Lutz Kämmerer

High Dimensional Fast Fourier Transform Based on Rank-1 Lattice Sampling

Lutz Kämmerer

High Dimensional Fast Fourier Transform Based on Rank-1 Lattice Sampling

TECHNISCHE UNIVERSITÄT
CHEMNITZ

Universitätsverlag Chemnitz
2014

Impressum

Bibliografische Information der Deutschen Nationalbibliothek

Die deutsche Nationalbibliothek verzeichnet diese Publikation in der Deutschen Nationalbibliografie; detaillierte bibliografische Angaben sind im Internet über `http://dnb.d-nb.de` abrufbar.

Diese Arbeit wurde von der Fakultät für Mathematik der Technischen Universität Chemnitz als Dissertation zur Erlangung des akademischen Grades Dr. rer. nat. genehmigt.
Die Arbeit wurde in englischer Sprache verfasst.

Tag der Einreichung: 30. Juni 2014

Betreuer: Prof. Dr. Daniel Potts, Technische Universität Chemnitz

1. Gutachter: Prof. Dr. Daniel Potts, Technische Universität Chemnitz
2. Gutachter: Prof. Dr. Peter Oswald, Jacobs University Bremen
3. Gutachter: Prof. Dr. Winfried Sickel, Friedrich–Schiller–Universität Jena

Tag der öffentlichen Prüfung: 21. November 2014

Technische Universität Chemnitz/Universitätsbibiliothek
Universitätsverlag Chemnitz
09107 Chemnitz
`http://www.tu-chemnitz.de/ub/univerlag`

Herstellung und Auslieferung
Verlagshaus Monsenstein und Vannerdat OHG
Am Hawerkamp 31
48155 Münster
`http://www.mv-verlag.de`

ISBN 978–3–944640–41–9

`http://nbn-resolving.de/urn:nbn:de:bsz:ch1-qucosa-157673`

Contents

1 Introduction **7**

2 Multivariate Trigonometric Polynomials **15**
2.1 Approximation of Multivariate Periodic Functions 17
2.2 Stability 19
2.3 Specific Frequency Index Sets 22
2.3.1 Weighted ℓ_p-balls 22
2.3.2 Weighted Hyperbolic Crosses 27
2.3.3 Energy-norm Based Hyperbolic Crosses 30
2.3.4 Arbitrary Sparse Frequency Index Sets 33
2.4 Summary 34

3 Rank-1 Lattices **35**
3.1 Evaluation of Multivariate Trigonometric Polynomials 38
3.2 Reconstruction of Multivariate Trigonometric Polynomials 38
3.3 Stability 47
3.4 Approximation of Multivariate Periodic Functions 49
3.5 Interpolation of Multivariate Periodic Functions 53
3.6 Tractability 54
3.7 Improvements on the Construction of Reconstructing Rank-1 Lattices 56
3.8 Specific Frequency Index Sets 58
3.8.1 Weighted ℓ_p-balls 60
3.8.2 Weighted Hyperbolic Crosses 66
3.8.3 Energy-norm Based Hyperbolic Crosses 71
3.8.4 Arbitrary Sparse Frequency Index Sets 75
3.9 Summary 76

4 Generated Sets **81**
4.1 Motivation 83
4.2 Evaluation of Multivariate Trigonometric Polynomials 84
4.3 Reconstruction of Multivariate Trigonometric Polynomials 85
4.4 Stability 89
4.5 Approximation of Multivariate Periodic Functions 96
4.6 Specific Frequency Index Sets 98
4.6.1 Weighted ℓ_p-balls 100
4.6.2 Weighted Hyperbolic Crosses 103
4.6.3 Arbitrary Sparse Frequency Index Sets 107
4.7 Summary 109

5 Applications and Numerical Examples **111**
5.1 Approximation of Periodic Functions 112
5.1.1 Polynomial Test Function 113
5.1.2 Periodic Test Function 121
5.2 Poisson's Equation in d Dimensions 127
5.2.1 Polynomial Test Function 130
5.3 Approximation of Non-periodic Functions 137
5.3.1 Non-periodic Polynomial Test Function 140
5.4 Summary 143

Bibliography **145**

Notations **151**

Chapter 1

Introduction

The approximation of functions is one basic problem in applied mathematics with a wide range of applications in almost all scientific fields.

We focus on the approximation of functions from sampling values. In general, one has to increase the number of sampling values, i.e., the amount of information, in order to achieve better approximations. Due to the possibly huge amount of data to be processed, highly efficient algorithms are of monumental interest. The fast Fourier transform (FFT), first introduced by C. F. Gauß and most popularly published by J. Cooley and J. W. Tukey in [CT65] in the mid-sixties of the last century, provides such a method that allows for extremely efficient computations of interpolations of one-dimensional functions by trigonometric polynomials. In the following decades, a huge list of papers presents modifications and improvements of this algorithm and, in particular, generalizations to spatial domains of higher dimensions d. Here, straightforward strategies, i.e., the consideration of tensor product grids, do not affect the efficiency of a corresponding FFT algorithm but fails due to the excessive amount of used data.

However, the originally introduced fast Fourier transform algorithm is an efficient implementation of the so-called one-dimensional discrete Fourier transform, which can be formally described by a matrix vector product. The corresponding matrix, called Fourier matrix, is unitary up to a scaling factor that might be present. Thus, the matrix has condition number one and, in addition, there exist stable and fast implementations of this discrete Fourier transform, cf. [Sch96, PST03]. Consequently, we notice that the approximation of univariate functions using the fast Fourier transform is also a stable method. In our considerations, we focus on the condition number of the Fourier matrices $\boldsymbol{A} = \left(\mathrm{e}^{2\pi \mathrm{i} \boldsymbol{k}\cdot\boldsymbol{x}}\right)_{\boldsymbol{x}\in\mathcal{X},\,\boldsymbol{k}\in I}$, where $\mathcal{X} \subset \mathbb{T}^d$ is a set of sampling nodes and $I \subset \mathbb{Z}^d$ the frequency index set of a multivariate trigonometric polynomial. More precisely, we ignore the stability of the concrete fast algorithms, and call the discrete Fourier transform stable whenever the condition number of the Fourier matrix is near one and perfectly stable if the condition number is exactly one.

In this work, we follow a very general approach. Specifically, we consider multivariate trigonometric polynomials with frequencies supported on a fixed but arbitrary frequency index set $I \subset \mathbb{Z}^d$ of finite cardinality. Naturally, one is interested in spatial discretizations in the d-dimensional torus $\mathbb{T}^d$ such that

- the sampling values of the trigonometric polynomial with frequencies supported on I at this spatial discretization uniquely determines the trigonometric polynomial,

- the corresponding discrete Fourier transform is fast realizable, and
- the corresponding fast Fourier transform is stable.

Throughout the work, we focus on specific structures of the frequency index sets I several times. We consider weighted ℓ_p-balls for $0 < p \leq \infty$, cf. (2.15), as frequency index sets. For full tensor product grids, i.e., weighted ℓ_∞-balls, in frequency domain there exist corresponding tensor product grids in the spatial domain such that the discrete Fourier transform is stable and efficiently realizable. As mentioned above, tensor product grids suffer from fast growing cardinalities and, thus, are not manageable for higher spatial dimensions d. For decreasing parameter p, the number of frequency indices that are contained in weighted ℓ_p-balls mildly reduces. Trigonometric polynomials with frequencies supported on weighted ℓ_p-balls, $0 < p < \infty$, well approximate specific functions and, thus, may succeed in various applications. Certainly, one is interested in sampling methods that allow for good approximations, see e.g. [LSX09] for an interpolation approach where the parameter $p = 1$ and dimension $d = 2$ is considered. Nevertheless, ℓ_p-balls suffer from fast growing cardinalities even for moderate expansions and dimensions d for all parameters $p > 0$. For that reason, hyperbolic cross approximations have become very popular. This approach severely reduces the number of frequency indices for approximations of functions that belong to spaces of dominating mixed smoothness, see e.g. [DS89, Tem93, DPT94]. Sampling at related so-called sparse grids allows for a unique interpolation, cf. e.g. [BD89, BG04], and corresponding fast computations, cf. [Hal92, Gra07, GH14]. Moreover, we consider arbitrary sparse frequency index sets without any structure. In [GPR10], it is proven that with "overwhelming" probability multivariate trigonometric polynomials supported on such arbitrary sparse frequency index sets can be reconstructed by using relatively few sampling values at randomly chosen nodes from the d-dimensional torus $\mathbb{T}^d$. However, the discrete Fourier transform related to the three mentioned types of frequency index sets suffer from different problems.

- The usually used spatial discretizations for ℓ_p-balls that allow for a corresponding fast Fourier transform are not well-adapted, in general.
- The Fourier matrices of the hyperbolic cross discrete Fourier transform suffers from growing condition numbers for increasing cardinality of the frequency index set I—at least for regular dyadic sparse grids, cf. [KK11].
- There exists no practicable fast algorithm for the sparse nonequispaced discrete Fourier transform for large dimensions d.

For these reasons, we suggest to use rank-1 lattices and a generalization as spatial discretizations in order to sample multivariate trigonometric polynomials not only of the mentioned types. Initially, rank-1 lattices were introduced as sampling schemes for numerical integration by several authors in the late 1950s and 1960s. In [Nie78], one finds a summary and an extensive reference list of early work on so-called lattice rules, i.e., cubature rules based on (rank-1) lattice sampling. On the contrary to the originated field of application, we use rank-1 lattices as sampling schemes for the approximation of whole functions by trigonometric polynomials. To the authors knowledge, this idea was first considered by V. N. Temlyakov for specific rank-1 lattices, i.e., rank-1 lattices of Korobov type, cf. [Tem86], and later on by D. Li and F. J. Hickernell in a more general setting, cf. [LH03]. Subsequently, the approximation properties of rank-1 lattices were investigated in the fields of information based complexity and applied analysis, cf. [ZLH06, KSW06, KSW08, KWW09, MS12]. However, there exist

only a few applicable construction methods for rank-1 lattices that are suitable for approximation, cf. [KSW06, KSW08, KWW09]. These methods crucially depend on the specific function spaces that are considered in these papers and are in fact component–by–component constructions.

Based on the considerations in [CKN10], we gave a universally applicable component–by–component construction strategy that determines reconstructing rank-1 lattices for given frequency index sets I, i.e., sampling sets that allow the perfectly stable reconstruction of trigonometric polynomials with frequencies supported on the frequency index set I. The presented construction method does not depend on the structure of the frequency index set I. Moreover, we generalize the concept of rank-1 lattices to so-called generated sets and present a continuous search method that also determines sampling sets that are very well suited for a fast and stable reconstruction of trigonometric polynomials. Due to the fact that the fast computation of the multi-dimensional discrete Fourier transforms using rank-1 lattices or generated sets as sampling schemes is realized by permutations and one-dimensional fast Fourier transforms or one-dimensional nonequispaced fast Fourier transforms, cf. [DR93, Bey95, Ste98], the stability of the one-dimensional fast algorithms spread to the presented algorithms in our work.

We analyze the reconstruction and stability properties of both sampling schemes and, in addition, apply the results in order to determine the excellent approximation properties of the corresponding sampling methods. Moreover, we discuss our findings on the basis of some approximation problems that are of crucial interest. Various numerical examples demonstrate the outstanding properties and the universality of the presented sampling schemes.

We point out that essential results of this thesis have already been published in [KKP12, Käm13a, Käm13b, Käm14, KPV13, KPV14]. Finally, we would like to encourage the practically orientated reader to make extensive use of our toolbox [Käm] which fundamentally consists of the algorithms that are presented here.

Outline of the Thesis

Chapter 2 : Multivariate Trigonometric Polynomials.
We introduce most of our notations and describe the approximation problem of multivariate periodic continuous functions using trigonometric polynomials. The main focus is on the approximation of functions that have absolutely convergent Fourier series.

We define function spaces $\mathcal{A}_\omega(\mathbb{T}^d)$, cf. (2.9), that contain functions f of a specific smoothness which is characterized by a so-called weight function ω that determines the decay of the Fourier coefficients of each function $f \in \mathcal{A}_\omega(\mathbb{T}^d)$. The corresponding norm of a function f in $\mathcal{A}_\omega(\mathbb{T}^d)$ is given by an ω-weighted ℓ_1-norm of the Fourier coefficients.

In particular, the weight function ω specifies more and also less important indices of Fourier coefficient by its function values. We define the frequency index sets $I_N := \{\boldsymbol{k} \in \mathbb{Z}^d \colon \omega(\boldsymbol{k}) \leq N\}$, $N \in \mathbb{R}$, that somehow collect the indices of the most important Fourier coefficients of the functions f that belong to $\mathcal{A}_\omega(\mathbb{T}^d)$. Moreover, we show that the Fourier partial sums of $f \in \mathcal{A}_\omega(\mathbb{T}^d)$ with frequencies supported on these frequency index sets I_N approximate the function f well.

In general, one cannot expect to approximate a function $f \in \mathcal{A}_\omega(\mathbb{T}^d)$ by its exact Fourier partial sums in numerical applications since one does not know the exact Fourier coefficients of f. Often, functions are given by its function values at specific sampling nodes. However, we would like to approximate multivariate continuous periodic functions f and we assume that it is possible to sample the function f at an arbitrary finite set of sampling nodes $\mathcal{X} \subset \mathbb{T}^d$.

We will use a finite set of function values of f, i.e., $f(\boldsymbol{x})$, $\boldsymbol{x} \in \mathcal{X}$, in order to compute a trigonometric polynomial with frequencies supported on a suitable given frequency index set, i.e., I_N, that approximates the function f. Naturally, one is interested in somehow good sampling schemes $\mathcal{X}$, that guarantees approximations of high quality.

In Section 2.2, we restrict our considerations to the reconstruction of multivariate trigonometric polynomials and, in addition, on the perfectly stable reconstruction of multivariate trigonometric polynomials, i.e., the corresponding Fourier matrix $\boldsymbol{A}$, cf. (2.7), should have a condition number that is exactly one.

We determine a general lower bound on the number of sampling values that are needed in order to perfectly stably reconstruct all trigonometric polynomials supported on the frequency index set I in Lemma 2.5. This lower bound mainly depends on the structure of the frequency index set I and is determined by the maximum of the cardinalities of all frequency index sets I' such that the difference sets fulfill $\mathcal{D}(I') \subset \mathcal{D}(I)$. The difference set of the frequency index set I is defined by $\mathcal{D}(I) := \{\boldsymbol{h} \in \mathbb{Z}^d \colon \boldsymbol{h} = \boldsymbol{k}_1 - \boldsymbol{k}_2, \boldsymbol{k}_1, \boldsymbol{k}_2 \in I\}$.

We apply these results on frequency index sets I of different structures in Section 2.3. In particular, we consider weighted ℓ_p-balls, $0 < p \leq \infty$, and weighted (energy-norm based) hyperbolic crosses, which are motivated by function spaces of isotropic and dominating mixed smoothness. Different types of such function spaces were of outstanding interest in approximation theory during the last decades. Finally, we summarize the findings of Chapter 2 in Section 2.4.

Chapter 3 : Rank-1 Lattices.

We consider rank-1 lattices $\Lambda(\boldsymbol{z}, M)$, cf. (3.1), which are structured discretizations in spatial domain, i.e., in the d-dimensional torus $\mathbb{T}^d$. The vector $\boldsymbol{z} \in \mathbb{Z}^d$ is called generating vector and $M \in \mathbb{N}$ is named lattice size of the rank-1 lattice $\Lambda(\boldsymbol{z}, M)$. The natural number M bounds the number of sampling nodes that are contained in $\Lambda(\boldsymbol{z}, M)$ from above. These kind of sampling sets are investigated extensively in the field of numerical integration. In particular, we focus on the approximation properties of these sampling sets.

First, we restrict our considerations on multivariate trigonometric polynomials and show that the structure of rank-1 lattices is well suited in order to fast evaluate multivariate trigonometric polynomials at all sampling nodes of a rank-1 lattice by means of a one-dimensional fast Fourier transform (FFT). In detail, the corresponding computational complexity is bounded by $\mathcal{O}\left(M \log M + d|I|\right)$, where I is the frequency index set of the multivariate trigonometric polynomial and M the number of sampling nodes. We emphasize that we evaluate multivariate trigonometric polynomials in linear time with respect to the maximum of the cardinality of the frequency index set I and the number of sampling nodes M up to some logarithmic factor $\log M$.

Subsequently, we determine necessary and sufficient conditions on a rank-1 lattice, such that sampling along this rank-1 lattice allows for the unique reconstruction of multivariate trigonometric polynomials with frequencies supported on a given frequency index set I, cf. Section 3.2. We call such a rank-1 lattice reconstructing rank-1 lattice for the frequency index set I. Within the framework of these considerations, we show that a unique reconstruction implies a perfectly stable reconstruction of multivariate trigonometric polynomials from samples along a rank-1 lattice naturally. We present an algorithm of a complexity in $\mathcal{O}\left(M \log M + d|I|\right)$ that computes this reconstruction.

However, a reconstructing rank-1 lattice for a frequency index set I is not explicitly given by the sufficient conditions we determined. Specifically, reconstructing rank-1 lattices of relatively small cardinalities are of our main interest in Section 3.2, since the computational costs

of the reconstruction algorithm mainly depends on the number of used sampling values. We develop a component–by–component approach that allows for the deterministic construction of reconstructing rank-1 lattices for a given frequency index set I in Corollary 3.4, which is based on the essential findings of Theorem 3.2. Moreover, we give bounds on the cardinality M of such a reconstructing rank-1 lattice, which mainly depends on the difference set $\mathcal{D}(I)$, cf. (2.11), and, thus, on the structure of the frequency index set I,

$$|I| \leq M \leq \max\left\{\frac{2|I|^2}{3}, \max\{3\|\boldsymbol{k}\|_\infty : \boldsymbol{k} \in I\}\right\}, \tag{1.1}$$

where the upper bound on the right hand side is roughly simplified, see Corollary 3.4 and the subsequent considerations for more details. We stress the fact that both bounds do not depend on the spatial dimension d but on the cardinality and the expansion of the frequency index set I.

In Section 3.4, we focus on the approximation properties of reconstructing rank-1 lattices for the index sets I_N in the spaces $\mathcal{A}_\omega(\mathbb{T}^d)$, i.e., we consider the trigonometric polynomial with frequencies supported on I_N that is determined from function values of f along the rank-1 lattice. We prove an upper bound on the $L_\infty(\mathbb{T}^d)$ approximation error that is only two times the upper bound of the $L_\infty(\mathbb{T}^d)$ approximation error which we obtained for the exact Fourier partial sum in Chapter 2, cf. Theorem 3.11. Furthermore, we extend the approximation approach to an interpolation approach that guarantees the same error estimates as we have shown for the approximation, cf. Section 3.5.

Additionally, we discuss improvements on the component–by–component construction of reconstructing rank-1 lattices in Section 3.7. In particular, we present two basic component–by–component strategies that deterministically constructs reconstructing rank-1 lattices without the computation of the difference sets $\mathcal{D}(I)$, which is a bottleneck of our previous determined algorithm due to the possibly huge memory requirements.

In addition, we apply the theoretical findings on rank-1 lattices to the specific frequency index sets that are introduced in Chapter 2. We prove that reconstructing rank-1 lattices are in some sense optimal sampling schemes, specifically, with respect to the perfectly stable reconstruction. Furthermore, we apply our component–by–component constructions of reconstructing rank-1 lattices to several examples, i.e., weighted ℓ_p-balls, weighted hyperbolic crosses, axis crosses, and randomly chosen frequency index sets, and discuss the corresponding results. We obtain the proved asymptotic behavior in general. Nevertheless, the rank-1 lattice sizes M of reconstructing rank-1 lattices are much smaller than the theoretical upper bounds in practice and, thus, reasonable even for frequency index sets I of cardinalities up to millions. We summarize the crucial findings of this chapter in Section 3.9.

Chapter 4: Generated Sets.

First, we introduce and motivate a generalization of rank-1 lattices, which we call generated sets. In contrast to rank-1 lattices, generated sets are sampling sets that are generated by a real valued vector $\boldsymbol{r} \in \mathbb{R}^d$. Our generalization retains the most important property of rank-1 lattices—the rank-1 structure.

In Section 4.2 we show that the evaluation of a multivariate trigonometric polynomial at all nodes of a generated set simplifies to a one-dimensional nonequispaced discrete Fourier transform. Thus, we simultaneously, fast evaluate a multivariate trigonometric polynomial at all nodes of a generated set by means of a one-dimensional nonequispaced fast Fourier transform (NFFT), cf. Algorithm 3.1. We would like to point out that the used one-dimensional NFFT is an approximate algorithm that has almost the same complexity as the FFT. In

detail, the computational complexity of Algorithm 3.1 is in $\mathcal{O}\left(M \log M + (|\log \varepsilon| + d)|I|\right)$, where ε characterizes the accuracy of the one-dimensional NFFT.

Subsequently, we shift our attention to the reconstruction problem, i.e., how to reconstruct the frequencies of a trigonometric polynomial from sampling values along a generated set, in Section 4.3. We show, that we can simply determine a generated set that allows for the unique reconstruction of trigonometric polynomials with frequencies supported on I by randomly choosing a generating vector $\boldsymbol{r}$ and fixing $M \geq |I|$. In our theoretical considerations, we show that one fixes a so-called reconstructing generated set for I with probability one in this way. In addition to it, we specify a fast algorithm that reconstructs a multivariate trigonometric polynomial with frequencies supported on the index set I from the sampling values along a reconstructing generated set for I. Due to the fact that there does not exist a direct fast computation of the pseudoinverse of a one-dimensional nonequispaced discrete Fourier transform, we apply an iterative method, i.e., a conjugate gradient method, that uses the NFFT and its adjoint algorithm. The computational complexity of one step of this iterative method is bounded by $\mathcal{O}\left(M \log M + (|\log \varepsilon| + d)|I|\right)$. In Lemma 4.5, we give an upper bound on the number of iterations that are sufficient in order to achieve a given relative error. As usual, this upper bound depends on the condition number of the Fourier matrix $\boldsymbol{A}$. However, the corresponding Fourier matrix $\boldsymbol{A}$ may suffer from huge condition numbers in general.

In Section 4.4, we show that the condition $|\{\boldsymbol{k} \cdot \boldsymbol{r} \bmod 1 \colon \boldsymbol{k} \in I\}| = |I|$ is necessary and also sufficient in order to determine a generated set with generating vector $\boldsymbol{r}$ that offers a stable discrete Fourier transform, i.e., a Fourier matrix $\boldsymbol{A}$ that has a condition number $\operatorname{cond}_2(\boldsymbol{A})$ near 1. We estimate the condition number by terms that are finite if and only if the condition $|\{\boldsymbol{k} \cdot \boldsymbol{r} \bmod 1 \colon \boldsymbol{k} \in I\}| = |I|$ is fulfilled. Furthermore, the almost surely finite upper bound on the condition number $\operatorname{cond}_2(\boldsymbol{A})$ is inversely proportional to the number of used sampling values M and tends to one if M tends to infinity. We use that property in order to determine an $M = M(I, \boldsymbol{r}, C) \in \mathbb{N}$ such that the related Fourier matrix $\boldsymbol{A}$, that is specified by the frequency index set I and the first $M(I, \boldsymbol{r}, C)$ multiples of $\boldsymbol{r}$ as sampling scheme, has a condition number $\operatorname{cond}_2(\boldsymbol{A})$ not larger than a specific target condition number $C > 1$, cf. Corollary 4.10.

Within this context, we develop an algorithm that allows for the fast computation of $M(I, \boldsymbol{r}, C)$ with a complexity of $\mathcal{O}\left(|I|(\log |I| + d)\right)$. Thus for a given frequency index set I and given target condition number C, we rate a vector $\boldsymbol{r}$ by the value of $M(I, \boldsymbol{r}, C)$. Since we are interested in suitable sampling sets, i.e., sampling sets that cause a Fourier matrix $\boldsymbol{A}$ with a small condition number $\operatorname{cond}_2(\boldsymbol{A}) < C$ and have a relatively small number of sampling nodes as well, we would like to determine generating vectors $\boldsymbol{r}$ such that $M(I, \boldsymbol{r}, C)$ is as small as possible. For that reason, we present a fast continuous search method based on a simplex search method that numerically determines local minimizers of $M(I, \circ, C)$.

Furthermore, we investigate the approximation properties of the presented sampling method and show that the $L_2(\mathbb{T}^d)$ error of approximations of Fourier partial sums of functions $f \in \mathcal{A}_\omega(\mathbb{T}^d)$ are of optimal order, provided that we determined the approximation of f from sampling values of f along a reconstructing generated set for I_N with a stable Fourier matrix $\boldsymbol{A}$, cf. Theorem 4.12.

Due to the fact that the concept of generated sets is a generalization of rank-1 lattices which also includes rank-1 lattices, we can apply the existence results for rank-1 lattices to generated sets. Our construction method for generated sets is based on a continuous optimization method that finds only local minimizers of an upper bound of the Gershgorin circle radius. In Section 4.6, we demonstrate the usability of the generated set search algorithm in

various examples and compare the results to rank-1 lattices that we determined in Section 3.8. Finally, we summarize the findings of this chapter in Section 4.7.

Chapter 5 : Applications and Numerical Examples.
The last chapter exemplifies some applications. In Section 5.1, we treat multivariate smooth periodic test functions and approximate these functions with approximated Fourier partial sums with frequencies supported on suitable frequency index sets, which are weighted ℓ_1-balls up to dimension $d = 22$ and equally weighted hyperbolic crosses up to dimension $d = 10$. In particular, we compare the rank-1 lattice approximation with the interpolation approach and point out and discuss the advantages of the interpolation in Sections 5.1.1 and 5.1.2. Additionally, we compare rank-1 lattice approximations to generated set approximations and obtain almost the same errors in Section 5.1.1.

In Section 5.2, we consider Poisson's equation in d dimensions with periodic boundary conditions. We give an error estimate for the rank-1 lattice sampling method and compare the errors of different sampling methods for trigonometric polynomials by means of an example that deals with functions up to dimension $d = 9$. In detail, we compare rank-1 lattice discretizations to full grid and standard sparse grid discretizations and demonstrate the differences in the asymptotics of these approaches.

As a last application, we treat multivariate non-periodic functions, explain how to periodize such functions, and discuss difficulties that may occur by approximating non-periodic functions using the algorithms that are adapted for periodic functions in Section 5.3.1. The periodized version of our non-periodic test function can be well approximated by trigonometric polynomials with frequencies supported on hyperbolic crosses with gaps. We determine reconstructing rank-1 lattices for these frequency index sets and compute approximations and interpolations in dimensions d up to $d = 10$. The error decay of the approximations is almost optimal with respect to the parameter N of the frequency index sets I_N.

Within all examples, we point out the advantages of well adapted frequency index sets I. At this point, we emphasize that all computed approximations are based on the approximation of functions using different Dirichlet kernels, see e.g. [Wei12]. We stress the fact that our sampling methods are not limited to such approximations. One may also compute approximations based on other trigonometric kernels, e.g., ℓ_q-Fejér and Riesz kernels, cf. [Wei12]. To this end, one determines the frequency index sets of the specific kernels and compute approximations from sampling values along reconstructing rank-1 lattices for those frequency index sets.

Acknowledgments

First, I feel the outstanding need to express my deep appreciation and gratitude to my advisor, Prof. Dr. Daniel Potts, for his great encouragement, his patient guidance, and his creativity that pave the way for this thesis. Additionally, I appreciate the valuable cooperations with Prof. Dr. Stefan Kunis and Toni Volkmer. I thank Dr. Manuel Gräf, Dr. Ralf Hielscher, Franziska Nestler, Michael Pippig, and the already above mentioned for the excellent working climate and fruitful on- and off-topic discussions.

Finally, I thank all the people who guided and / or supported me on my way throughout the years.

Chapter 2

Approximation using Multivariate Trigonometric Polynomials

In the wide field of approximation theory, one mostly uses smoothness properties of a function in order to determine the quality of a specific approximation method. In particular for sufficiently smooth multivariate periodic functions $f\colon \mathbb{T}^d \to \mathbb{C}$, $d \in \mathbb{N}$ is the spatial dimension, one takes the function f as its Fourier series

$$f(\boldsymbol{x}) = \sum_{\boldsymbol{k}\in\mathbb{Z}^d} \hat{f}_{\boldsymbol{k}} \mathrm{e}^{2\pi\mathrm{i}\boldsymbol{k}\cdot\boldsymbol{x}}$$

and characterizes the smoothness of the function f using properties of its Fourier coefficients

$$\hat{f}_{\boldsymbol{k}} := \int_{\mathbb{T}^d} f(\boldsymbol{x}) \mathrm{e}^{-2\pi\mathrm{i}\boldsymbol{k}\cdot\boldsymbol{x}} \mathrm{d}\boldsymbol{x}. \tag{2.1}$$

We assume that the function f belongs to the function space $L_1(\mathbb{T}^d)$ in order to guarantee the existence of all Fourier coefficients $\hat{f}_{\boldsymbol{k}}$, $\boldsymbol{k} \in \mathbb{Z}^d$, of f. The function spaces $L_p(\mathbb{T}^d)$, $1 \leq p < \infty$, are defined by

$$L_p(\mathbb{T}^d) := \left\{ f\colon \mathbb{T}^d \to \mathbb{C}, \int_{\mathbb{T}^d} |f(\boldsymbol{x})|^p \mathrm{d}\boldsymbol{x} < \infty \right\} \tag{2.2}$$

and for $p = \infty$

$$L_\infty(\mathbb{T}^d) := \left\{ f\colon \mathbb{T}^d \to \mathbb{C}, \operatorname{ess\,sup}_{\boldsymbol{x}\in\mathbb{T}^d} |f(\boldsymbol{x})| < \infty \right\}. \tag{2.3}$$

As usual, the norm of a function $f \in L_p(\mathbb{T}^d)$ is denoted and given by $\|f|L_p(\mathbb{T}^d)\| := \left(\int_{\mathbb{T}^d} |f(\boldsymbol{x})|^p \mathrm{d}\boldsymbol{x}\right)^{1/p}$ for $1 \leq p < \infty$, and $\|f|L_\infty(\mathbb{T}^d)\| := \operatorname{ess\,sup}_{\boldsymbol{x}\in\mathbb{T}^d} |f(\boldsymbol{x})|$ for $p = \infty$.

In the following, we consider the Fourier coefficients $\hat{f}_{\boldsymbol{k}}$ in dependence on $\boldsymbol{k} \in \mathbb{Z}^d$. If the absolute values of the Fourier coefficients decrease sufficiently fast for growing frequency index $\boldsymbol{k}$, we may approximate the function f using only a few terms $\hat{f}_{\boldsymbol{k}} \mathrm{e}^{2\pi\mathrm{i}\boldsymbol{k}\cdot\boldsymbol{x}}$, $\boldsymbol{k} \in I \subset \mathbb{Z}^d$, $|I| < \infty$, very well. We call the set I frequency index set of the Fourier partial sum

$$S_I f(\boldsymbol{x}) := \sum_{\boldsymbol{k}\in I} \hat{f}_{\boldsymbol{k}} \mathrm{e}^{2\pi\mathrm{i}\boldsymbol{k}\cdot\boldsymbol{x}} \tag{2.4}$$

which is a trigonometric polynomial with frequencies supported on the index set I, in fact.

We emphasize that we left out a lot of details in the last sentences. Specifically, the reader may ask the following questions:

- What means "sufficiently fast decreasing Fourier coefficients"?
- How do we define the growth of a vector $\boldsymbol{k} \in \mathbb{Z}^d$?
- How do we get the Fourier coefficients $\hat{f}_{\boldsymbol{k}}$ of the function f for specific $\boldsymbol{k} \in \mathbb{Z}^d$, i.e., how do we evaluate the integrals in (2.1)?

A lot of details on the characterizations of periodic functions and suitable function spaces, particularly concerning the properties of the Fourier coefficients of f, can be found in [ST87, Chapter 3].

In this chapter, we consider the approximation of functions f using Fourier partial sums $S_I f$, where the frequency index set I should be carefully chosen with respect to the properties of the sequence of the Fourier coefficients $(\hat{f}_{\boldsymbol{k}})_{\boldsymbol{k} \in \mathbb{Z}^d}$. In detail, we are interested in the approximation of functions f that belongs to a subspace of $L_2(\mathbb{T}^d)$, which is a Hilbert space with the scalar product

$$\langle f, g \rangle_{L_2(\mathbb{T}^d)} := \int_{\mathbb{T}^d} f(\boldsymbol{x}) \overline{g(\boldsymbol{x})} \mathrm{d}\boldsymbol{x}, \tag{2.5}$$

where $\overline{g}$ is the complex conjugate of g. More specifically, we consider periodic functions $f \in L_1(\mathbb{T}^d)$, where the sequence of Fourier coefficients of f is absolutely summable, which implies that the considered functions f have continuous representatives within $L_1(\mathbb{T}^d)$. We call the function space

$$\mathcal{A}(\mathbb{T}^d) := \{ f \in L_1(\mathbb{T}^d) : \sum_{\boldsymbol{k} \in \mathbb{Z}^d} |\hat{f}_{\boldsymbol{k}}| < \infty \} \tag{2.6}$$

the Wiener algebra and define the related norm of f by $\|f|\mathcal{A}(\mathbb{T}^d)\| := \sum_{\boldsymbol{k} \in \mathbb{Z}^d} |\hat{f}_{\boldsymbol{k}}|$. Since we would like to sample the functions $f \in \mathcal{A}(\mathbb{T}^d)$ in the following chapters, we identify each function $f \in \mathcal{A}(\mathbb{T}^d)$ with its continuous representative $\sum_{\boldsymbol{k} \in \mathbb{Z}^d} \hat{f}_{\boldsymbol{k}} \mathrm{e}^{2\pi \mathrm{i} \boldsymbol{k} \cdot \circ}$. Furthermore, we introduce subspaces of the Wiener algebra. The corresponding function spaces may consist of functions that have a specific type of smoothness, i.e., isotropic smoothness or dominating mixed smoothness.

We consider the approximation properties of Fourier partial sums $S_I f$, see (2.4), where the frequency index set I has to be suitably chosen with respect to a function space that contains the function f. Later on, our goal will be the approximation of the Fourier partial sum $S_I f$ from sampling values of the function f. For that reason, we study the corresponding Fourier matrix

$$\boldsymbol{A} := \left(\mathrm{e}^{2\pi \mathrm{i} \boldsymbol{k} \cdot \boldsymbol{x}} \right)_{\boldsymbol{x} \in \mathcal{X}, \, \boldsymbol{k} \in I}, \tag{2.7}$$

where $\mathcal{X} := \{ \boldsymbol{x}_j \in \mathbb{T}^d : j = 0, \ldots, M-1 \}$ is a sampling scheme on the d-dimensional torus $\mathbb{T}^d$. Note that we assume to run through the sets I and $\mathcal{X}$ in some fixed order whenever we use $\boldsymbol{k} \in I$ or $\boldsymbol{x} \in \mathcal{X}$ as running index of matrices or vectors.

We assume that the frequency index set I is fixed and determine some specific necessary conditions on the Fourier matrix $\boldsymbol{A}$ and, in particular, the cardinality of the sampling set $\mathcal{X}$ in order to guarantee pairwise orthogonal columns within the Fourier matrix $\boldsymbol{A}$, i.e.,

the condition number of $\boldsymbol{A}$ is one and, thus, the corresponding discrete Fourier transform perfectly stable, cf. Lemma 2.5. In particular, we prove a lower bound on the number of sampling values in $\mathcal{X}$ that are necessarily needed in order to obtain such perfectly stable Fourier matrices $\boldsymbol{A}$.

Furthermore, we apply our general findings on different well-known structures of frequency index sets I and give specific lower bounds on the number of sampling values that are needed in order to achieve Fourier matrices $\boldsymbol{A}$ that have orthogonal columns. Specifically, we consider so-called weighted l_p-balls, $0 < p \leq \infty$, as frequency index sets I, that may occur if one approximates functions in spaces of isotropic smoothness. In addition, we also deal with (energy-norm based) hyperbolic cross type frequency index sets I, that are very well suited to the approximation of functions of dominating mixed smoothness.

2.1 Approximation of Multivariate Periodic Functions

We denote by Π_I the space of all multivariate trigonometric polynomials with frequencies supported on the index set $I \subset \mathbb{Z}^d$, which is a set of finitely many integer vectors. The cardinality of the set I is denoted by $|I|$. In formula, we gain

$$\Pi_I := \operatorname{span}\{\mathrm{e}^{2\pi\mathrm{i}\boldsymbol{k}\cdot\circ} \colon \boldsymbol{k} \in I\}. \tag{2.8}$$

The space Π_I is spanned by orthogonal basis functions with respect to the scalar product in $L_2(\mathbb{T}^d)$, cf. (2.5), which implies that each element $f \in \Pi_I$ is uniquely determined by its vector of Fourier coefficients $\left(\hat{f}_{\boldsymbol{k}}\right)_{\boldsymbol{k}\in I}$ with $f(\boldsymbol{x}) = \sum_{\boldsymbol{k}\in I} \hat{f}_{\boldsymbol{k}} \mathrm{e}^{2\pi\mathrm{i}\boldsymbol{k}\cdot\boldsymbol{x}}$.

In general, a suitable chosen frequency index set I ensures good approximating Fourier partial sums $S_I f \in \Pi_I$, see (2.4), in specific function spaces. We define the weighted function spaces

$$\mathcal{A}_\omega(\mathbb{T}^d) := \{f \in L_1(\mathbb{T}^d) : \ f(\boldsymbol{x}) = \sum_{\boldsymbol{k}\in\mathbb{Z}^d} \hat{f}_{\boldsymbol{k}} \mathrm{e}^{2\pi\mathrm{i}\boldsymbol{k}\cdot\boldsymbol{x}}, \ \sum_{\boldsymbol{k}\in\mathbb{Z}^d} \omega(\boldsymbol{k})|\hat{f}_{\boldsymbol{k}}| < \infty\}, \tag{2.9}$$

where $\omega : \mathbb{Z}^d \to [1, \infty]$ is called *weight function* and characterizes the decay of the Fourier coefficients of all functions $f \in \mathcal{A}_\omega(\mathbb{T}^d)$, i.e., the Fourier coefficients $\hat{f}_{\boldsymbol{k}}$ have to decrease faster than the weight function ω increases with respect to $\boldsymbol{k}$ in order to obtain $f \in \mathcal{A}_\omega(\mathbb{T}^d)$. Specifically, the decay of the Fourier coefficients $\hat{f}_{\boldsymbol{k}}$ describe the smoothness of the function f. Moreover, we define the norm of a function $f \in \mathcal{A}_\omega(\mathbb{T}^d)$ by $\|f|\mathcal{A}_\omega(\mathbb{T}^d)\| := \sum_{\boldsymbol{k}\in\mathbb{Z}^d} \omega(\boldsymbol{k})|\hat{f}_{\boldsymbol{k}}|$. The space of continuous $\mathbb{T}^d$-periodic functions is represented by $\mathcal{C}(\mathbb{T}^d)$. The norm in the vector space $\mathcal{C}(\mathbb{T}^d)$ coincides with the norm in $L_\infty(\mathbb{T}^d)$. The next Lemma states that the embeddings $\mathcal{A}_\omega(\mathbb{T}^d) \subset \mathcal{A}_{\omega_1}(\mathbb{T}^d) = \mathcal{A}(\mathbb{T}^d) \cap \mathcal{C}(\mathbb{T}^d)$ hold, where $\omega_1(\boldsymbol{k}) = 1$ for all $\boldsymbol{k} \in \mathbb{Z}^d$. $\mathcal{A}(\mathbb{T}^d)$ is called *Wiener algebra*.

Lemma 2.1. *Each function $f \in \mathcal{A}(\mathbb{T}^d)$ has a continuous representative. In particular, we obtain $\mathcal{A}_\omega(\mathbb{T}^d) \subset \mathcal{A}(\mathbb{T}^d) \subset \mathcal{C}(\mathbb{T}^d)$ with the usual interpretation.*

Proof. Let $f \in \mathcal{A}_\omega(\mathbb{T}^d)$ be given. Then the function f belongs to $\mathcal{A}(\mathbb{T}^d)$ since the estimate

$$\infty > \sum_{\boldsymbol{k}\in\mathbb{Z}^d} \omega(\boldsymbol{k})|\hat{f}_{\boldsymbol{k}}| \geq \sum_{\boldsymbol{k}\in\mathbb{Z}^d} |\hat{f}_{\boldsymbol{k}}|$$

holds.

Now, let $f \in \mathcal{A}(\mathbb{T}^d)$ be given. The summability of the sequence $(|\hat{f}_{\boldsymbol{k}}|)_{\boldsymbol{k}\in\mathbb{Z}^d}$ of the absolute values of the Fourier coefficients implies the summability of the sequence $(|\hat{f}_{\boldsymbol{k}}|^2)_{\boldsymbol{k}\in\mathbb{Z}^d}$ of the squared absolute values of the Fourier coefficients and, thus, the embeddings $\mathcal{A}(\mathbb{T}^d) \subset L_2(\mathbb{T}^d)$ is proved using Parseval's identity and a standard estimate.

Clearly, the function $g = \sum_{\boldsymbol{k}\in\mathbb{Z}^d} \hat{f}_{\boldsymbol{k}} \mathrm{e}^{2\pi\mathrm{i}\boldsymbol{k}\cdot\circ}$ is a representative of f in $L_2(\mathbb{T}^d)$ and also in $\mathcal{A}(\mathbb{T}^d)$. We show, that g is the continuous representative of f.

The absolute values of the Fourier coefficients of $f \in \mathcal{A}(\mathbb{T}^d)$ are summable. So, for each $\varepsilon > 0$ there exists an index set $I \subset \mathbb{Z}^d$ of finite cardinality with $\sum_{\boldsymbol{k}\in\mathbb{Z}^d\setminus I} |\hat{f}_{\boldsymbol{k}}| < \frac{\varepsilon}{4}$. For a fixed $\boldsymbol{x}_0 \in \mathbb{T}^d$, we estimate

$$\begin{aligned} |g(\boldsymbol{x}_0) - g(\boldsymbol{x})| &= \left| \sum_{\boldsymbol{k}\in\mathbb{Z}^d} \hat{f}_{\boldsymbol{k}} \mathrm{e}^{2\pi\mathrm{i}\boldsymbol{k}\cdot\boldsymbol{x}_0} - \sum_{\boldsymbol{k}\in\mathbb{Z}^d} \hat{f}_{\boldsymbol{k}} \mathrm{e}^{2\pi\mathrm{i}\boldsymbol{k}\cdot\boldsymbol{x}} \right| \\ &\leq \left| \sum_{\boldsymbol{k}\in I} \hat{f}_{\boldsymbol{k}} \mathrm{e}^{2\pi\mathrm{i}\boldsymbol{k}\cdot\boldsymbol{x}_0} - \sum_{\boldsymbol{k}\in I} \hat{f}_{\boldsymbol{k}} \mathrm{e}^{2\pi\mathrm{i}\boldsymbol{k}\cdot\boldsymbol{x}} \right| + \frac{\varepsilon}{2}. \end{aligned}$$

The trigonometric polynomial $S_I f(\boldsymbol{x}) = \sum_{\boldsymbol{k}\in I} \hat{f}_{\boldsymbol{k}} \mathrm{e}^{2\pi\mathrm{i}\boldsymbol{k}\cdot\boldsymbol{x}}$ is a continuous function. Accordingly, for $\varepsilon > 0$ and $\boldsymbol{x}_0 \in \mathbb{T}^d$ there exists $\delta_0 > 0$ such that $\|\boldsymbol{x}_0 - \boldsymbol{x}\|_1 < \delta_0$ implies $|S_I f(\boldsymbol{x}_0) - S_I f(\boldsymbol{x})| < \frac{\varepsilon}{2}$ and we obtain

$$|g(\boldsymbol{x}_0) - g(\boldsymbol{x})| < \varepsilon \quad \text{for all } \boldsymbol{x} \text{ with } \|\boldsymbol{x}_0 - \boldsymbol{x}\|_1 < \delta_0.$$

■

In particular for further considerations on sampling methods, cf. Sections 3.4, 3.5, and 4.5, it is essential that we identify each function $f \in \mathcal{A}(\mathbb{T}^d)$ with its continuous representative in the following. Note that the definition of $\mathcal{A}_\omega(\mathbb{T}^d)$ in (2.9) already comprises the continuity of the contained functions.

Lemma 2.2. *Assuming the cardinality $|I_N|$ of the index set $I_N = \{\boldsymbol{k} \in \mathbb{Z}^d : \omega(\boldsymbol{k}) \leq N\}$, $N \in \mathbb{R}$, being finite, the exact Fourier partial sum*

$$S_{I_N} f(\boldsymbol{x}) := \sum_{\boldsymbol{k}\in I_N} \hat{f}_{\boldsymbol{k}} \mathrm{e}^{2\pi\mathrm{i}\boldsymbol{k}\cdot\boldsymbol{x}} \tag{2.10}$$

approximates the function $f \in \mathcal{A}_\omega(\mathbb{T}^d)$ and we estimate the error by

$$\|f - S_{I_N} f | L_\infty(\mathbb{T}^d)\| \leq N^{-1} \|f | \mathcal{A}_\omega(\mathbb{T}^d)\|.$$

Proof. Let $f \in \mathcal{A}_\omega(\mathbb{T}^d)$. We obtain $S_{I_N} f \in \mathcal{A}_\omega(\mathbb{T}^d) \subset \mathcal{C}(\mathbb{T}^d)$ and straightforward calculation yields

$$\begin{aligned} \|f - S_{I_N} f | L_\infty(\mathbb{T}^d)\| &= \operatorname{ess\,sup}_{\boldsymbol{x}\in\mathbb{T}^d} |(f - S_{I_N} f)(\boldsymbol{x})| = \operatorname{ess\,sup}_{\boldsymbol{x}\in\mathbb{T}^d} \left| \sum_{\boldsymbol{k}\in\mathbb{Z}^d\setminus I_N} \hat{f}_{\boldsymbol{k}} \mathrm{e}^{2\pi\mathrm{i}\boldsymbol{k}\cdot\boldsymbol{x}} \right| \\ &\leq \sum_{\boldsymbol{k}\in\mathbb{Z}^d\setminus I_N} |\hat{f}_{\boldsymbol{k}}| \leq \frac{1}{\inf_{\boldsymbol{k}\in\mathbb{Z}^d\setminus I_N} \omega(\boldsymbol{k})} \sum_{\boldsymbol{k}\in\mathbb{Z}^d\setminus I_N} \omega(\boldsymbol{k}) |\hat{f}_{\boldsymbol{k}}| \\ &\leq \frac{1}{N} \sum_{\boldsymbol{k}\in\mathbb{Z}^d} \omega(\boldsymbol{k}) |\hat{f}_{\boldsymbol{k}}| = N^{-1} \|f | \mathcal{A}_\omega(\mathbb{T}^d)\|. \end{aligned}$$

■

Lemma 2.3. *Let $N \in \mathbb{R}$ and the index set $I_N := \{\boldsymbol{k} \in \mathbb{Z}^d : \omega(\boldsymbol{k}) \leq N\}$ with the cardinality $0 < |I_N| < \infty$ be given. The norm of the operator S_{I_N} is bounded by*

$$\frac{1}{\min_{\boldsymbol{k}\in\mathbb{Z}^d} \omega(\boldsymbol{k})} \leq \|S_{I_N}|\mathcal{A}_\omega(\mathbb{T}^d) \to \mathcal{C}(\mathbb{T}^d)\| \leq \frac{1}{\min_{\boldsymbol{k}\in\mathbb{Z}^d} \omega(\boldsymbol{k})} + \frac{1}{N}.$$

Proof. Due to $0 < |I_N| < \infty$ there exists $\min_{\boldsymbol{k}\in I_N} \omega(\boldsymbol{k})$ and $\min_{\boldsymbol{k}\in\mathbb{Z}^d} \omega(\boldsymbol{k}) = \min_{\boldsymbol{k}\in I_N} \omega(\boldsymbol{k})$. In order to obtain the upper bound we apply the triangle inequality and Lemma 2.2. We estimate

$$\begin{aligned}
\|S_{I_N}|\mathcal{A}_\omega(\mathbb{T}^d) \to \mathcal{C}(\mathbb{T}^d)\| &= \sup_{\substack{f\in\mathcal{A}_\omega \\ \|f|\mathcal{A}_\omega\|=1}} \|S_{I_N} f|\mathcal{C}(\mathbb{T}^d)\| \\
&\leq \sup_{\substack{f\in\mathcal{A}_\omega \\ \|f|\mathcal{A}_\omega\|=1}} \|S_{I_N} f - f|\mathcal{C}(\mathbb{T}^d)\| + \sup_{\substack{f\in\mathcal{A}_\omega \\ \|f|\mathcal{A}_\omega\|=1}} \|f|\mathcal{C}(\mathbb{T}^d)\| \\
&\leq \sup_{\substack{f\in\mathcal{A}_\omega \\ \|f|\mathcal{A}_\omega\|=1}} \sum_{\boldsymbol{k}\in\mathbb{Z}^d} |\hat{f}(\boldsymbol{k})| + N^{-1}\|f|\mathcal{A}_\omega(\mathbb{T}^d)\| \\
&\leq \sup_{\substack{f\in\mathcal{A}_\omega \\ \|f|\mathcal{A}_\omega\|=1}} \sum_{\boldsymbol{k}\in\mathbb{Z}^d} \frac{\omega(\boldsymbol{k})}{\min_{\boldsymbol{k}\in\mathbb{Z}^d} \omega(\boldsymbol{k})} |\hat{f}(\boldsymbol{k})| + N^{-1}\|f|\mathcal{A}_\omega(\mathbb{T}^d)\| \\
&\leq \frac{1}{\min_{\boldsymbol{k}\in\mathbb{Z}^d} \omega(\boldsymbol{k})} + \frac{1}{N}.
\end{aligned}$$

To prove the lower bound we construct a suitable example. Let $\boldsymbol{k}' \in I_N$ be a frequency index with $\omega(\boldsymbol{k}') = \min_{\boldsymbol{k}\in\mathbb{Z}^d} \omega(\boldsymbol{k})$. The trigonometric polynomial $g(\boldsymbol{x}) = \frac{1}{\omega(\boldsymbol{k}')} \mathrm{e}^{2\pi \mathrm{i} \boldsymbol{k}'\cdot\boldsymbol{x}}$ is an element of $\mathcal{A}_\omega(\mathbb{T}^d)$ and the corresponding norm amounts to $\|g|\mathcal{A}_\omega(\mathbb{T}^d)\| = 1$. With $S_{I_N} g = g$, we achieve

$$\|S_{I_N}|\mathcal{A}_\omega(\mathbb{T}^d) \to \mathcal{C}(\mathbb{T}^d)\| \geq \|S_{I_N} g|\mathcal{C}(\mathbb{T}^d)\| = \|g|\mathcal{C}(\mathbb{T}^d)\| = g(\boldsymbol{0}) = \frac{1}{\omega(\boldsymbol{k}')} = \frac{1}{\min_{\boldsymbol{k}\in I_N} \omega(\boldsymbol{k})}.$$

■

2.2 Stability

It is well known that for full grid discretizations $\mathcal{X}$ in spatial domain and corresponding full grid I in frequency domain the related Fourier matrix

$$\boldsymbol{A} := \boldsymbol{A}(I, \mathcal{X}) := \left(\mathrm{e}^{2\pi \mathrm{i} \boldsymbol{k}\cdot\boldsymbol{x}}\right)_{\boldsymbol{x}\in\mathcal{X}, \boldsymbol{k}\in I} \in \mathbb{C}^{|\mathcal{X}|\times|I|}$$

is a unitary one up to some constant. This basically means that the columns of the matrix $\boldsymbol{A}$ are pairwise orthogonal, i.e., $\boldsymbol{A}^*\boldsymbol{A} = M\boldsymbol{I}$, where $M = |\mathcal{X}|$ is the number of discretization nodes in the spatial domain, $\boldsymbol{A}^* \in \mathbb{C}^{|I|\times|\mathcal{X}|}$ is the adjoint matrix of $\boldsymbol{A}$, and $\boldsymbol{I} \in \mathbb{C}^{|I|\times|I|}$ is the identity matrix. In particular for full grid discretizations I in frequency domain and corresponding full grid discretization $\mathcal{X}$ in spatial domain, the Fourier matrix $\boldsymbol{A}$ is a squared matrix, i.e., $|I| = |\mathcal{X}|$, and describes a bijective mapping from frequencies supported on the frequency index set I to function values at the spatial discretization $\mathcal{X}$.

Lemma 2.4. *For $\boldsymbol{a}, \boldsymbol{b} \in \mathbb{Z}^d$ with $a_s \leq b_s$, $s = 1, \ldots, d$, let $I = \left(\times_{s=1}^{d} [a_s, b_s]\right) \cap \mathbb{Z}^d$ be a full grid discretization in frequency domain. The sampling set $\mathcal{X} = \times_{s=1}^{d} \{0, \frac{1}{b_s - a_s + 1}, \ldots, \frac{b_s - a_s}{b_s - a_s + 1}\}$ entails a Fourier matrix*

$$\boldsymbol{A} = \left(\mathrm{e}^{2\pi \mathrm{i} \boldsymbol{k} \cdot \boldsymbol{x}}\right)_{\boldsymbol{x} \in \mathcal{X}, \boldsymbol{k} \in I}$$

such that $\boldsymbol{A}^* \boldsymbol{A} = \prod_{s=1}^{d} (b_s - a_s + 1)\, \boldsymbol{I}$.

Proof. For each $\boldsymbol{k}$, $\boldsymbol{h} \in I$ we obtain

$$\begin{aligned}(\boldsymbol{A}^* \boldsymbol{A})_{\boldsymbol{k}, \boldsymbol{h}} &= \sum_{\boldsymbol{x} \in \mathcal{X}} \mathrm{e}^{2\pi \mathrm{i} (\boldsymbol{h} - \boldsymbol{k}) \cdot \boldsymbol{x}} = \prod_{s=1}^{d} \sum_{j_s = 0}^{b_s - a_s} \mathrm{e}^{2\pi \mathrm{i} (h_s - k_s) \frac{j_s}{b_s - a_s + 1}} \\ &= \prod_{s=1}^{d} (b_s - a_s + 1) \delta_0(h_s - k_s) = \begin{cases} 0 & \text{for } \boldsymbol{h} \neq \boldsymbol{k}, \\ \prod_{s=1}^{d} (b_s - a_s + 1) & \text{for } \boldsymbol{h} = \boldsymbol{k}. \end{cases}\end{aligned}$$

The function δ_0 is the Dirac delta function, i.e., $\delta_0(x) = \begin{cases} 1 & \text{for } x = 0, \\ 0 & \text{otherwise.} \end{cases}$ ∎

In Chapter 3 of this work, we will show that we can construct a suitable spatial discretization for each arbitrary index set I such that $\boldsymbol{A}^* \boldsymbol{A} = M \boldsymbol{I}$ takes effect. In general, we have to expect some oversampling. That means the matrices $\boldsymbol{A}$ are rectangular matrices with a number of rows at least as big as the number of columns, i.e. $M \geq |I|$. Note that the full grid spatial discretization corresponding to the full frequency grid $\times_{s=1}^{d} ([\min\{k_s \in \mathbb{Z} \colon \boldsymbol{k} \in I\}, \max\{k_s \in \mathbb{Z} \colon \boldsymbol{k} \in I\}] \cap \mathbb{Z})$ that contains I fulfills $\boldsymbol{A}^* \boldsymbol{A} = M \boldsymbol{I}$, for example. But in general, the cardinality of this full grid in spatial domain is huge and so impractical for higher dimensions d. Nevertheless this cardinality is a simple upper bound for the number of samples needed to perfectly stable evaluate and reconstruct trigonometric polynomials with frequencies supported on the index set I. The next lemma gives a lower bound of this number of samples. Prior to this, we have to define an operator working on sets in the following sense

$$\mathcal{D}(I) := \{\boldsymbol{h} \in \mathbb{Z}^d : \boldsymbol{h} = \boldsymbol{k}_1 - \boldsymbol{k}_2, \boldsymbol{k}_1, \boldsymbol{k}_2 \in I\}. \tag{2.11}$$

Thus, the operator $\mathcal{D}$ applied on the set I results in a set containing all possible differences of two elements of the set I. We call the set $\mathcal{D}(I)$ *difference set* of the frequency index set I.

Lemma 2.5. *Let $I \subset \mathbb{Z}^d$ be an arbitrary frequency index set of finite cardinality. We need at least $M \geq \max_{I' \subset \mathbb{Z}^d} \{|I'| : \mathcal{D}(I') \subset \mathcal{D}(I)\}$ samples to achieve a Fourier matrix $\boldsymbol{A}$ with orthogonal columns.*

Proof. Let I' be a frequency index set such that $|I'| = \max_{I'' \subset \mathbb{Z}^d} \{|I''| : \mathcal{D}(I'') \subset \mathcal{D}(I)\}$ and $\mathcal{D}(I') \subset \mathcal{D}(I)$. Furthermore let the cardinality $M = |\mathcal{X}|$ of the sampling set $\mathcal{X}$ and the elements of $\mathcal{X}$ labeled by $\boldsymbol{x}_0, \ldots, \boldsymbol{x}_{M-1}$. The condition $\boldsymbol{A}^* \boldsymbol{A} = M \boldsymbol{I}$ reads as follows

$$(\boldsymbol{A}^* \boldsymbol{A})_{\boldsymbol{k}, \boldsymbol{h}} = \sum_{j=0}^{M-1} \mathrm{e}^{2\pi \mathrm{i} (\boldsymbol{h} - \boldsymbol{k}) \cdot \boldsymbol{x}_j} = M \prod_{s=1}^{d} \delta_0(h_s - k_s)$$

for all $\boldsymbol{k}, \boldsymbol{h} \in I$ and $\delta_0(x) = \begin{cases} 1 & \text{for } x = 0, \\ 0 & \text{for } x \neq 0. \end{cases}$ Since $\{\boldsymbol{h} - \boldsymbol{k} \in \mathbb{Z}^d : \ \boldsymbol{h}, \boldsymbol{k} \in I\} = \mathcal{D}(I) \supset \mathcal{D}(I') = \{\boldsymbol{h} - \boldsymbol{k} \in \mathbb{Z}^d : \ \boldsymbol{h}, \boldsymbol{k} \in I'\}$, we obtain

$$\left(\tilde{\boldsymbol{A}}^* \tilde{\boldsymbol{A}}\right)_{\boldsymbol{k},\boldsymbol{h}} := \sum_{j=0}^{M-1} \mathrm{e}^{2\pi \mathrm{i}(\boldsymbol{h}-\boldsymbol{k})\cdot\boldsymbol{x}_j} = M \prod_{s=1}^{d} \delta_0(h_s - k_s)$$

for all $\boldsymbol{h}, \boldsymbol{k} \in I'$ with $\tilde{\boldsymbol{A}} = \left(\mathrm{e}^{2\pi \mathrm{i} \boldsymbol{h} \boldsymbol{x}_j}\right)_{j=0,\ldots,M-1,\boldsymbol{h}\in I'}$. Obviously the columns of $\tilde{\boldsymbol{A}}$ need to be pairwise orthogonal. According to that, the matrix $\tilde{\boldsymbol{A}}$ has full column rank. This implies that $M \geq |I'|$ is necessary. ■

Another point of view leads us to the following interpretation of orthogonality of the Fourier matrix $\boldsymbol{A}$, i.e.,

$$(\boldsymbol{A}^* \boldsymbol{A})_{\boldsymbol{k}_1,\boldsymbol{k}_2} = \sum_{j=0}^{M-1} \mathrm{e}^{2\pi \mathrm{i}(\boldsymbol{k}_2-\boldsymbol{k}_1)\cdot\boldsymbol{x}_j}.$$

The condition $\boldsymbol{A}^*\boldsymbol{A} = M\boldsymbol{I}$ implies that all monomials $\mathrm{e}^{2\pi \mathrm{i} \boldsymbol{h}\cdot\boldsymbol{x}}$ with frequencies supported on the difference set of I, i.e., $\boldsymbol{h} \in \mathcal{D}(I)$, can be exactly integrated using the quasi–Monte Carlo method

$$\mathrm{Q}_{\mathcal{X}}[f] := \frac{1}{M} \sum_{j=0}^{M-1} f(\boldsymbol{x}_j) \tag{2.12}$$

that is given by the sampling set $\mathcal{X} := \{\boldsymbol{x}_j \in \mathbb{T}^d \colon j = 0, \ldots, M-1\}$, i.e., we achieve

$$\mathrm{Q}_{\mathcal{X}}[p] := \frac{1}{M} \sum_{j=0}^{M-1} p(\boldsymbol{x}_j) = \int_{\mathbb{T}^d} p(\boldsymbol{x}) \mathrm{d}\boldsymbol{x} \tag{2.13}$$

for all $p \in \Pi_{\mathcal{D}(I)}$. According to this notion, S. M. Ermakov explains in his monograph [Erm75, Chap. IV] that there exist sampling sets $\tilde{\mathcal{X}} = \{\boldsymbol{x}_j \in \mathbb{T}^d \colon j = 0, \ldots, |\mathcal{D}(I)| - 1\}$ of cardinality $|\tilde{\mathcal{X}}| = |\mathcal{D}(I)|$ such that each of the linear independent monomials $\mathrm{e}^{2\pi \mathrm{i} \boldsymbol{h}\cdot\boldsymbol{x}}$, $\boldsymbol{h} \in \mathcal{D}(I)$, and thus also all of their linear combinations $p \in \Pi_{\mathcal{D}(I)}$, can be numerically integrated in an exact way using a weighted cubature formula

$$\mathrm{Q}_{\tilde{\mathcal{X}}}[p] = \sum_{j=0}^{|\tilde{\mathcal{X}}|-1} w_j p(\boldsymbol{x}_j),$$

where $(w_j)_{j=0}^{|\tilde{\mathcal{X}}|-1}$ are the weights. In short words, there exist sampling sets $\tilde{\mathcal{X}}$ of a cardinality $|\tilde{\mathcal{X}}| = |\mathcal{D}(I)|$, such that we obtain

$$\mathrm{Q}_{\tilde{\mathcal{X}}}[p] = \int_{\mathbb{T}^d} p(\boldsymbol{x}) \mathrm{d}\boldsymbol{x}$$

for all $p \in \Pi_{\mathcal{D}(I)}$.

One of the main targets of Chapter 3 is the construction of sampling sets $\mathcal{X}$ such that the quasi–Monte Carlo rule (2.12) is exact for all trigonometric polynomials supported on the difference set $\mathcal{D}(I)$, i.e., (2.13) holds for all $p \in \Pi_{\mathcal{D}(I)}$. To be more precise, we are eagerly

interested in sampling sets $\mathcal{X}$ with additional "rank-1" structure in Chapters 3 and 4. This additional structure of $\mathcal{X}$ allows us to break a multidimensional discrete Fourier transform down to a one-dimensional discrete Fourier transform. Accordingly, we can compute the matrix vector products concerning the Fourier matrix $\boldsymbol{A}$ and its (pseudo–)inverse using known fast algorithms.

2.3 Specific Frequency Index Sets

In this section, we consider different structures of frequency index sets that appear in a wide variety of applications. More precisely, we consider frequency index sets $I_N := \{\boldsymbol{k} \in \mathbb{Z}^d \colon \omega(\boldsymbol{k}) \leq N\}$ determined by ω such that functions $f \in \mathcal{A}_\omega(\mathbb{T}^d)$ may be well approximated by trigonometric polynomials with frequencies supported on the specific index sets I_N. The subsections are named after these index sets. In the following we use dimension-dependent weight-sequences $\boldsymbol{\gamma} = (\gamma_s)_{s=1}^\infty \in [0,1]^{\mathbb{N}}$ and we assume that the components of the variable $\boldsymbol{x} = (x_1, x_2, \ldots, x_d)^\top$ are ordered in their importance, i.e. $\gamma_1 \geq \gamma_2 \geq \ldots$. We stress the fact that the weight sequence $\boldsymbol{\gamma}$ may moderate the dependence on the different dimensions and, in addition, the dependencies between different dimensions. In particular, in the field of information based complexity such weights are used in order to determine tractability results on the integration problem in different weighted function spaces, see e.g. [SW01, HW01, NW01]. Furthermore some additional papers also deal with the approximation of functions that belong to those function spaces, cf. e.g. [HW00, NSW04]. We suggest the monographs of E. Novak and H. Woźniakowski, see [NW08, NW10, NW12], that give a great overview about existing tractability results and open questions, and in particular [NW08, Chapter 2] that greatly motivates the considerations of dimension dependent weights from the point of view of the experts in information based complexity. We discuss in Chapter 5 the relevance of the weights $\boldsymbol{\gamma}$ in concrete applications.

2.3.1 Weighted ℓ_p-balls

In this subsection, we consider the weight functions

$$\omega_p^{d,\boldsymbol{\gamma}}(\boldsymbol{k}) = \max\left(1, \|\boldsymbol{k}|\ell_p^{d,\boldsymbol{\gamma}}\|\right) \qquad \text{for } 0 < p \leq \infty, \tag{2.14}$$

where

$$\|\boldsymbol{k}|\ell_p^{d,\boldsymbol{\gamma}}\| = \begin{cases} \left(\sum_{s=1}^d \left(\gamma_s^{-1}|k_s|\right)^p\right)^{1/p} & \text{for } 0 < p < \infty, \\ \max_{s=1,\ldots,d} \gamma_s^{-1}|k_s| & \text{for } p = \infty \end{cases}$$

and $\boldsymbol{\gamma} = (\gamma_s)_{s=1}^\infty \in [0,1]^{\mathbb{N}}$. We define $0^{-1}l = \begin{cases} 0 & \text{for } l = 0, \\ \infty & \text{for } l \in \mathbb{N}. \end{cases}$ As described above we generate index sets

$$I_{p,N}^{d,\boldsymbol{\gamma}} := \{\boldsymbol{k} \in \mathbb{Z}^d : \omega_p^{d,\boldsymbol{\gamma}}(\boldsymbol{k}) \leq N\} \tag{2.15}$$

and call them *weighted ℓ_p-balls* of size N. We prove the following inclusions and a universal upper bound of the cardinality of $I_{p,N}^{d,\boldsymbol{\gamma}}$.

Lemma 2.6. *Let $0 < p < q \leq \infty$, the parameter $N \in \mathbb{R}$, $N \geq 1$, the dimension $d \in \mathbb{N}$, and the weights $\boldsymbol{\gamma} = (\gamma_s)_{s=1}^{\infty} \in [0,1]^{\mathbb{N}}$ be given. Then the inclusion*

$$I_{p,N}^{d,\boldsymbol{\gamma}} \subset I_{q,N}^{d,\boldsymbol{\gamma}} \qquad \text{and the estimates} \qquad |I_{p,N}^{d,\boldsymbol{\gamma}}| \leq |I_{q,N}^{d,\boldsymbol{\gamma}}| \leq |I_{\infty,N}^{d,\boldsymbol{\gamma}}| \leq 2^{2N \sum_{s=1}^{d} \gamma_s}$$

hold.

Proof. Obviously, for $N \geq 1$ we obtain $\mathbf{0} \in I_{p,N}^{d,\boldsymbol{\gamma}}$ for all $0 < p \leq \infty$. Consequently, in the following we only consider elements $\boldsymbol{k} \in I_{p,N}^{d,\boldsymbol{\gamma}} \setminus \{\mathbf{0}\}$ and show that $\boldsymbol{k} \in I_{q,N}^{d,\boldsymbol{\gamma}}$ holds for all $q > p$. Note that for $\boldsymbol{k} \neq \mathbf{0}$ the equality $\omega_p^{d,\boldsymbol{\gamma}}(\boldsymbol{k}) = \|\boldsymbol{k}|\ell_p^{d,\boldsymbol{\gamma}}\|$ holds. We start with the special case $q = \infty$. Let $\boldsymbol{k} \in I_{p,N}^{d,\boldsymbol{\gamma}} \setminus \{\mathbf{0}\}$. We estimate

$$\begin{aligned} N \geq \omega_p^{d,\boldsymbol{\gamma}}(\boldsymbol{k}) = \|\boldsymbol{k}|\ell_p^{d,\boldsymbol{\gamma}}\| &= \left(\sum_{s=1}^{d} |\gamma_s^{-1} k_s|^p \right)^{1/p} \\ &\geq \left(\max_{s=1,\ldots,d} |\gamma_s^{-1} k_s|^p \right)^{1/p} = \max_{s=1,\ldots,d} \gamma_s^{-1} |k_s| = \omega_\infty^{d,\boldsymbol{\gamma}}(\boldsymbol{k}). \end{aligned}$$

Hence, we obtain $\boldsymbol{k} \in I_{\infty,N}^{d,\boldsymbol{\gamma}}$ for all $\boldsymbol{k} \in I_{p,N}^{d,\boldsymbol{\gamma}}$ and we conclude $I_{p,N}^{d,\boldsymbol{\gamma}} \subset I_{\infty,N}^{d,\boldsymbol{\gamma}}$. Next, we show the inclusions for $0 < p < q < \infty$. We take $\boldsymbol{k} \in I_{p,N}^{d,\boldsymbol{\gamma}} \setminus \{\mathbf{0}\}$ and obtain

$$\begin{aligned} 1 = \frac{\omega_q^{d,\boldsymbol{\gamma}}(\boldsymbol{k})}{\omega_q^{d,\boldsymbol{\gamma}}(\boldsymbol{k})} &= \left\| \frac{\boldsymbol{k}}{\|\boldsymbol{k}|\ell_q^{d,\boldsymbol{\gamma}}\|} \middle| \ell_q^{d,\boldsymbol{\gamma}} \right\| = \left(\sum_{s=1}^{d} \left(\frac{\gamma_s^{-1}|k_s|}{\|\boldsymbol{k}|\ell_q^{d,\boldsymbol{\gamma}}\|} \right)^q \right)^{1/q} \\ &\leq \left(\sum_{s=1}^{d} \left(\frac{\gamma_s^{-1}|k_s|}{\|\boldsymbol{k}|\ell_q^{d,\boldsymbol{\gamma}}\|} \right)^p \right)^{1/q} \leq \frac{\|\boldsymbol{k}|\ell_p^{d,\boldsymbol{\gamma}}\|^{p/q}}{\|\boldsymbol{k}|\ell_q^{d,\boldsymbol{\gamma}}\|^{p/q}} = \left(\frac{\omega_p^{d,\boldsymbol{\gamma}}(\boldsymbol{k})}{\omega_q^{d,\boldsymbol{\gamma}}(\boldsymbol{k})} \right)^{p/q}. \end{aligned}$$

Since the function $t^{p/q}$ is monotonically increasing for fixed $0 < \frac{p}{q} < 1$ and $0 < t < \infty$, we conclude

$$N \geq \omega_p^{d,\boldsymbol{\gamma}}(\boldsymbol{k}) \geq \omega_q^{d,\boldsymbol{\gamma}}(\boldsymbol{k})$$

for all $\boldsymbol{k} \in I_{p,N}^{d,\boldsymbol{\gamma}}$ and get $I_{p,N}^{d,\boldsymbol{\gamma}} \subset I_{q,N}^{d,\boldsymbol{\gamma}}$.

The inclusions from above imply the inequalities $|I_{p,N}^{d,\boldsymbol{\gamma}}| \leq |I_{q,N}^{d,\boldsymbol{\gamma}}| \leq |I_{\infty,N}^{d,\boldsymbol{\gamma}}|$ for $0 < p < q \leq \infty$. Consequently, we only show the upper bound of the cardinality of $I_{\infty,N}^{d,\boldsymbol{\gamma}}$, $N \geq 1$,

$$|I_{\infty,N}^{d,\boldsymbol{\gamma}}| = \prod_{s=1}^{d} (1 + 2\lfloor \gamma_s N \rfloor) \leq \prod_{s=1}^{d} 2^{2\lfloor \gamma_s N \rfloor} \leq 2^{2N \sum_{s=1}^{d} \gamma_s}.$$

■

Note that this upper bound of the cardinalities of $I_{p,N}^{d,\boldsymbol{\gamma}}$, $0 < p \leq \infty$, is bounded independently of d if $\sum_{s=1}^{\infty} \gamma_s < \infty$.

In order to apply Lemma 2.5 we show some inclusions concerning the difference sets $\mathcal{D}(I_{p,N}^{d,\boldsymbol{\gamma}})$, see (2.11), of weighted ℓ_p-balls and, in addition, lower and upper bounds on the cardinality of weighted ℓ_p-balls.

Lemma 2.7. *Let the parameter $N \in \mathbb{R}$, $N \geq 1$, the dimension $d \in \mathbb{N}$, and the weights $\boldsymbol{\gamma} = (\gamma_s)_{s=1}^{\infty}$, $\gamma_1 \geq \gamma_2 \geq \ldots \geq \gamma_d > 0$, be given. Then for the difference set $\mathcal{D}(I_{p,N}^{d,\boldsymbol{\gamma}})$ the inclusions*

$$I_{1,2N-\gamma_d^{-1}}^{d,\boldsymbol{\gamma}} \cup I_{p,N}^{d,\boldsymbol{\gamma}} \subset \mathcal{D}(I_{p,N}^{d,\boldsymbol{\gamma}}) \subset I_{p,2N}^{d,\boldsymbol{\gamma}} \quad \text{for } 1 \leq p \leq \infty,$$

and

$$I_{1,d^{\frac{p-1}{p}}N}^{d,\boldsymbol{\gamma}} \subset I_{p,N}^{d,\boldsymbol{\gamma}} \subset \mathcal{D}(I_{p,N}^{d,\boldsymbol{\gamma}}) \subset I_{p,2^{1/p}N}^{d,\boldsymbol{\gamma}} \quad \text{for } 0 < p < 1$$

hold.

Proof. At first we consider the case $1 \leq p \leq \infty$. For arbitrary $\boldsymbol{k}, \boldsymbol{l} \in I_{p,N}^{d,\boldsymbol{\gamma}}$ we estimate by the triangle inequality

$$\|\boldsymbol{k} - \boldsymbol{l}|\ell_p^{d,\boldsymbol{\gamma}}\| \leq \|\boldsymbol{k}|\ell_p^{d,\boldsymbol{\gamma}}\| + \|\boldsymbol{l}|\ell_p^{d,\boldsymbol{\gamma}}\| \leq 2N.$$

Accordingly, we obtain $\mathcal{D}(I_{p,N}^{d,\boldsymbol{\gamma}}) \subset I_{p,2N}^{d,\boldsymbol{\gamma}}$.

In the following we consider the first inclusion from above. Due to $\mathbf{0} \in I_{p,N}^{d,\boldsymbol{\gamma}}$ we obtain $I_{p,N}^{d,\boldsymbol{\gamma}} \subset \mathcal{D}(I_{p,N}^{d,\boldsymbol{\gamma}})$. Because of $I_{1,2N-\gamma_d^{-1}}^{d,\boldsymbol{\gamma}} = \emptyset$ for $2N - \gamma_d^{-1} < 1$, we consider w.l.o.g. $2N - \gamma_d^{-1} \geq 1$. Due to $I_{1,N}^{d,\boldsymbol{\gamma}} \subset I_{p,N}^{d,\boldsymbol{\gamma}}$ and accordingly $\mathcal{D}(I_{1,N}^{d,\boldsymbol{\gamma}}) \subset \mathcal{D}(I_{p,N}^{d,\boldsymbol{\gamma}})$, $1 \leq p \leq \infty$, it is sufficient to prove the inclusion $I_{1,2N-\gamma_d^{-1}}^{d,\boldsymbol{\gamma}} \subset \mathcal{D}(I_{1,N}^{d,\boldsymbol{\gamma}})$. Considering that, we take an arbitrary $\boldsymbol{h} \in I_{1,2N-\gamma_d^{-1}}^{d,\boldsymbol{\gamma}}$ and show that there exist $\boldsymbol{l}, \boldsymbol{k} \in I_{1,N}^{d,\boldsymbol{\gamma}}$ such that $\boldsymbol{h} = \boldsymbol{k} - \boldsymbol{l}$. We split the indices of the components of $\boldsymbol{h} \in I_{1,2N-\gamma_d^{-1}}^{d,\boldsymbol{\gamma}}$ in two subsets

$$\mathcal{I}_1 := \left\{ s \in \mathbb{N} \colon 1 \leq s \leq d,\ \frac{h_s}{2} \in \mathbb{Z} \right\} \qquad \text{and} \qquad \mathcal{I}_2 := \left\{ s \in \mathbb{N} \colon 1 \leq s \leq d,\ \frac{h_s}{2} \notin \mathbb{Z} \right\}$$

and order the elements of the set $\mathcal{I}_2$ following $1 \leq s_1 < \ldots < s_{|\mathcal{I}_2|} \leq d$. We define

$$k_s = \begin{cases} \frac{h_s}{2} & \text{for } s \in \mathcal{I}_1, \\ \operatorname{sgn}(h_s)\frac{|h_s|-1}{2} & \text{for } s \in \mathcal{I}_2, s = s_t, t/2 \in \mathbb{Z}, \\ \operatorname{sgn}(h_s)\frac{|h_s|+1}{2} & \text{for } s \in \mathcal{I}_2, s = s_t, t/2 \notin \mathbb{Z}, \end{cases} \qquad \text{and} \qquad \boldsymbol{l} = \boldsymbol{k} - \boldsymbol{h},$$

where sgn denotes the sign function, and estimate the norms of $\boldsymbol{k}$ and $\boldsymbol{l}$

$$\begin{aligned} \|\boldsymbol{k}|\ell_1^{d,\boldsymbol{\gamma}}\| &= \sum_{s=1}^{d} \gamma_s^{-1}|k_s| = \sum_{s\in\mathcal{I}_1} \gamma_s^{-1}\frac{|h_s|}{2} + \sum_{t=1}^{|\mathcal{I}_2|} \gamma_{s_t}^{-1}\frac{|h_{s_t}| + (-1)^{t+1}}{2} \\ &= \frac{1}{2}\sum_{s=1}^{d} \gamma_s^{-1}|h_s| + \frac{1}{2}\sum_{t=1}^{|\mathcal{I}_2|}(-1)^{t+1}\gamma_{s_t}^{-1} \leq \frac{\|\boldsymbol{h}|\ell_1^{d,\boldsymbol{\gamma}}\| + \gamma_d^{-1}}{2} \leq N, \\ \|\boldsymbol{l}|\ell_1^{d,\boldsymbol{\gamma}}\| &= \sum_{s=1}^{d} \gamma_s^{-1}|k_s - h_s| = \sum_{s\in\mathcal{I}_1} \gamma_s^{-1}\frac{|h_s|}{2} + \sum_{t=1}^{|\mathcal{I}_2|} \gamma_{s_t}^{-1}\frac{|h_{s_t}| + (-1)^{t}}{2} \\ &= \frac{1}{2}\sum_{s=1}^{d} \gamma_s^{-1}|h_s| + \frac{1}{2}\sum_{t=1}^{|\mathcal{I}_2|}(-1)^{t}\gamma_{s_t}^{-1} \leq \frac{\|\boldsymbol{h}|\ell_1^{d,\boldsymbol{\gamma}}\| + \gamma_d^{-1}}{2} \leq N \end{aligned}$$

since the ordered sequence $1 \geq \gamma_1 \geq \ldots \geq \gamma_d > 0$ implies the estimate $\sum_{t=1}^{|\mathcal{I}_2|}(-1)^{t+j}\gamma_{s_t}^{-1} \leq \gamma_d^{-1}$, $j = 0, 1$.

Considering the case $0 < p < 1$, we obtain that the functions t^p and $t^{1/p}$ are concave and convex, respectively. Due to $N \geq 1$, we know $\mathbf{0} \in I_{p,N}^{d,\boldsymbol{\gamma}}$ and $I_{p,N}^{d,\boldsymbol{\gamma}} \subset \mathcal{D}(I_{p,N}^{d,\boldsymbol{\gamma}})$. Showing the third inclusion, we assume $\boldsymbol{h} \in \mathcal{D}(I_{p,N}^{d,\boldsymbol{\gamma}})$. Consequently, we determine $\boldsymbol{k}, \boldsymbol{l}' \in I_{p,N}^{d,\boldsymbol{\gamma}}$ with $\boldsymbol{h} = \boldsymbol{k} - \boldsymbol{l}'$. The set $I_{p,N}^{d,\boldsymbol{\gamma}}$ is symmetric to the origin. Accordingly, there exists $\boldsymbol{l} = -\boldsymbol{l}' \in I_{p,N}^{d,\boldsymbol{\gamma}}$ and we obtain $\boldsymbol{h} = \boldsymbol{k} + \boldsymbol{l}$. We apply the concaveness of the function t^p and obtain

$$\|\boldsymbol{h}|\ell_p^{d,\boldsymbol{\gamma}}\|^p = \|\boldsymbol{k} + \boldsymbol{l}|\ell_p^{d,\boldsymbol{\gamma}}\|^p = \sum_{s=1}^{d} \gamma_s^{-p} |k_s + l_s|^p \leq \sum_{s=1}^{d} \gamma_s^{-p} |k_s|^p + \sum_{s=1}^{d} \gamma_s^{-p} |l_s|^p.$$

Using the homogeneity of the p-norm and the convexity of $t^{1/p}$ yields

$$\begin{aligned}\|\boldsymbol{h}|\ell_p^{d,\boldsymbol{\gamma}}\| &\leq \left(\|\boldsymbol{k}|\ell_p^{d,\boldsymbol{\gamma}}\|^p + \|\boldsymbol{l}|\ell_p^{d,\boldsymbol{\gamma}}\|^p\right)^{1/p} = 2^{1/p} \left(\frac{1}{2}\left\|\boldsymbol{k}|\ell_p^{d,\boldsymbol{\gamma}}\right\|^p + \frac{1}{2}\left\|\boldsymbol{l}|\ell_p^{d,\boldsymbol{\gamma}}\right\|^p\right)^{1/p} \\ &\leq 2^{1/p-1}(\|\boldsymbol{k}|\ell_p^{d,\boldsymbol{\gamma}}\| + \|\boldsymbol{l}|\ell_p^{d,\boldsymbol{\gamma}}\|) \leq 2^{1/p} N.\end{aligned}$$

The embedding $\mathcal{D}(I_{p,N}^{d,\boldsymbol{\gamma}}) \subset I_{p,2^{1/p}N}^{d,\boldsymbol{\gamma}}$ is the best possible one, since

$$\boldsymbol{k} = (\lfloor \gamma_1 N \rfloor, 0, \ldots, 0)^\top \quad \text{and} \quad \boldsymbol{l} = (0, \lfloor \gamma_2 N \rfloor, 0, \ldots, 0)$$

implies $\boldsymbol{k}, \boldsymbol{l} \in I_{p,N}^{d,\boldsymbol{\gamma}}$ and

$$\|\boldsymbol{k} - \boldsymbol{l}|\ell_p^{d,\boldsymbol{\gamma}}\| = (\gamma_1^{-p} \lfloor \gamma_1 N \rfloor^p + \gamma_2^{-p} \lfloor \gamma_2 N \rfloor^p)^{1/p} \geq (c_1 N^p + c_2 N^p)^{1/p} = (c_1 + c_2)^{1/p} N,$$

where $c_1 \leq 1$ and $c_2 \leq 1$. The constants c_1 and c_2 can come arbitrarily close to 1 depending on N, and the values of γ_1 and γ_2.

In order to show the first inclusion, we assume $\boldsymbol{k} \in I_{1,d^{\frac{p-1}{p}}N}^{d,\boldsymbol{\gamma}}$ and estimate

$$\left(d^{\frac{p-1}{p}} N\right)^p \geq \|\boldsymbol{k}|\ell_1^{d,\boldsymbol{\gamma}}\|^p = \left(\sum_{s=1}^{d} \gamma_s^{-1} |k_s|\right)^p.$$

Again, we apply the concaveness of t^p, $0 < p < 1$, and Jensen's inequality and obtain

$$\left(d^{\frac{p-1}{p}} N\right)^p \geq d^p \left(\frac{1}{d} \sum_{s=1}^{d} \gamma_s^{-1} |k_s|\right)^p \geq \frac{d^p}{d} \sum_{s=1}^{d} (\gamma_s^{-1} |k_s|)^p = d^{p-1} \|\boldsymbol{k}|\ell_p^{d,\boldsymbol{\gamma}}\|^p,$$

which implies $d^{\frac{p-1}{p}} N \geq d^{\frac{p-1}{p}} \|\boldsymbol{k}|\ell_p^{d,\boldsymbol{\gamma}}\|$ and $\boldsymbol{k} \in I_{p,N}^{d,\boldsymbol{\gamma}}$. ∎

Lemma 2.8. *For fixed dimension $d \in \mathbb{N}$, parameter $1 \leq p \leq \infty$, weights $\boldsymbol{\gamma}$ with $1 \geq \gamma_1 \geq \gamma_2 \geq \ldots \geq \gamma_d > 0$, and parameter $N \in \mathbb{R}$, $\gamma_d N \geq 2d$, we estimate the cardinality of $I_{p,N}^{d,\boldsymbol{\gamma}}$*

$$\frac{\gamma_d^d N^d}{d!} \leq |I_{1,N}^{d,\boldsymbol{\gamma}}| \leq |I_{p,N}^{d,\boldsymbol{\gamma}}| \leq |I_{\infty,N}^{d,\boldsymbol{\gamma}}| = \prod_{s=1}^{d} (1 + 2 \lfloor \gamma_s N \rfloor).$$

Proof. The inclusions $I_{1,N}^{d,\boldsymbol{\gamma}} \subset I_{p,N}^{d,\boldsymbol{\gamma}} \subset I_{\infty,N}^{d,\boldsymbol{\gamma}}$ are shown in Lemma 2.6. We show the inclusion $I_{1,\lfloor\gamma_d N\rfloor}^{d,\mathbf{1}} \subset I_{1,N}^{d,\boldsymbol{\gamma}}$ and prove a lower bound on the cardinality of $I_{1,\lfloor\gamma_d N\rfloor}^{d,\mathbf{1}}$.

Obviously, we obtain $\mathbf{0} \in I_{1,\lfloor\gamma_d N\rfloor}^{d,\mathbf{1}}$ and $\mathbf{0} \in I_{1,N}^{d,\boldsymbol{\gamma}}$ for $d \in \mathbb{N}$, $\gamma_d \in (0,1]$, and $N \in \mathbb{R}$, $\gamma_d N \geq 2d$. With $\boldsymbol{h} \in I_{1,\lfloor\gamma_d N\rfloor}^{d,\mathbf{1}} \setminus \{\mathbf{0}\}$ we have

$$N \geq \gamma_d^{-1} \lfloor \gamma_d N \rfloor \geq \gamma_d^{-1} \|\boldsymbol{h}|\ell_1^{d,\mathbf{1}}\| = \sum_{s=1}^{d} \gamma_d^{-1} |h_s| \geq \sum_{s=1}^{d} \gamma_s^{-1} |h_s| = \|\boldsymbol{h}|\ell_1^{d,\boldsymbol{\gamma}}\|$$

and hence $\boldsymbol{h} \in I_{1,N}^{d,\boldsymbol{\gamma}}$.

In [Mys01] one finds a detailed proof of the cardinality of unweighted ℓ_1-balls, which yields

$$\begin{aligned}
|I_{1,\lfloor\gamma_d N\rfloor}^{d,\mathbf{1}}| &\geq \sum_{l=0}^{\min(d,\lfloor\gamma_d N\rfloor)} \binom{d}{l} \binom{\lfloor\gamma_d N\rfloor}{l} 2^l \\
&= \sum_{l=0}^{d} \binom{d}{l} \binom{\lfloor\gamma_d N\rfloor}{l} 2^l \geq \binom{d}{d} \binom{\lfloor\gamma_d N\rfloor}{d} 2^d \\
&\geq \frac{2^d(\gamma_d N - 1)\dots(\gamma_d N - d)}{d!} \geq \frac{2^d(\gamma_d N - d)^d}{d!} \geq \frac{(\gamma_d N)^d}{d!}.
\end{aligned}$$

■

The last lemma motivates the next

Corollary 2.9. *Let $d \in \mathbb{N}$, $0 < p \leq \infty$, and $\boldsymbol{\gamma} = (\gamma_s)_{s=1}^{\infty}$ with $1 \geq \gamma_1 \geq \ldots \geq \gamma_d > 0$ be fixed. In addition, we assume $N \in \mathbb{R}$ and $\gamma_d c_{d,p} N \geq 2d$, where $c_{d,p} = \begin{cases} 1 & \text{for } 1 \leq p \leq \infty, \\ d^{(p-1)/p} & \text{for } 0 < p < 1. \end{cases}$ In order to obtain orthogonal columns of the Fourier matrix $\boldsymbol{A} = \left(\mathrm{e}^{2\pi\mathrm{i}\boldsymbol{h}\cdot\boldsymbol{x}}\right)_{\boldsymbol{x}\in\mathcal{X},\boldsymbol{h}\in I_{p,N}^{d,\boldsymbol{\gamma}}}$ the cardinality of the sampling set $\mathcal{X}$ necessarily fulfills*

$$|\mathcal{X}| \geq C_{d,p,\boldsymbol{\gamma}} N^d.$$

Proof. We obtain $I_{1,c_{d,p}N}^{d,\boldsymbol{\gamma}} \subset I_{p,N}^{d,\boldsymbol{\gamma}}$ with $c_{d,p} = \begin{cases} 1 & \text{for } 1 \leq p \leq \infty, \\ d^{(p-1)/p} & \text{for } 0 < p < 1, \end{cases}$ cf. Lemmas 2.6 and 2.7. Obviously, we have $\mathcal{D}(I_{1,c_{d,p}N}^{d,\boldsymbol{\gamma}}) \subset \mathcal{D}(I_{p,N}^{d,\boldsymbol{\gamma}})$ and Lemmas 2.5 and 2.8 yields that each sampling set $\mathcal{X}$ that entails orthogonal columns of the Fourier matrix $\boldsymbol{A}(I_{p,N}^{d,\boldsymbol{\gamma}}, \mathcal{X})$ needs at least

$$|I_{1,c_{d,p}N}^{d,\boldsymbol{\gamma}}| \geq \frac{\gamma_d^d c_{d,p}^d N^d}{d!}$$

different sampling nodes. ■

Figures 2.1a – 2.1d show unweighted (i.e., $\boldsymbol{\gamma} = \mathbf{1}$) two-dimensional ℓ_p-balls for $p = \frac{1}{2}, 1, 2$, and ∞. Since each d-dimensional ℓ_p-ball $I_{p,N}^{d,\boldsymbol{\gamma}}$, $0 < p \leq \infty$, contains a d-dimensional ℓ_1-ball of appropriate size, cf. Lemma 2.7, we conclude that the cardinality of each ℓ_p-ball is bounded from above and below by $c_{d,p,\boldsymbol{\gamma}} N^d \leq |I_{p,N}^{d,\boldsymbol{\gamma}}| \leq C_{d,p,\boldsymbol{\gamma}} N^d$. Accordingly, we obtain that the cardinalities of the frequency index sets $I_{p,N}^{d,\boldsymbol{\gamma}}$ grow like N^d with increasing N and fixed parameter p, dimension d, and weights $(\gamma_s)_{s=1}^d \in (0,1]^d$. Due to their fast growing

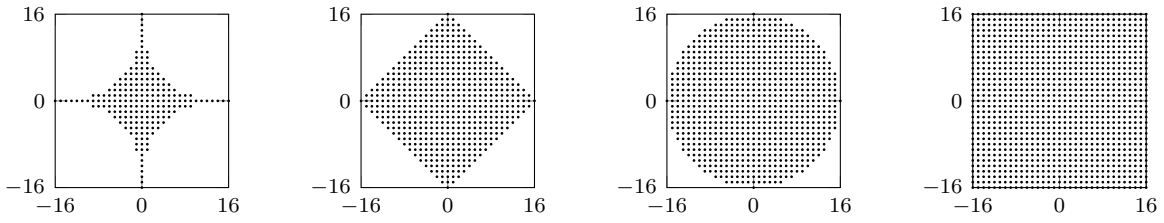

(a) $I^{2,\mathbf{1}}_{\frac{1}{2},16}$ (b) $I^{2,\mathbf{1}}_{1,16}$ (c) $I^{2,\mathbf{1}}_{2,16}$ (d) $I^{2,\mathbf{1}}_{\infty,16}$

Figure 2.1: Two-dimensional ℓ_p-balls $I^{2,\mathbf{1}}_{p,16}$ for $p \in \{\frac{1}{2}, 1, 2, \infty\}$.

cardinality, the frequency index sets $I^{d,\boldsymbol{\gamma}}_{p,N}$ are unmanageable, at least for dimensions $d \geq 6$ and fast growing values of the parameter N.

In principle, the function spaces $\mathcal{A}_{\omega^{d,\boldsymbol{\gamma}}_p}(\mathbb{T}^d)$ are equivalent for fixed dimension d, and different $\boldsymbol{\gamma}$, $1 \geq \gamma_1 \geq \ldots \geq \gamma_d > 0$ and p. Nevertheless, if one considers the approximation properties within the spaces $\mathcal{A}_{\omega^{d,\boldsymbol{\gamma}}_p}(\mathbb{T}^d)$ for growing dimension d, the particular choice of p may cause differences in the results, cf. [KSU14] for similar considerations in Hilbert spaces.

However, a lot of numerical applications in higher dimensions d allow for further restrictions on the functions that should be approximated. A very popular concept is to consider function spaces of dominating mixed smoothness, see e.g. the sparse grid sampling results in [DS89, Zen91, DPT94, SS99a, SS99b, Spr00, BG04, SU07, Ull08, Yse10] for various function spaces of dominating mixed smoothness and [Tem86] for a specific rank-1 lattice approach. In detail, one assumes that the mixed partial derivatives decay as fast as the unmixed partial derivatives of the same order. These additional assumptions shrinks the function spaces enormously and, thus, reduces the number of degrees of freedom of specific approximation problems. More precisely, trigonometric polynomials with frequencies supported on ℓ_p-balls are ill-suited in order to approximate functions of such function spaces due to their fast growing cardinality with respect to the parameter N. The naturally well-suited discretizations in frequency domain are so-called hyperbolic crosses. The cardinalities of these index sets grow much slower with increasing N and fixed other parameters, which is one of the main advantages of hyperbolic crosses.

2.3.2 Weighted Hyperbolic Crosses

This subsection treats so-called weighted hyperbolic crosses. Trigonometric polynomials with frequencies supported on hyperbolic crosses are suitable to approximate functions from spaces of dominating mixed smoothness. Those spaces are often called Korobov spaces in the field of information based complexity and applications in numerical integration. We are interested in frequency index sets I of relatively small cardinality, such that the indices of the most important frequencies of functions of dominating mixed smoothness are collected in there. With weights $\boldsymbol{\gamma} = (\gamma_s)_{s=1}^{\infty}$, $1 \geq \gamma_s \geq 0$, $s \in \mathbb{N}$, we define the weight function

$$\omega^{d,\boldsymbol{\gamma}}_{\mathrm{hc}}(\boldsymbol{k}) = \prod_{s=1}^{d} \max(1, \gamma_s^{-1}|k_s|). \tag{2.16}$$

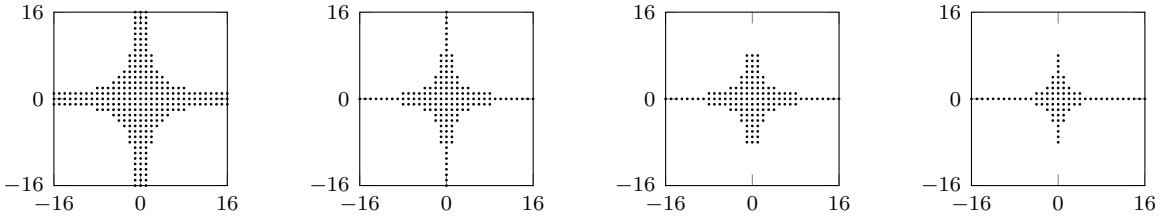

(a) $I^{2,\boldsymbol{\gamma}}_{\mathrm{hc},16}, \gamma_1 = \gamma_2 = 1$ (b) $I^{2,\boldsymbol{\gamma}}_{\mathrm{hc},32}, \gamma_1 = \gamma_2 = \frac{1}{2}$ (c) $I^{2,\boldsymbol{\gamma}}_{\mathrm{hc},16}, \gamma_1 = 1, \gamma_2 = \frac{1}{2}$ (d) $I^{2,\boldsymbol{\gamma}}_{\mathrm{hc},32}, \gamma_1 = \frac{1}{2}, \gamma_2 = \frac{1}{4}$

Figure 2.2: Two-dimensional weighted hyperbolic crosses $I^{2,\boldsymbol{\gamma}}_{\mathrm{hc},N}$ for different N and $\boldsymbol{\gamma}$.

Here, we also set $0^{-1}l = \begin{cases} 0 & \text{for } l = 0, \\ \infty & \text{for } l \in \mathbb{N}. \end{cases}$ For $N \in \mathbb{R}$ and fixed weights $\boldsymbol{\gamma}$, we consider the index set

$$I^{d,\boldsymbol{\gamma}}_{\mathrm{hc},N} := \{\boldsymbol{k} \in \mathbb{Z}^d : \omega^{d,\boldsymbol{\gamma}}_{\mathrm{hc}}(\boldsymbol{k}) \leq N\} \tag{2.17}$$

and call it *weighted hyperbolic cross*. Figure 2.2 shows some two-dimensional weighted hyperbolic crosses and illustrates the effects of different weights $\boldsymbol{\gamma}$. At a first glance on Figures 2.1a and 2.2a the $\ell_{1/2}$-ball seems to be more sparse than the unweighted hyperbolic cross $I^{d,\mathbf{1}}_{\mathrm{hc},N}$. In fact, for larger values of N and, in particular, higher dimensions $d > 2$ one observes and proves the contrary.

Specifically, the cardinalities of weighted hyperbolic crosses do not depend on the refinement N to the power of the dimension d in contrast to weighted ℓ_p-balls. We denote by $\zeta(\tau) = \sum_{k=1}^{\infty} k^{-\tau}$ the Riemann zeta function and estimate the cardinality of $I^{d,\boldsymbol{\gamma}}_{\mathrm{hc},N}$ in the following lemma.

Lemma 2.10. *Let $d \in \mathbb{N}$, $N \in \mathbb{R}$, $N \geq 1$, and $\boldsymbol{\gamma} = (\gamma_s)_{s=1}^{\infty}$ with $1 \geq \gamma_1 \geq \gamma_2 \geq \ldots \geq \gamma_d \geq 0$. The cardinality of $I^{d,\boldsymbol{\gamma}}_{\mathrm{hc},N}$ is bounded from above by*

$$|I^{d,\boldsymbol{\gamma}}_{\mathrm{hc},N}| \leq N^{\tau} \prod_{s=1}^{d} (1 + 2\zeta(\tau)\gamma_s^{\tau}) \qquad \text{for all } \tau > 1. \tag{2.18}$$

In addition, we obtain

$$I^{d,\mathbf{1}}_{\mathrm{hc},N'} \subset I^{d,\boldsymbol{\gamma}}_{\mathrm{hc},N} \subset I^{d,\mathbf{1}}_{\mathrm{hc},N}, \quad \text{where } N' = N \prod_{s=1}^{d} \gamma_s,$$

and, as a consequence, $|I^{d,\boldsymbol{\gamma}}_{\mathrm{hc},N}| \in \Theta\left(N(\log N)^{d-1}\right)$ for fixed dimension d and weights $\boldsymbol{\gamma}$ with $\gamma_d > 0$.

Proof. A proof of the inequality in (2.18) can be found in [CKN10, Section 2.5].

The embeddings are proven by the inequalities

$$\prod_{s=1}^{d} \max(1, |k_s|) \leq \prod_{s=1}^{d} \max(1, \gamma_s^{-1}|k_s|)$$

and

$$\prod_{s=1}^{d} \max(1, \gamma_s^{-1}|k_s|) \leq \prod_{s=1}^{d} \max(\gamma_s^{-1}, \gamma_s^{-1}|k_s|) = \left(\prod_{s=1}^{d} \gamma_s^{-1}\right) \left(\prod_{s=1}^{d} \max(1, |k_s|)\right).$$

for each $\boldsymbol{k} \in \mathbb{Z}^d$.

Using a simple induction, one shows the cardinality estimates for the index sets $I_{\mathrm{hc},N}^{d,\mathbf{1}}$

$$c_d N \max(\log N, 1)^{d-1} \leq |I_{\mathrm{hc},N}^{d,\mathbf{1}}| \leq C_d N \max(\log N, 1)^{d-1}. \tag{2.19}$$

Alternatively, one concludes the lower bound in (2.19) using some embedding arguments for so-called dyadic hyperbolic crosses, cf. [KKP12, Lemma 2.1], and the estimates for the cardinality of dyadic hyperbolic crosses in [Hal92, Section 5.3]. The upper bound is explicitly proved in [Käm13a, Remark 4.10]. We apply the estimates in (2.19) and achieve

$$c_{d,\boldsymbol{\gamma}} N \max\left(\log N, 1\right)^{d-1} \leq c_d N' \max\left(\log N', 1\right)^{d-1} \leq |I_{\mathrm{hc},N}^{d,\boldsymbol{\gamma}}| \leq C_d N \max(\log N, 1)^{d-1}.$$

■

Note that for fixed $\tau > 1$ and a summable $\boldsymbol{\gamma}$, i.e. $\sum_{s=1}^{\infty} \gamma_s < \infty$, the upper bound from (2.18) of the cardinality of $I_{\mathrm{hc},N}^{d,\boldsymbol{\gamma}}$ is independent of the dimension d, cf. [Kno54, Chapter VII, Theorem 7].

We apply Lemma 2.5 on weighted hyperbolic crosses and obtain that we have to expect oversampling to achieve a perfectly stable spatial discretization for trigonometric polynomials with frequencies supported on weighted hyperbolic crosses. The used proof technique is illustrated in Figure 2.3.

Lemma 2.11. *Let $\boldsymbol{\gamma} = (\gamma_s)_{s=1}^{\infty}$ with $1 \geq \gamma_1 \geq \gamma_2 \geq \ldots \geq \gamma_d \geq 0$, $d \geq 2$, and $N \in \mathbb{R}$. In order to obtain orthogonal columns in the Fourier matrix $\boldsymbol{A} := \left(\mathrm{e}^{2\pi \mathrm{i} \boldsymbol{k} \cdot \boldsymbol{x}}\right)_{\boldsymbol{x} \in \mathcal{X}, \boldsymbol{k} \in I_{\mathrm{hc},N}^{d,\boldsymbol{\gamma}}}$ the cardinality M of the sampling set $\mathcal{X}$ has to be at least as big as $(\lfloor \gamma_1 N \rfloor + 1)(\lfloor \gamma_2 N \rfloor + 1)$.*

Proof. We define

$$I' = \{0, \ldots, \lfloor \gamma_1 N \rfloor\} \times \{0, \ldots, \lfloor \gamma_2 N \rfloor\} \times \underbrace{\{0\} \times \cdots \times \{0\}}_{d-2-\text{times}} \subset \mathbb{Z}^d$$

and obtain

$$\begin{aligned}
\mathcal{D}(I') &= \{-\lfloor \gamma_1 N \rfloor, \ldots, \lfloor \gamma_1 N \rfloor\} \times \{-\lfloor \gamma_2 N \rfloor, \ldots, \lfloor \gamma_2 N \rfloor\} \times \underbrace{\{0\} \times \cdots \times \{0\}}_{d-2-\text{times}} \\
&\subset \{\boldsymbol{k} - \boldsymbol{l} \in \mathbb{Z}^d : l_1 \in [-\lfloor \gamma_1 N \rfloor, \lfloor \gamma_1 N \rfloor] \cap \mathbb{Z}, l_2 = \ldots = l_d = 0, \\
&\qquad\qquad k_2 \in [-\lfloor \gamma_2 N \rfloor, \lfloor \gamma_2 N \rfloor] \cap \mathbb{Z},\ k_1 = k_3 = \ldots = k_d = 0\} \\
&\subset \{\boldsymbol{k} - \boldsymbol{l} \in \mathbb{Z}^d : \boldsymbol{k}, \boldsymbol{l} \in I_{\mathrm{hc},N}^{d,\boldsymbol{\gamma}}\} = \mathcal{D}(I_{\mathrm{hc},N}^{d,\boldsymbol{\gamma}}).
\end{aligned}$$

We apply Lemma 2.5 and get that the number M of samples needed to achieve a Fourier matrix with orthogonal columns is at least as big as the cardinality of I'. Consequently, we obtain the necessary condition $|\mathcal{X}| \geq (\lfloor \gamma_1 N \rfloor + 1)(\lfloor \gamma_2 N \rfloor + 1)$. ■

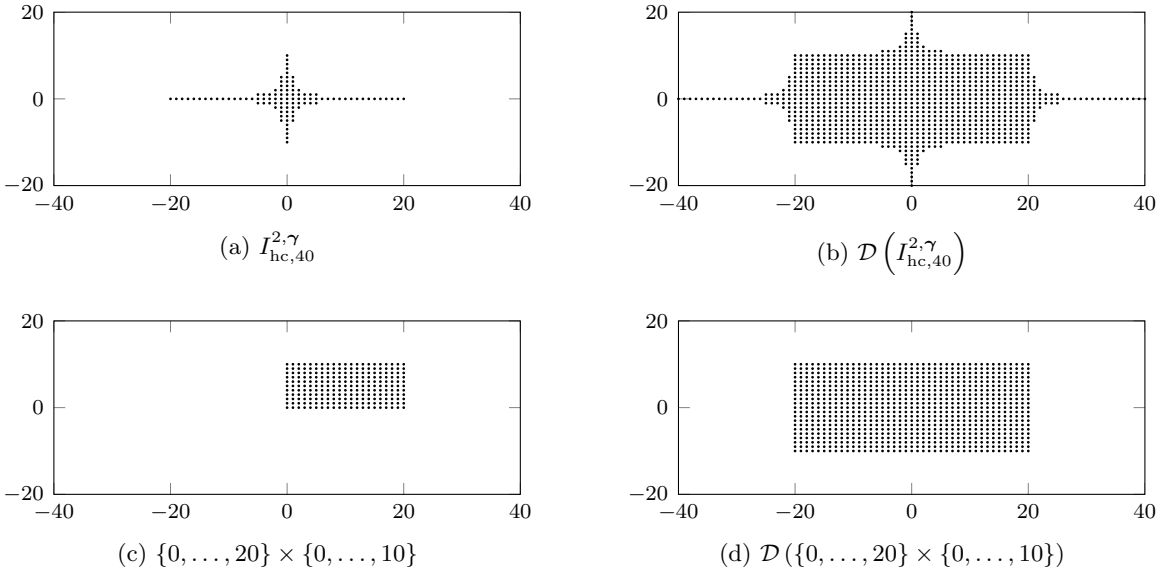

(a) $I^{2,\boldsymbol{\gamma}}_{\mathrm{hc},40}$ (b) $\mathcal{D}\left(I^{2,\boldsymbol{\gamma}}_{\mathrm{hc},40}\right)$

(c) $\{0,\dots,20\}\times\{0,\dots,10\}$ (d) $\mathcal{D}\left(\{0,\dots,20\}\times\{0,\dots,10\}\right)$

Figure 2.3: Weighted hyperbolic cross $I^{2,\boldsymbol{\gamma}}_{\mathrm{hc},40}$, $\boldsymbol{\gamma} = (1/2, 1/4, 0, \dots)$, its difference set $\mathcal{D}\left(I^{2,\boldsymbol{\gamma}}_{\mathrm{hc},40}\right)$, a corresponding subset $\{-20,\dots,20\}\times\{-10,\dots,10\} \subset \mathcal{D}\left(I^{2,\boldsymbol{\gamma}}_{\mathrm{hc},40}\right)$ and a two-dimensional tensor product grid $\{0,\dots,20\}\times\{0,\dots,10\}$ with difference set $\mathcal{D}\left(\{0,\dots,20\}\times\{0,\dots,10\}\right) = \{-20,\dots,20\}\times\{-10,\dots,10\}$.

Due to the fact that the cardinality of weighted hyperbolic crosses is bounded by (2.19), i.e., by terms $C_d N \max(\log N, 1)^{d-1}$ and perfectly stable sampling schemes need at least $C_{\boldsymbol{\gamma}} N^2$ sampling values, we have to expect much more sampling nodes in $\mathcal{X}$ than the number of frequency indices $|I^{d,\boldsymbol{\gamma}}_{\mathrm{hc},N}|$ in order to obtain a perfectly stable Fourier matrix $\boldsymbol{A}$—at least for fixed dimension d, fixed weights $\boldsymbol{\gamma}$, and large N.

At this point, we stress the fact that the cardinality of the weighted hyperbolic crosses may not suffer from the curse of dimension if the weight sequence $\boldsymbol{\gamma}$ is summable, cf. (2.18). Nevertheless, if we fix the dimension d and increases N the cardinality of the weighted hyperbolic cross $|I^{d,\boldsymbol{\gamma}}_{\mathrm{hc},N}|$ grows approximately as $C_d N \max(\log N, 1)^{d-1}$. Regardless of the factor C_d that does not depend on N, already the terms $(\log N)^{d-1}$ will grow fast for small N and dimensions $d \geq 10$, e.g., $(\log 150)^9 \geq 5^9 = 1\,953\,125$.

In specific applications, one can further shrink the frequency index sets to so-called (weighted) energy-norm based hyperbolic crosses without losing approximation quality. In particular, the cardinalities of those energy-norm based hyperbolic crosses can be bounded by terms $C_d N$, i.e., the dependence on the dimension d and the parameter N can be separated in different factors. We would like to emphasize that the cardinality of energy-norm based hyperbolic crosses can be bounded by terms that are even linear in N. However, the term C_d may depend exponentially on the dimension d.

2.3.3 Energy-norm Based Hyperbolic Crosses

In some specific applications, one approximates functions with dominating mixed smoothness and is interested in approximations that cause small errors with respect to norms that mainly depends on the isotropic smoothness. The so-called energy norm, which is the (L_2-)norm of the sum of all first partial derivatives of a function, is of particular interest, cf. [BG04].

Some work [BG99, BG04, Kna00, GH14] published during the last fifteen years treat different kinds of so-called energy norms and corresponding energy-norm based hyperbolic crosses. With $\boldsymbol{\gamma} = (\gamma_s)_{s=1}^{\infty} \in [0,1]^{\mathbb{N}}$, $\beta \geq 0$, and $\beta > -\alpha$, we define the weight function

$$\omega_{\mathrm{ehc}}^{d,\boldsymbol{\gamma},\alpha,\beta}(\boldsymbol{k}) = \max(1, \|\boldsymbol{k}\|_1)^{\frac{\alpha}{\alpha+\beta}} \prod_{s=1}^{d} \max(1, \gamma_s^{-1}|k_s|)^{\frac{\beta}{\alpha+\beta}}. \tag{2.20}$$

The corresponding frequency index sets are given by

$$I_{\mathrm{ehc},N}^{d,\boldsymbol{\gamma},\alpha,\beta} := \{\boldsymbol{k} \in \mathbb{Z}^d : \omega_{\mathrm{ehc}}^{d,\boldsymbol{\gamma},\alpha,\beta}(\boldsymbol{k}) \leq N\} = \{\boldsymbol{k} \in \mathbb{Z}^d : \omega_{\mathrm{ehc}}^{d,\boldsymbol{\gamma},\frac{\alpha}{\beta},1}(\boldsymbol{k}) \leq N^{1+\frac{\alpha}{\beta}}\},\ N \geq 1. \tag{2.21}$$

Considering the weight function $\omega_{\mathrm{ehc}}^{d,\boldsymbol{\gamma},\alpha,\beta}$ in detail, we obtain the equalities

$$\omega_{\mathrm{ehc}}^{d,\boldsymbol{\gamma},0,\beta} = \omega_{\mathrm{hc}}^{d,\boldsymbol{\gamma}} \qquad \text{and} \qquad \omega_{\mathrm{ehc}}^{d,\boldsymbol{\gamma},\alpha,0} = \omega_{p}^{d,\mathbf{1}},$$

cf. (2.14) and (2.16). Accordingly, the frequency index sets $I_{\mathrm{ehc},N}^{d,\boldsymbol{\gamma},0,\beta}$ and $I_{\mathrm{ehc},N}^{d,\boldsymbol{\gamma},\alpha,0}$ are weighted hyperbolic crosses and unweighted ℓ_1-balls, respectively. The most interesting frequency index sets resulting from (2.21) are those, where the parameters α and β fulfill $\alpha < 0$ and $\beta > -\alpha$, cf. Figure 2.4 for illustrations in dimension 2. These frequency index sets are even sparser than weighted hyperbolic crosses in some sense—for fixed dimension d, fixed weights $\boldsymbol{\gamma} \in [0,1]^{\mathbb{N}}$, and parameters $\alpha < 0$ and $\beta > -\alpha$, we obtain a cardinality $|I_{\mathrm{ehc},N}^{d,\boldsymbol{\gamma},\alpha,\beta}| \in \mathcal{O}(N)$, cf. [KPV13, Lemma 2.6]. In other words, increasing N causes expanding frequency index sets $I_{\mathrm{ehc},N}^{d,\boldsymbol{\gamma},\alpha,\beta}$ and the cardinality $|I_{\mathrm{ehc},N}^{d,\boldsymbol{\gamma},\alpha,\beta}|$ can be bounded by terms that grows linearly in N. We call the index sets $I_{\mathrm{ehc},N}^{d,\boldsymbol{\gamma},\alpha,\beta}$ with $\alpha < 0$ and $\beta > -\alpha$ *energy-norm based hyperbolic crosses*. Due to the sparsity of energy-norm based hyperbolic crosses, we focus on the parameter configuration $\alpha < 0$ and $\beta > -\alpha$ and recognize, that the quotient of $-\alpha$ and β fulfills $0 < -\frac{\alpha}{\beta} < 1$. This quotient $-\frac{\alpha}{\beta}$ indicates somehow the sparsity of corresponding weighted energy-norm based hyperbolic crosses, i.e., for fixed dimension d, fixed weight sequence $\boldsymbol{\gamma}$, and fixed N, $I_{\mathrm{ehc},N}^{d,\boldsymbol{\gamma},\alpha,\beta}$ becomes sparser the larger $-\frac{\alpha}{\beta}$ is, cf. Figure 2.4.

Lemma 2.12. *Let the dimension $d \in \mathbb{N}$, the parameter $N \in \mathbb{R}$, $N \geq 1$, the weights $\boldsymbol{\gamma} \in [0,1]^{\mathbb{N}}$, $\alpha \leq 0$ and $\beta > -\alpha$ be given. The following inclusions hold*

$$\bigcup_{s=1}^{d} \left\{(0)_{j=1}^{s-1}\right\} \times \{-\left\lfloor \gamma_s^{\frac{\beta}{\alpha+\beta}} N \right\rfloor, \dots, \left\lfloor \gamma_s^{\frac{\beta}{\alpha+\beta}} N \right\rfloor\} \times \left\{(0)_{j=s+1}^{d}\right\} \subset I_{\mathrm{ehc},N}^{d,\boldsymbol{\gamma},\alpha,\beta} \subset I_{\mathrm{hc},d^{-\frac{\alpha}{\alpha+\beta}}N}^{d,\boldsymbol{\gamma}}.$$

Proof. Due to $N \geq 1$, we have $\mathbf{0}$ included in all three sets from above. Hence, in the following we consider $\boldsymbol{k} \neq \mathbf{0}$. We prove the first inclusion. Let $\mathbf{0} \neq \boldsymbol{k} \in \bigcup_{s=1}^{d} \left\{(0)_{j=1}^{s-1}\right\} \times \{-\left\lfloor \gamma_s^{\frac{\beta}{\alpha+\beta}} N \right\rfloor, \dots, \left\lfloor \gamma_s^{\frac{\beta}{\alpha+\beta}} N \right\rfloor\} \times \left\{(0)_{j=s+1}^{d}\right\}$. Then we determine $s_0 \in \{1, \dots, d\}$ with $k_s = 0$ for all $s \neq s_0$. Consequently, we estimate

$$\omega_{\mathrm{ehc}}^{d,\boldsymbol{\gamma},\alpha,\beta}(\boldsymbol{k}) = |k_{s_0}|^{\frac{\alpha}{\alpha+\beta}} \max(1, \gamma_{s_0}^{-1}|k_{s_0}|)^{\frac{\beta}{\alpha+\beta}} = \gamma_{s_0}^{-\frac{\beta}{\alpha+\beta}} |k_{s_0}| \leq N.$$

We prove the second inclusion. We calculate $\omega_{\mathrm{ehc}}^{d,\boldsymbol{\gamma},\alpha,\beta}(\mathbf{0}) = 1$. With $\mathbf{0} \in I_{\mathrm{ehc},N}^{d,\boldsymbol{\gamma},\alpha,\beta}$ and $d \geq 1$ we have $N \geq 1$ and $d^{-\frac{\alpha}{\alpha+\beta}} N \geq 1$. Due to $\omega_{\mathrm{hc}}^{d,\boldsymbol{\gamma}}(\mathbf{0}) = 1$, we obtain $\mathbf{0} \in I_{\mathrm{hc},d^{-\frac{\alpha}{\alpha+\beta}}N}^{d,\boldsymbol{\gamma}}$. For arbitrary

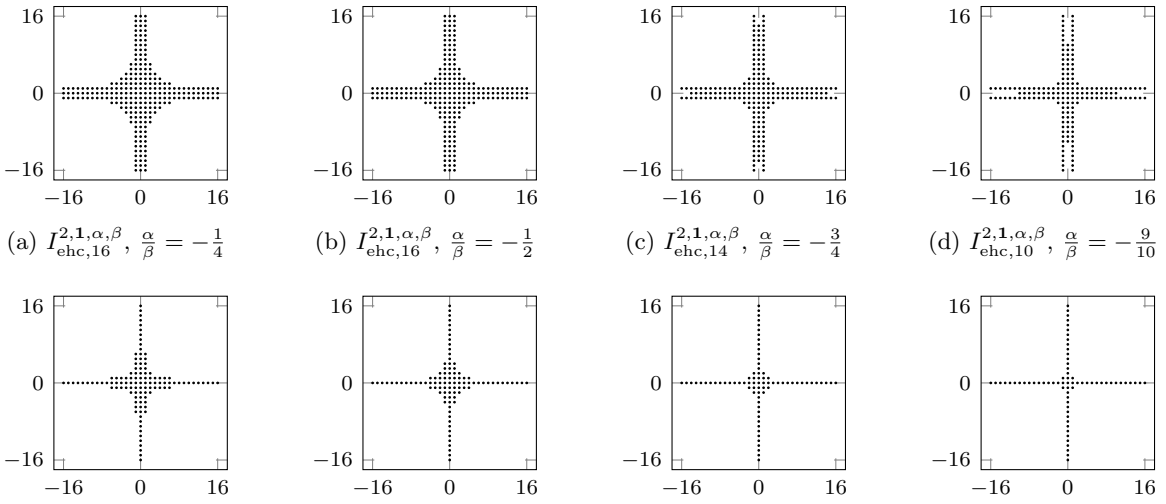

(a) $I^{2,\mathbf{1},\alpha,\beta}_{\mathrm{ehc},16}$, $\frac{\alpha}{\beta} = -\frac{1}{4}$ (b) $I^{2,\mathbf{1},\alpha,\beta}_{\mathrm{ehc},16}$, $\frac{\alpha}{\beta} = -\frac{1}{2}$ (c) $I^{2,\mathbf{1},\alpha,\beta}_{\mathrm{ehc},14}$, $\frac{\alpha}{\beta} = -\frac{3}{4}$ (d) $I^{2,\mathbf{1},\alpha,\beta}_{\mathrm{ehc},10}$, $\frac{\alpha}{\beta} = -\frac{9}{10}$

(e) $I^{2,\frac{1}{2}\mathbf{1},\alpha,\beta}_{\mathrm{ehc},2^{1/3}32}$, $\frac{\alpha}{\beta} = -\frac{1}{4}$ (f) $I^{2,\frac{1}{2}\mathbf{1},\alpha,\beta}_{\mathrm{ehc},64}$, $\frac{\alpha}{\beta} = -\frac{1}{2}$ (g) $I^{2,\frac{1}{2}\mathbf{1},\alpha,\beta}_{\mathrm{ehc},256}$, $\frac{\alpha}{\beta} = -\frac{3}{4}$ (h) $I^{2,\frac{1}{2}\mathbf{1},\alpha,\beta}_{\mathrm{ehc},2^{14}}$, $\frac{\alpha}{\beta} = -\frac{9}{10}$

Figure 2.4: Two-dimensional weighted energy-norm based hyperbolic crosses $I^{2,\boldsymbol{\gamma}}_{\mathrm{ehc},N}$ for different N, $\boldsymbol{\gamma}$, and relations of α and β.

$\boldsymbol{k} \in I^{d,\boldsymbol{\gamma},\alpha,\beta}_{\mathrm{ehc},N} \setminus \{\mathbf{0}\}$ we estimate

$$N \geq \omega^{d,\boldsymbol{\gamma},\alpha,\beta}_{\mathrm{ehc}}(\boldsymbol{k}) = \max(1, \|\boldsymbol{k}\|_1)^{\frac{\alpha}{\alpha+\beta}} \prod_{s=1}^{d} \max(1, \gamma_s^{-1}|k_s|)^{\frac{\beta}{\alpha+\beta}}$$
$$\geq d^{\frac{\alpha}{\alpha+\beta}} \max(1, \|\boldsymbol{k}\|_\infty)^{\frac{\alpha}{\alpha+\beta}} \prod_{s=1}^{d} \max(1, \gamma_s^{-1}|k_s|)^{\frac{\beta}{\alpha+\beta}}.$$

With $s_0 \in \{s \in \mathbb{N} \cap [1, \ldots, d] : k_s = \|\boldsymbol{k}\|_\infty\}$ we estimate

$$d^{-\frac{\alpha}{\alpha+\beta}} N \geq \left(\frac{1}{\gamma_{s_0}}\right)^{\frac{\beta}{\alpha+\beta}} |k_{s_0}| \prod_{\substack{s=1 \\ s\neq s_0}}^{d} \max(1, \gamma_s^{-1}|k_s|)^{\frac{\beta}{\alpha+\beta}}.$$

Due to $\frac{\beta}{\alpha+\beta} \geq 1$, $\frac{1}{\gamma_{s_0}} \geq 1$ and $\max(1, \gamma_s^{-1}|k_s|) \geq 1$, $s = 1, \ldots, d$, we obtain

$$d^{-\frac{\alpha}{\alpha+\beta}} N \geq \gamma_{s_0}^{-1}|k_{s_0}| \prod_{\substack{s=1 \\ s\neq s_0}}^{d} \max(1, \gamma_s^{-1}|k_s|) = \prod_{s=1}^{d} \max(1, \gamma_s^{-1}|k_s|) = \omega^{d,\boldsymbol{\gamma}}_{\mathrm{hc}}(\boldsymbol{k}).$$

■

Lemma 2.13. *Let the weights $\boldsymbol{\gamma} = (\gamma_s)_{s=1}^{\infty} \in [0,1]^{\mathbb{N}}$ with $1 \geq \gamma_1 \geq \gamma_2 \geq \ldots \geq \gamma_d \geq 0$, the dimension $d \geq 2$, and the parameters $0 \leq -\alpha < \beta$ and $N \in \mathbb{R}$, $N \geq 1$ be given. In order to obtain orthogonal columns in the Fourier matrix $\boldsymbol{A} := \left(\mathrm{e}^{2\pi \mathrm{i} \boldsymbol{k}\cdot\boldsymbol{x}}\right)_{\boldsymbol{x}\in\mathcal{X},\, \boldsymbol{k}\in I^{d,\boldsymbol{\gamma},\alpha,\beta}_{\mathrm{ehc},N}}$ the cardinality M of the sampling set $\mathcal{X}$ has to be at least as big as $\left(\left\lfloor \gamma_1^{\frac{\beta}{\alpha+\beta}} N \right\rfloor + 1\right)\left(\left\lfloor \gamma_2^{\frac{\beta}{\alpha+\beta}} N \right\rfloor + 1\right)$.*

Proof. Similar to the proof of Lemma 2.11, we define

$$I' = \left\{0, \ldots, \left\lfloor \gamma_1^{\frac{\beta}{\alpha+\beta}} N \right\rfloor\right\} \times \left\{0, \ldots, \left\lfloor \gamma_2^{\frac{\beta}{\alpha+\beta}} N \right\rfloor\right\} \times \underbrace{\{0\} \times \cdots \times \{0\}}_{d-2\text{-times}} \subset \mathbb{Z}^d$$

and obtain

$$\begin{aligned}
\mathcal{D}(I') &= \left\{-\left\lfloor \gamma_1^{\frac{\beta}{\alpha+\beta}} N \right\rfloor, \ldots, \left\lfloor \gamma_1^{\frac{\beta}{\alpha+\beta}} N \right\rfloor\right\} \times \left\{-\left\lfloor \gamma_2^{\frac{\beta}{\alpha+\beta}} N \right\rfloor, \ldots, \left\lfloor \gamma_2^{\frac{\beta}{\alpha+\beta}} N \right\rfloor\right\} \times \underbrace{\{0\} \times \cdots \times \{0\}}_{d-2\text{-times}} \\
&\subset \{\boldsymbol{k} - \boldsymbol{l} \in \mathbb{Z}^d \colon\ l_1 \in [-\left\lfloor \gamma_1^{\frac{\beta}{\alpha+\beta}} N \right\rfloor, \left\lfloor \gamma_1^{\frac{\beta}{\alpha+\beta}} N \right\rfloor] \cap \mathbb{Z}, l_2 = \ldots = l_d = 0; \\
&\qquad\qquad k_2 \in [-\left\lfloor \gamma_2^{\frac{\beta}{\alpha+\beta}} N \right\rfloor, \left\lfloor \gamma_2^{\frac{\beta}{\alpha+\beta}} N \right\rfloor] \cap \mathbb{Z},\ k_1 = k_3 = \ldots = k_d = 0\} \\
&\subset \{\boldsymbol{k} - \boldsymbol{l} \colon\ \boldsymbol{k}, \boldsymbol{l} \in I_{\mathrm{ehc},N}^{d,\boldsymbol{\gamma},\alpha,\beta}\} = \mathcal{D}(I_{\mathrm{ehc},N}^{d,\boldsymbol{\gamma},\alpha,\beta}).
\end{aligned}$$

We apply Lemma 2.5 and get that the number M of samples needed to achieve a Fourier matrix with orthogonal columns is at least as big as the cardinality of I'. Consequently, we obtain the necessary condition $|\mathcal{X}| \geq \left(\left\lfloor \gamma_1^{\frac{\beta}{\alpha+\beta}} N \right\rfloor + 1\right)\left(\left\lfloor \gamma_2^{\frac{\beta}{\alpha+\beta}} N \right\rfloor + 1\right)$. ∎

The last lemma shows that perfectly stable sampling schemes for energy-norm based hyperbolic cross trigonometric polynomials suffers from an oversampling that depends on N, in general. In detail, we need $\Omega(N^2)$ sampling values at different nodes in $\mathcal{X}$ in order to reconstruct a trigonometric polynomial with frequencies supported on the index set $I_{\mathrm{ehc},N}^{d,\boldsymbol{\gamma},\alpha,\beta}$, $|I_{\mathrm{ehc},N}^{d,\boldsymbol{\gamma},\alpha,\beta}| \in \mathcal{O}(N)$, in a perfectly stable way.

At the end, we would like to stress that the weight function $\omega_{\mathrm{ehc}}^{d,\boldsymbol{\gamma},\alpha,\beta}$ may takes values that are smaller than one. However, for fixed dimension d, weights $\boldsymbol{\gamma}$ and smoothness parameters α and β, the range of $\omega_{\mathrm{ehc}}^{d,\boldsymbol{\gamma},\alpha,\beta}$ is contained in $[c_{d,\boldsymbol{\gamma},\alpha,\beta}, \infty)$, where the term $c_{d,\boldsymbol{\gamma},\alpha,\beta}$ fulfills $c_{d,\boldsymbol{\gamma},\alpha,\beta} > 0$. Accordingly, we also obtain the embedding $\mathcal{A}_{\omega_{\mathrm{ehc}}^{d,\boldsymbol{\gamma},\alpha,\beta}}(\mathbb{T}^d) \subset \mathcal{A}(\mathbb{T}^d)$.

2.3.4 Arbitrary Sparse Frequency Index Sets

In this section, we assume that the frequency index set I is a sparse one and given. Since we consider only frequency index sets of finite cardinality, it is quite natural that the frequency index set is contained in a d-dimensional box of a certain edge length. We assume no structure on the frequency index set I. Applying the more or less nonconstructive results of S. M. Ermakov [Erm75, Chapter IV], we know that there exist sampling sets $\mathcal{X}$ of a cardinality $|\mathcal{X}| \leq |\mathcal{D}(I)|$ such that the matrix $\boldsymbol{A}^* \boldsymbol{W} \boldsymbol{A}$,

$$(\boldsymbol{A}^* \boldsymbol{W} \boldsymbol{A})_{\boldsymbol{k}_1, \boldsymbol{k}_2} = \sum_{j=0}^{|\mathcal{X}|-1} w_j \mathrm{e}^{2\pi \mathrm{i} (\boldsymbol{k}_2 - \boldsymbol{k}_1) \cdot \boldsymbol{x}_j} = \begin{cases} 1 & \text{for } \boldsymbol{k}_1 = \boldsymbol{k}_2, \\ 0 & \text{else,} \end{cases} \tag{2.22}$$

is the identity matrix, cf. Section 2.2 on page 21. The matrix $\boldsymbol{W}$ is a diagonal matrix that contains the weights w_j as its diagonal entries.

Due to the non-existing structure of the frequency index set, the best possible estimate of the cardinality of the difference set $\mathcal{D}(I)$ is given by $|\mathcal{D}(I)| \leq |I|(|I| - 1) + 1$.

At a first glance, the assumption that one knows an arbitrary sparse frequency index set I is not quite natural. But under certain circumstances, such an arbitrary frequency index set I may be identified using for example an orthogonal matching pursuit as described in [KR08] or [Xu11]. Specifically, if one has to treat the identified trigonometric polynomial $p \in \Pi_I$ further, a suitable sampling scheme allowing fast computations may be of quite particular interest. Since we cannot assume structure on the resulting frequency index set $I \subset \mathbb{Z}^d$, we have to deal with arbitrary frequency index sets and need strategies in order to construct corresponding suitable sampling schemes.

In Chapter 3, some weak additional assumptions on I will allow us to determine sampling sets $\mathcal{X}$ that fulfills $|\mathcal{X}| \leq |\mathcal{D}(I)|$ and (2.22). Particularly, the sampling sets $\mathcal{X}$ are rank-1 lattices and the matrices $\boldsymbol{W}$ scaled identity matrices, i.e., $\boldsymbol{W} = \frac{1}{|\mathcal{X}|}\boldsymbol{I}$. In other words, we determine quasi-Monte Carlo rules that allow for the perfectly stable reconstruction of trigonometric polynomials with frequencies supported on given frequency index sets I.

2.4 Summary

At the beginning of this chapter, we introduced the function spaces $\mathcal{A}_\omega(\mathbb{T}^d)$ that we will treat during the whole work. We showed that the functions f that belongs to those function spaces can be well approximated using the Fourier partial sums $S_{I_N} f$, where $S_{I_N} f \in \Pi_{I_N}$ are trigonometric polynomials with frequencies supported on the index sets $I_N \subset \mathbb{Z}^d$, cf. Lemma 2.2. The frequency index sets I_N crucially depend on the weight function ω.

We brought in mind that it is easily possible to sample trigonometric polynomials with frequencies supported on d-dimensional full grids in a perfectly stable and unique way. One may uses the corresponding sampling schemes, i.e., full grids in the spatial domain, as sampling schemes for approximation problems, which yields perfectly stable approximation algorithms.

Subsequently, we considered the same approaches for arbitrary frequency index sets I and determined a lower bound on the number of sampling values that are necessary in order to uniquely sample trigonometric polynomials $f \in \Pi_I$ in a perfectly stable way, cf. Lemma 2.5. The corresponding lower bound mainly depends on the structure of the frequency index set I. Specifically, the largest possible cardinality of all frequency index sets I' such that the difference sets fulfill $\mathcal{D}(I') \subset \mathcal{D}(I)$ bounds the necessary number of sampling values of a perfectly stable sampling scheme for I from below.

Additionally, we applied the findings on specific structures of frequency index sets, i.e., ℓ_p-balls, weighted hyperbolic crosses and weighted energy-norm based hyperbolic crosses. Thereby, we were interested in the dependence on the parameter N of the lower bound of the necessary number of sampling values. In particular, the lower bound is of optimal order in N with respect to the cardinality of the corresponding frequency index set I for ℓ_p-balls, cf. Corollary 2.9. Furthermore, we determined that weighted (energy-norm) based hyperbolic cross trigonometric polynomials can not be uniquely sampled in a perfectly stable way using the optimal number of sampling values with respect to N, cf. Lemmas 2.11 and 2.13.

Finally, we applied our results on arbitrary sparse frequency index sets and discussed the relations to already known results in the field of numerical integration. In particular, the interest in arbitrary sparse frequency index sets is caused by already existing adaptive methods that determines the concrete support of trigonometric polynomials in frequency domain.

Chapter 3

Rank-1 Lattices

At first, we give the central definition of this chapter. For a given vector $\boldsymbol{z} \in \mathbb{Z}^d$ and a number $M \in \mathbb{N}$ we define the *rank-1 lattice*

$$\Lambda(\boldsymbol{z}, M) := \{\boldsymbol{x}_j := \frac{j}{M}\boldsymbol{z} \bmod \mathbf{1} \in \mathbb{T}^d \colon j = 0, \ldots, M-1\} \tag{3.1}$$

as spatial discretization in the d-dimensional torus $\mathbb{T}^d$. We name the vector $\boldsymbol{z}$ the *generating vector* and the number M the *lattice size* of the rank-1 lattice $\Lambda(\boldsymbol{z}, M)$. Figure 3.1 sketches the construction of a two-dimensional rank-1 lattice.

Initially, rank-1 lattices were introduced as sampling schemes for (equally weighted) cubature rules in the late 1950s and 1960s. In [Nie78], one finds a summary and an extensive reference list of the early work on so-called lattice rules, i.e., cubature rules based on (rank-1) lattice sampling.

The increased interest in rank-1 lattices during the last years is caused by the seminal result of I. H. Sloan and A. V. Reztsov, see [SR02], where a component–by–component

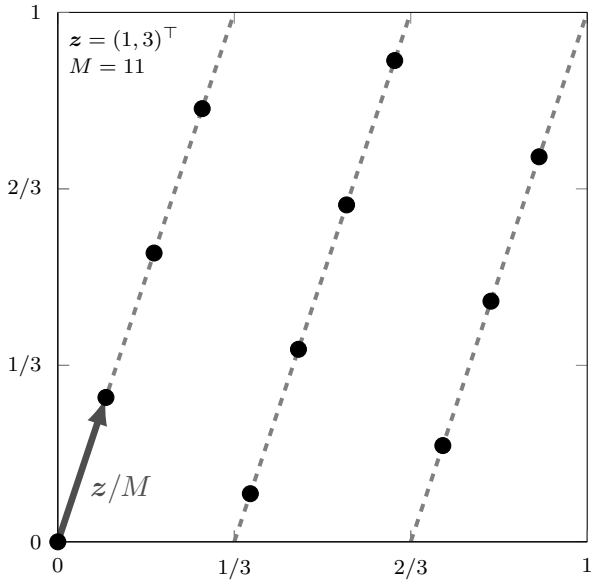

Figure 3.1: Rank-1 lattice construction sketch.

approach is described that constructs good lattice rules, which are cubature formulas that guarantee somehow optimal theoretical error estimates for functions of specific classes. In detail, the theoretical error estimates are optimal with respect to the number of used sampling values up to some logarithmic factors. The expression component–by–component refers to the construction of the generating vector $\boldsymbol{z}$, i.e., for a given lattice size M one determines the components of the vector $\boldsymbol{z}$ one after another and builds up good lattice rules in dimension s from a good lattice rule in dimension $s-1$, $s=2,\dots,d$.

The presented construction method in [SR02] allows to determine good lattice rules in very high dimensions due to computational costs of $\mathcal{O}\left(dM^2\right)$, where d is the spatial dimension, M is the number of used sampling values, and one uses $\mathcal{O}\left(M\right)$ memory. The additional findings of R. Cools and D. Nuyens, cf. [CN04], allow for a fast construction of such good lattice rules, which enormously improves the applicability of these cubature rules in practice. Specifically, the so-called fast component–by–component construction of (almost) optimal rank-1 lattice rules improves the computational costs to $\mathcal{O}\left(dM\log M\right)$ and uses $\mathcal{O}\left(M\right)$ memory. Thus, this construction method provides the user with good lattice rules in large dimensions d with a high accuracy due to the huge number, i.e., up to several millions, of sampling values.

The book of I. H. Sloan and S. Joe, [SJ94], offers a great introduction to lattice methods for numerical integration. Furthermore, we would like to recommend the survey paper [DKS13] that presents recent developments in quasi-Monte Carlo cubature methods and focuses, among others, on lattice methods.

The idea to approximate whole functions—and not only the integrals of the functions—from sampling values along a specific type of rank-1 lattices was considered in the 1980s by V. N. Temlyakov, cf. [Tem86]. Only much later, i.e., after 2000, researchers considered the approximation properties of rank-1 lattices in general, cf. [LH03, ZLH06, KSW06, KSW08, KWW09, MS12]. Specifically, the outstanding properties of rank-1 lattices are investigated in the fields of information based complexity as well as applied analysis. None of these papers gave universally applicable construction methods for rank-1 lattices that are suitable for approximation. Either there are nonconstructive existence results, cf. [Tem86, LH03, ZLH06], or the corresponding construction methods are heavily adapted to the considered function spaces, cf. [KSW06, KSW08, KWW09].

In this chapter, we present a component–by–component construction of rank-1 lattices that allows the unique reconstruction of trigonometric polynomials $f \in \Pi_I$. We name a rank-1 lattice that allows the unique reconstruction of all trigonometric polynomials with frequencies supported on the index set I *reconstructing rank-1 lattice* for I. We would like to point out that $I \subset \mathbb{Z}^d$ may be an arbitrary frequency index set, e.g., I is without any structure or with gaps.

Furthermore, we prove that our method determines such so-called reconstructing rank-1 lattices for the frequency index set I with a number of sampling nodes M that is bounded by terms

$$|I| \leq M \leq \max\left\{\frac{2|I|^2}{3}, \max\{3\|\boldsymbol{k}\|_\infty \colon \boldsymbol{k} \in I\}\right\}, \quad |I| \geq 8, \tag{3.2}$$

where the right hand side is already simplified, see Corollary 3.4 for the details. We stress on the fact that it mainly depends on the structure of the frequency index set I whether there exists rank-1 lattices of a size M that is close to $|I|$ or not, but in all cases M is bounded from above by the term on the right hand side in (3.2). In particular for $I \subset [-|I|,|I|]^d$, $|I| \geq 8$, the number of needed sampling values M is not larger than $\frac{2}{3}|I|^2$ independent of the dimension d and the structure of I.

In Section 3.4, we consider the approximation properties of these reconstructing rank-1 lattices. Certainly, one may sample a sufficiently smooth function f along a reconstructing rank-1 lattice and compute an approximation of the Fourier partial sum $S_I f$ from the sampling values of f. We show, that for suitably chosen frequency index sets I the approximated Fourier partial sum $\tilde{S}_I f$ is close to the exact Fourier partial sum $S_I f$. In detail, we prove the error estimate

$$\|f - \tilde{S}_{I_N} f | L_\infty(\mathbb{T}^d)\| \leq 2N^{-1} \|f | \mathcal{A}_\omega(\mathbb{T}^d)\|, \tag{3.3}$$

where we assume that the frequency index set $I_N = \{\boldsymbol{k} \in \mathbb{Z}^d \colon \omega(\boldsymbol{k}) \leq N\}$ is of finite cardinality and $\tilde{S}_{I_N} f$ is the approximated Fourier partial sum computed from the sampling values of a reconstructing rank-1 lattice for I_N. The function spaces $\mathcal{A}_\omega(\mathbb{T}^d)$ consist of multivariate continuous periodic functions of a certain smoothness that belongs to the Wiener algebra $\mathcal{A}(\mathbb{T}^d)$, cf. (2.9). We stress on the fact that the right hand side of (3.3) is only two times the worst case $L_\infty(\mathbb{T}^d)$ error of f approximated by the exact Fourier partial sum $S_{I_N} f$, cf. Lemma 2.2.

The main advantage of using rank-1 lattices as sampling schemes for the reconstruction of trigonometric polynomials $f \in \Pi_I$ and the approximation of functions $f \in \mathcal{A}_\omega(\mathbb{T}^d)$ by $\tilde{S}_{I_N} f$ is the simplicity of the corresponding computation and its independence on the structure of the frequency index set I and I_N, respectively. In detail, the corresponding discrete Fourier transform simplifies to some easily realizable post-computations subsequent to a one-dimensional equispaced discrete Fourier transform. Clearly, we apply the one-dimensional fast Fourier transform, in order to compute the discrete Fourier transform that is needed for the reconstruction or the approximation. If one uses reconstructing rank-1 lattices for the frequency index set I (or I_N) as sampling schemes, all the computations are extremely stable, since the post-computations consists of (perfectly stable) permutations and the one-dimensional equispaced fast Fourier transform is also known to be stable, cf. [Sch96, PST03]. We stress on the fact, that our approximation strategy can also be extended to an interpolation strategy as described in Section 3.5.

In Section 3.8, we apply our findings on rank-1 lattices to specific frequency index sets that occur in various numerical applications. To this end, we analyze the structures of the specific frequency index sets I that are introduced in Chapter 2 and estimate the number of sampling values that are needed in order to uniquely sample the trigonometric polynomials $f \in \Pi_I$ along a rank-1 lattice. We show, that we can uniquely reconstruct trigonometric polynomials with frequencies supported on weighted ℓ_p-balls $I_{p,N}^{d,\boldsymbol{\gamma}}$ with the asymptotically optimal number of sampling values with respect to N. In addition, we consider trigonometric polynomials with frequencies supported on energy-norm based hyperbolic crosses $I_{\mathrm{ehc},N}^{d,\boldsymbol{\gamma}}$. Under the assumption that the Fourier matrix $\boldsymbol{A}$, cf. (2.7), shall consist of pairwise orthogonal columns, our findings allow us to determine sampling schemes, i.e., reconstructing rank-1 lattices for $I_{\mathrm{ehc},N}^{d,\boldsymbol{\gamma}}$, that are asymptotically optimal with respect to the parameter N. Furthermore, rank-1 lattices can also be used in order to sample weighted hyperbolic cross trigonometric polynomials $f \in \Pi_{I_{\mathrm{hc},N}^{d,\boldsymbol{\gamma}}}$ in a perfectly stable way. The corresponding number of used sampling values is also asymptotically optimal with respect to N up to some logarithmic factors $\log N$, provided that we require pairwise orthogonal columns within the Fourier matrices $\boldsymbol{A}$. Additionally, we discuss some numerical experiments for randomly chosen frequency index sets $I \subset [-128, 128]^d$, $|I| \geq 750$, which demonstrates that the number of sampling values of reconstructing rank-1 lattices for the frequency index set I does not depend on the dimension d, but on the cardinality $|I|$ and is bounded by $\mathcal{O}\left(|I|^2\right)$ in general.

Algorithm 3.1 Evaluation at rank-1 lattice

Input:	$M \in \mathbb{N}$	lattice size of rank-1 lattice $\Lambda(\boldsymbol{z}, M)$
	$\boldsymbol{z} \in \mathbb{Z}^d$	generating vector of rank-1 lattice $\Lambda(\boldsymbol{z}, M)$
	$I \subset \mathbb{Z}^d$	frequency index set
	$\hat{\boldsymbol{f}} = \left(\hat{f}_{\boldsymbol{k}}\right)_{\boldsymbol{k}\in I}$	Fourier coefficients of $f \in \Pi_I$

$\hat{\boldsymbol{g}} = (0)_{l=0}^{M-1}$
for each $\boldsymbol{k} \in I$ ***do***
  $\hat{g}_{\boldsymbol{k}\cdot\boldsymbol{z} \bmod M} = \hat{g}_{\boldsymbol{k}\cdot\boldsymbol{z} \bmod M} + \hat{f}_{\boldsymbol{k}}$
end for
$\boldsymbol{f} = \text{iFFT\_1D}(\hat{\boldsymbol{g}})$
$\boldsymbol{f} = M\boldsymbol{f}$

Output:	$\boldsymbol{f} = \boldsymbol{A}\hat{\boldsymbol{f}} = \left(f\left(\frac{j\boldsymbol{z}}{M} \bmod \boldsymbol{1}\right)\right)_{j=0}^{M-1}$	function values of $f \in \Pi_I$

3.1 Evaluation of Multivariate Trigonometric Polynomials

We consider the trigonometric polynomial $f \in \Pi_I$, $f(\boldsymbol{x}) = \sum_{\boldsymbol{k}\in I} \hat{f}_{\boldsymbol{k}} \mathrm{e}^{2\pi\mathrm{i}\boldsymbol{k}\boldsymbol{x}}$, where the Fourier coefficients $\hat{f}_{\boldsymbol{k}}$, $\boldsymbol{k} \in I$, are given. Following [LH03], the simultaneous evaluation of a trigonometric polynomial $f \in \Pi_I$ at all nodes of the rank-1 lattice $\Lambda(\boldsymbol{z}, M)$ simplifies to a one-dimensional discrete Fourier transform, i.e.,

$$f(\boldsymbol{x}_j) = \sum_{\boldsymbol{k}\in I} \hat{f}_{\boldsymbol{k}} \mathrm{e}^{2\pi\mathrm{i}\boldsymbol{k}\cdot\boldsymbol{x}_j} = \sum_{\boldsymbol{k}\in I} \hat{f}_{\boldsymbol{k}} \mathrm{e}^{2\pi\mathrm{i}\frac{j\boldsymbol{k}\cdot\boldsymbol{z}}{M}} = \sum_{l=0}^{M-1} \left(\sum_{\substack{\boldsymbol{k}\in I \\ \boldsymbol{k}\cdot\boldsymbol{z}\equiv l \pmod M}} \hat{f}_{\boldsymbol{k}} \right) \mathrm{e}^{2\pi\mathrm{i}\frac{jl}{M}}$$
$$= \sum_{l=0}^{M-1} \hat{g}_l \mathrm{e}^{2\pi\mathrm{i}\frac{jl}{M}}, \qquad \text{where} \qquad \hat{g}_l = \sum_{\substack{\boldsymbol{k}\in I \\ \boldsymbol{k}\cdot\boldsymbol{z}\equiv l \pmod M}} \hat{f}_{\boldsymbol{k}}.$$

We pre-compute the sequence $(\hat{g}_l)_{l=0}^{M-1}$ and apply a one-dimensional inverse fast Fourier transform to evaluate f at all nodes of the rank-1 lattice $\Lambda(\boldsymbol{z}, M)$, cf. [CT65]. We obtain a complexity of $\mathcal{O}(d|I|)$ to compute all values $\boldsymbol{k}\cdot\boldsymbol{z} \bmod M$, $\boldsymbol{k} \in I$, and the vector $(\hat{g}_l)_{l=0}^{M-1}$ and further a complexity of $\mathcal{O}(M \log M)$ to evaluate all values $f(\boldsymbol{x}_j)$, $j = 0, \ldots, M-1$, using a single one-dimensional fast Fourier transform. Thus the total complexity is $\mathcal{O}(M \log M + d|I|)$, cf. Algorithm 3.1. In the case of multiple using $\Lambda(\boldsymbol{z}, M)$ in combination with the index set I one has to compute all values of $\boldsymbol{k}\cdot\boldsymbol{z} \bmod M$ only once. Thus we obtain a lower complexity of $\mathcal{O}(M \log M + |I|)$ for one evaluation here. Note that the complexity only depends linearly on the maximum of the cardinality of the frequency index set I and the cardinality of the sampling set $\Lambda(\boldsymbol{z}, M)$ up to some logarithmic factor $\log M$.

3.2 Reconstruction of Multivariate Trigonometric Polynomials

As the fast evaluation of trigonometric polynomials at all sampling nodes of $\boldsymbol{x}_j$ of the rank-1 lattice $\Lambda(\boldsymbol{z}, M)$ is guaranteed, see Algorithm 3.1, we draw our attention to the reconstruction of a trigonometric polynomial $f \in \Pi_I$ with frequencies supported on I using function values at the nodes $\boldsymbol{x}_j$ of a rank-1 lattice $\Lambda(\boldsymbol{z}, M)$. We consider the corresponding Fourier matrix

$\boldsymbol{A}$ and its adjoint $\boldsymbol{A}^*$,

$$\boldsymbol{A} := \left(\mathrm{e}^{2\pi\mathrm{i}\boldsymbol{k}\cdot\boldsymbol{x}}\right)_{\boldsymbol{x}\in\Lambda(\boldsymbol{z},M),\,\boldsymbol{k}\in I} \in \mathbb{C}^{M\times|I|} \quad \text{and} \quad \boldsymbol{A}^* := \left(\mathrm{e}^{-2\pi\mathrm{i}\boldsymbol{k}\cdot\boldsymbol{x}}\right)_{\boldsymbol{k}\in I,\,\boldsymbol{x}\in\Lambda(\boldsymbol{z},M)} \in \mathbb{C}^{|I|\times M},$$

in order to determine necessary and sufficient conditions on rank-1 lattices $\Lambda(\boldsymbol{z}, M)$ that allow for a unique reconstruction of all Fourier coefficients of $f \in \Pi_I$. The reconstruction of the Fourier coefficients $\hat{\boldsymbol{f}} = (\hat{f}_{\boldsymbol{k}})_{\boldsymbol{k}\in I} \in \mathbb{C}^{|I|}$ from sampling values $\boldsymbol{f} = (f(\boldsymbol{x}))_{\boldsymbol{x}\in\Lambda(\boldsymbol{z},M)} \in \mathbb{C}^M$ can be realized by solving the normal equation $\boldsymbol{A}^*\boldsymbol{A}\hat{\boldsymbol{f}} = \boldsymbol{A}^*\boldsymbol{f}$, which is equivalent to solve the least squares problem

$$\text{find } \hat{\boldsymbol{f}} \in \mathbb{C}^{|I|} \text{ such that } \|\boldsymbol{A}\hat{\boldsymbol{f}} - \boldsymbol{f}\|_2 \to \min,$$

cf. [Bjö96]. Assuming $\boldsymbol{f} = (f(\boldsymbol{x}))_{\boldsymbol{x}\in\Lambda(\boldsymbol{z},M)}$ being a vector of sampling values of the trigonometric polynomial $f \in \Pi_I$, the vector $\boldsymbol{f}$ belongs to the range of $\boldsymbol{A}$ and we can find a possibly non-unique solution $\hat{\boldsymbol{f}}$ of $\boldsymbol{A}\hat{\boldsymbol{f}} = \boldsymbol{f}$. We compute a unique solution of the normal equation, iff the Fourier matrix $\boldsymbol{A}$ has full column rank.

Lemma 3.1. *Let a frequency index set $I \subset \mathbb{Z}^d$ of finite cardinality and a rank-1 lattice $\Lambda(\boldsymbol{z}, M)$ be given. Then two distinct columns of the corresponding Fourier matrix $\boldsymbol{A}$ are orthogonal or equal, i.e., $(\boldsymbol{A}^*\boldsymbol{A})_{\boldsymbol{h},\boldsymbol{k}} \in \{0, M\}$ for $\boldsymbol{h}, \boldsymbol{k} \in I$.*

Proof. The matrix $\boldsymbol{A}^*\boldsymbol{A}$ contains all scalar products of two columns of the Fourier matrix $\boldsymbol{A}$, i.e., $(\boldsymbol{A}^*\boldsymbol{A})_{\boldsymbol{h},\boldsymbol{k}}$ is the scalar product of column $\boldsymbol{k}$ with column $\boldsymbol{h}$ of the Fourier matrix $\boldsymbol{A}$. We obtain

$$(\boldsymbol{A}^*\boldsymbol{A})_{\boldsymbol{h},\boldsymbol{k}} = \sum_{j=0}^{M-1} \left(\mathrm{e}^{2\pi\mathrm{i}\frac{(\boldsymbol{k}-\boldsymbol{h})\cdot\boldsymbol{z}}{M}}\right)^j = \begin{cases} M & \text{for } \boldsymbol{k}\cdot\boldsymbol{z} \equiv \boldsymbol{h}\cdot\boldsymbol{z} \pmod{M}, \\ \frac{\mathrm{e}^{2\pi\mathrm{i}(\boldsymbol{k}-\boldsymbol{h})\cdot\boldsymbol{z}}-1}{\mathrm{e}^{2\pi\mathrm{i}\frac{(\boldsymbol{k}-\boldsymbol{h})\cdot\boldsymbol{z}}{M}}-1} = 0 & \text{else.} \end{cases}$$

■

According to Lemma 3.1 the matrix $\boldsymbol{A}$ has full column rank, iff

$$\boldsymbol{k}\cdot\boldsymbol{z} \not\equiv \boldsymbol{h}\cdot\boldsymbol{z} \pmod{M} \qquad \text{for all} \quad \boldsymbol{k} \neq \boldsymbol{h};\ \boldsymbol{k}, \boldsymbol{h} \in I, \tag{3.4}$$

or, equivalent,

$$\boldsymbol{k}\cdot\boldsymbol{z} \not\equiv 0 \pmod{M} \qquad \text{for all} \quad \boldsymbol{k} \in \mathcal{D}(I) \setminus \{\boldsymbol{0}\}, \tag{3.5}$$

where $\mathcal{D}(I)$ is the difference set of the frequency index set I as defined in (2.11). We call a rank-1 lattice $\Lambda(\boldsymbol{z}, M)$ ensuring (3.4) or equivalently (3.5) *reconstructing rank-1 lattice* for the index set I. In particular, condition (3.5) ensures the exact integration of all trigonometric polynomials $g \in \Pi_{\mathcal{D}(I)}$ applying the lattice rule given by the rank-1 lattice $\Lambda(\boldsymbol{z}, M)$, i.e., the identity $\int_{\mathbb{T}^d} g(\boldsymbol{x})\mathrm{d}\boldsymbol{x} = \frac{1}{M}\sum_{j=0}^{M-1} g(\boldsymbol{x}_j)$ holds for all $g \in \Pi_{\mathcal{D}(I)}$, cf. [SK87]. Certainly, $f \in \Pi_I$ and $\boldsymbol{k} \in I$ implies that $f(\circ)\mathrm{e}^{-2\pi\mathrm{i}\boldsymbol{k}\cdot\circ} \in \Pi_{\mathcal{D}(I)}$ and we obtain

$$\frac{1}{M}\sum_{j=0}^{M-1} f\left(\frac{j\boldsymbol{z}}{M} \bmod \boldsymbol{1}\right)\mathrm{e}^{-2\pi\mathrm{i}j\frac{\boldsymbol{k}\cdot\boldsymbol{z}}{M}} = \int_{\mathbb{T}^d} f(\boldsymbol{x})\mathrm{e}^{-2\pi\mathrm{i}\boldsymbol{k}\cdot\boldsymbol{x}}\mathrm{d}\boldsymbol{x} =: \hat{f}_{\boldsymbol{k}},$$

where the right equality is the usual definition of the Fourier coefficients. We symbolize the reconstruction property of the rank-1 lattice $\Lambda(\boldsymbol{z}, M)$ with respect to I using the notation $\Lambda(\boldsymbol{z}, M, I)$.

Algorithm 3.2 Reconstruction from sampling values along a reconstructing rank-1 lattice

Input:	$I \subset \mathbb{Z}^d$	frequency index set of finite cardinality
	$M \in \mathbb{N}$	lattice size of rank-1 lattice $\Lambda(\boldsymbol{z}, M, I)$
	$\boldsymbol{z} \in \mathbb{Z}^d$	generating vector of rank-1 lattice $\Lambda(\boldsymbol{z}, M, I)$
	$\boldsymbol{f} = \left(f\left(\frac{j\boldsymbol{z}}{M} \bmod \mathbf{1}\right)\right)_{j=0}^{M-1}$	function values of $f \in \Pi_I$

$\hat{\boldsymbol{g}} = \mathrm{FFT\_1D}(\boldsymbol{f})$
for each $\boldsymbol{k} \in I$ ***do***
  $\hat{f}_{\boldsymbol{k}} = \frac{1}{M}\hat{g}_{\boldsymbol{k}\cdot\boldsymbol{z} \bmod M}$
end for

Output:	$\hat{\boldsymbol{f}} = M^{-1}\boldsymbol{A}^*\boldsymbol{f} = \left(\hat{f}_{\boldsymbol{k}}\right)_{\boldsymbol{k}\in I}$	Fourier coefficients supported on I

Another fact, which comes out of Lemma 3.1, is that the matrix $\boldsymbol{A}$ fulfills $\boldsymbol{A}^*\boldsymbol{A} = M\boldsymbol{I}$ in the case of $\Lambda(\boldsymbol{z}, M)$ being a reconstructing rank-1 lattice for I. The normalized normal equation simplifies to

$$\hat{\boldsymbol{f}} = \frac{1}{M}\boldsymbol{A}^*\boldsymbol{A}\hat{\boldsymbol{f}} = \frac{1}{M}\boldsymbol{A}^*\boldsymbol{f},$$

and in fact we reconstruct the Fourier coefficients of $f \in \Pi_I$ applying the lattice rule

$$\hat{f}_{\boldsymbol{k}} = \frac{1}{M}\sum_{j=0}^{M-1} f(\boldsymbol{x}_j)\mathrm{e}^{-2\pi\mathrm{i}\frac{j\boldsymbol{k}\cdot\boldsymbol{z}}{M}} = \frac{1}{M}\sum_{j=0}^{M-1} f(\boldsymbol{x}_j)\mathrm{e}^{-2\pi\mathrm{i}\frac{jl}{M}}$$

for all $\boldsymbol{k} \in I$ and $l = \boldsymbol{k}\cdot\boldsymbol{z} \bmod M$. In particular, one computes all Fourier coefficients using one one-dimensional FFT and the unique inverse mapping of $\boldsymbol{k} \mapsto \boldsymbol{k}\cdot\boldsymbol{z} \bmod M$, cf. Algorithm 3.2. The corresponding complexity is given by $\mathcal{O}(M\log M + d|I|)$.

A reconstructing rank-1 lattice for the frequency index set I is characterized by (3.4) and (3.5), respectively. Similar to the construction of rank-1 lattices for the exact integration of trigonometric polynomials of specific trigonometric degrees, see [CKN10], we are interested in existence results and suitable construction algorithms for reconstructing rank-1 lattices. In order to prepare the main theorem of this section, we define the projection of an index set $I \subset \mathbb{Z}^d$ on $\mathbb{Z}^s$, $d \geq s \in \mathbb{N}$,

$$I_{\downarrow s} := \{(k_j)_{j=1}^s \in \mathbb{Z}^s \colon \boldsymbol{k} = (k_j)_{j=1}^d \in I\}. \tag{3.6}$$

Furthermore, we name a frequency index set $I \subset \mathbb{Z}^d$ *symmetric to the origin* iff $I = \{-\boldsymbol{k} \colon \boldsymbol{k} \in I\}$, i.e., $\boldsymbol{k} \in I$ implies $-\boldsymbol{k} \in I$ for all $\boldsymbol{k} \in I$.

Theorem 3.2. *Let $s \in \mathbb{N}$, $d \geq s \geq 2$, $\tilde{I} \subset \mathbb{Z}^d$ be an arbitrary d-dimensional set of finite cardinality that is symmetric to the origin, and M be a prime number satisfying*

$$M \geq \frac{|\{\boldsymbol{k} \in \tilde{I}_{\downarrow s} : \boldsymbol{k} = (\boldsymbol{h}, h_s), \boldsymbol{h} \in \tilde{I}_{\downarrow s-1} \setminus \{\mathbf{0}\} \text{ and } h_s \in \mathbb{Z}\setminus\{0\}\}|}{2} + 2.$$

Additionally, we assume that each nonzero element of the set of the sth component of $\tilde{I}_{\downarrow s}$ and M are coprime, i.e., $M \nmid l$ for all $l \in \{h_s \in \mathbb{Z}\setminus\{0\} : \boldsymbol{k} = (\boldsymbol{h}, h_s) \in \tilde{I}_{\downarrow s}, \boldsymbol{h} \in \tilde{I}_{\downarrow s-1}\}$, and that there exists a generating vector $\boldsymbol{z}^* \in \mathbb{N}^{s-1}$ that guarantees

$$\boldsymbol{h}\cdot\boldsymbol{z}^* \not\equiv 0 \pmod{M} \quad \text{for all } \boldsymbol{h} \in \tilde{I}_{\downarrow s-1} \setminus \{\mathbf{0}\}.$$

Then, there exists at least one $z_s^* \in \{1, \dots, M-1\}$ *such that*

$$(\boldsymbol{h}, h_s) \cdot (\boldsymbol{z}^*, z_s^*) \not\equiv 0 \pmod{M} \quad \text{for all } (\boldsymbol{h}, h_s) \in \tilde{I}_{\downarrow s} \setminus \{\mathbf{0}\}.$$

Proof. We adapt the proof of [CKN10, Theorem 1]. Let us assume that

$$\boldsymbol{h} \cdot \boldsymbol{z}^* \not\equiv 0 \pmod{M} \text{ for all } \boldsymbol{h} \in \tilde{I}_{\downarrow s-1} \setminus \{\mathbf{0}\}.$$

Basically, we determine an upper bound on the number of elements $z_s \in \{1, \dots, M-1\}$ with

$$(\boldsymbol{h}, h_s) \cdot (\boldsymbol{z}^*, z_s) \equiv 0 \pmod{M} \text{ for at least one } (\boldsymbol{h}, h_s) \in \tilde{I}_{\downarrow s} \setminus \{\mathbf{0}\}$$

or, equivalent,

$$\boldsymbol{h} \cdot \boldsymbol{z}^* \equiv -h_s z_s \pmod{M} \text{ for at least one } (\boldsymbol{h}, h_s) \in \tilde{I}_{\downarrow s} \setminus \{\mathbf{0}\}.$$

Similar to [CKN10] we consider three cases:

$h_s = 0$: With $(\boldsymbol{h}, h_s) \in \tilde{I}_{\downarrow s} \setminus \{\mathbf{0}\}$ we have $\mathbf{0} \neq \boldsymbol{h} \in \tilde{I}_{\downarrow s-1} \setminus \{\mathbf{0}\}$. Consequently, $\boldsymbol{h} \cdot \boldsymbol{z}^* \equiv -0 z_s \pmod{M}$ never holds because of $\boldsymbol{h} \cdot \boldsymbol{z}^* \not\equiv 0 \pmod{M}$ for all $\boldsymbol{h} \in \tilde{I}_{\downarrow s-1} \setminus \{\mathbf{0}\}$.

$\boldsymbol{h} = \mathbf{0}$: We consider $z_s \in \{1, \dots, M-1\}$. We required M being prime, so z_s and M are coprime. Due to $(\boldsymbol{h}, h_s) \in \tilde{I}_{\downarrow s} \setminus \{\mathbf{0}\}$, we obtain $h_s \neq 0$ and we assumed M and $h_s \neq 0$ are coprime. Consequently, we realize $z_s h_s \neq 0$ and $z_s h_s$ and M are relatively prime. So $\mathbf{0}\boldsymbol{z}^* \equiv -h_s z_s \pmod{M}$ never holds for $(\mathbf{0}, h_s) \in \tilde{I}_{\downarrow s} \setminus \{\mathbf{0}\}$ and $z_s \in \{1, \dots, M-1\}$.

else: Since $0 \neq h_s$ and M are coprime and $\boldsymbol{h} \cdot \boldsymbol{z}^* \not\equiv 0 \pmod{M}$, there is at most one $z_s \in \{1, \dots, M-1\}$ that fulfills $\boldsymbol{h} \cdot \boldsymbol{z}^* \equiv -h_s z_s \pmod{M}$. Due to the symmetry of the considered index set $\{(\boldsymbol{h}, h_s) \in \tilde{I}_{\downarrow s} \setminus \{\mathbf{0}\} : \boldsymbol{h} \in \tilde{I}_{\downarrow s-1} \setminus \{\mathbf{0}\} \text{ and } h_s \in \mathbb{Z} \setminus \{0\}\}$ we have to count at most one z_s for the two elements $(\boldsymbol{h}, h_s)$ and $-(\boldsymbol{h}, h_s)$.

Hence, we have at most

$$\frac{|\{(\boldsymbol{h}, h_s) \in \tilde{I}_{\downarrow s} \setminus \{\mathbf{0}\} : \boldsymbol{h} \in \tilde{I}_{\downarrow s-1} \setminus \{\mathbf{0}\} \text{ and } h_s \in \mathbb{Z} \setminus \{0\}\}|}{2} \tag{3.7}$$

elements of $\{1, \dots, M-1\}$ with

$$\boldsymbol{h} \cdot \boldsymbol{z}^* \equiv -h_s z_s \pmod{M} \text{ for at least one } (\boldsymbol{h}, h_s) \in \tilde{I}_{\downarrow s} \setminus \{\mathbf{0}\}.$$

If the candidate set $\{1, \dots, M-1\}$ for z_s^* contains more elements than (3.7), we can determine at least one z_s^* with

$$\boldsymbol{h} \cdot \boldsymbol{z}^* \not\equiv -h_s z_s^* \pmod{M} \text{ for all } (\boldsymbol{h}, h_s) \in \tilde{I}_{\downarrow s} \setminus \{\mathbf{0}\}.$$

Consequently, the number of elements in $\{1, \dots, M-1\}$ with

$$|\{1, \dots, M-1\}| \geq \frac{|\{(\boldsymbol{h}, h_s) \in \tilde{I}_{\downarrow s} \setminus \{\mathbf{0}\} : \boldsymbol{h} \in \tilde{I}_{\downarrow s-1} \setminus \{\mathbf{0}\} \text{ and } h_s \in \mathbb{Z} \setminus \{0\}\}|}{2} + 1$$

and M is prime guarantees that there exists such a z_s^*. Since we assumed M being prime and

$$\begin{aligned} M &= |\{1, \dots, M-1\}| + 1 \\ &\geq \frac{|\{(\boldsymbol{h}, h_s) \in \tilde{I}_{\downarrow s} \setminus \{\mathbf{0}\} : \boldsymbol{h} \in \tilde{I}_{\downarrow s-1} \setminus \{\mathbf{0}\} \text{ and } h_s \in \mathbb{Z} \setminus \{0\}\}|}{2} + 2 \end{aligned}$$

we can find at least one z_s by testing out all possible candidates $\{1, 2, \dots, M-1\}$. ∎

Theorem 3.2 outlines one step of a component-by-component construction of a rank-1 lattice, guaranteeing the exact integration of trigonometric polynomials with frequencies supported on index sets $\tilde{I}$ which are symmetric to the origin.

We obtain this symmetry of the difference sets $\mathcal{D}(I)_{\downarrow s}$

$$\boldsymbol{h} \in \mathcal{D}(I)_{\downarrow s} \Rightarrow \exists \boldsymbol{k}_1, \boldsymbol{k}_2 \in I_{\downarrow s} \colon \boldsymbol{h} = \boldsymbol{k}_1 - \boldsymbol{k}_2 \Rightarrow -\boldsymbol{h} = \boldsymbol{k}_2 - \boldsymbol{k}_1 \in \mathcal{D}(I)_{\downarrow s}.$$

So, our strategy is to apply Theorem 3.2 to the difference set $\mathcal{D}(I)_{\downarrow s}$ of the frequency index set $I_{\downarrow s}$ for all $2 \leq s \leq d$. In order to use Theorem 3.2, we have to find sufficient conditions on rank-1 lattices of dimension $d = 1$ guaranteeing that $hz_1 \not\equiv 0 \pmod{M}$ for all $h \in \mathcal{D}(I)_{\downarrow 1} \setminus \{0\}$.

Lemma 3.3. *Let $I \subset \mathbb{Z}$ be a one-dimensional frequency index set of finite cardinality and M be a prime number satisfying $M \geq |I|$. Additionally, we assume M and h being coprime for all $h \in \mathcal{D}(I) \setminus \{0\}$. Then we can uniquely reconstruct the Fourier coefficients of all $f \in \Pi_I$ applying the one-dimensional lattice rule given by $\Lambda(1, M)$.*

Proof. Applying the lattice rule given by $\Lambda(1, M)$ to the integrands of the integrals computing the Fourier coefficient $\hat{f}_k$, $k \in I$, of $f \in \Pi_I$, we obtain

$$\begin{aligned}\frac{1}{M} \sum_{j=0}^{M-1} f\left(\frac{j}{M}\right) \mathrm{e}^{-2\pi \mathrm{i} \frac{kj}{M}} &= \frac{1}{M} \sum_{j=0}^{M-1} \sum_{h \in I} \hat{f}_h \mathrm{e}^{2\pi \mathrm{i} \frac{hj}{M}} \mathrm{e}^{-2\pi \mathrm{i} \frac{kj}{M}} \\ &= \frac{1}{M} \sum_{h \in I} \hat{f}_h \sum_{j=0}^{M-1} \mathrm{e}^{2\pi \mathrm{i} \frac{(h-k)j}{M}} = \hat{f}_k = \int_0^1 f(x) \mathrm{e}^{-2\pi \mathrm{i} k x} dx\end{aligned}$$

due to $h - k \in \mathcal{D}(I) \setminus \{0\}$ and M are coprime. ∎

We summarize the results of Theorem 3.2 and Lemma 3.3 and figure out the following

Corollary 3.4. *Let $I \subset \mathbb{Z}^d$ be an arbitrary d-dimensional index set of finite cardinality and M be a prime number satisfying $M \geq M_{\mathrm{lb}}$ with a lower bound*

$$M_{\mathrm{lb}} := \max\left(|I_{\downarrow 1}|, \max_{s=2,\ldots,d} \frac{|\{\boldsymbol{k} \in \mathcal{D}(I)_{\downarrow s} : \boldsymbol{k} = (\boldsymbol{h}, h_s), \boldsymbol{h} \in \mathcal{D}(I)_{\downarrow s-1} \setminus \{\boldsymbol{0}\} \text{ and } h_s \in \mathbb{Z} \setminus \{0\}\}|}{2} + 2\right).$$

In addition, we assume that $M \nmid l$ for all $l \in \{k = \boldsymbol{e}_s \cdot \boldsymbol{h} : \boldsymbol{h} \in \mathcal{D}(I), s = 1, \ldots, d\} \setminus \{0\}$, where $\boldsymbol{e}_s \in \mathbb{N}^d$ is a d-dimensional unit vector with $e_{s,j} = \begin{cases} 0 & \text{for } j \neq s \\ 1 & \text{for } j = s. \end{cases}$. Then, there exists a rank-1 lattice of cardinality M that allows the reconstruction of all trigonometric polynomials with frequencies supported on I by sampling along the rank-1 lattice. Furthermore, once we determined a suitable M the proof of Theorem 3.2 verifies that we can find at least one appropriate generating vector component-by-component. Algorithm 3.3 indicates the corresponding strategy.

The essential part of the last corollary is the lower bound M_{lb} of the prime number M. In order to estimate M from above, we apply some results about the distribution of primes. Thus, the existence of a prime number M with

$$M_{\mathrm{lb}} \leq M \leq \frac{4}{3}(M_{\mathrm{lb}} + 2) \leq \frac{2}{3}(|\mathcal{D}(I)| + 7) \leq \frac{2}{3}(|I|^2 - |I| + 8), \text{ cf. [Loo11, Cor. 2.2]}, \quad (3.8)$$

Algorithm 3.3 Component-by-component lattice search

Input:	$M \in \mathbb{N}$	cardinality of rank-1 lattice
	$I \subset \mathbb{Z}^d$	frequency index set

$\boldsymbol{z} = \emptyset$
for $s = 1, \dots, d$ ***do***
  form the set $I_{\downarrow s}$ as defined in (3.6)
  search for one $z_s \in [1, M-1] \cap \mathbb{Z}$ with $|\{(\boldsymbol{z}, z_s) \cdot \boldsymbol{k} \bmod M : \ \boldsymbol{k} \in I_{\downarrow s}\}| = |I_{\downarrow s}|$
  $\boldsymbol{z} = (\boldsymbol{z}, z_s)$
end for

Output:	$\boldsymbol{z} \in \mathbb{Z}^d$	generating vector

and for $M_{\mathrm{lb}} \geq 396\,738$

$$M_{\mathrm{lb}} \leq M \leq \left(1 + \frac{1}{25 \log^2 M_{\mathrm{lb}}}\right) M_{\mathrm{lb}} \leq 1.00025 M_{\mathrm{lb}} \leq \frac{4\,001}{8\,000}(|\mathcal{D}(I)| + 3) \leq \frac{4\,001}{8\,000}|I|^2, \quad (3.9)$$

cf. [Dus10, Prop. 6.8], is guaranteed. For most specific high-dimensional frequency index sets I, the condition that M is coprime to all components of the elements of the difference set $\mathcal{D}(I)$ is fulfilled a priori, since the embedding $I \subset \boldsymbol{k} + [0, M_{\mathrm{lb}} - 1]^d$ often holds for at least one $\boldsymbol{k} \in \mathbb{Z}^d$. In particular, let us assume that $I \subset \{\boldsymbol{k} + \boldsymbol{h} : \boldsymbol{h} \in [0, M-1]^d\}$ holds for a specific $\boldsymbol{k} \in \mathbb{Z}^d$. Obviously the difference set $\mathcal{D}(I)$ is covered by $[-M+1, M-1]^d$. Accordingly, all prime factors of the absolute value $|l|$ of each number $l \in \{k = \boldsymbol{e}_s \cdot \boldsymbol{h} : \ \boldsymbol{h} \in \mathcal{D}(I), s = 1, \dots, d\} \setminus \{0\} \subset [-M+1, M-1] \setminus \{0\}$ is smaller than the prime number M.

Remark 3.5. Since M is a prime number, we note that each frequency index set $I \subset \mathbb{Z}^d$ which is contained in a d-dimensional cube of edge length $M-1$ a priori fulfills the assumption $M \nmid l$ for all $l \in \{k = \boldsymbol{e}_s \cdot \boldsymbol{h} \in \mathbb{Z} : \ \boldsymbol{h} \in \mathcal{D}(I), s = 1, \dots, d\} \setminus \{0\}$. ■

In the following, we focus on the coprimality condition of M and the components of the difference set $\mathcal{D}(I)$ that we have specified in Theorem 3.2 and Corollary 3.4. The next remark verifies that this sufficient condition on M can not be dropped in general.

Remark 3.6. For arbitrary $d \in \mathbb{N}$ and arbitrary $M' \in \mathbb{N}$ there exist index sets $I \subset \mathbb{Z}^d$ with $|I| = 2$, such that there exists no rank-1 lattice of size $M \leq M'$ allowing a reconstruction of trigonometric polynomials $f \in \Pi_I$.

Proof. We fix $d \in \mathbb{N}$ and $M' \in \mathbb{N}$, define $c := \prod_{\substack{p \leq M' \\ p \text{ prime}}} p^{\lfloor \log_p M' \rfloor}$, and indicate for arbitrary $\boldsymbol{a} \in \mathbb{Z}^d$ and $\boldsymbol{b} \in \mathbb{Z}^d \setminus \{\boldsymbol{0}\}$ the concrete index set $I = \{\boldsymbol{a}, \boldsymbol{a} + c\boldsymbol{b}\} \subset \mathbb{Z}^d$.

Now, we reconstruct the Fourier coefficients of $f(\boldsymbol{x}) = \sum_{\boldsymbol{h} \in I} \hat{f}_{\boldsymbol{h}} \mathrm{e}^{2\pi \mathrm{i} \boldsymbol{h} \cdot \boldsymbol{x}}$ by numerically integrating the function $f_{\boldsymbol{k}} = f(\circ)\mathrm{e}^{-2\pi \mathrm{i} \boldsymbol{k} \cdot \circ}$ by a lattice rule of $M \leq M'$ lattice nodes. We obtain

$$\begin{aligned} Qf_{\boldsymbol{a}} &= \frac{1}{M} \sum_{j=0}^{M-1} f\left(\frac{j\boldsymbol{z}}{M}\right) \mathrm{e}^{-2\pi \mathrm{i} j \frac{\boldsymbol{a} \cdot \boldsymbol{z}}{M}} = \frac{1}{M} \sum_{j=0}^{M-1} \sum_{\boldsymbol{h} \in I} \hat{f}_{\boldsymbol{h}} \prod_{s=1}^{d} \mathrm{e}^{2\pi \mathrm{i} j \frac{(h_s - a_s) z_s}{M}} \\ &= \hat{f}_{\boldsymbol{a}} + \hat{f}_{\boldsymbol{a} + c\boldsymbol{b}} \frac{1}{M} \sum_{j=0}^{M-1} \prod_{s=1}^{d} \mathrm{e}^{2\pi \mathrm{i} j b_s z_s \frac{c}{M}}. \end{aligned}$$

Steps	worst case arithmetic complexity
1. Compute the difference sets $\mathcal{D}(I)_{\downarrow s}$, $s = 1, \dots, d$	$\mathcal{O}\left(\lvert I\rvert^2(d + \log\lvert I\rvert)\right)$
2. Compute M_{lb} as given in Corollary 3.4	$\mathcal{O}\left(d\lvert\mathcal{D}(I)\rvert\right)$
3. Determine the smallest prime $M \geq M_{\mathrm{lb}}$	$\mathcal{O}\left(M_{\mathrm{lb}}/\log\log M_{\mathrm{lb}}\right)$
4. Increase the prime number M as long as $M \mid l$ for at least one $l \in \{k = \boldsymbol{e}_s \cdot \boldsymbol{h} : \boldsymbol{h} \in \mathcal{D}(I), s = 1, \dots, d\} \setminus \{0\}$	$\mathcal{O}\left(d\lvert\mathcal{D}(I)\rvert + L \log L\right)$
5. Search for a suitable generating vector $\boldsymbol{z}$ component–by–component by Algorithm 3.3	$\mathcal{O}\left(d\lvert I\rvert M\right)$
Total:	$\mathcal{O}\left(d\lvert I\rvert(M + \lvert I\rvert \log\lvert I\rvert) + L \log L\right)$

Table 3.1: The five steps of determining reconstructing rank-1 lattices and their arithmetic complexities.

Due to all prime factors of M are also prime factors of $c = \prod_{\substack{p \leq M' \\ p \text{ prime}}} p^{\lfloor \log_p M' \rfloor}$, we know $\frac{c}{M} \in \mathbb{Z} \setminus \{0\}$. This yields

$$Qf_{\boldsymbol{a}} = \hat{f}_{\boldsymbol{a}} + \hat{f}_{\boldsymbol{a}+c\boldsymbol{b}} = Qf_{\boldsymbol{a}+c\boldsymbol{b}}$$

and we cannot reconstruct the Fourier coefficients of $f \in \Pi_I$ uniquely. ■

Nevertheless, we indicate a strategy that determines reconstructing rank-1 lattices for arbitrary frequency index sets $I \subset \mathbb{Z}^d$ of finite cardinality and analyze the arithmetical complexities of each step in the following. To this end, we additionally determine the numbers

$$k_s^{\max} = \max\{\boldsymbol{k} \cdot \boldsymbol{e}_s : \boldsymbol{k} \in I\} \quad \text{and} \quad k_s^{\min} = \min\{\boldsymbol{k} \cdot \boldsymbol{e}_s : \boldsymbol{k} \in I\} \quad \text{for } s = 1, \dots, d,$$

and

$$L = \max_{s=1,\dots,d} (k_s^{\max} - k_s^{\min}). \tag{3.10}$$

Hence, we obtain the embeddings $I \subset \{\boldsymbol{k}^{\min} + \boldsymbol{h} : \boldsymbol{h} \in [0, L]^d \cap \mathbb{Z}^d\}$ and $\mathcal{D}(I) \subset [-L, L]^d$. We give a short explanation on the complexities given in the listing of Table 3.1.

The first step is the computation of the difference sets $\mathcal{D}(I)_{\downarrow s}$. In detail, we compute the difference set $\mathcal{D}(I) = \mathcal{D}(I)_{\downarrow d}$ using Algorithm 3.4 in a naive way. The computation of all elements $\boldsymbol{h} = \boldsymbol{k}_j - \boldsymbol{k}_l$ has a complexity bounded by $Cd|I|^2$. Since the $\mathcal{D}(I)$ is a set, duplicates must be recognized and eliminated. In principle, one uses a sorted list in order to store the set $\mathcal{D}(I)$. In addition one can store a whole bunch of $\boldsymbol{h}$'s in a sorted block and insert them in one go. The computation of $\mathcal{D}(I)_{\downarrow s}$, $s < d$, is then a simple projection on the first s variables, i.e., we drop the last $d - s$ components of all elements $\boldsymbol{h} \in \mathcal{D}(I)$ and eliminate all duplicates. This approach can be done for $s = d - 1$ down to 1 using the recurrence $\mathcal{D}(I)_{\downarrow s} = \left\{(\boldsymbol{h})_{l=1}^{s} : \boldsymbol{h} \in \mathcal{D}(I)_{\downarrow s+1}\right\}$. Consequently, the arithmetic complexity of the first step is bounded by $\mathcal{O}\left(|I|^2(d + \log|I|)\right)$.

In order to compute M_{lb} as given in Corollary 3.4, we have to count the elements of $I_{\downarrow 1}$, which is in principle the projection of the frequency index set I on its first dimension and one of the inexpensive computations here. Furthermore, we have to take a look at each vector

Algorithm 3.4 Computation of the difference set

Input: $I \subset \mathbb{Z}^d$ frequency index set

$\mathcal{D}(I) = \{\mathbf{0}\}$
for $j = 1, \ldots, |I|$ ***do***
  for $l = j+1, \ldots, |I|$ ***do***
    $\boldsymbol{h} = \boldsymbol{k}_j - \boldsymbol{k}_l$
    $\mathcal{D}(I) = \mathcal{D}(I) \cup \{\boldsymbol{h}, -\boldsymbol{h}\}$
  end for
end for

Output: $\mathcal{D}(I)$ difference set of the frequency index set I

of integers $\boldsymbol{h} \in \mathcal{D}(I)_{\downarrow s}$, $s = 2, \ldots, d$ and have to count all these vectors having the special property $\boldsymbol{h} \in \{\boldsymbol{k} \in \mathcal{D}(I)_{\downarrow s} : \boldsymbol{k} = (\boldsymbol{l}, l_s), \boldsymbol{l} \in \mathcal{D}(I)_{\downarrow s-1} \setminus \{\mathbf{0}\} \text{ and } l_s \in \mathbb{Z} \setminus \{0\}\}$. In the worst case, we obtain $\mathcal{D}(I)_{\downarrow 2} \lesssim \mathcal{D}(I)_{\downarrow 3} \lesssim \ldots \lesssim \mathcal{D}(I)_{\downarrow d}$. Accordingly, the upper bound on the arithmetic complexity of the second step is $\mathcal{O}\left(d|\mathcal{D}(I)|\right)$.

Due to Bertrand's postulate or Equations (3.8) and (3.9), the smallest prime number not smaller than M_{lb} is smaller than $2M_{\mathrm{lb}}$. Using one of the prime sieves presented in [AB04], one determines the smallest prime M not smaller than M_{lb} in $\mathcal{O}\left(M_{\mathrm{lb}}/\log\log M_{\mathrm{lb}}\right)$ arithmetic operations in the third step.

The computational effort of step four mainly depends on the structure of the frequency index set I. Next, we determine the set $\mathcal{K}(I) := \{k = \boldsymbol{e}_s \cdot \boldsymbol{h} : \boldsymbol{h} \in \mathcal{D}(I), s = 1, \ldots, d\} \setminus \{0\} \subset \{-L, \ldots, L\}$, cf. (3.10). All elements $k \in \mathcal{K}(I)$ with $|k| < M$ are not of our interest since those k fulfill $M' \nmid k$ for all numbers $M' > M$, $M' \in \mathbb{N}$, a priori. Accordingly, we sort all elements of $\mathcal{K}(I, M) := \{k = |\boldsymbol{e}_s \cdot \boldsymbol{h}| : \boldsymbol{h} \in \mathcal{D}(I), s = 1, \ldots, d\} \setminus \{0, \ldots, M-1\}$ and compute a sorted list of all prime numbers starting with M up to the smallest prime number larger than L. Now, we pass sequentially through these two sorted lists and determine the smallest prime that is not contained in $\mathcal{K}(I, M)$. The corresponding arithmetic complexity is bounded by the complexity of the computation of $\mathcal{K}(I)$, which is in $\mathcal{O}\left(d|\mathcal{D}(I)|\right)$, and the sorting of the list containing the elements of $\mathcal{K}(I, M)$ and the list of the prime numbers from M up to L, which is in $\mathcal{O}\left(L \log L\right)$.

Once, we determined an M fulfilling all requirements of Corollary 3.4, we proved that Algorithm 3.3 determines a generating vector $\boldsymbol{z}$, such that $\Lambda(\boldsymbol{z}, M)$ is a reconstructing rank-1 lattice for the frequency index set I, i.e., $\Lambda(\boldsymbol{z}, M) = \Lambda(\boldsymbol{z}, M, I)$. For each dimension $s = 2, \ldots, d$, we search for a number z_s within the set $\{1, \ldots, M-1\}$. Using the buffered scalar products $(h_l)_{l=1}^{s} \cdot (z_l)_{l=1}^{s}$, the computational costs for each s is bounded by $C|I|M$, and, hence, the fifth step of our strategy has an arithmetic complexity of $\mathcal{O}\left(d|I|M\right)$.

The total complexity of all steps together is bounded by $\mathcal{O}\left(d|I|(M + |I|\log|I|) + L\log L\right)$, where M mainly depends on the structure of the frequency index set I and its difference set $\mathcal{D}(I)$ and on L, which itself depends on the expansion of the frequency index set I. In higher dimensions, one often considers frequency index sets I, that are contained in a d-dimensional box of edge length $|I|$, i.e., $L \leq |I|$. In that cases, we know a priori that $L \leq |I| \leq M$ and the fourth step is not needed. The corresponding arithmetic complexity reduces to $\mathcal{O}\left(d|I|(M + |I|\log|I|)\right)$, where M is bounded by the terms given in (3.8) or (3.9). Thus, we estimate $d|I|^2 \log|I| \lesssim d|I|(M + |I|\log|I|) \lesssim d|I|^3$.

Anyway, once one has discovered a reconstructing rank-1 lattice $\Lambda(\boldsymbol{z}, M, I)$ for the fre-

Algorithm 3.5 Lattice size decreasing

Input:	$I \subset \mathbb{Z}^d$	frequency index set
	$M \in \mathbb{N}$	cardinality of rank-1 lattice
	$\boldsymbol{z} \in \mathbb{N}^d$	$\Lambda(\boldsymbol{z}, M, I)$ is reconstructing rank-1 lattice for I

for $j = |I|, \ldots, M$ ***do***
  if $|\{\boldsymbol{z} \cdot \boldsymbol{k} \bmod j : \ \boldsymbol{k} \in I\}| = |I|$ ***then***
    $M_{\min} = j$
    break
  end if
end for

Output:	$M_{\min}$	reduced lattice size

quency index set I, the condition

$$\boldsymbol{k} \cdot \boldsymbol{z} \neq \boldsymbol{h} \cdot \boldsymbol{z} \qquad \text{for all} \quad \boldsymbol{k} \neq \boldsymbol{h};\ \boldsymbol{k}, \boldsymbol{h} \in I,$$

holds and one can ask for $M' < M$ fulfilling

$$\boldsymbol{k} \cdot \boldsymbol{z} \not\equiv \boldsymbol{h} \cdot \boldsymbol{z} \pmod{M'} \qquad \text{for all} \quad \boldsymbol{k} \neq \boldsymbol{h};\ \boldsymbol{k}, \boldsymbol{h} \in I.$$

For a fixed frequency index set I and a fixed generating vector $\boldsymbol{z}$ we assume the rank-1 lattice $\Lambda(\boldsymbol{z}, M, I)$ being a reconstructing rank-1 lattice. Then, Algorithm 3.5 computes the smallest lattice size $M_{\min}$ guaranteeing the reconstruction property of the rank-1 lattice $\Lambda(\boldsymbol{z}, M_{\min}, I)$. We obtain an arithmetic complexity of Algorithm 3.5 in the order of $|I|(d + M)$ in the worst case.

Relationship to Lattice Rules Used for Numerical Integration

The final point in this section connects our results in Theorem 3.2 and Corollary 3.4 to known results for numerical integration. In particular, one is mainly interested in lattice rules that exactly integrates all trigonometric polynomials $f \in \Pi_I$ of a specific trigonometric degree, cf. [Zar72, CR97, CKN10], i.e., the frequency index set I has a specific structure. The paper of R. Cools, F. Kuo, and D. Nuyens [CKN10] treats the most popular definitions of even weighted trigonometric degrees, namely the weighted trigonometric degree ($I = I^{d,\boldsymbol{\gamma}}_{1,N}$), the weighted product trigonometric degree ($I = I^{d,\boldsymbol{\gamma}}_{\infty,N}$), and the weighted Zaremba cross degree ($I = I^{d,\boldsymbol{\gamma}}_{\mathrm{hc},N}$). Theorem 3.2 and Corollary 3.4 are essentially based on the ideas that they used in order to determine rank-1 lattices that exactly integrates the trigonometric polynomials of the mentioned trigonometric degrees.

Our considerations allow us to extend their results for more general frequency index sets I. To this end, we take Theorem 3.2 and Corollary 3.4 into account and formulate some facts about lattice rules that have a generalized trigonometric degree of exactness in the following sense. We consider the space of trigonometric polynomials Π_I, where the frequency index set I has finite cardinality. By definition, the rank-1 lattice $\Lambda(\boldsymbol{z}, M)$ has the generalized trigonometric degree of exactness I, iff the lattice rule given by $\Lambda(\boldsymbol{z}, M)$ integrates exactly all trigonometric polynomials supported on I. Then, Theorem 3.2, Corollary 3.4, and Equations (3.8) and (3.9) verify the next

Remark 3.7. Let the frequency index set $I \subset \mathbb{Z}^d$ be a frequency index set that is symmetric to the origin and contained in $[-|I|/4, |I|/4]^d$. Then, there exists a rank-1 lattice of size $M \leq C|I|$ that has a trigonometric degree of exactness I and the generating vector can be determined using a component–by–component approach. In detail, the constant C is less than 1 for $|I| > 14$ and is close to $\frac{1}{2}$ for large cardinalities $|I|$. ■

Due to the results of S. M. Ermakov, see [Erm75, Chapter IV], for each frequency index set $I \subset \mathbb{Z}^d$, $|I| < \infty$, there exist sampling sets $\mathcal{X} \subset \mathbb{T}^d$, $|\mathcal{X}| \leq |\Pi_I| = |I|$, such that a corresponding suitable cubature formula is exact for all trigonometric polynomials from Π_I. Actually, at least for frequency index sets I that are symmetric to the origin and contained in a suitably small box, we can find rank-1 lattices of a size M smaller or equal $|I|$ and use the corresponding lattice rules in order to integrate exactly all elements of Π_I. We stress the fact that these rank-1 lattices can be found by adapting our component–by–component approach. In detail, we have to search generating vectors $\boldsymbol{z}$ in Algorithm 3.3 such that the equivalences of the scalar products $\boldsymbol{k} \cdot \boldsymbol{z} \not\equiv 0 \pmod{M}$ hold for all $\boldsymbol{k} \in I \setminus \{\boldsymbol{0}\}$.

3.3 Stability

In this section, we analyze the stability of our sampling method. In other words, we determine the condition number

$$\operatorname{cond}_2(\boldsymbol{A}^*\boldsymbol{A}) = \frac{\lambda_{\max}(\boldsymbol{A}^*\boldsymbol{A})}{\lambda_{\min}(\boldsymbol{A}^*\boldsymbol{A})}$$

of the matrices $\boldsymbol{A}^*\boldsymbol{A}$, where $\boldsymbol{A} = \left(\mathrm{e}^{2\pi \mathrm{i} j \frac{\boldsymbol{k}\cdot\boldsymbol{z}}{M}}\right)_{j=0,\ldots,M-1;\, \boldsymbol{k}\in I}$ is the Fourier matrix given by the frequency index set I and the rank-1 lattice $\Lambda(\boldsymbol{z}, M)$, and $\lambda_{\max}(\boldsymbol{A}^*\boldsymbol{A})$ and $\lambda_{\min}(\boldsymbol{A}^*\boldsymbol{A})$ are the maximal and minimal eigenvalues of the matrix $\boldsymbol{A}^*\boldsymbol{A}$. The condition number of the matrix $\boldsymbol{A}^*\boldsymbol{A}$ is finite iff the matrix $\boldsymbol{A}$ has full column rank, i.e., all singular values of the matrix $\boldsymbol{A}$ are positive real numbers and, in other words, all eigenvalues of the self-adjoint matrix $\boldsymbol{A}^*\boldsymbol{A}$ are positive real numbers. The next theorem determines eigenvalues of the matrix $\boldsymbol{A}^*\boldsymbol{A}$. In principle, we obtain two different cases depending on the reconstruction property of the rank-1 lattice $\Lambda(\boldsymbol{z}, M)$ with respect to I. On the one hand, all eigenvalues of $\boldsymbol{A}^*\boldsymbol{A}$ are equal to M iff $\Lambda(\boldsymbol{z}, M)$ is a reconstructing rank-1 lattice for I, i.e., $\Lambda(\boldsymbol{z}, M, I) = \Lambda(\boldsymbol{z}, M)$. On the other hand, there exist zero valued eigenvalues of $\boldsymbol{A}^*\boldsymbol{A}$ iff $\Lambda(\boldsymbol{z}, M)$ is not a reconstructing rank-1 lattice for I and, thus, the matrix $\boldsymbol{A}^*\boldsymbol{A}$ is not of full rank, the condition number is infinite, and we call the Fourier transform given by the matrix $\boldsymbol{A}$ unstable.

Theorem 3.8. *Let the dimension $d \in \mathbb{N}$, $I \subset \mathbb{Z}^d$ be an arbitrary frequency index set of finite cardinality, and $\Lambda(\boldsymbol{z}, M)$ be a rank-1 lattice. Then the matrix $\boldsymbol{A} = \left(\mathrm{e}^{2\pi \mathrm{i} j \frac{\boldsymbol{k}\cdot\boldsymbol{z}}{M}}\right)_{j=0,\ldots,M-1;\, \boldsymbol{k}\in I}$ has either*

- *orthogonal columns, i.e., we obtain $\boldsymbol{A}^*\boldsymbol{A} = M\boldsymbol{I}$ and $\Lambda(\boldsymbol{z}, M)$ is a reconstructing rank-1 lattice,*

or

- *the matrix $\boldsymbol{A}^*\boldsymbol{A}$ is not of full rank, i.e., the smallest eigenvalue $\lambda_{\min}(\boldsymbol{A}^*\boldsymbol{A})$ of $\boldsymbol{A}^*\boldsymbol{A}$ is zero.*

Proof. Analogous to the proof of Lemma 3.1, we consider the elements of the matrix $\boldsymbol{A}^*\boldsymbol{A}$ and obtain

$$(\boldsymbol{A}^*\boldsymbol{A})_{\boldsymbol{l},\boldsymbol{k}} = \sum_{j=0}^{M-1} \mathrm{e}^{2\pi \mathrm{i} j \frac{(\boldsymbol{k}-\boldsymbol{l})\cdot\boldsymbol{z}}{M}} = \begin{cases} M & \text{for } \boldsymbol{k}\cdot\boldsymbol{z} \equiv \boldsymbol{l}\cdot\boldsymbol{z} \pmod{M}, \\ 0 & \text{else.} \end{cases}$$

We obtain $\boldsymbol{k}\cdot\boldsymbol{z} \not\equiv \boldsymbol{l}\cdot\boldsymbol{z} \pmod{M}$ for all $\boldsymbol{k},\boldsymbol{l} \in I$, $\boldsymbol{k} \neq \boldsymbol{l}$, iff $\Lambda(\boldsymbol{z}, M)$ is a reconstructing rank-1 lattice.

On the other hand, let us assume that there exists a pair $\boldsymbol{k}_1, \boldsymbol{k}_2 \in I$, $\boldsymbol{k}_1 \neq \boldsymbol{k}_2$, that fulfills $\boldsymbol{k}_1\cdot\boldsymbol{z} \equiv \boldsymbol{k}_2\cdot\boldsymbol{z} \pmod{M}$. Then, the rank-1 lattice $\Lambda(\boldsymbol{z}, M)$ is no reconstructing rank-1 lattice for I and we determine equality of the $\boldsymbol{k}_1$th and the $\boldsymbol{k}_2$th rows and, hence, the smallest eigenvalue of $\boldsymbol{A}^*\boldsymbol{A}$ is zero. ∎

The last theorem justified, that we have to deal with reconstructing rank-1 lattices in order to obtain stable discrete Fourier transforms that use rank-1 lattices as spatial discretizations. In detail, the corresponding discrete Fourier transforms have the minimal condition number 1 and we call the transforms perfectly stable.

Corollary 3.9. *Let the dimension $d \in \mathbb{N}$, $I \subset \mathbb{Z}^d$ an arbitrary frequency index set of finite cardinality, and $\Lambda(\boldsymbol{z}, M, I)$ a reconstructing rank-1 lattice for I. The corresponding discrete Fourier transform is well-conditioned, in particular the condition number $\mathrm{cond}_2(\boldsymbol{A})$ of the Fourier matrix $\boldsymbol{A} = \left(\mathrm{e}^{2\pi \mathrm{i} j \frac{\boldsymbol{k}\cdot\boldsymbol{z}}{M}}\right)_{j=0,\ldots,M-1;\, \boldsymbol{k}\in I}$ fulfills*

$$\mathrm{cond}_2(\boldsymbol{A}) = \frac{\sigma_{\max}(\boldsymbol{A})}{\sigma_{\min}(\boldsymbol{A})} = 1.$$

In this sense the problem is perfectly stable. Here, $\sigma_{\min}(\boldsymbol{A})$ and $\sigma_{\max}(\boldsymbol{A})$ denotes the minimal and the maximal singular value of $\boldsymbol{A}$, respectively.

Proof. Due to

$$\sigma_{\max}(\boldsymbol{A}) = \sqrt{\lambda_{\max}(\boldsymbol{A}^*\boldsymbol{A})} = \sqrt{\lambda_{\max}(M\boldsymbol{I})} = \sqrt{M} = \sqrt{\lambda_{\min}(\boldsymbol{A}^*\boldsymbol{A})} = \sigma_{\min}(\boldsymbol{A})$$

with $\lambda_{\min}(\boldsymbol{A}^*\boldsymbol{A})$ and $\lambda_{\max}(\boldsymbol{A}^*\boldsymbol{A})$ the minimal and maximal eigenvalue of $\boldsymbol{A}^*\boldsymbol{A}$, we obtain the assertion from above. ∎

We showed in Section 3.1, that the evaluation of multivariate trigonometric polynomials along rank-1 lattices leads to a one-dimensional discrete Fourier transform of the length of the used rank-1 lattice. In advance of this one-dimensional DFT we have to compute the corresponding Fourier coefficients using the formula $\hat{g}_l = \sum_{\substack{\boldsymbol{k}\in I \\ \boldsymbol{k}\cdot\boldsymbol{z}\equiv l \bmod M}} \hat{f}_{\boldsymbol{k}}$, $l = 0,\ldots,M-1$. Due to this aliasing formula, we may not be able to reconstruct trigonometric polynomials supported on the frequency index set I. In detail, if we consider a rank-1 lattice $\Lambda(\boldsymbol{z}, M)$ that has not the reconstruction property with respect to the considered frequency index set I, we obtain at least one $l_0 \in \{0,\ldots,M-1\}$ such that $|\boldsymbol{k} \in I\colon \boldsymbol{k}\cdot\boldsymbol{z} \equiv l_0 \bmod M| > 1$ and we cannot reconstruct the summands of $\hat{g}_l = \sum_{\substack{\boldsymbol{k}\in I \\ \boldsymbol{k}\cdot\boldsymbol{z}\equiv l \bmod M}} \hat{f}_{\boldsymbol{k}}$. Hence, we have a Fourier matrix $\boldsymbol{A}$ that is not of full column rank, the condition number is given by $\mathrm{cond}_2(\boldsymbol{A}) = \infty$, and a unique reconstruction of all $f \in \Pi_I$ is impossible.

Using reconstructing rank-1 lattices, we guarantee that the mapping $I \to \{0,\ldots,M-1\}$, $\boldsymbol{k} \mapsto \boldsymbol{k}\cdot\boldsymbol{z} \pmod{M}$ is an injective one. As a consequence, the computation of the one-dimensional Fourier coefficients $\hat{g}_l$, $l = 0,\ldots,M-1$, is in principle a permutation of the

multi-dimensional Fourier coefficients $\hat{f}_{\boldsymbol{k}}$, $\boldsymbol{k} \in I$, which is perfectly stable. Accordingly, this permutation and a subsequently applied one-dimensional equispaced discrete Fourier transform yield a perfectly stable strategy in order to compute the multi-dimensional discrete Fourier transform.

We would like to stress that sampling multivariate trigonometric polynomials along reconstructing rank- 1 lattices leads to a perfectly stable Fourier transform similar to the discrete Fourier transform on full multi-dimensional grids, cf. Lemma 2.4.

3.4 Approximation of Multivariate Periodic Functions

For $M \in \mathbb{N}$ we consider the rank-1 lattice $\Lambda(\boldsymbol{z}, M)$ with generating vector $\boldsymbol{z} \in \mathbb{Z}^d$. We call the set

$$\Lambda^{\perp}(\boldsymbol{z}, M) := \{\boldsymbol{k} \in \mathbb{Z}^d : \boldsymbol{k} \cdot \boldsymbol{z} \equiv 0 \pmod{M}\} \tag{3.11}$$

the *integer dual lattice* of $\Lambda(\boldsymbol{z}, M)$.

Approximating functions using trigonometric polynomials computed from sampling values along a rank-1 lattice is closely connected with the integer dual lattice and a corresponding aliasing of the Fourier coefficients of the approximated function. So, let us approximate the $\boldsymbol{k}$th Fourier coefficient $\hat{f}_{\boldsymbol{k}}$ of an arbitrary continuous function $f \in \mathcal{A}(\mathbb{T}^d) \cap \mathcal{C}(\mathbb{T}^d)$ that belongs to the Wiener algebra from the sampling values at a rank-1 lattice $\Lambda(\boldsymbol{z}, M)$. We compute the approximation of the Fourier coefficients $\hat{f}_{\boldsymbol{k}}$ using the lattice rule given by $\Lambda(\boldsymbol{z}, M)$ in the following way:

$$\begin{aligned}\hat{\tilde{f}}_{\boldsymbol{k}} &:= \frac{1}{M} \sum_{j=0}^{M-1} f\left(\frac{j\boldsymbol{z}}{M}\right) \mathrm{e}^{-2\pi \mathrm{i} j \frac{\boldsymbol{k}\cdot\boldsymbol{z}}{M}} = \frac{1}{M} \sum_{j=0}^{M-1} \sum_{\boldsymbol{h}\in\mathbb{Z}^d} \hat{f}_{\boldsymbol{h}} \mathrm{e}^{2\pi \mathrm{i} j \frac{(\boldsymbol{h}-\boldsymbol{k})\cdot\boldsymbol{z}}{M}} \\ &= \sum_{\boldsymbol{h}\in\mathbb{Z}^d} \hat{f}_{\boldsymbol{k}+\boldsymbol{h}} \frac{1}{M} \sum_{j=0}^{M-1} \mathrm{e}^{2\pi \mathrm{i} j \frac{\boldsymbol{h}\cdot\boldsymbol{z}}{M}} = \sum_{\boldsymbol{h}\in\Lambda^{\perp}(\boldsymbol{z},M)} \hat{f}_{\boldsymbol{k}+\boldsymbol{h}}.\end{aligned}$$

Obviously we obtain $\boldsymbol{0} \in \Lambda^{\perp}(\boldsymbol{z}, M)$ and, accordingly,

$$\hat{\tilde{f}}_{\boldsymbol{k}} = \hat{f}_{\boldsymbol{k}} + \sum_{\boldsymbol{h}\in\Lambda^{\perp}(\boldsymbol{z},M)\setminus\{\boldsymbol{0}\}} \hat{f}_{\boldsymbol{k}+\boldsymbol{h}}. \tag{3.12}$$

The absolute convergence of the series of the Fourier coefficients of f allows for the calculations of the last lines. We call $\hat{\tilde{f}}_{\boldsymbol{k}}$ the approximated Fourier coefficients of f. Furthermore, we name equation (3.12) *aliasing formula for the rank-1 lattice* $\Lambda(\boldsymbol{z}, M)$. The corresponding fast computation of all $\hat{\tilde{f}}_{\boldsymbol{k}}$, $\boldsymbol{k} \in I$, can be realized using Algorithm 3.2 where we input the lattice size M, the generating vector $\boldsymbol{z}$, the frequency index set I, and the vector of sampling values $\boldsymbol{f} = \left(f\left(\frac{j\boldsymbol{z}}{M} \bmod \boldsymbol{1}\right)\right)_{j=0}^{M-1}$. We emphasize that the vector $\boldsymbol{f}$ contains function values of a function f that may not be a trigonometric polynomial supported on the frequency index set I, i.e., $f \notin \Pi_I$. In fact, Algorithm 3.2 expects function values from trigonometric polynomials with frequencies supported on the index set I. Nevertheless, Algorithm 3.2 computes the approximated Fourier coefficients $\hat{\tilde{f}}_{\boldsymbol{k}}$, $\boldsymbol{k} \in I$, as given in (3.12). In particular, Algorithm 3.2 calculates the unique solution $\hat{\tilde{\boldsymbol{f}}} = \left(\hat{\tilde{f}}_{\boldsymbol{k}}\right)_{\boldsymbol{k}\in I}$ of the normal equation $\boldsymbol{A}^* \boldsymbol{A} \hat{\tilde{\boldsymbol{f}}} = \boldsymbol{A}^* \boldsymbol{f}$ if $\Lambda(\boldsymbol{z}, M)$ is a reconstructing rank-1 lattice for I.

An error analysis, which is based on a given rank-1 lattice $\Lambda(\boldsymbol{z}, M)$ and a given weight function ω, has been presented by D. Li and F. J. Hickernell in [LH03]. They gave an approximation error, depending on the aliasing formula, cf. (3.12), for the given rank-1 lattice $\Lambda(\boldsymbol{z}, M)$, i.e., one can measure the quality of a given rank-1 lattice but has no constructive way in order to determine rank-1 lattices of high quality. In contrast to their approach, we fix an arbitrary weight function ω construct the frequency index set $I_N := \{\boldsymbol{k} \in \mathbb{Z}^d \colon \omega(\boldsymbol{k}) \leq N\}$, $|I_N| < \infty$, and a suitable reconstructing rank-1 lattice $\Lambda(\boldsymbol{z}, M, I_N)$ which is well adapted for the frequency index set I_N. The resulting approximation property of our strategy depends mainly on the frequency index set I_N and the reconstruction property of the rank-1 lattice $\Lambda(\boldsymbol{z}, M, I_N)$ and not on the concrete generating vector $\boldsymbol{z}$ and the lattice size M.

We prepare the theorem that discusses the approximation properties of our method and show the relation between the frequency index set I and the dual lattice $\Lambda^\perp(\boldsymbol{z}, M, I)$ of a reconstructing rank-1 lattice $\Lambda(\boldsymbol{z}, M, I)$.

Lemma 3.10. *Let $I \subset \mathbb{Z}^d$ be an arbitrary index set of finite cardinality and $\Lambda(\boldsymbol{z}, M, I)$ a corresponding reconstructing rank-1 lattice. Then the following inclusion holds*

$$\{\boldsymbol{k} + \boldsymbol{h} : \boldsymbol{k} \in I, \boldsymbol{h} \in \Lambda^\perp(\boldsymbol{z}, M, I) \setminus \{\boldsymbol{0}\}\} \subset \mathbb{Z}^d \setminus I.$$

Proof. Let us assume that there exist $\boldsymbol{k} \in I$ and $\boldsymbol{h} \in \Lambda^\perp(\boldsymbol{z}, M, I) \setminus \{\boldsymbol{0}\}$ such that $\boldsymbol{k} + \boldsymbol{h} \in I$. Due to $\Lambda(\boldsymbol{z}, M, I)$ is a reconstructing rank-1 lattice for I and $\boldsymbol{0} \neq \boldsymbol{h} = (\boldsymbol{k} + \boldsymbol{h}) - \boldsymbol{k} \in \mathcal{D}(I) \cap \Lambda^\perp(\boldsymbol{z}, M, I) \setminus \{\boldsymbol{0}\}$ we are in contradiction with $\boldsymbol{l} \cdot \boldsymbol{z} \not\equiv 0 \mod M$ for all $\boldsymbol{l} \in \mathcal{D}(I) \setminus \{\boldsymbol{0}\}$. Accordingly the assertion holds. ∎

A first approximation result is given in the next theorem.

Theorem 3.11. *Let the function f belonging to the weighted function space $\mathcal{A}_\omega(\mathbb{T}^d)$, i.e., $f \in \mathcal{A}_\omega(\mathbb{T}^d)$, cf. (2.9), and the frequency index set $I_N = \{\boldsymbol{k} \in \mathbb{Z}^d : \omega(\boldsymbol{k}) \leq N\}$ of finite cardinality be given. Additionally, we assume that $\Lambda(\boldsymbol{z}, M, I_N)$ is a reconstructing rank-1 lattice for I_N. Then we estimate the error of the approximation*

$$\tilde{S}_{I_N} f(\boldsymbol{x}) = \sum_{\boldsymbol{k} \in I_N} \hat{\tilde{f}}_{\boldsymbol{k}} \mathrm{e}^{2\pi \mathrm{i} \boldsymbol{k} \boldsymbol{x}}, \quad \hat{\tilde{f}}_{\boldsymbol{k}} = \sum_{j=0}^{M-1} f\left(\frac{j\boldsymbol{z}}{M}\right) \mathrm{e}^{-2\pi \mathrm{i} j \frac{\boldsymbol{k} \cdot \boldsymbol{z}}{M}}, \boldsymbol{k} \in I_N, , \tag{3.13}$$

of f by

$$\|f - \tilde{S}_{I_N} f | L_\infty(\mathbb{T}^d)\| \leq 2N^{-1} \|f | \mathcal{A}_\omega(\mathbb{T}^d)\|. \tag{3.14}$$

Proof. We split up the estimation in two parts using the triangle inequality

$$\|f - \tilde{S}_{I_N} f | L_\infty(\mathbb{T}^d)\| \leq \|f - S_{I_N} f | L_\infty(\mathbb{T}^d)\| + \|\tilde{S}_{I_N} f - S_{I_N} f | L_\infty(\mathbb{T}^d)\|.$$

Lemma 2.2 yields

$$\|f - S_{I_N} f | L_\infty(\mathbb{T}^d)\| \leq N^{-1} \|f | \mathcal{A}_\omega(\mathbb{T}^d)\|$$

and we only have to treat the second summand using (3.12)

$$\begin{aligned} \|\tilde{S}_{I_N} f - S_{I_N} f | L_\infty(\mathbb{T}^d)\| &= \operatorname{ess\,sup}_{\boldsymbol{x} \in \mathbb{T}^d} \left| \sum_{\boldsymbol{k} \in I_N} (\hat{\tilde{f}}_{\boldsymbol{k}} - \hat{f}_{\boldsymbol{k}}) \mathrm{e}^{2\pi \mathrm{i} \boldsymbol{k} \cdot \boldsymbol{x}} \right| \\ &\leq \sum_{\boldsymbol{k} \in I_N} \left| \sum_{\boldsymbol{h} \in \Lambda^\perp(\boldsymbol{z}, M) \setminus \{\boldsymbol{0}\}} \hat{f}_{\boldsymbol{k} + \boldsymbol{h}} \right| \leq \sum_{\boldsymbol{k} \in I_N} \sum_{\boldsymbol{h} \in \Lambda^\perp(\boldsymbol{z}, M) \setminus \{\boldsymbol{0}\}} \left| \hat{f}_{\boldsymbol{k} + \boldsymbol{h}} \right|. \end{aligned}$$

Due to Lemma 3.10 we estimate

$$\begin{aligned}\|\tilde{S}_{I_N} f - S_{I_N} f | L_\infty(\mathbb{T}^d)\| &\leq \sum_{\boldsymbol{k}\in\mathbb{Z}^d\setminus I_N} \left|\hat{f}_{\boldsymbol{k}}\right| \leq \frac{1}{\inf_{\boldsymbol{h}\in\mathbb{Z}^d\setminus I_N} \omega(\boldsymbol{h})} \sum_{\boldsymbol{k}\in\mathbb{Z}^d} \omega(\boldsymbol{k}) \left|\hat{f}_{\boldsymbol{k}}\right| \\ &\leq N^{-1} \|f|\mathcal{A}_\omega(\mathbb{T}^d)\|\end{aligned}$$

and obtain the assertion. ∎

Theorem 3.11 states, that the worst case error of an approximation $\tilde{S}_{I_N} f$ of the function f, which is the Fourier partial sum given by the approximated Fourier coefficients that are computed from samples along a reconstructing rank-1 lattice $\Lambda(\boldsymbol{z}, M, I_N)$, is almost as good as the worst case error of the approximation $S_{I_N} f$, which is the exact Fourier partial sum.

We stress the fact that the approximation properties mainly depends on the norms one considers. In particular, we focus on the $L_\infty(\mathbb{T}^d)$-norm on the left hand side and the weighted ℓ_1-norm of the Fourier coefficients on the right hand side.

Remark 3.12. Some more specific results, additionally concerning a Hilbert space setting of particular interest, cf. [GH14], can be found in [KPV13] and [KPV14]. In [KPV13] we focussed on the approximation of functions belonging to the subspace of the Wiener algebra $\mathcal{A}(\mathbb{T}^d)$

$$\mathcal{A}^{\alpha,\beta,\boldsymbol{\gamma}}(\mathbb{T}^d) := \mathcal{A}_{\omega_{\mathrm{ehc}}^{d,\boldsymbol{\gamma},\alpha,\beta}}(\mathbb{T}^d) := \left\{ f \in \mathcal{A}(\mathbb{T}^d) \cap \mathcal{C}(\mathbb{T}^d) \colon \|f|\mathcal{A}_{\omega_{\mathrm{ehc}}^{d,\boldsymbol{\gamma},\alpha,\beta}}(\mathbb{T}^d)\| := \sum_{\boldsymbol{k}\in\mathbb{Z}^d} (\omega_{\mathrm{ehc}}^{d,\boldsymbol{\gamma},\alpha,\beta}(\boldsymbol{k}))^{\alpha+\beta} |\hat{f}_{\boldsymbol{k}}| < \infty \right\}$$

or the Hilbert space

$$\mathcal{H}^{\alpha,\beta,\boldsymbol{\gamma}}(\mathbb{T}^d) := \mathcal{H}_{\omega_{\mathrm{ehc}}^{d,\boldsymbol{\gamma},\alpha,\beta}}(\mathbb{T}^d) := \left\{ f \in L_1(\mathbb{T}^d) \colon \|f|\mathcal{H}_{\omega_{\mathrm{ehc}}^{d,\boldsymbol{\gamma},\alpha,\beta}}(\mathbb{T}^d)\| := \sqrt{\sum_{\boldsymbol{k}\in\mathbb{Z}^d} (\omega_{\mathrm{ehc}}^{d,\boldsymbol{\gamma},\alpha,\beta}(\boldsymbol{k}))^{2(\alpha+\beta)} |\hat{f}_{\boldsymbol{k}}|^2} < \infty \right\}$$

and consider the approximation error caused by sampling continuous functions $f \in \mathcal{A}^{\alpha,\beta,\boldsymbol{\gamma}}(\mathbb{T}^d)$ or $f \in \mathcal{H}^{\alpha,\beta,\boldsymbol{\gamma}}(\mathbb{T}^d)$ along reconstructing rank-1 lattices $\Lambda(\boldsymbol{z}, M, I_{\mathrm{ehc},N}^{d,\boldsymbol{\gamma},\alpha,\beta})$ for the frequency index set $I_{\mathrm{ehc},N}^{d,\boldsymbol{\gamma},\alpha,\beta}$. The weights $\omega_{\mathrm{ehc}}^{d,\boldsymbol{\gamma},\alpha,\beta}$ are given in (2.20). A similar Hilbert space setting has been studied by M. Griebel and J. Hamaekers in [GH14]. This paper deals with sparse grids and energy-norm based sparse grids as sampling schemes. Their impressive approximation estimates encouraged us to consider the properties of the rank-1 lattice sampling method used for approximating functions from the function spaces $\mathcal{A}^{\alpha,\beta,\boldsymbol{\gamma}}(\mathbb{T}^d)$ and $\mathcal{H}^{\alpha,\beta,\boldsymbol{\gamma}}(\mathbb{T}^d)$ defined above.

In detail, we proved the following error estimates

$$\|f - \tilde{S}_{\mathcal{I}_{\mathrm{ehc},N}^{d,\boldsymbol{\gamma},\alpha,\beta}} f | L_\infty(\mathbb{T}^d)\| \leq 2\, N^{-(\alpha+\beta)}\, \|f|\mathcal{A}^{\alpha,\beta,\boldsymbol{\gamma}}(\mathbb{T}^d)\| \tag{3.15}$$

$$\leq \left(1 + (1 + 2\zeta(2\lambda))^{\frac{d}{2}}\right) N^{-(\alpha+\beta)}\, \|f|\mathcal{H}^{\alpha,\beta+\lambda,\boldsymbol{\gamma}}(\mathbb{T}^d)\|, \tag{3.16}$$

see [KPV13, Theorem 3.4], where the parameters have to fulfill $N \geq 1$, $\beta \geq 0$, $\alpha + \beta > 0$, $\boldsymbol{\gamma} \in (0,1]^d$, $\lambda > 1/2$, and ζ is the Riemann zeta function.

The result in (3.15) is given by Theorem 3.11 and of optimal order. In our estimate (3.16), we could not prove the optimal order of convergence. Our proof technique does not allow to get better results. Nevertheless, the paper [KPV13] contains extensive numerical tests that indicates that the optimal order of convergence can be reached by sampling along reconstructing rank-1 lattices.

Based on this work, we have been pointed on the work of V. N. Temlyakov [Tem86], who treats a similar approximation problem. He considered the $L_2(\mathbb{T}^d)$ error of the approximation in the Hilbert space $\mathcal{H}^{0,\beta,\mathbf{1}}(\mathbb{T}^d)$ and used rank-1 lattice sampling along specific rank-1 lattices of Korobov type. These are rank-1 lattices $\Lambda(\boldsymbol{z}, M)$ with a generating vector of the form $\boldsymbol{z} = (1, a, a^2, a^3, \ldots, a^{d-1})$. The additional structure of the generating vector allowed him to prove that there exist rank-1 lattices of this specific structure, such that the approximation $\tilde{S}_{\mathcal{I}^{d,\boldsymbol{\gamma},0,\beta}_{\mathrm{ehc},N}} f$ computed from samples of f along these rank-1 lattices is optimal with respect to the order in N, i.e.,

$$\|f - \tilde{S}_{\mathcal{I}^{d,\boldsymbol{\gamma}}_{\mathrm{hc},N^{1/\beta}}} f | L_2(\mathbb{T}^d)\| \leq C_{d,\boldsymbol{\gamma}} N^{-\beta} \, \|f | \mathcal{H}^{0,\beta,\boldsymbol{\gamma}}(\mathbb{T}^d)\|.$$

Based on his ideas, we extended the results of V. N. Temlyakov to more general function spaces $\mathcal{H}^{\alpha,\beta,\mathbf{1}}(\mathbb{T}^d)$ in [KPV14], where we had to deal with the additional parameter α which describes some additional isotropic smoothness. We would like to mention our most interesting innovative finding, i.e., the error estimate for the parameters $\alpha < 0$, $\beta > 1 - \alpha$. We showed that there exist prime numbers M, $M \leq c_{d,\alpha,\beta} N^2$ and generating vectors of Korobov type such that the error of the corresponding approximation $\tilde{S}_{\mathcal{I}^{d,\mathbf{1},\alpha,\beta}_{\mathrm{ehc},N}} f$ is given by

$$\|f - \tilde{S}_{\mathcal{I}^{d,\mathbf{1},\alpha,\beta}_{\mathrm{ehc},N}} f | L_2(\mathbb{T}^d)\| \leq C_{d,\alpha,\beta} N^{-(\alpha+\beta)} \, \|f | \mathcal{H}^{\alpha,\beta,\mathbf{1}}(\mathbb{T}^d)\|,$$

see [KPV14, Lemma 4.4 & Theorem 4.10], which is optimal with respect to the order in N and the frequency index set $\mathcal{I}^{d,\mathbf{1},\alpha,\beta}_{\mathrm{ehc},N}$. Unfortunately, this existence proof is not constructive and, even worse, the corresponding reconstructing rank-1 lattice with a generating vector of Korobov type has to fulfill an infinite number of conditions in order to guarantee the error bounds. Consequently, we are not able to test all necessary requirements on a given generating vector of Korobov type and, thus, cannot determine such a vector. In our paper [KPV14], there are also some numerical tests, that uses generating vectors that we have found by our component–by–component approach. In particular, these results emphasize the outstanding properties of the reconstructing rank-1 lattices determined by our component–by–component strategies. All mentioned error estimates deals with terms C and c that only depend on the parameters that are given as indices. Unfortunately, these constants grow exponentially with the dimension d.

In addition, our paper [KPV13] contains approximation results about the approximation used sampling along perturbed rank-1 lattice nodes. The idea there is to use Taylor approximation in order to compute the function values at the perturbed rank-1 lattice nodes. Under additional assumptions, we are also able to approximate functions from sampling values at perturbed rank-1 lattice nodes, for details see [KPV13, Sec. 3.3]. The corresponding error estimates are quite similar to the estimates in (3.15) and (3.16) up to the constants.

Furthermore, our paper [KPV13] contains error estimates for approximations $S_I f$, where the structure of the frequency index set I does not fit exactly to the norms of the estimates in some specific kind. ■

Algorithm 3.6 Construction of interpolating frequency index set

Input: $I \subset \mathbb{Z}^d$ frequency index set
$\boldsymbol{z} \in \mathbb{N}^d$ generating vector of reconstructing rank-1 lattice $\Lambda(\boldsymbol{z}, M, I)$
$M \in \mathbb{N}$ rank-1 lattice size of reconstructing rank-1 lattice $\Lambda(\boldsymbol{z}, M, I)$

$l = 1$
$\tilde{I} = I$
$\tilde{I}^{\mathrm{SP}} = \{\boldsymbol{k} \cdot \boldsymbol{z} \bmod M \colon \boldsymbol{k} \in I\}$
while $|\tilde{I}^{\mathrm{SP}}| < M$ ***do***
  construct the set $K_l := \{\boldsymbol{k} \in \mathbb{Z}^d \colon l - 1 < \omega(\boldsymbol{k}) <= l\}$
  order the elements in K_l with respect to ω, i.e., $\omega(\boldsymbol{k}_1) \leq \omega(\boldsymbol{k}_2) \leq \ldots \leq \omega(\boldsymbol{k}_{|K_l|})$
  for $j = 1, \ldots, |K_l|$ ***do***
    if $\boldsymbol{k}_j \cdot \boldsymbol{z} \bmod M \notin \tilde{I}^{\mathrm{SP}}$ ***then***
      $\tilde{I} = \tilde{I} \cup \{\boldsymbol{k}_j\}$
      $\tilde{I}^{\mathrm{SP}} = \tilde{I}^{\mathrm{SP}} \cup \{\boldsymbol{k}_j \cdot \boldsymbol{z} \bmod M\}$
    end if
  end for
  $l = l + 1$
end while

Output: $\tilde{I}$ interpolating frequency index set for $\Lambda(\boldsymbol{z}, M)$

3.5 Interpolation of Multivariate Periodic Functions

Up to now, we treated approximation problems. In general, we computed the approximated Fourier coefficients with frequencies supported on the frequency index set I_N from $M \geq |I_N|$ function values along the reconstructing rank-1 lattice $\Lambda(\boldsymbol{z}, M, I_N)$. Some of the theoretical findings, cf. Lemmas 2.11 and 2.13, verify that there exist frequency index sets I_N, such that we cannot find a reconstructing rank-1 lattice $\Lambda(\boldsymbol{z}, |I_N|, I_N)$. Consequently, the approximation $\tilde{S}_{I_N} f$, cf. (3.13), may not be an interpolation on the rank-1 lattice nodes for $f \notin \Pi_{I_N}$. In [MS12], H. Munthe-Kaas and T. Sørevik describe a constructive strategy in order to find suitable frequency indices $\boldsymbol{k} \in \mathbb{Z}^d$ with respect to a given weight function $\omega : \mathbb{Z}^d \to [0, \infty)$ such that the union of all these frequency indices is a space of trigonometric polynomials $\Pi_{\tilde{I}}$ that allow a unique interpolation on a given rank-1 lattice $\Lambda(\boldsymbol{z}, M)$. In detail, the strategy indicated by Algorithm 3.6 with input $\boldsymbol{z}$, M, and $I = \emptyset$ lead us to the, maybe non-unique, frequency index set $\tilde{I}$. The idea in [MS12] is to take a rank-1 lattice $\Lambda(\boldsymbol{z}, M)$ that is optimized for some kind of an integration error, compute the frequency index set $\tilde{I}$, and approximate the function f by $\tilde{S}_{\tilde{I}} f$. Clearly, the rank-1 lattice $\Lambda(\boldsymbol{z}, M) = \Lambda(\boldsymbol{z}, M, \tilde{I})$ is a reconstructing rank-1 lattice for $\tilde{I}$. Unfortunately, the strategy to construct $\tilde{I}$ may discard frequencies $\boldsymbol{k}$ that have a low value $\omega(\boldsymbol{k})$ and thus the approximation error may be of a high order in the worst case.

In order to avoid these problems, we advice to plug in reconstructing rank-1 lattices $\Lambda(\boldsymbol{z}, M, I)$ and, additionally, the frequency index set I in Algorithm 3.6. The strategy is as follows. For a fixed weight function ω, we determine the frequency index set $I_N := \{\boldsymbol{k} \in \mathbb{Z}^d \colon \omega(\boldsymbol{k}) \leq N\}$ and a corresponding reconstructing rank-1 lattice $\Lambda(\boldsymbol{z}, M, I_N)$ using the approach mentioned in Table 3.1 or Algorithms 3.7 or 3.8. Then, we determine $\tilde{I}$ as sketched in Algorithm 3.6. Due to the reconstruction property of $\Lambda(\boldsymbol{z}, M, I_N)$, we obtain $I_N \subset \tilde{I} =: \tilde{I}_N$, $|\tilde{I}_N| = M$, and $\Lambda(\boldsymbol{z}, M, I_N) = \Lambda(\boldsymbol{z}, |\tilde{I}_N|, \tilde{I}_N)$. Now, we are able to compute an interpolation

$S_{\tilde{I}_N} f$ of $f \in \mathcal{A}_\omega(\mathbb{T}^d)$ and, in addition, we get an error estimate similar to Theorem 3.11.

Theorem 3.13. *Let the function $f \in \mathcal{A}_\omega(\mathbb{T}^d)$ and the frequency index set $I_N = \{\boldsymbol{k} \in \mathbb{Z}^d : \omega(\boldsymbol{k}) \leq N\}$ of finite cardinality be given. Additionally, we assume that the frequency index set $\tilde{I}_N$ fulfills $I_N \subset \tilde{I}_N$ and there exists a reconstructing rank-1 lattice $\Lambda(\boldsymbol{z}, |\tilde{I}_N|, \tilde{I}_N)$ for the frequency index set $\tilde{I}_N$. Then, the approximation $\tilde{S}_{\tilde{I}_N} f$ of f is in fact an interpolation of f at all rank-1 lattice nodes of $\Lambda(\boldsymbol{z}, |\tilde{I}_N|, \tilde{I}_N)$ and we estimate*

$$\|f - \tilde{S}_{\tilde{I}_N} f | L_\infty(\mathbb{T}^d)\| \leq 2N^{-1} \|f | \mathcal{A}_\omega(\mathbb{T}^d)\|. \tag{3.17}$$

Proof. The reconstruction property of $\Lambda(\boldsymbol{z}, |\tilde{I}_N|, \tilde{I}_N)$ for $\tilde{I}_N$ and the equality of the lattice size and the number of frequencies, that are contained in $\tilde{I}_N$, yield that the Fourier matrix $\boldsymbol{A} = \left(\mathrm{e}^{2\pi \mathrm{i} j \frac{\boldsymbol{k}\cdot\boldsymbol{z}}{M}}\right)_{j=0,\ldots,|\tilde{I}_N|-1, \boldsymbol{k}\in\tilde{I}_N}$ is a regular squared matrix and, thus, directly invertible. The corresponding solution $\hat{\tilde{\boldsymbol{f}}} = \boldsymbol{A}^{-1}\boldsymbol{f}$ interpolates f at all rank-1 lattice nodes of $\Lambda(\boldsymbol{z}, |\tilde{I}_N|, \tilde{I}_N)$, since we obtain $\boldsymbol{A}\hat{\tilde{\boldsymbol{f}}} = \boldsymbol{f}$. The proof of the error estimate follows the proof of Theorem 3.11. ∎

Remark 3.14. Besides the general result presented here, there can be found some error estimates for specific weight functions in [KPV13]. In particular, we treat an interpolation problem in a Hilbert space setting therein, that is similar to the approximation problems explained in Remark 3.12. The corresponding error estimates are also of the same type and quality. ∎

We discuss the advantages of the interpolation approach in Chapter 5. In particular, the numerical examples in Section 5.1 and 5.3 demonstrate the advantages of interpolating frequency index sets $\tilde{I}_N$. At this point, we should mention that the computation of a suitable interpolating frequency index set $\tilde{I}_N$ may take a lot of memory and in addition computational time, cf. Algorithm 3.6.

3.6 Tractability

In the last sections, we showed that there exists a rank-1 lattice of size M, $|I_N| \leq M \lesssim |I_N|^2$, with $I_N = \{\boldsymbol{k} \in \mathbb{Z}^d : \omega(\boldsymbol{k}) \leq N\}$, $I_N \subset \{\boldsymbol{k} + [0, M]^d\}$, $\boldsymbol{k} \in \mathbb{Z}^d$, that allows for the approximation of $f \in \mathcal{A}_\omega(\mathbb{T}^d)$ with a relative error not larger than $2N^{-1}$. In other words, assuming the frequency index set I_N contained in a d-dimensional cube of edge length smaller than $|I_N|^2$, we need not more than $|I_N|^2$ samples to approximate f with an error not larger than $2N^{-1}$, cf. Remark 3.5 and Corollary 3.4. Depending on ω, the cardinality of I_N possibly depends on N and d.

Regarding the tractability of our approximation problem we consider the cardinality of I_N. We can determine different types of tractability, see, e.g. [NW08]. We call the problem *polynomial tractable* if the number of information we need to achieve an approximation error not larger than ε depends only polynomial on ε^{-1} and d. If we have additional independence of d the problem is called *strongly tractable*. Furthermore, we call the problem *weakly tractable* iff the information complexity is not exponential in ε^{-1} and not exponential in d. Obviously, we can reduce these conditions to conditions on the number $M \leq |I_N|^2$ of samples we need to achieve the approximation error not larger than $2N^{-1}$. In order to obtain tractability the cardinality of I_N has to be polynomial in N and d. Moreover, the cardinality of I_N has to be

independent of d in order to obtain strong tractability. Finally, we prove weak tractability, if $\lim_{d+N\to\infty} \frac{2\ln|I_N|}{d+N} = 0$ holds. In the following we consider some of the examples from Section 2.3.

Lemma 3.15. *Let $\boldsymbol{\gamma} = (\gamma_s)_{s=1}^{\infty} \in [0,1]^{\mathbb{N}}$, $0 < \epsilon \in \mathbb{R}$, $0 < c \in \mathbb{R}$, $\gamma_s \leq \frac{c}{s^{1+\epsilon}}$ and $0 < p \leq \infty$ be given. The approximation of the function $f \in \mathcal{A}_{\omega_p^{d,\boldsymbol{\gamma}}}(\mathbb{T}^d)$ using trigonometric polynomials with frequencies supported on weighted ℓ_p-balls $I_{p,N}^{d,\boldsymbol{\gamma}} := \{\boldsymbol{k} \in \mathbb{Z}^d : \omega_p^{d,\boldsymbol{\gamma}}(\boldsymbol{k}) \leq N\}$, see (2.15), is at least weakly tractable.*

Proof. Following Lemma 2.6, we estimate

$$\begin{aligned}\frac{2\ln|I_{p,N}^{d,\boldsymbol{\gamma}}|}{d+N} \leq \frac{2\ln|I_{\infty,N}^{d,\boldsymbol{\gamma}}|}{d+N} = \frac{2\sum_{s=1}^{d}\ln(1+2\lfloor\gamma_s N\rfloor)}{d+N} \leq \frac{2\sum_{\substack{s\in\mathbb{N}\\ s^{1+\epsilon}\leq cN}}\ln(1+2cs^{-1-\epsilon}N)}{d+N}\\ \leq \frac{4\sum_{\substack{s\in\mathbb{N}\\ s^{1+\epsilon}\leq cN}}\ln(2cs^{-1-\epsilon}N)}{d+N} \leq \frac{4s_N\ln 2 + 4(1+\epsilon)s_N\ln s_N}{d+c^{-1}s_N^{1+\epsilon}}\end{aligned}$$

with $s_N = (cN)^{\frac{1}{1+\epsilon}}$ and $N = \frac{s_N^{1+\epsilon}}{c}$. We conclude

$$\lim_{d+c^{-1}s_N^{1+\epsilon}\to\infty} \frac{4s_N\ln 2 + 4(1+\epsilon)s_N\ln s_N}{d+c^{-1}s_N^{1+\epsilon}} = 0.$$

■

Lemma 3.16. *With $\sum_{s=1}^{\infty}\gamma_s < \infty$ the cardinality of the weighted hyperbolic cross $I_{\mathrm{hc},N}^{d,\boldsymbol{\gamma}}$, cf. (2.17), is bounded from above by $|I_{\mathrm{hc},N}^{d,\boldsymbol{\gamma}}| \leq C_{\boldsymbol{\gamma}} N^2$ where $C_{\boldsymbol{\gamma}}$ is independent of the dimension d. Consequently $|I_{\mathrm{hc},N}^{d,\boldsymbol{\gamma}}|^2$ is independent of d and polynomial in N. The corresponding approximation problem in $\mathcal{A}_{\omega_p^{d,\boldsymbol{\gamma}}}(\mathbb{T}^d)$ is strongly tractable.*

Proof. We refer to [CKN10, Equation (6)]. There, one finds the estimate

$$|I_{\mathrm{hc},N}^{d,\boldsymbol{\gamma}}| \leq N^{\tau}\prod_{s=1}^{d}(1+2\zeta(\tau)\gamma_s^{\tau})$$

for all $\tau > 1$. The product converges for all $\tau > 1$ and $d \to \infty$. So, we achieve

$$|I_{\mathrm{hc},N}^{d,\boldsymbol{\gamma}}| \leq C_{\boldsymbol{\gamma},\tau} N^{\tau}.$$

We plug in $\tau = 2$ and obtain the assertion from above. ■

The last two lemmas treat different kinds of weights ω and determines positive tractability results of the corresponding approximation problem from the number of frequency indices given by I_N. In a similar way, one can analyze other weight functions and the corresponding cardinalities of the arising frequency index sets I_N. In detail, the positive tractability results concerning the cardinalities of I_N directly causes positive tractability result on the approximation method that computes approximated Fourier partial sums $\tilde{S}_{I_N} f$ from sampling values of f along reconstructing rank-1 lattices for I_N.

3.7 Improvements on the Construction of Reconstructing Rank-1 Lattices

In Table 3.1, we listed the basic steps that we determined from our theoretical results in Corollary 3.4 in order to construct reconstructing rank-1 lattices. Even if we additionally assume that the frequency index set I is contained in a d-dimensional cube of edge length $|I|$, we may have to expect a computational complexity of $\Omega\left(d|I|^3\right)$ and a memory requirement in $\Omega\left(d|I|^2\right)$ in the worst case.

According to the usual practice, we are interested in improvements on the deterministic way, cf. Table 3.1, for finding reconstructing rank-1 lattices.

One can consider modifications that reduce the arithmetic complexity or the memory requirements of the costly steps. In general, this may be successful if one restricts the frequency index I to a specific structure. In detail, convexity of I may be helpful or the embedding of the difference set $\mathcal{D}(I)$ into a frequency index set that is often considered in numerical integration, e.g., ℓ_1-balls or hyperbolic crosses which are often called Zaremba crosses in numerical integration. In particular, the famous fast component–by–component construction of rank-1 lattices for numerical integration developed by R. Cools and D. Nuyens, cf. [CN04, CN06, CN07, CN08, CKN10], offers a possibility in order to improve step 5 of our strategy, see Table 3.1. In short words, the fast component–by–component construction is a component–by–component construction, which computes for a fixed rank-1 lattice size M and a fixed generating vector $(z_1,\dots,z_{s-1})^\top$ a specific integration error in dimension s for each $z_s = 1,\dots,M-1$ using a fast Fourier transform. Consequently, we can try to improve the fifth step of our strategy, cf. Table 3.1, in the following way. We assume, that we have an integration error functional that somehow fits to the structure of the difference set $\mathcal{D}(I)$ and fulfills the assumptions of the fast component–by–component construction, cf. [CN07]. Then, we order the candidates $l = \{1,\dots,M-1\}$ for z_s with respect to the integration error of the rank-1 lattice $\Lambda((z_1,\dots,z_{s-1},l)^\top, M)$, ascendingly. Subsequently, we test the rank-1 lattices $\Lambda((z_1,\dots,z_{s-1},l)^\top, M)$ for the reconstruction property for the frequency index set I starting with the generating vectors $(z_1,\dots,z_{s-1},l)^\top$ bringing the smallest integration errors. The explained approach is based on the following necessity. Due to the assumption that the integration error functional fits to the structure of the difference set, we obtain that for rank-1 lattices that have a large worst case integration error the integer dual lattice, cf. (3.11), may touches the difference set $\mathcal{D}(I)$ with high probability. Thus, we pass through all candidates $l \in \{1,\dots,M-1\}$ in a way, such that, hopefully, only a few tests are necessary in order to find a reconstructing rank-1 lattice. There are at least two crucial disadvantages on that approach:

1. The approach is severely limited to specific structures of difference sets $\mathcal{D}(I)$, cf. [CN07].
2. We have to analyze the structure of the difference set $\mathcal{D}(I)$ in order to find (or may not find) a suitable error functional.

Besides these two disadvantages, we usually observe that the fifth step of our strategy, cf. Table 3.1, is not as costly as the worst case arithmetic complexity promises.

Hence, we focus on another improvement. In detail, the first step of our strategy, i.e., the computation of the difference sets $\mathcal{D}(I)_{\downarrow s}$, requires high computational costs and, in addition, a lot of memory. Thus, we are interested in deterministic strategies in order to determine reconstructing rank-1 lattices that avoid the computation of the difference set $\mathcal{D}(I)$. Moreover, further simplifications of the search strategy can mainly improve the practicability

of our sampling method. In particular, we have in mind applications, that identify the frequency index set I dimension–by–dimension. Consequently, the assumption of Corollary 3.4 cannot be fulfilled, since we do not know all s-dimensional difference sets $\mathcal{D}(I)_{\downarrow s}$ a priori.

Algorithms determining generating vectors z and lattice sizes M

One of the main disadvantages of Algorithm 3.3 arises from the necessity of the input of a suitable rank-1 lattice size M. In this section we introduce a strategy to compute generating vectors $\boldsymbol{z}$ and corresponding lattice sizes M for fixed frequency index sets I. In particular, the specified algorithms seems to be useful for higher dimensions d and frequency index sets $I \subset \boldsymbol{k} + [\boldsymbol{0}, \boldsymbol{a}]$, $\boldsymbol{k} \in \mathbb{Z}^d$, $\boldsymbol{a} \in \mathbb{N}^d$, contained in boxes of relatively small edge lengths $a_1, a_2, \ldots, a_d$.

Lemma 3.17. *Let the dimension $d \in \mathbb{N}$, $d \geq 2$, and the frequency index set $I \subset \mathbb{Z}^d$ of finite cardinality, $|I| \geq 2$, be given. We assume that $\Lambda(\boldsymbol{z}, M, I_{\downarrow d-1})$ with $\boldsymbol{z} = (z_1, \ldots, z_{d-1})^\top$ is a reconstructing rank-1 lattice for the frequency index set $I_{\downarrow d-1} := \{(h_s)_{s=1}^{d-1} : \boldsymbol{h} \in I\}$. With $S = \min\{m \in \mathbb{N} : |\{h_d \bmod m : \boldsymbol{h} \in I\}| = |\{h_d : \boldsymbol{h} \in I\}|\}$, we create a reconstructing rank-1 lattice $\Lambda((z_1, \ldots, z_{d-1}, M)^\top, MS, I)$ for the frequency index set I.*

Proof. We assume the rank-1 lattice $\Lambda((z_1, \ldots, z_{d-1})^\top, M)$ is a reconstructing rank-1 lattice for $I_{\downarrow d-1}$ and $\Lambda((z_1, \ldots, z_{d-1}, M)^\top, MS)$ is not a reconstructing rank-1 lattice for I, i.e., there exist at least two different elements $(\boldsymbol{h}, h_d), (\boldsymbol{k}, k_d) \in I$, $(\boldsymbol{h}, h_d) \neq (\boldsymbol{k}, k_d)$, such that

$$\boldsymbol{h} \cdot \boldsymbol{z} + h_d M \equiv \boldsymbol{k} \cdot \boldsymbol{z} + k_d M \pmod{MS}.$$

We distinguish three different possible cases of $(\boldsymbol{h}, h_d), (\boldsymbol{k}, k_d) \in I$, $(\boldsymbol{h}, h_d) \neq (\boldsymbol{k}, k_d)$:

- $\boldsymbol{h} = \boldsymbol{k}$ and $h_d \neq k_d$
  We consider the corresponding residue classes

  $$0 \equiv \boldsymbol{k} \cdot \boldsymbol{z} + k_d M - \boldsymbol{h} \cdot \boldsymbol{z} - h_d M \equiv (k_d - h_d) M \pmod{MS}$$

  and obtain $S \mid (k_d - h_d)$, i.e., $k_d \equiv h_d \pmod{S}$. Thus, we estimate $|\{h_d \bmod S : \boldsymbol{h} \in I\}| < |\{h_d : \boldsymbol{h} \in I\}|$, which is in contradiction to the definition of S.

- $\boldsymbol{h} \neq \boldsymbol{k}$ and $h_d = k_d$
  Accordingly, we calculate

  $$0 \equiv \boldsymbol{k} \cdot \boldsymbol{z} + k_d M - \boldsymbol{h} \cdot \boldsymbol{z} - h_d M \equiv (\boldsymbol{k} - \boldsymbol{h}) \cdot \boldsymbol{z} \pmod{MS}$$

  and obtain $MS \mid (\boldsymbol{k} - \boldsymbol{h}) \cdot \boldsymbol{z}$ and $M \mid (\boldsymbol{k} - \boldsymbol{h}) \cdot \boldsymbol{z}$ as well. According to that, we obtain $\boldsymbol{h} \cdot \boldsymbol{z} \equiv \boldsymbol{k} \cdot \boldsymbol{z} \pmod{M}$, which is in contradiction to the assumption $\Lambda(\boldsymbol{z}, M)$ is a reconstructing rank-1 lattice for $I_{\downarrow d-1}$.

- $\boldsymbol{h} \neq \boldsymbol{k}$ and $h_d \neq k_d$
  Due to $\Lambda(\boldsymbol{z}, M)$ is a reconstructing rank-1 lattice for $I_{\downarrow d-1}$ we have

  $$0 \not\equiv \boldsymbol{k} \cdot \boldsymbol{z} - \boldsymbol{h} \cdot \boldsymbol{z} \pmod{M}.$$

  Thus, we can find uniquely specified $a_{\boldsymbol{k},\boldsymbol{h}} \in \mathbb{Z}$ and $b_{\boldsymbol{k},\boldsymbol{h}} \in \{1, \ldots, M-1\}$ such that $\boldsymbol{k} \cdot \boldsymbol{z} - \boldsymbol{h} \cdot \boldsymbol{z} = a_{\boldsymbol{k},\boldsymbol{h}} M + b_{\boldsymbol{k},\boldsymbol{h}}$. We calculate

  $$0 \equiv \boldsymbol{k} \cdot \boldsymbol{z} + k_d M - \boldsymbol{h} \cdot \boldsymbol{z} - h_d M \equiv (a_{\boldsymbol{k},\boldsymbol{h}} + k_d - h_d) M + b_{\boldsymbol{k},\boldsymbol{h}} \pmod{MS}$$

  and obtain $MS \mid (a_{\boldsymbol{k},\boldsymbol{h}} + k_d - h_d) M + b_{\boldsymbol{k},\boldsymbol{h}}$. As a consequence, we deduce $M \mid b_{\boldsymbol{k},\boldsymbol{h}}$, which is in conflict with $b_{\boldsymbol{k},\boldsymbol{h}} \in \{1, \ldots, M-1\}$.

Algorithm 3.7 Component-by-component lattice search (unknown lattice size M)

Input: $I \subset \mathbb{Z}^d$ frequency index set

$M_1 = \min \{m \in \mathbb{N} : |\{h_1 \bmod m : \boldsymbol{h} \in I\}| = |\{h_1 : \boldsymbol{h} \in I\}|\}$
$z_1 = 1$
for $s = 2, \ldots, d$ ***do***
  $S = \min \{m \in \mathbb{N} : |\{h_s \bmod m : \boldsymbol{h} \in I\}| = |\{h_s : \boldsymbol{h} \in I\}|\}$
  $z_s = M_{s-1}$
  $\boldsymbol{z} = (\boldsymbol{z}, z_s)$
  form the set $I_{\downarrow s}$
  $M_s = \min \left\{m \in \mathbb{N} : |\{\boldsymbol{z} \cdot \boldsymbol{h} \bmod m : \boldsymbol{h} \in I_{\downarrow s}\}| = |I_{\downarrow s}|\right\} \leq SM_{s-1}$ (Algorithm 3.5)
end for

Output: $\boldsymbol{z} \in \mathbb{Z}^d$ generating vector
$\boldsymbol{M} \in \mathbb{N}^d$ rank-1 lattice sizes for dimension $s = 1, \ldots, d$ of reconstructing rank-1 lattices $\Lambda((1, M_1, \ldots, M_{s-1})^\top, M_s, I_{\downarrow s})$, $s = 1, \ldots, d$

Extending the reconstructing rank-1 lattice $\Lambda(\boldsymbol{z}, M, I_{\downarrow d-1})$ for $I_{\downarrow d-1}$ to $\Lambda((\boldsymbol{z}^\top, M)^\top, MS)$ with S as defined above, we actually get a reconstructing rank-1 lattice for the frequency index set $I \subset \mathbb{Z}^d$. ■

Lemma 3.17 lead us directly to the specification of Algorithm 3.7. We stress the fact that the corresponding output of Algorithm 3.7 is a vector $\boldsymbol{M}$ and a generating vector $\boldsymbol{z} = (1, M_1, \ldots, M_{d-1})^\top$ that specify reconstructing rank-1 lattices $\Lambda((z_1, \ldots, z_s)^\top, M_s)$ for the index sets $I_{\downarrow s}$, $s = 1, \ldots, d$.

In addition, Algorithm 3.8 extends this strategy. In contrast to Algorithm 3.7, knowing M_{s-1} we do not fix $z_s = M_{s-1}$. We search for a suitable component $z_s \in [0, M_{s-1}]$ of the generating vector $\boldsymbol{z}$. In that way, Algorithm 3.8 may find even smaller rank-1 lattices than Algorithm 3.7 does. Please note, that the determination of a rank-1 lattice is also guaranteed due to M_{s-1} is one of the candidates for z_s. Furthermore, we allow $z_s = 0$. A generating vector $\boldsymbol{z}$ that is returned by Algorithm 3.8 and has a zero component in dimension s states that the information of the sth component of the integer vectors $\boldsymbol{k}$ contained in the frequency index set I is not necessary in order to find a reconstructing rank-1 lattice. In other words, all vectors $\boldsymbol{k} \in I_{\downarrow s}$ are uniquely determined by its first $s-1$ components and the trigonometric polynomial $f \in \Pi_{I_{\downarrow s}}$ can be uniquely reconstructed from sampling values that depends only on the first $s-1$ dimensions.

3.8 Specific Frequency Index Sets

In this section, we treat the same frequency index sets I as considered in Section 2.3. In particular, we use the introduced frequency index sets in order to demonstrate different features of the corresponding reconstructing rank-1 lattices, cf. Section 3.2. In the following discussions we focus on fixed dimensions d and apply the existence results from Corollary 3.4 to the different structures of frequency index sets that are defined in Section 2.3, i.e., we estimate lattice sizes M guaranteeing the existence of reconstructing rank-1 lattices $\Lambda(\boldsymbol{z}, M, I)$ for the frequency index sets I. In particular, we are interested in the relations of the lattice size M and the cardinality $|I|$, where the frequency index sets I are weighed ℓ_p-balls $I_{p,N}^{d,\gamma}$,

Algorithm 3.8 Component-by-component lattice search (unknown lattice size M, extended)

Input: $I \subset \mathbb{Z}^d$ frequency index set

$M_1 = \min\{m \in \mathbb{N}\colon |\{h_1 \bmod m\colon \boldsymbol{h} \in I\}| = |\{h_1 : \boldsymbol{h} \in I\}|\}$
$z_1 = 1$
for $s = 2, \ldots, d$ ***do***
  $S = \min\{m \in \mathbb{N}\colon |\{h_s \bmod m\colon \boldsymbol{h} \in I\}| = |\{h_s : \boldsymbol{h} \in I\}|\}$
  form the set $I_{\downarrow s}$
  search for the smallest $z_s \in [0, M_{s-1}] \cap \mathbb{Z}$ with $|\{(\boldsymbol{z}, z_s) \cdot \boldsymbol{h} \bmod SM_{s-1}\colon \boldsymbol{h} \in I_{\downarrow s}\}| = |I_{\downarrow s}|$
  $\boldsymbol{z} = (\boldsymbol{z}, z_s)$
  $M_s = \min\left\{m \in \mathbb{N}\colon |\{\boldsymbol{z} \cdot \boldsymbol{h} \bmod m :\ \boldsymbol{h} \in I_{\downarrow s}\}| = |I_{\downarrow s}|\right\} \leq SM_{s-1}$ (Algorithm 3.5)
end for

Output: $\boldsymbol{z} \in \mathbb{Z}^d$ generating vector
$\boldsymbol{M} \in \mathbb{N}^d$ rank-1 lattice sizes for dimension $s = 1, \ldots, d$ of reconstructing rank-1 lattices $\Lambda((z_1, z_2, \ldots, z_s)^\top, M_s, I_{\downarrow s})$, $s = 1, \ldots, d$

weighted hyperbolic crosses $I^{d,\boldsymbol{\gamma}}_{\mathrm{hc},N}$, energy-norm based hyperbolic crosses $I^{d,\boldsymbol{\gamma},\alpha,\beta}_{\mathrm{ehc},N}$ and arbitrary sparse frequency index sets.

We demonstrate that reconstructing rank-1 lattices are a good choice in order to sample multivariate trigonometric polynomials. At least for weighted ℓ_p-balls and energy-norm based hyperbolic crosses, we use Corollary 3.4 in order to show that reconstructing rank-1 lattices are perfectly stable sampling schemes of optimal order with respect to the parameter N and the stability.

The numerical examples of this section are presented in tables, that have all a similar structure. The most left columns contain the parameters determining the frequency index set I and the cardinality $|I|$ of the corresponding frequency index set. The following four columns present lattice sizes $M_{\mathrm{Cor3.4}}$, $M_{\mathrm{Alg3.3+Alg3.5}}$, $M_{\mathrm{Alg3.7}}$, and $M_{\mathrm{Alg3.8}}$ of reconstructing rank-1 lattices, where

- $M_{\mathrm{Cor3.4}}$ is the lattice size that we found using the strategy indicated in Table 3.1 applied on the frequency index set I, i.e., the lattice size for which we proved the existence of a generating vector $\boldsymbol{z}$ that can be determined component–by–component such that the rank-1 lattice $\Lambda(\boldsymbol{z}, M_{\mathrm{Cor3.4}}, I)$ is a reconstructing one for I,

- $M_{\mathrm{Alg3.3+Alg3.5}}$ is the lattice size that we determined by applying Algorithm 3.5 on the rank-1 lattice we determined by the strategy from Table 3.1,

- $M_{\mathrm{Alg3.7}}$ is the size of the reconstructing rank-1 lattice that we computed using Algorithm 3.7, and

- $M_{\mathrm{Alg3.8}}$ is the cardinality of the reconstructing rank-1 lattice that is found by Algorithm 3.8 for the input I.

In appropriate cases, we specified the generating vector $\boldsymbol{z}_{\mathrm{Alg3.8}}$ that is determined by Algorithm 3.8 in the last column. Again, we stress on the fact that the strategy shown in Table 3.1 suffers from huge memory requirements. According to this, several values of $M_{\mathrm{Cor3.4}}$ and $M_{\mathrm{Alg3.3+Alg3.5}}$ are not listed in the tables of this section.

3.8.1 Weighted ℓ_p-balls

In this section we consider weighted ℓ_p-balls $I_{p,N}^{d,\boldsymbol{\gamma}}$, defined in (2.15), as frequency index sets. We apply Corollary 3.4 and show that the relation $M/|I_{p,N}^{d,\boldsymbol{\gamma}}|$ of the lattice size M of a suitable reconstructing rank-1 lattice $\Lambda(\boldsymbol{z}, M, I_{p,N}^{d,\boldsymbol{\gamma}})$ and the cardinality $|I_{p,N}^{d,\boldsymbol{\gamma}}|$ of the weighted ℓ_p-ball is bounded independently of N.

Corollary 3.18. *Let the fixed dimension $d \in \mathbb{N}$, the parameter $p \in (0,\infty]$, the weights $\boldsymbol{\gamma} \in [0,1]^{\mathbb{N}}$ with $\gamma_1 \geq \ldots \geq \gamma_d > 0$, and $N \in \mathbb{R}$, $d^{\min(0,(p-1)/p)}\gamma_d N \geq 2d$, be given. Then, there exists a reconstructing rank-1 lattice $\Lambda(\boldsymbol{z}, M, I_{p,N}^{d,\boldsymbol{\gamma}})$ of size $M \lesssim |I_{p,N}^{d,\boldsymbol{\gamma}}|$, i.e., the oversampling factor $\frac{M}{|I_{p,N}^{d,\boldsymbol{\gamma}}|}$ is bounded from above by a number $C_{p,d,\boldsymbol{\gamma}}$ depending only on the dimension d, the parameter p, and the weights $\gamma_1, \ldots, \gamma_d$. The constant $C_{p,d,\boldsymbol{\gamma}}$ can be bounded by $\tilde{C}_{p,d,\boldsymbol{\gamma}} = \frac{16}{3}\gamma_d^{-d} d^{d\max(0,-(p-1)/p)} d! \prod_{s=1}^{d}(1+\gamma_s 2^{\max(2,1+1/p)})$ roughly.*

Proof. We proved the embeddings

$$I_{1,d^{\min(0,(p-1)/p)}N}^{d,\boldsymbol{\gamma}} \subset I_{p,N}^{d,\boldsymbol{\gamma}} \subset \mathcal{D}(I_{p,N}^{d,\boldsymbol{\gamma}}) \subset I_{p,2^{\max(1,1/p)}N}^{d,\boldsymbol{\gamma}} \subset I_{\infty,2^{\max(1,1/p)}N}^{d,\boldsymbol{\gamma}}$$

in Lemmas 2.6 and 2.7. We take Corollary 3.4, Remark 3.5, and (3.8) into account and determine a prime number $M \leq \frac{2}{3}(|\mathcal{D}(I_{p,N}^{d,\boldsymbol{\gamma}})|+7) \leq \frac{16}{3}|I_{\infty,2^{\max(1,1/p)}N}^{d,\boldsymbol{\gamma}}|$ fulfilling the assumptions of Corollary 3.4, i.e., we find a generating vector $\boldsymbol{z}$ such that the resulting rank-1 lattice is a reconstructing rank-1 lattice $\Lambda(\boldsymbol{z}, M, I_{p,N}^{d,\boldsymbol{\gamma}})$ for the frequency index set $I_{p,N}^{d,\boldsymbol{\gamma}}$. We use Lemma 2.8 and estimate

$$\begin{aligned}\frac{M}{|I_{p,N}^{d,\boldsymbol{\gamma}}|} &\leq \frac{16}{3}\frac{|I_{\infty,2^{\max(1,1/p)}N}^{d,\boldsymbol{\gamma}}|}{|I_{1,d^{\min(0,(p-1)/p)}N}^{d,\boldsymbol{\gamma}}|} \leq \frac{16}{3}\frac{\prod_{s=1}^{d}(1+2\lfloor\gamma_s 2^{\max(1,1/p)}N\rfloor)}{\frac{\gamma_d^d d^{d\min(0,(p-1)/p)}N^d}{d!}} \\ &\leq \frac{16}{3}\gamma_d^{-d} d^{d\max(0,-(p-1)/p)} d! \prod_{s=1}^{d}(1+\gamma_s 2^{\max(2,1+1/p)}) =: \tilde{C}_{p,d,\boldsymbol{\gamma}}.\end{aligned}$$

■

We stress the fact that the order in N is the best possible in the asymptotic with respect to N, since we proved that there exist reconstructing rank-1 lattices $\Lambda(\boldsymbol{z}, M, |I_{p,N}^{d,\boldsymbol{\gamma}}|)$ of size M such that the oversampling factor $M/|I_{p,N}^{d,\boldsymbol{\gamma}}|$ is bounded independently of N, provided that N is large enough. Nevertheless, we have to expect lattice sizes $M \sim N^d$ due to the fact that the cardinalities of the frequency index sets fulfill $|I_{p,N}^{d,\boldsymbol{\gamma}}| \sim N^d$ for large enough parameters N, cf. Lemma 2.7 and Corollary 2.9. Anyway, the upper bound on the constant $C_{p,d,\boldsymbol{\gamma}}$ may be huge. Certainly, we did not take care on the best possible estimates with respect to the weights $\boldsymbol{\gamma}$ and the parameter p in order to calculate $\tilde{C}_{p,d,\boldsymbol{\gamma}}$. Thus, for specific parameter constellations, we will not observe constants that are as big as $\tilde{C}_{p,d,\boldsymbol{\gamma}}$ from Corollary 3.18.

In the following we consider weighted ℓ_p-balls of a specific structure in detail. We start with ℓ_∞-balls, which are in principle so-called (weighted) full frequency index sets. In addition, we treat weighted ℓ_1-balls that are convex subsets of the ℓ_∞-balls. Appropriate weighted ℓ_1-balls may severely decrease the number of frequencies compared to ℓ_∞-balls. Furthermore, we consider $\ell_{1/2}$-balls, that have cardinalities that are even smaller than those of the corresponding ℓ_1-balls. The non-convexity of ℓ_p-balls, $p < 1$, is of our particular interest.

Example 3.19. As a first example, we treat weighted ℓ_∞-balls and determine a rank-1 lattice size $M \leq \frac{16}{3}|I^{d,\boldsymbol{\gamma}}_{\infty,2N}|$ such that we can find a reconstructing rank-1 lattices $\Lambda(\boldsymbol{z}, M, I^{d,\boldsymbol{\gamma}}_{\infty,N})$ for the weighted l_∞-balls $I^{d,\boldsymbol{\gamma}}_{\infty,N}$, cf. Corollary 3.4, Remark 3.5, Lemma 2.7 and (3.8). Consequently, we can estimate the oversampling factor $M/|I^{d,\boldsymbol{\gamma}}_{\infty,N}|$ by

$$\frac{M}{|I^{d,\boldsymbol{\gamma}}_{\infty,N}|} \leq \frac{16}{3}\frac{\prod_{s=1}^{d}(1+2\lfloor\gamma_s 2N\rfloor)}{\prod_{s=1}^{d}(1+2\lfloor\gamma_s N\rfloor)} \leq \frac{16}{3}\frac{\prod_{s=1}^{d}(3+4\lfloor\gamma_s N\rfloor)}{\prod_{s=1}^{d}(1+2\lfloor\gamma_s N\rfloor)} \leq 16\cdot 3^d,$$

which is much better than the upper bound given in Corollary 3.18.

Since the ℓ_∞-ball is the classical frequency index set in higher dimensions d which one obtains by the tensor product of one-dimensional discrete Fourier transforms, this type of frequency index sets is well investigated. In particular, the paper of G. Steidl and M. Tasche, [ST89], deals with so-called index transforms, where they transform the indices of s-dimensional full frequency index sets, i.e., s-dimensional ℓ_∞-balls, to d-dimensional ℓ_∞-balls, $d > s$. In principle, we consider a similar but inverse transform to those index transforms. In detail, we have a transform of a d-dimensional ℓ_∞-ball $I^{d,\boldsymbol{\gamma}}_{\infty,N}$ to a (shifted) one-dimensional ℓ_∞-ball $[0, M-1]\cap\mathbb{Z}$ given by the mapping $\boldsymbol{k} \mapsto \boldsymbol{k}\cdot\boldsymbol{z} \bmod M$, $\boldsymbol{k} \in I^{d,\boldsymbol{\gamma}}_{\infty,N}$. In order to find a reconstructing rank-1 lattice for $I^{d,\boldsymbol{\gamma}}_{\infty,N}$ our index mapping has to be injective.

In particular, we can apply the results of G. Steidl and M. Tasche, cf. [ST89], in the following way. We embed the frequency index set $I^{d,\boldsymbol{\gamma}}_{\infty,N}$ in a suitable ℓ_∞-ball $I^{d,\boldsymbol{\gamma}}_{\infty,N} \subset \times_{s=1}^{d}\left[-\frac{a_s-1}{2}, \frac{a_s-1}{2}\right]$ where the integers a_s are one or pairwise coprime. Then there exists a bijective index transform from $\times_{s=1}^{d}\left[-\frac{a_s-1}{2}, \frac{a_s-1}{2}\right]$ to $[0, \prod_{s=1}^{d} a_s - 1]\cap\mathbb{Z}$ due to the results of [ST89]. In detail, we can give such an index transform using rank-1 lattices. We define the generating vector $\boldsymbol{z}$ with components

$$z_s := \prod_{\substack{t=1\\ t\neq s}}^{d} a_s$$

and a rank-1 lattice size $M := \prod_{s=1}^{d} a_s$. Then, the corresponding mapping $\boldsymbol{k} \mapsto \boldsymbol{k}\cdot\boldsymbol{z} \bmod M$ is bijective between $\times_{s=1}^{d}\left[-\frac{a_s-1}{2}, \frac{a_s-1}{2}\right]$ and $[0, M-1]\cap\mathbb{Z}$ and consequently, we have found a generating vector $\boldsymbol{z}$ and lattice size M such that the mapping $\boldsymbol{k} \mapsto \boldsymbol{k}\cdot\boldsymbol{z} \bmod M$ is injective for all $\boldsymbol{k} \in I^{d,\boldsymbol{\gamma}}_{\infty,N}$. Thus, we gain a reconstructing rank-1 lattice $\Lambda(\boldsymbol{z}, M, I^{d,\boldsymbol{\gamma}}_{\infty,N})$ for $I^{d,\boldsymbol{\gamma}}_{\infty,N}$.

Now, we estimate the cardinality of the found reconstructing rank-1 lattice $\Lambda(\boldsymbol{z}, M, I^{d,\boldsymbol{\gamma}}_{\infty,N})$, i.e., we would like to determine a close bound on $M := \prod_{s=1}^{d} a_s$. Clearly, the d coprime numbers a_s, $s = 1,\ldots,d$, should be chosen very carefully. For specific frequency index sets $I^{d,\boldsymbol{\gamma}}_{\infty,N}$ and suitable chosen a_s, $s = 1,\ldots,d$, we obtain $I^{d,\boldsymbol{\gamma}}_{\infty,N} = \times_{s=1}^{d}\left[-\frac{a_s-1}{2}, \frac{a_s-1}{2}\right]$ and, thus, we do not observe oversampling, i.e., the oversampling factor $M/|I^{d,\boldsymbol{\gamma}}_{\infty,N}|$ is determined by one. In particular for a constant sequence $\boldsymbol{\gamma}$, we may find sequences a_s, $s = 1,\ldots,d$, that are d successive coprime numbers and its product is much larger than $|I^{d,\boldsymbol{\gamma}}_{\infty,N}|$. In fact, the quotient $\prod_{s=1}^{d} a_s/|I^{d,\boldsymbol{\gamma}}_{\infty,N}|$ may grow exponentially in d. □

Example 3.20. Our second example also deals with convex frequency index sets. We consider weighted ℓ_1-balls $I^{d,\boldsymbol{\gamma}}_{1,N}$. The theoretical findings in Corollary 3.18 verify that we can find reconstructing rank-1 lattices $\Lambda(\boldsymbol{z}, M, I^{d,\boldsymbol{\gamma}}_{1,N})$ of sizes M that are not greater than $C_{p,d,\boldsymbol{\gamma}}|I^{d,\boldsymbol{\gamma}}_{1,N}|$. Certainly, the constant $C_{p,d,\boldsymbol{\gamma}}$ is an asymptotic bound and we cannot expect to observe fixed

Weighted convex ℓ_p-balls $I_{1,N}^{d,\boldsymbol{\gamma}}$, $I_{1,N}^{d,\mathbf{1}}$, $I_{\infty,N}^{d,\boldsymbol{\gamma}}$ – Comparison of Cardinalities						
		N				
	d	2	4	6	8	10
$\lvert I_{1,N}^{d,\boldsymbol{\gamma}}\rvert$	3	9	65	227	515	983
	6	15	241	1 567	6 955	23 431
	9	17	333	3 121	19 671	94 693
	10	17	351	3 433	23 193	120 251
$\lvert I_{1,N}^{d,\mathbf{1}}\rvert$	3	25	129	377	833	1 561
	6	85	1 289	8 989	40 081	134 245
	9	181	5 641	75 517	598 417	3 317 445
	10	221	8 361	134 245	1 256 465	8 097 453
$\lvert I_{\infty,N}^{d,\boldsymbol{\gamma}}\rvert$	3	45	441	1 287	3 315	6 783
	6	1 215	55 125	567 567	3 610 035	14 549 535
	9	3 645	2 480 625	99 324 225	1 592 025 435	12 963 635 685
	10	3 645	7 441 875	496 621 125	11 144 178 045	90 745 449 795

Table 3.2: Cardinalities of ℓ_p-ball frequency index sets $I_{1,N}^{d,\boldsymbol{\gamma}}$, $I_{1,N}^{d,\mathbf{1}}$, and $I_{\infty,N}^{d,\boldsymbol{\gamma}}$ for comparison, $\boldsymbol{\gamma} = \left(0.9^{s-1}\right)_{s\in\mathbb{N}}$.

oversampling factors in specific numerical examples. In particular, for fixed dimension d, the cardinalities of the ℓ_1-ball $I_{1,N}^{d,\boldsymbol{\gamma}}$ grows very fast and we showed in Lemma 2.8 that $|I_{1,N}^{d,\boldsymbol{\gamma}}| \gtrsim N^d$. Thus, we expect large cardinalities $|I_{1,N}^{d,\boldsymbol{\gamma}}|$ for even moderate dimensions $d > 3$ and moderate parameters N.

On the other hand, we can choose suitable weights $\boldsymbol{\gamma}$ in order to consider ℓ_1-balls of reasonable cardinalities in higher dimensions. Decreasing weights $\boldsymbol{\gamma}$, that tends to zero, cause decreasing expansions of the frequency index sets in higher dimensions, i.e., the absolute value of the sth component of the integer vector $\boldsymbol{k} \in I_{1,N}^{d,\boldsymbol{\gamma}}$ is bounded by $\lfloor \gamma_s N \rfloor$.

For our numerical example, we fixed the weights $\boldsymbol{\gamma} = \left(0.9^{s-1}\right)_{s\in\mathbb{N}}$ and the parameter $p = 1$. Table 3.2 presents the cardinalities of some frequency index sets $I_{1,N}^{d,\boldsymbol{\gamma}}$ of specific dimensions $d = 3, 6, 9, 10$ and parameters $N = 2, 4, 6, 8, 10$.

Often, one uses embeddings of the frequency index sets in order to reconstruct trigonometric polynomials (or approximate functions). We explain this strategy in a few words: One considers the trigonometric polynomial $f \in \Pi_{I_{1,N}^{d,\boldsymbol{\gamma}}}$ as a trigonometric polynomial that has its frequency support on a superset of $I_{1,N}^{d,\boldsymbol{\gamma}}$. Then, one reconstructs all frequencies of f supported on this superset using sampling values along a known sampling scheme and a corresponding fast algorithm that matches with the superset. Subsequently, one can project the solution f onto the space of trigonometric polynomials $\Pi_{I_{1,N}^{d,\boldsymbol{\gamma}}}$. Clearly, the supersets of $I_{1,N}^{d,\boldsymbol{\gamma}}$ should not cause huge additional costs for the reconstruction of f. The costs mainly depend on the cardinality of the superset. We consider two different approaches.

The first is the embedding of the weighted ℓ_1-ball $I_{1,N}^{d,\boldsymbol{\gamma}}$ in an unweighted ℓ_1-ball $I_{1,N}^{d,\mathbf{1}}$, which is as close as possible. We also specified the corresponding cardinalities of these frequency index sets in Table 3.2. According to those cardinalities, we have to expect large additional costs in order to reconstruct trigonometric polynomials supported on $I_{1,N}^{d,\mathbf{1}}$ instead of $I_{1,N}^{d,\boldsymbol{\gamma}}$

Weighted ℓ_1-balls $I_{1,2}^{d,\boldsymbol{\gamma}}$ – Reconstructing Rank-1 Lattices $\Lambda(\boldsymbol{z}, M, I_{1,2}^{d,\boldsymbol{\gamma}})$						
d	$\lvert I_{1,2}^{d,\boldsymbol{\gamma}}\rvert$	$M_{\text{Cor3.4}}$	$M_{\text{Alg3.3+Alg3.5}}$	$M_{\text{Alg3.7}}$	$M_{\text{Alg3.8}}$	$z_{\text{Alg3.8},d}$
1	5	5	5	5	5	1
2	7	7	7	8	7	3
3	9	11	9	11	9	4
4	11	11	11	14	11	5
5	13	13	13	17	13	6
6	15	17	15	20	15	7
7	17	17	17	23	17	8
8	17	17	17	23	17	0

Table 3.3: Cardinalities of reconstructing rank-1 lattices for weighted ℓ_1-ball frequency index sets $I_{1,2}^{d,\boldsymbol{\gamma}}$ found by applying Corollary 3.4, Algorithm 3.3 and 3.5, Algorithm 3.7, and Algorithm 3.8, $\boldsymbol{\gamma} = \left(0.9^{s-1}\right)_{s\in\mathbb{N}}$. Last column: generating vector $\boldsymbol{z}_{\text{Alg3.8}} = (z_{\text{Alg3.8},s})_{s=1}^{d}$ returned by Algorithm 3.8.

since we expect a large number of samples $M \geq |I_{1,N}^{d,\mathbf{1}}|$ compared to the cardinality of the weighted ℓ_1-ball.

On the other hand, we can also embed the weighted ℓ_1-ball $I_{1,N}^{d,\boldsymbol{\gamma}}$ to the weighted ℓ_∞-ball $I_{\infty,N}^{d,\boldsymbol{\gamma}}$. The main advantage of this embedding is that there are fast algorithms available in order to compute the d-dimensional discrete Fourier transform and we know, that we need exactly $|I_{\infty,N}^{d,\boldsymbol{\gamma}}|$ many sampling values in order to uniquely and stably reconstruct all trigonometric polynomials with frequencies supported on $I_{\infty,N}^{d,\boldsymbol{\gamma}}$. Anyway, Table 3.2 shows corresponding cardinalities of the closest supersets of $I_{1,N}^{d,\boldsymbol{\gamma}}$ of the weighted ℓ_∞-type. Obviously, this approach cannot be very successful even for dimensions $d \geq 6$. We would need a huge number of samples in order to reconstruct the trigonometric polynomial supported on the frequency index set $I_{1,N}^{d,\boldsymbol{\gamma}}$. Consequently, the embedding approach fails unless the corresponding embedding is really close.

As a consequence, we would like to give specific sampling schemes that allows the unique and stable direct reconstruction of all trigonometric polynomials with frequency supported on the weighted ℓ_1-ball $I_{1,N}^{d,\boldsymbol{\gamma}}$. In particular, we shift our attention to reconstructing rank-1 lattices for weighted ℓ_1-balls.

Since the weights $\boldsymbol{\gamma}$ decrease monotonically, we specify the effective dimension d_{eff} of the frequency index set $I_{1,N}^{d,\boldsymbol{\gamma}}$ by

$$d_{\text{eff}} := \max\{s \in \mathbb{N}\colon 0.9^{s-1}N \geq 1\} = \left\lfloor \frac{\log N}{\log(10/9)} \right\rfloor + 1. \tag{3.18}$$

Accordingly, the frequency index set $I_{1,N}^{d,\boldsymbol{\gamma}}$ has a maximal effective dimension d_{eff} depending on N, i.e., $I_{1,N}^{d,\boldsymbol{\gamma}} = I_{1,N}^{d_{\text{eff}},\boldsymbol{\gamma}} \times \left\{(0)_{s=d_{\text{eff}}+1}^{d}\right\}$ for $d > d_{\text{eff}}$.

We computed reconstructing rank-1 lattices of sizes $M_{\text{Cor3.4}}$, $M_{\text{Alg3.3+Alg3.5}}$, $M_{\text{Alg3.7}}$, and $M_{\text{Alg3.8}}$ for the weighted ℓ_1-balls $I_{1,N}^{d,\boldsymbol{\gamma}}$ having different parameter $N = 2, 6, 10$ and dimensions d up to the effective dimension d_{eff}, cf. Tables 3.3, 3.4, and 3.5.

The theoretical results $M_{\text{Cor3.4}}$ are much smaller than the very pessimistic right hand sides of (3.8) and (3.9), that bounds the number $M_{\text{Cor3.4}}$ by the term $c|I_{1,N}^{d,\boldsymbol{\gamma}}|^2$, where c is not

Weighted ℓ_1-balls $I_{1,6}^{d,\boldsymbol{\gamma}}$ – Reconstructing Rank-1 Lattices $\Lambda(\boldsymbol{z}, M, I_{1,6}^{d,\boldsymbol{\gamma}})$						
d	$\lvert I_{1,6}^{d,\boldsymbol{\gamma}}\rvert$	$M_{\text{Cor3.4}}$	$M_{\text{Alg3.3+Alg3.5}}$	$M_{\text{Alg3.7}}$	$M_{\text{Alg3.8}}$	$z_{\text{Alg3.8},d}$
1	13	13	13	13	13	1
2	63	103	71	72	71	11
3	227	701	317	367	317	60
4	551	2 857	918	1 192	918	256
5	997	8 461	1 964	2 559	1 964	601
6	1 567	19 163	3 699	5 612	3 699	1 363
7	2 169	34 511	6 238	9 456	6 238	2 324
8	2 697	49 169	7 902	13 009	7 902	3 139
9	3 121	59 281	9 634	19 097	9 634	4 011
10	3 433	62 533	9 881	25 249	9 881	4 373
11	3 653	62 533	11 666	29 397	11 666	4 486
12	3 799	62 533	12 180	31 436	11 666	2 513
13	3 877	62 533	12 319	34 061	11 666	1 258
14	3 911	62 533	12 319	38 790	11 666	678
15	3 933	62 533	12 721	39 342	11 666	309
16	3 943	62 533	12 721	40 236	11 666	155
17	3 945	62 533	12 721	42 512	11 666	17
18	3 947	62 533	12 721	42 975	11 666	18
19	3 947	62 533	12 721	42 975	11 666	0

Table 3.4: Cardinalities of reconstructing rank-1 lattices for weighted ℓ_1-ball frequency index sets $I_{1,6}^{d,\boldsymbol{\gamma}}$ found by applying Corollary 3.4, Algorithm 3.3 and 3.5, Algorithm 3.7, and Algorithm 3.8, $\boldsymbol{\gamma} = \left(0.9^{s-1}\right)_{s\in\mathbb{N}}$. Last column: generating vector $\boldsymbol{z}_{\text{Alg3.8}} = (z_{\text{Alg3.8},s})_{s=1}^{d}$ returned by Algorithm 3.8.

smaller than $\frac{1}{2}$. This behavior is caused by the convexity of the frequency index sets $I_{1,N}^{d,\boldsymbol{\gamma}}$. Since the frequency index sets $I_{1,N}^{d,\boldsymbol{\gamma}}$ are convex, a lot of differences $\boldsymbol{k}-\boldsymbol{h}$, $\boldsymbol{k},\boldsymbol{h} \in I_{1,N}^{d,\boldsymbol{\gamma}}$ coincides and the cardinalities of the corresponding difference sets $\mathcal{D}(I_{1,N}^{d,\boldsymbol{\gamma}})$ are much smaller than the upper bound $|I_{1,N}^{d,\boldsymbol{\gamma}}|(|I_{1,N}^{d,\boldsymbol{\gamma}}|-1)+1 \geq \mathcal{D}(I_{1,N}^{d,\boldsymbol{\gamma}})$. We go into detail and observe fast growing oversampling factors $M_{\text{Cor3.4}}/|I_{1,N}^{d,\boldsymbol{\gamma}}|$ for growing parameters N, even though we know that this factor is universally bounded for fixed dimension d, parameter p, and weight sequence $\boldsymbol{\gamma}$. In principle, even for $N = 10$, we are in some kind of a start-up. That means that the oversampling factors grow up to a specific bound. Since the cardinalities of the frequency index sets $I_{1,N}^{d,\boldsymbol{\gamma}}$ grow very fast, we may not be able to observe the upper bound by numerical tests, at least for larger dimensions d.

Anyway, the reconstructing rank-1 lattices $\Lambda(\boldsymbol{z}, M, I_{1,N}^{d,\boldsymbol{\gamma}})$ of practical interest, i.e., $M = M_{\text{Alg3.3+Alg3.5}}$, $M = M_{\text{Alg3.7}}$, or $M = M_{\text{Alg3.8}}$, are of moderately smaller size M than $M_{\text{Cor3.4}}$. Nevertheless, we also observe oversampling factors that grow with respect to N. In our examples, these oversampling factors are bounded by a constant smaller than eleven and, thus, are of moderate size.

Again, we take the embedding approaches from above into account and recognize that well adapted reconstructing rank-1 lattices offers a much more suitable possibility in order to reconstruct trigonometric polynomials supported on specific frequency index sets than the

Weighted ℓ_1-balls $I^{d,\boldsymbol{\gamma}}_{1,10}$ – Reconstructing Rank-1 Lattices $\Lambda(\boldsymbol{z}, M, I^{d,\boldsymbol{\gamma}}_{1,10})$						
d	$\lvert I^{d,\boldsymbol{\gamma}}_{1,10}\rvert$	$M_{\text{Cor3.4}}$	$M_{\text{Alg3.3+Alg3.5}}$	$M_{\text{Alg3.7}}$	$M_{\text{Alg3.8}}$	$z_{\text{Alg3.8},d}$
1	21	23	21	21	21	1
2	183	331	199	200	199	19
3	983	3 491	1 326	1 611	1 326	162
4	3 741	24 473	6 387	7 135	6 387	1 164
5	10 569	123 973	24 322	30 606	24 322	5 205
6	23 431	468 527	64 015	80 243	64 015	18 175
7	43 081	1 371 301	165 954	225 421	165 954	45 840
8	67 857	3 197 449	358 751	490 560	358 751	116 926
9	94 693	6 057 319	561 453	806 439	561 453	182 295
10	120 251	–	–	1 395 338	806 670	310 294
11	142 261	–	–	2 006 409	1 021 007	387 494
12	159 611	–	–	2 988 396	1 228 093	510 199
13	172 079	–	–	3 555 604	1 409 797	541 049
14	180 383	–	–	3 908 777	1 517 004	571 769
15	185 551	–	–	4 652 512	1 553 233	227 367
16	188 531	–	–	4 757 505	1 553 253	148 906
17	190 085	–	–	5 259 209	1 553 253	79 117
18	190 819	–	–	5 536 902	1 578 919	27 290
19	191 105	–	–	5 650 176	1 578 919	3 503
20	191 207	–	–	5 857 071	1 578 919	1 600
21	191 233	–	–	5 905 635	1 578 919	414
22	191 235	–	–	5 922 089	1 578 919	28
23	191 235	–	–	5 922 089	1 578 919	0

Table 3.5: Cardinalities of reconstructing rank-1 lattices for weighted ℓ_1-ball frequency index sets $I^{d,\boldsymbol{\gamma}}_{1,10}$ found by applying Corollary 3.4, Algorithm 3.3 and 3.5, Algorithm 3.7, and Algorithm 3.8, $\boldsymbol{\gamma} = \left(0.9^{s-1}\right)_{s\in\mathbb{N}}$. Last column: generating vector $\boldsymbol{z}_{\text{Alg3.8}} = (z_{\text{Alg3.8},s})^d_{s=1}$ returned by Algorithm 3.8.

discussed embedding approaches. □

Example 3.21. The first non-convex frequency index set under consideration are weighted ℓ_p-balls, where p is less than one. In particular, we focus on $\ell_{1/2}$-balls $|I^{d,\boldsymbol{\gamma}}_{\frac{1}{2},N}|$ and even summable $\boldsymbol{\gamma} = \left(0.9^{s-1}\right)_{s\in\mathbb{N}}$. Due to Lemma 2.6, we know that the cardinality of $I^{d,\boldsymbol{\gamma}}_{\frac{1}{2},N}$ can be bounded from above by terms that are independent of the dimension d. However, we expect a fast growing sequence $\left(|I^{d,\boldsymbol{\gamma}}_{\frac{1}{2},N}|\right)_{N\in\mathbb{N}}$ even for fixed moderate dimension $d \geq 3$, since there exists a weighted ℓ_1-ball $I^{d,\boldsymbol{\gamma}}_{1,d^{-1/2}N}$ of appropriate size that is embedded within the $\ell_{1/2}$-ball $|I^{d,\boldsymbol{\gamma}}_{\frac{1}{2},N}|$.

In particular for parameters $p < 1$, the upper bound $\tilde{C}_{p,d,\boldsymbol{\gamma}}$ on the oversampling factors $M_{\text{Cor3.4}}/|I^{d,\boldsymbol{\gamma}}_{p,N}|$ from Corollary 3.18 is very huge, i.e., for $p = 1/2$ we calculate $\tilde{C}_{1/2,d,\boldsymbol{\gamma}} \geq \frac{16}{3} d^{d/2} d!$, where we uniformly estimated the terms depending on $\boldsymbol{\gamma}$.

Since we found small reconstructing rank-1 lattices for the weighted ℓ_1-balls, cf. Example 3.20, and we showed the embeddings $I^{d,\boldsymbol{\gamma}}_{\frac{1}{2},N} \subset I^{d,\boldsymbol{\gamma}}_{1,N}$ in Lemma 2.6, we conjecture that there exist reasonable reconstructing rank-1 lattices $\Lambda(\boldsymbol{z}, M, I^{d,\boldsymbol{\gamma}}_{\frac{1}{2},N})$ for reasonable parameters N and moderate dimensions d. In Tables 3.6 and 3.7, we present rank-1 lattice sizes of reconstructing rank-1 lattices $\Lambda(\boldsymbol{z}, M, I^{d,\boldsymbol{\gamma}}_{\frac{1}{2},N})$, $N = 16, 35$. We applied the strategy mentioned in Table 3.1 only on the frequency index sets $I^{d,\boldsymbol{\gamma}}_{\frac{1}{2},35}$ that have a cardinality smaller than 100 000 since the computation of the difference sets $\mathcal{D}(I^{d,\boldsymbol{\gamma}}_{\frac{1}{2},35})$ takes a lot of computational time and memory.

Clearly, the $\ell_{1/2}$-balls are much smaller than the ℓ_1-balls for fixed parameters. However, we compare the reconstructing rank-1 lattice sizes $|\Lambda(\boldsymbol{z}, M, I^{d,\boldsymbol{\gamma}}_{\frac{1}{2},N})|$ with those $|\Lambda(\boldsymbol{z}, M, I^{d,\boldsymbol{\gamma}}_{1,N})|$ of weighted ℓ_1-balls of a similar cardinality, cf. Tables 3.4 and 3.5.

We observe that the theoretical lattice size $M_{\text{Cor3.4}}$ for the $\ell_{1/2}$-balls is much larger than those for the convex ℓ_1-balls of a similar cardinality. The reason for this observation is the non-convexity of the $\ell_{1/2}$-balls, that implies that the difference sets $\mathcal{D}(I^{d,\boldsymbol{\gamma}}_{\frac{1}{2},N})$ are much larger than those for the convex ℓ_1-balls. In detail, the number of coinciding differences $\boldsymbol{k} - \boldsymbol{h}$, $\boldsymbol{k}, \boldsymbol{h} \in I^{d,\boldsymbol{\gamma}}_{\frac{1}{2},N}$, is significantly smaller.

We call back to our mind that each lattice rule given by a reconstructing rank-1 lattice for a frequency index set I exactly integrates all trigonometric polynomials with frequencies supported on the corresponding difference set $\mathcal{D}(I)$. Thus, we expect larger reconstructing rank-1 lattice sizes with higher cardinalities of the difference set.

In accordance to that, we observe larger reconstructing rank-1 lattice sizes $M_{\text{Alg3.3+Alg3.5}}$, $M_{\text{Alg3.7}}$, $M_{\text{Alg3.8}}$ for $\ell_{1/2}$-balls compared to the reconstructing rank-1 lattice sizes for ℓ_1-balls of a similar cardinality. The two improvements, presented in Algorithms 3.7 and 3.8, allow for the faster computation of reconstructing rank-1 lattices even for frequency index sets $I^{d,\boldsymbol{\gamma}}_{\frac{1}{2},35}$ of higher cardinalities and, thus, higher dimensions.

We obtain that almost all reconstructing rank-1 lattice sizes $M_{\text{Alg3.3+Alg3.5}}$ and $M_{\text{Alg3.8}}$ are the same, in Table 3.7 at least for dimensions d up to ten. Algorithm 3.7 determines reconstructing rank-1 lattices for the frequency index sets $I^{d,\boldsymbol{\gamma}}_{\frac{1}{2},35}$ of larger sizes $M_{\text{Alg3.7}}$ in most cases. This observation is very probably caused by the inflexible choice of the generating vector. However, the determined rank-1 lattice sizes $M_{\text{Alg3.8}}$ of practical interest yield moderate oversampling factors $M_{\text{Alg3.8}}/|I^{d,\boldsymbol{\gamma}}_{\frac{1}{2},35}|$ smaller than 40.

We stress on the fact that the embedding approach mentioned in Example 3.20, now using the embedding $I^{d,\boldsymbol{\gamma}}_{\frac{1}{2},N} \subset I^{d,\boldsymbol{\gamma}}_{1,N}$, is also not successfully applicable in general. In particular, we observe huge differences in the cardinalities of the $\ell_{1/2}$ and ℓ_1-balls that fulfills the closest embedding, already for dimension $d = 4$. For example, we determine $|I^{4,\boldsymbol{\gamma}}_{1,35}| = 534\,055$ whereas the 8 835 frequencies of a trigonometric polynomial supported on the $\ell_{1/2}$-ball $I^{d,\boldsymbol{\gamma}}_{\frac{1}{2},35}$ can be uniquely reconstructed from 66 851 samples along the well adapted reconstructing rank-1 lattice $\Lambda((1, 59, 1264, 9300)^\top, 66\,851, I^{d,\boldsymbol{\gamma}}_{\frac{1}{2},35})$, cf. Table 3.7. □

3.8.2 Weighted Hyperbolic Crosses

Since the cardinality of all ℓ_p-balls grows approximately like N^d, the use of even sparser frequency grids has become very popular. In particular, one is interested in frequency index sets that relax the curse of dimension. One of the most famous strategy is to use so-called

Weighted $\ell_{\frac{1}{2}}$-balls $I^{d,\boldsymbol{\gamma}}_{\frac{1}{2},16}$ – Reconstructing Rank-1 Lattices $\Lambda(\boldsymbol{z}, M, I^{d,\boldsymbol{\gamma}}_{\frac{1}{2},16})$						
d	$\lvert I^{d,\boldsymbol{\gamma}}_{\frac{1}{2},16}\rvert$	$M_{\text{Cor3.4}}$	$M_{\text{Alg3.3+Alg3.5}}$	$M_{\text{Alg3.7}}$	$M_{\text{Alg3.8}}$	$z_{\text{Alg3.8},d}$
1	33	37	33	33	33	1
2	169	563	384	479	384	25
3	429	4 177	1 381	1 559	1 381	210
4	783	15 581	3 498	4 894	3 498	564
5	1 219	37 463	6 141	8 651	6 141	1 374
6	1 661	67 537	9 956	18 691	9 956	2 446
7	2 105	99 679	14 175	21 888	14 175	3 302
8	2 527	128 311	17 579	39 373	17 579	4 275
9	2 895	143 413	19 908	47 312	19 908	4 317
10	3 195	149 341	21 655	61 844	20 598	3 391
11	3 453	152 183	23 445	69 700	23 336	4 622
12	3 639	152 183	23 986	83 264	24 558	5 146
13	3 791	152 183	24 894	87 259	24 843	5 872
14	3 911	152 183	24 894	88 446	24 894	5 055
15	4 005	152 183	24 894	96 737	24 894	2 222
16	4 083	152 183	24 894	99 017	24 894	1 706
17	4 143	152 183	24 894	108 846	24 894	1 036
18	4 191	152 183	24 894	111 341	24 894	341
19	4 227	152 183	24 894	119 421	24 894	670
20	4 251	152 183	24 894	125 520	24 894	172
21	4 265	152 183	24 894	128 878	24 894	141
22	4 267	152 183	24 894	129 819	24 894	34
23	4 269	152 183	24 894	130 488	24 894	36
24	4 271	152 183	24 894	133 701	24 894	37
25	4 273	152 183	24 894	133 915	24 894	39
26	4 275	152 183	24 894	137 272	24 894	40
27	4 277	152 183	24 894	138 021	24 894	57
28	4 277	152 183	24 894	138 021	24 894	0

Table 3.6: Cardinalities of reconstructing rank-1 lattices for weighted $\ell_{\frac{1}{2}}$-ball frequency index sets $I^{d,\boldsymbol{\gamma}}_{1/2,16}$ found by applying Corollary 3.4, Algorithm 3.3 and 3.5, Algorithm 3.7, and Algorithm 3.8, $\boldsymbol{\gamma} = \left(0.9^{s-1}\right)_{s\in\mathbb{N}}$. Last column: generating vector $\boldsymbol{z}_{\text{Alg3.8}} = (z_{\text{Alg3.8},s})_{s=1}^{d}$ returned by Algorithm 3.8.

hyperbolic crosses in the frequency domain in order to reduce the number of degrees of freedom for different basis functions.

Certainly, we treat trigonometric polynomials with frequencies supported on weighted hyperbolic crosses $I^{d,\boldsymbol{\gamma}}_{\text{hc},N}$ as defined in (2.17). In some sense, one uses the weights in order to describe the interactions between the different spatial variables.

We would like to apply Corollary 3.4. For that reason, we estimate the cardinality of the difference sets $\mathcal{D}(I^{d,\boldsymbol{\gamma}}_{\text{hc},N})$, cf. (2.11), of weighted hyperbolic crosses $I^{d,\boldsymbol{\gamma}}_{\text{hc},N}$.

Lemma 3.22. *Let the dimension $d \in \mathbb{N}$, the parameter $N \in \mathbb{R}$, $N \geq 1$, and the weights $\boldsymbol{\gamma}$ with $1 \geq \gamma_1 \geq \ldots \geq \gamma_d > 0$ be given. Then, there exists a constant $C_{d,\boldsymbol{\gamma}} \in \mathbb{R}$, $C_{d,\boldsymbol{\gamma}} < \infty$,*

Weighted $\ell_{\frac{1}{2}}$-balls $I^{d,\boldsymbol{\gamma}}_{\frac{1}{2},35}$ – Reconstructing Rank-1 Lattices $\Lambda(\boldsymbol{z}, M, I^{d,\boldsymbol{\gamma}}_{\frac{1}{2},35})$						
d	$\lvert I^{d,\boldsymbol{\gamma}}_{\frac{1}{2},35}\rvert$	$M_{\text{Cor3.4}}$	$M_{\text{Alg3.3+Alg3.5}}$	$M_{\text{Alg3.7}}$	$M_{\text{Alg3.8}}$	$z_{\text{Alg3.8},d}$
1	0	71	71	71	71	1
2	749	2 789	1 912	2 237	1 912	59
3	3 285	47 111	14 797	14 228	14 797	1 264
4	8 835	379 273	66 851	82 447	66 851	9 300
5	18 019	1 757 221	210 991	269 545	210 991	32 239
6	30 263	5 456 317	493 713	818 346	493 713	84 684
7	44 867	12 521 473	919 065	1 740 252	919 065	199 329
8	60 479	22 765 229	1 668 126	2 954 608	1 668 126	369 750
9	76 109	35 109 583	2 423 987	4 860 233	2 423 987	544 787
10	90 983	47 048 609	3 168 384	7 174 048	3 168 384	835 846
11	104 615	–	–	9 967 618	3 947 025	675 582
12	116 571	–	–	12 767 667	4 315 244	947 574
13	126 761	–	–	14 897 553	5 021 560	1 124 837
14	135 105	–	–	18 605 649	5 535 857	1 158 645
15	141 877	–	–	20 634 382	5 753 575	1 130 537
16	147 195	–	–	23 862 830	5 991 436	1 185 121
17	151 371	–	–	25 975 777	6 001 930	776 496
18	154 569	–	–	27 269 873	6 001 930	303 222
19	156 955	–	–	28 281 941	6 001 930	243 504
20	158 715	–	–	31 061 843	6 001 930	127 198
21	159 999	–	–	31 195 936	6 001 930	53 173
22	160 917	–	–	31 284 480	6 001 930	8 602
23	161 551	–	–	32 151 152	6 001 930	10 878
24	161 965	–	–	32 506 567	6 001 930	4 745
25	162 221	–	–	32 763 537	6 140 573	1 846
26	162 381	–	–	33 034 181	6 140 573	2 045
27	162 477	–	–	33 080 498	6 140 573	271
28	162 549	–	–	33 180 624	6 140 573	257
29	162 595	–	–	33 484 046	6 140 573	207
30	162 621	–	–	33 778 321	6 140 573	145
31	162 631	–	–	33 941 110	6 140 573	151
32	162 633	–	–	34 012 574	6 140 573	83
33	162 635	–	–	34 121 356	6 140 573	85
34	162 637	–	–	34 322 520	6 140 573	87
35	162 637	–	–	34 322 520	6 140 573	0

Table 3.7: Cardinalities of reconstructing rank-1 lattices for weighted $\ell_{\frac{1}{2}}$-ball frequency index sets $I^{d,\boldsymbol{\gamma}}_{1/2,35}$ found by applying Corollary 3.4, Algorithm 3.3 and 3.5, Algorithm 3.7, and Algorithm 3.8, $\boldsymbol{\gamma} = \left(0.9^{s-1}\right)_{s\in\mathbb{N}}$. Last column: generating vector $\boldsymbol{z}_{\text{Alg3.8}} = (z_{\text{Alg3.8},s})_{s=1}^{d}$ returned by Algorithm 3.8.

which is independent of N, such that the cardinality of the difference set $\mathcal{D}(I^{d,\boldsymbol{\gamma}}_{\mathrm{hc},N})$ is bounded by

$$\mathcal{D}(I^{d,\boldsymbol{\gamma}}_{\mathrm{hc},N}) \leq C_{d,\boldsymbol{\gamma}} N^2 \max(\log N, 1)^{d-2}.$$

Proof. The technical proof of this lemma can be found in [Käm13a, Sec. 4]. ∎

A cheaper but less sharper upper bound of the cardinality $|\mathcal{D}(I^{d,\boldsymbol{\gamma}}_{\mathrm{hc},N})|$ of the difference set $\mathcal{D}(I^{d,\boldsymbol{\gamma}}_{\mathrm{hc},N})$ can be achieved using embedding arguments. In detail, we use Lemma 2.10, follow the arguments of [Käm13a, Lemma 4.1 and Remark 4.10], and estimate

$$\begin{aligned}\mathcal{D}(I^{d,\boldsymbol{\gamma}}_{\mathrm{hc},N}) &\subset \mathcal{D}(I^{d,\mathbf{1}}_{\mathrm{hc},N}) \subset I^{d,\mathbf{1}}_{\mathrm{hc},2^d N^2} \\ |\mathcal{D}(I^{d,\boldsymbol{\gamma}}_{\mathrm{hc},N})| &\leq |I^{d,\mathbf{1}}_{\mathrm{hc},2^d N^2}| \leq C_d N^2 \max(\log N, 1)^{d-1}.\end{aligned}$$

However, we use the result of Lemma 3.22 in order to bound the oversampling factor $M/|I^{d,\boldsymbol{\gamma}}_{\mathrm{hc},N}|$, where M is the size of a reconstructing rank-1 lattice $\Lambda(\boldsymbol{z}, M, I^{d,\boldsymbol{\gamma}}_{\mathrm{hc},N})$ determined by Corollary 3.4.

Corollary 3.23. *Let the dimension $d \in \mathbb{N}$, the parameter $N \in \mathbb{R}$, $N \geq 1$, and the weights $\boldsymbol{\gamma} \in [0,1]^{\mathbb{N}}$ with $\gamma_1 \geq \ldots \geq \gamma_d > 0$ be given. There exists a reconstructing rank-1 lattice $\Lambda(\boldsymbol{z}, M, I^{d,\boldsymbol{\gamma}}_{\mathrm{hc},N})$ of size $M \lesssim \frac{N}{\max(\log N,1)} |I^{d,\boldsymbol{\gamma}}_{\mathrm{hc},N}|$, i.e., the oversampling factor $\frac{M}{|I^{d,\boldsymbol{\gamma}}_{\mathrm{hc},N}|}$ can be bounded by a term $C_{d,\boldsymbol{\gamma}} \frac{N}{\max(\log N,1)}$, where the term $C_{d,\boldsymbol{\gamma}}$ is independent of N.*

Proof. We treat the case $d = 1$ separately. The frequency index set $I^{1,\boldsymbol{\gamma}}_{\mathrm{hc},N}$ is the set $\{-\lfloor \gamma_1 N \rfloor, \ldots, \lfloor \gamma_1 N \rfloor\}$. The rank-1 lattice $\Lambda(1, 2\lfloor \gamma_1 N \rfloor + 1, I^{1,\boldsymbol{\gamma}}_{\mathrm{hc},N})$ is a reconstructing one for this frequency index set. Accordingly, the condition $1 = \frac{M}{|I^{1,\boldsymbol{\gamma}}_{\mathrm{hc},N}|} \leq C_{1,\boldsymbol{\gamma}} \frac{N}{\max(\log N,1)}$ holds for all $C_{1,\boldsymbol{\gamma}} \geq 1$.

We consider higher dimensional cases, i.e., $d > 1$. Assuming $\lfloor \gamma_2 N \rfloor = 0$, the frequency index set $I^{d,\boldsymbol{\gamma}}_{\mathrm{hc},N}$ is in fact $I^{1,\boldsymbol{\gamma}}_{\mathrm{hc},N} \times \{(0)^d_{s=2}\}$ and we refer to the one-dimensional case. So, w.l.o.g., we require $\gamma_1 N \geq \gamma_2 N \geq 1$ and obtain that $I^{d,\boldsymbol{\gamma}}_{\mathrm{hc},N} \subset I^{d,\boldsymbol{\gamma}}_{\infty,N}$ the hyperbolic cross is contained in the d-dimensional box of edge length $2\lfloor \gamma_1 N \rfloor + 1$. On the other hand, M is a prime number that necessarily satisfies the inequality $M \geq |I^{d,\boldsymbol{\gamma}}_{\mathrm{hc},N}| \geq 2\lfloor \gamma_1 N \rfloor + 2\lfloor \gamma_2 N \rfloor + 1 > 2\lfloor \gamma_1 N \rfloor + 1$. Accordingly, each prime number M with $M \geq |I^{d,\boldsymbol{\gamma}}_{\mathrm{hc},N}|$ is coprime to all components of the elements of the difference set $\mathcal{D}(I^{d,\boldsymbol{\gamma}}_{\mathrm{hc},N})$, cf. Remark 3.5. The condition $M \geq |I^{d,\boldsymbol{\gamma}}_{\mathrm{hc},N}|$ is already necessary, due to the fact that we need at least as many sampling nodes as the number of frequency indices contained in $I^{d,\boldsymbol{\gamma}}_{\mathrm{hc},N}$.

Taking Lemma 2.10, 3.22, and equations (3.8) and (3.9) into account, we estimate

$$\frac{M}{|I^{d,\boldsymbol{\gamma}}_{\mathrm{hc},N}|} \leq \frac{\tilde{C}_{d,\boldsymbol{\gamma}} |\mathcal{D}(I^{d,\boldsymbol{\gamma}}_{\mathrm{hc},N})|}{|I^{d,\boldsymbol{\gamma}}_{\mathrm{hc},N}|} \leq \frac{\tilde{C}'_{d,\boldsymbol{\gamma}} N^2 \max(\log N, 1)^{d-2}}{c_{d,\boldsymbol{\gamma}} N \max(\log N, 1)^{d-1}} \leq C_{d,\boldsymbol{\gamma}} \frac{N}{\max(\log N, 1)}.$$

∎

According to Lemma 2.11 each sampling set $\mathcal{X}$ guaranteeing that the corresponding Fourier matrix $\boldsymbol{A} = \left(\mathrm{e}^{2\pi \mathrm{i} \boldsymbol{k} \cdot \boldsymbol{x}}\right)_{\boldsymbol{x} \in \mathcal{X},\, \boldsymbol{k} \in I^{d,\boldsymbol{\gamma}}_{\mathrm{hc},N}}$ has orthogonal columns needs not less than $|\mathcal{X}| \geq \gamma_1 \gamma_2 N^2$ many sampling nodes. Since the reconstruction property of a rank-1 lattice $\mathcal{X} = \Lambda(\boldsymbol{z}, M, I^{d,\boldsymbol{\gamma}}_{\mathrm{hc},N})$ implies the pairwise orthogonality of all columns of the corresponding Fourier matrix $\boldsymbol{A}$, we conclude $M \geq \gamma_1 \gamma_2 N^2$. Consequently, we determine an oversampling factor

$\frac{M}{|I^{d,\boldsymbol{\gamma}}_{\mathrm{hc},N}|} \gtrsim \frac{N}{\max(\log N,1)^{d-1}}$ in the asymptotic with respect to the parameter N, i.e., in general, we have to expect an oversampling factor $\frac{M}{|I^{d,\boldsymbol{\gamma}}_{\mathrm{hc},N}|}$ that depends on the dimension d, the weights $\boldsymbol{\gamma}$, and in particular N if we uniquely reconstruct hyperbolic cross trigonometric polynomials from sampling values along rank-1 lattices. Corollary 3.23 bounds this asymptotic oversampling factor from above. Thus, we estimate

$$\frac{N}{\max(\log N,1)^{d-1}} \lesssim \frac{M}{|I^{d,\boldsymbol{\gamma}}_{\mathrm{hc},N}|} \lesssim \frac{N}{\max(\log N,1)}. \tag{3.19}$$

Example 3.24. In order to illustrate the oversampling factors that we expect for reconstructing rank-1 lattices for weighted hyperbolic crosses, we fixed the weights $\boldsymbol{\gamma} = \left(\frac{1}{2}\right)_{s\in\mathbb{N}}$ and computed corresponding reconstructing rank-1 lattices for the weighted hyperbolic crosses $I^{d,\boldsymbol{\gamma}}_{\mathrm{hc},N}$, $d = 2,\dots,5$, $N = 2^1, 2^2, \dots, 2^{10}$. Due to Lemma 2.11 and Corollary 3.23 we are sure that there exist reconstructing rank-1 lattice sizes M for $I^{d,\boldsymbol{\gamma}}_{\mathrm{hc},N}$ such that $N^2/4 \leq M \leq C_{d,\boldsymbol{\gamma}} N^2 (\log N)^{d-2}$. We are interested in the asymptotic behavior on the dimension d. Thus we calculate

$$\frac{1}{4} \leq M/N^2 \leq C_{d,\boldsymbol{\gamma}} (\log N)^{d-2}$$

and

$$\log 1/4 \leq \log(M/N^2) \leq \log C_{d,\boldsymbol{\gamma}} + (d-2)\log\log N.$$

Accordingly, for fixed dimension d the slope of the graphs of M/N^2 on a log-log scale may illustrate the number a of the log factors, i.e., $M/N^2 \sim (\log N)^a$. Corresponding plots are presented in Figure 3.2 for dimensions $d = 2,3,4,5$. In particular, we see that the slopes of $2(\log N)^{d-2}$ and $M_{\mathrm{Cor3.4}}/N^2$ are very close to each other. Since the lattice sizes $M_{\mathrm{Cor3.4}}$ mainly depends on the cardinality of the difference sets $\mathcal{D}(I^{d,\boldsymbol{\gamma}}_{\mathrm{hc},N})$, all the figures indicate that the upper bound on the cardinality of $\mathcal{D}(I^{d,\boldsymbol{\gamma}}_{\mathrm{hc},N})$, cf. Lemma 3.22, is of the right order even in the log terms. Thus, we cannot achieve better theoretical results applying Corollary 3.4 in order to estimate sufficient oversampling factors of reconstructing rank-1 lattices.

Furthermore, the slopes of the log-log scaled plots of $M_{\mathrm{Alg3.7}}/N^2$ and $M_{\mathrm{Alg3.8}}/N^2$ can be found in the plots of Figures 3.2. We observe even smaller slopes than those obtained from the theoretical results. Thus, the oversampling factors $M_{\mathrm{Alg3.7}}/|I^{d,\boldsymbol{\gamma}}_{\mathrm{hc},N}|$ and $M_{\mathrm{Alg3.8}}/|I^{d,\boldsymbol{\gamma}}_{\mathrm{hc},N}|$ for these reconstructing rank-1 lattices might not grow as fast as the upper bounds. Nevertheless, Figures 3.2c and 3.2d suggest that also the lower bound on the oversampling factor in (3.19) is not sharp. □

Example 3.25. This example treat so-called symmetric weighted hyperbolic crosses $I^{d,\boldsymbol{\gamma}}_{\mathrm{hc},N}$ of different dimensions d and parameters $N = 4, 2^{2.5}$. We fixed the weights $\gamma_s = \left(\frac{108972864000}{2122061\pi^{10}}\right)^{1/10} \approx 0.941686$, $s = 1,\dots,d$ and determined reconstructing rank-1 lattices for weighted hyperbolic crosses $I^{d,\boldsymbol{\gamma}}_{\mathrm{hc},N}$, $d = 1,\dots,10$.

Since the parameters N are relatively small, we do not observe the asymptotic behavior but we realize mildly increasing oversampling factors $M_{\mathrm{Cor3.4}}/|I^{d,\boldsymbol{\gamma}}_{\mathrm{hc},N}|$, $M_{\mathrm{Alg3.3+Alg3.5}}/|I^{d,\boldsymbol{\gamma}}_{\mathrm{hc},N}|$, $M_{\mathrm{Alg3.7}}/|I^{d,\boldsymbol{\gamma}}_{\mathrm{hc},N}|$, and $M_{\mathrm{Alg3.8}}/|I^{d,\boldsymbol{\gamma}}_{\mathrm{hc},N}|$ with growing dimension d and/or growing parameter N, cf. Table 3.8. □

A lot of additional details and numerical examples on rank-1 lattices used for sampling hyperbolic cross trigonometric polynomials can be found in [Käm13a].

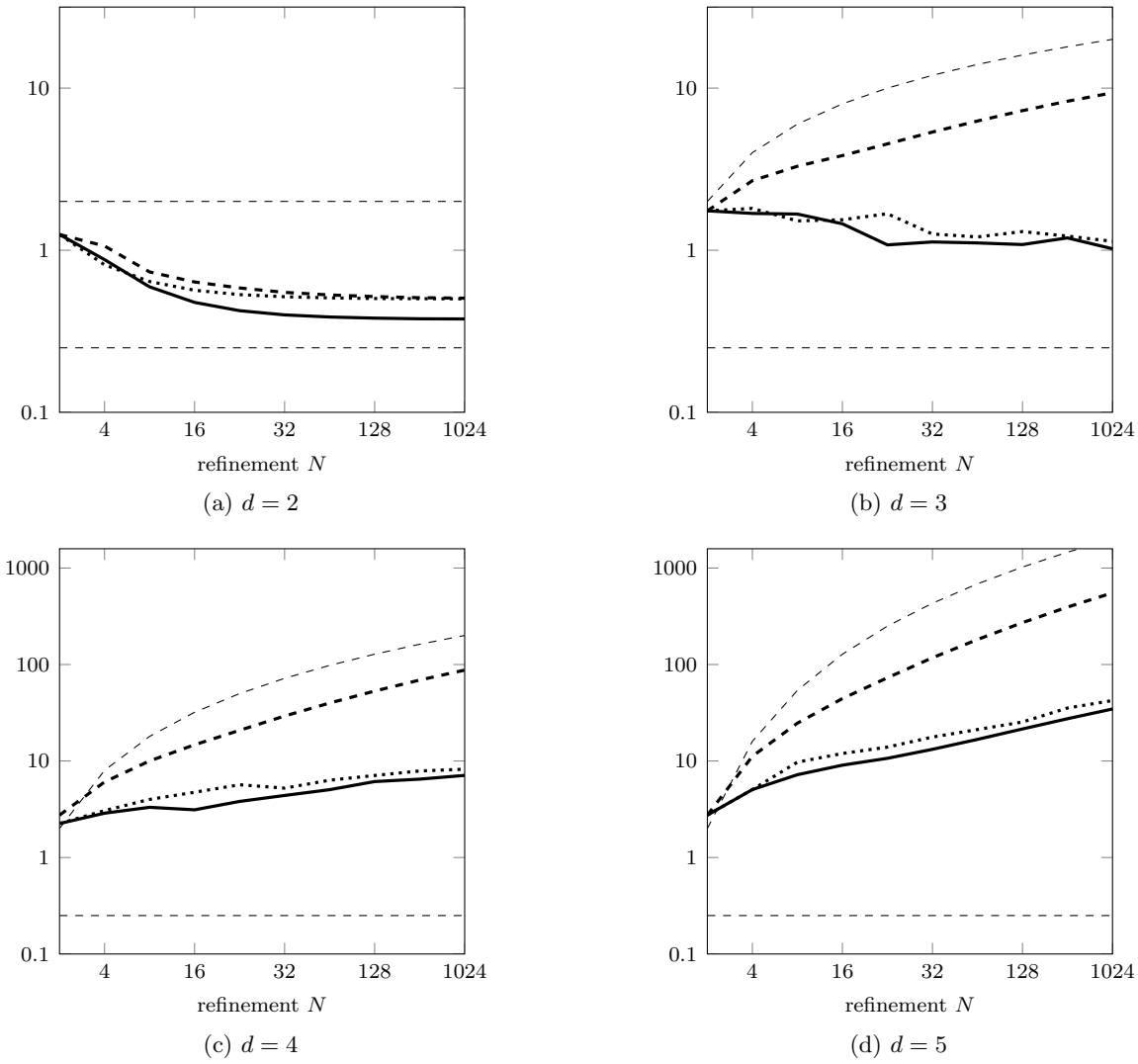

(a) $d = 2$ (b) $d = 3$

(c) $d = 4$ (d) $d = 5$

Figure 3.2: Cardinalities of reconstructing rank-1 lattices for weighted hyperbolic crosses $I^{d,\boldsymbol{\gamma}}_{\mathrm{hc},N}$ of different dimensions d for comparison. Upper dashed: $2(\log_2 N)^{d-2}$, lower dashed: $1/4$, thick dashed: $M_{\mathrm{Cor3.4}}/N^2$, thick dotted: $M_{\mathrm{Alg3.7}}/N^2$, thick solid: $M_{\mathrm{Alg3.8}}/N^2$, $\boldsymbol{\gamma} = \left(\frac{1}{2}\right)_{s\in\mathbb{N}}$.

3.8.3 Energy-norm Based Hyperbolic Crosses

We consider the last structured frequency index set from Section 2.3, the so-called energy-norm based hyperbolic crosses $|I^{d,\boldsymbol{\gamma},\alpha,\beta}_{\mathrm{ehc},N}|$, cf. (2.21). In particular, we fix the dimension d, the weights $\boldsymbol{\gamma}$, and the smoothness parameters $0 < -\alpha < \beta$ and consider the cardinalities of the frequency index sets $|I^{d,\boldsymbol{\gamma},\alpha,\beta}_{\mathrm{ehc},N}|$ and corresponding reconstructing rank-1 lattices $\Lambda(\boldsymbol{z}, M, I^{d,\boldsymbol{\gamma},\alpha,\beta}_{\mathrm{ehc},N})$ as a function of the parameter N.

Corollary 3.26. *Let the fixed dimension $d \in \mathbb{N}$, the parameter $N \in \mathbb{R}$, $N \geq 1$, the smoothness parameters $0 < -\alpha < \beta$ and the weights $\boldsymbol{\gamma} \in [0,1]^{\mathbb{N}}$ with $\gamma_1 \geq \ldots \geq \gamma_d > 0$ be given. Then, there exists a reconstructing rank-1 lattice $\Lambda(\boldsymbol{z}, M, I^{d,\boldsymbol{\gamma},\alpha,\beta}_{\mathrm{ehc},N})$ of size $M \lesssim N|I^{d,\boldsymbol{\gamma},\alpha,\beta}_{\mathrm{ehc},N}|$,*

Weighted hyperbolic crosses $I^{d,\boldsymbol{\gamma}}_{\mathrm{hc},N}$ – Reconstructing Rank-1 Lattices $\Lambda(\boldsymbol{z}, M, I^{d,\boldsymbol{\gamma}}_{\mathrm{hc},N})$							
	d	$\lvert I^{d,\boldsymbol{\gamma}}_{\mathrm{hc},N}\rvert$	$M_{\mathrm{Cor3.4}}$	$M_{\mathrm{Alg3.3+Alg3.5}}$	$M_{\mathrm{Alg3.7}}$	$M_{\mathrm{Alg3.8}}$	$z_{\mathrm{Alg3.8},d}$
$N = 4$	1	7	7	7	7	7	1
	2	33	53	38	38	38	7
	3	135	419	186	186	186	38
	4	513	3 037	875	875	875	186
	5	1 703	19 121	4 037	4 037	4 037	875
	6	5 217	108 413	17 060	14 836	17 060	3 937
	7	15 655	589 187	61 334	57 150	61 334	17 060
	8	47 617	–	–	238 087	238 682	61 334
	9	148 167	–	–	930 406	1 001 977	237 807
	10	469 409	–	–	3 934 421	3 458 502	898 550
$N = 2^{5/2}$	1	11	11	11	11	11	1
	2	61	113	73	73	73	11
	3	255	977	449	402	449	72
	4	1 001	7 451	2 497	2 185	2 497	449
	5	3 843	53 569	11 144	11 941	11 144	2 497
	6	13 125	344 423	45 393	53 048	45 393	11 059
	7	40 407	2 022 481	218 084	232 368	218 084	42 896
	8	117 905	–	–	1 020 265	916 888	199 813
	9	341 307	–	–	4 473 854	3 979 598	914 534
	10	1 007 629	–	–	19 632 641	17 436 325	3 979 598

Table 3.8: Cardinalities of reconstructing rank-1 lattices for equally weighted hyperbolic cross frequency index sets $I^{d,\boldsymbol{\gamma}}_{\mathrm{hc},N}$ found by applying Corollary 3.4, Algorithm 3.3 and 3.5, Algorithm 3.7, and Algorithm 3.8, $\boldsymbol{\gamma} = \left(\frac{108972864000}{2122061\pi^{10}}\right)^{1/10}\mathbf{1}$. Last column: generating vector $\boldsymbol{z}_{\mathrm{Alg3.8}} = (z_{\mathrm{Alg3.8},s})_{s=1}^{d}$ returned by Algorithm 3.8.

i.e., the oversampling factor $\frac{M}{|I^{d,\boldsymbol{\gamma},\alpha,\beta}_{\mathrm{ehc},N}|}$ *can be bounded by a term* $C_{d,\boldsymbol{\gamma},\alpha,\beta}N$*, where the term* $C_{d,\boldsymbol{\gamma},\alpha,\beta}$ *is independent of* N*.*

Proof. According to [KPV13, Lemma 2.6], the cardinality of $I^{d,\boldsymbol{\gamma},\alpha,\beta}_{\mathrm{ehc},N}$ is bounded from above by $|I^{d,\boldsymbol{\gamma},\alpha,\beta}_{\mathrm{ehc},N}| \leq \check{C}_{d,\boldsymbol{\gamma},\alpha,\beta}N$, where $\check{C}_{d,\boldsymbol{\gamma},\alpha,\beta}$ is a term that may depend on its subscripted parameters but not on N. W.l.o.g., we only consider frequency index sets $I^{d,\boldsymbol{\gamma},\alpha,\beta}_{\mathrm{ehc},N}$, where $|I^{d,\boldsymbol{\gamma},\alpha,\beta}_{\mathrm{ehc},N}| \geq 4$. Otherwise, i.e., $|I^{d,\boldsymbol{\gamma},\alpha,\beta}_{\mathrm{ehc},N}| < 4$, the frequency index set $I^{d,\boldsymbol{\gamma},\alpha,\beta}_{\mathrm{ehc},N}$ is in fact a one-dimensional frequency index set on the first axis and we refer to the first lines of the proof of Corollary 3.23.

So, we assume $|I^{d,\boldsymbol{\gamma},\alpha,\beta}_{\mathrm{ehc},N}| \geq 4$, apply equations (3.8) and (3.9), and determine a prime number $M_1 \geq M_{\mathrm{lb}}$, cf. Corollary 3.4, with

$$M_{\mathrm{lb}} \leq M_1 \leq |I^{d,\boldsymbol{\gamma},\alpha,\beta}_{\mathrm{ehc},N}|^2 \leq \check{C}_{d,\boldsymbol{\gamma},\alpha,\beta}N|I^{d,\boldsymbol{\gamma},\alpha,\beta}_{\mathrm{ehc},N}|.$$

On the other hand the frequency index set $I^{d,\boldsymbol{\gamma},\alpha,\beta}_{\mathrm{ehc},N}$ is contained in a d-dimensional box of edge length $2d^{-\alpha/(\alpha+\beta)}N + 1$, in detail, $I^{d,\boldsymbol{\gamma},\alpha,\beta}_{\mathrm{ehc},N} \subset I^{d,\mathbf{1}}_{\infty,d^{-\alpha/(\alpha+\beta)}N}$, cf. [KPV13, Lemma 2.2].

Applying Bertrand's postulate, we determine a prime number M_2 fulfilling

$$2d^{-\alpha/(\alpha+\beta)}N + 1 \leq 3d^{-\alpha/(\alpha+\beta)}N|I_{\mathrm{ehc},N}^{d,\boldsymbol{\gamma},\alpha,\beta}| \leq M_2 \leq 6d^{-\alpha/(\alpha+\beta)}N|I_{\mathrm{ehc},N}^{d,\boldsymbol{\gamma},\alpha,\beta}|.$$

Clearly, the prime number $M = \max(M_1, M_2) \geq M_{\mathrm{lb}}$ is coprime to all components of the elements of the difference set $\mathcal{D}(I_{\mathrm{ehc},N}^{d,\boldsymbol{\gamma},\alpha,\beta})$. Consequently, according to Corollary 3.4, we use a component–by–component strategy in order to find a generating vector $\boldsymbol{z} \in [1, M-1]^d$ such that the arising rank-1 lattice $\Lambda(\boldsymbol{z}, M)$ is a reconstructing one for the frequency index set $I_{\mathrm{ehc},N}^{d,\boldsymbol{\gamma},\alpha,\beta}$. At the end we estimate M and obtain

$$\max(M_{\mathrm{lb}}, 2d^{-\alpha/(\alpha+\beta)}N + 1) \leq M \leq \underbrace{\max(\check{C}_{d,\boldsymbol{\gamma},\alpha,\beta}, 6d^{-\alpha/(\alpha+\beta)})}_{=:C_{d,\boldsymbol{\gamma},\alpha,\beta}} N|I_{\mathrm{ehc},N}^{d,\boldsymbol{\gamma},\alpha,\beta}|.$$

■

Due to the fact that the cardinality of energy-norm based hyperbolic crosses $I_{\mathrm{ehc},N}^{d,\boldsymbol{\gamma},\alpha,\beta}$, i.e., $-\beta < \alpha < 0$, can be bounded by

$$\check{c}_{d,\boldsymbol{\gamma},\alpha,\beta}N \leq |I_{\mathrm{ehc},N}^{d,\boldsymbol{\gamma},\alpha,\beta}| \leq \check{C}_{d,\boldsymbol{\gamma},\alpha,\beta}N,$$

where $0 < \check{c}_{d,\boldsymbol{\gamma},\alpha,\beta} < \check{C}_{d,\boldsymbol{\gamma},\alpha,\beta} < \infty$, Corollary 3.26 gives us a constructive method in order to determine a reconstructing rank-1 lattice $\Lambda(\boldsymbol{z}, M, I_{\mathrm{ehc},N}^{d,\boldsymbol{\gamma},\alpha,\beta})$ of size $M \lesssim C_{d,\boldsymbol{\gamma},\alpha,\beta}N^2$. In general, the sampling scheme $\Lambda(\boldsymbol{z}, M, I_{\mathrm{ehc},N}^{d,\boldsymbol{\gamma},\alpha,\beta})$ suffers from an oversampling factor $M/|I_{\mathrm{ehc},N}^{d,\boldsymbol{\gamma},\alpha,\beta}|$ that depends linearly on N.

The following point of view shows in some sense the optimality of rank-1 lattices used for sampling trigonometric polynomials contained in $\Pi_{I_{\mathrm{ehc},N}^{d,\boldsymbol{\gamma},\alpha,\beta}}$. Considering only perfectly stable sampling schemes $\mathcal{X}$, i.e., the Fourier matrix $\boldsymbol{A} = \left(\mathrm{e}^{2\pi\mathrm{i}\boldsymbol{k}\cdot\boldsymbol{x}}\right)_{\boldsymbol{x}\in\mathcal{X},\,\boldsymbol{k}\in I_{\mathrm{ehc},N}^{d,\boldsymbol{\gamma},\alpha,\beta}}$ has orthogonal columns, then rank-1 lattices are asymptotically optimal in the number of sampling nodes with respect to the parameter N. In detail, on the one hand, a perfectly stable sampling scheme for trigonometric polynomials in $\Pi_{I_{\mathrm{ehc},N}^{d,\boldsymbol{\gamma},\alpha,\beta}}$ needs at least a cardinality of $\Omega\left(N^2\right)$, cf. Lemma 2.13. On the other hand, there exist reconstructing rank-1 lattices $\Lambda(\boldsymbol{z}, M, I_{\mathrm{ehc},N}^{d,\boldsymbol{\gamma},\alpha,\beta})$ that allow the perfectly stable reconstruction of all trigonometric polynomials $f \in \Pi_{I_{\mathrm{ehc},N}^{d,\boldsymbol{\gamma},\alpha,\beta}}$, where the lattice size $M \in \mathcal{O}\left(N^2\right)$ is bounded by terms depending on N in the optimal order. We stress on the fact, that Algorithm 3.3 and Corollary 3.26 present a deterministic component–by-component strategy in order to determine such reconstructing rank-1 lattices $\Lambda(\boldsymbol{z}, M, I_{\mathrm{ehc},N}^{d,\boldsymbol{\gamma},\alpha,\beta})$ of size M matching $M \leq |I_{\mathrm{ehc},N}^{d,\boldsymbol{\gamma},\alpha,\beta}|^2$.

At this point, we would like to mention that generalized sparse grids and, in particular, so-called energy-norm based sparse grids, cf. [BG99, BG04, Kna00, GH14], offer a suitable possibility to reconstruct trigonometric polynomials $f \in \Pi_{I_{\mathrm{ehc},N}^{d,\boldsymbol{\gamma},\alpha,\beta}}$ with a lower number of sampling values and an asymptotically lower number of arithmetical operations. In particular, $\mathcal{O}\left(|I_{\mathrm{ehc},N}^{d,\boldsymbol{\gamma},\alpha,\beta}|\right)$ sampling values and $\mathcal{O}\left(|I_{\mathrm{ehc},N}^{d,\boldsymbol{\gamma},\alpha,\beta}|\log(|I_{\mathrm{ehc},N}^{d,\boldsymbol{\gamma},\alpha,\beta}|)\right)$ arithmetical operations are needed in order to reconstruct trigonometric polynomials with frequencies supported on energy-norm based hyperbolic crosses $I_{\mathrm{ehc},N}^{d,\boldsymbol{\gamma},\alpha,\beta}$ using a sparse grid approach. Due to Lemma 2.13, we cannot expect a perfectly stable Fourier transform using energy-norm based sparse grids as sampling scheme in general. However, we demonstrate the asymptotic behavior of reconstructing rank-1 lattice sizes in N on subsets of weighted energy-norm based hyperbolic crosses.

Axis crosses $I^2_{\mathrm{ac},K}$ – Reconstructing Rank-1 Lattices $\Lambda(\boldsymbol{z}, M, I^2_{\mathrm{ac},K})$					
K	$\lvert I^2_{\mathrm{ac},K}\rvert$	$M_{\mathrm{Cor3.4}}$	$M_{\mathrm{Alg3.3+Alg3.5}}$	$M_{\mathrm{Alg3.7}}$	$M_{\mathrm{Alg3.8}}$
2	9	11	10	13	10
4	17	37	26	41	26
8	33	131	82	145	82
16	65	521	290	545	290
32	129	2 053	1 090	2 113	1 090
64	257	8 209	4 226	8 321	4 226
128	513	32 771	16 642	33 025	16 642
256	1 025	131 101	66 050	131 585	66 050
512	2 049	524 309	263 170	525 313	263 170
1 024	4 097	2 097 169	1 050 626	2 099 201	1 050 626

Table 3.9: Cardinalities of reconstructing rank-1 lattices for axis cross frequency index sets $I^2_{\mathrm{ac},2^l}$ found by applying Corollary 3.4, Algorithm 3.3 and 3.5, Algorithm 3.7, and Algorithm 3.8.

Example 3.27. Since the sparsity of an energy-norm based hyperbolic cross $I^{d,\boldsymbol{\gamma},\alpha,\beta}_{\mathrm{ehc},N}$ mainly depends on the parameters α and β, more precise on the quotient α/β, we would like to focus on even sparser frequency index sets, so-called d-dimensional axis crosses

$$I^d_{\mathrm{ac},K} := \bigcup_{s=1}^{d} \left\{ \left\{ (0)_{j=1}^{s-1} \right\} \times \{-\lfloor K \rfloor, \ldots, \lfloor K \rfloor\} \times \left\{ (0)_{j=s+1}^{d} \right\} \right\}. \tag{3.20}$$

In general, weighted energy-norm based hyperbolic crosses are supersets of axis crosses of appropriate size, cf. Lemma 2.12. In particular, for a fixed dimension d and fixed weights $\boldsymbol{\gamma}$, $1 \geq \gamma_1 \geq \gamma_2 \geq \ldots \geq \gamma_d > 0$, we determine the size K of the axis cross, that is contained in $I^{d,\boldsymbol{\gamma},\alpha,\beta}_{\mathrm{ehc},N}$ by $K = \left\lfloor \gamma_d^{\frac{\beta}{\alpha+\beta}} N \right\rfloor$. Accordingly, the size K of the largest axis cross $I^d_{\mathrm{ac},K}$ that is embedded in the weighted energy-norm based hyperbolic cross $I^{d,\boldsymbol{\gamma},\alpha,\beta}_{\mathrm{ehc},N}$ depends linearly on N.

Taking Lemma 2.13 into account, a perfectly stable sampling scheme for the energy-norm based hyperbolic cross $I^{d,\boldsymbol{\gamma},\alpha,\beta}_{\mathrm{ehc},N}$ needs at least $\left(\left\lfloor \gamma_1^{\frac{\beta}{\alpha+\beta}} N \right\rfloor + 1 \right) \left(\left\lfloor \gamma_2^{\frac{\beta}{\alpha+\beta}} N \right\rfloor + 1 \right) \geq (K+1)^2$ sampling nodes. In fact, we expose this using axis crosses of an appropriate size.

Our numerical test demonstrate this behavior for rank-1 lattices as perfectly stable spatial discretizations, see Tables 3.9 and 3.10. In particular, we determined reconstructing rank-1 lattices for axis crosses $I^d_{\mathrm{ac},K}$ of different dimensions d and sizes K. Since the embeddings $I^d_{\mathrm{ac},K} \subset I^{d,\boldsymbol{\gamma},\alpha,\beta}_{\mathrm{ehc},N}$ hold we have to expect reconstructing rank-1 lattices for $I^{d,\boldsymbol{\gamma},\alpha,\beta}_{\mathrm{ehc},N}$ which are of at least the same size as the reconstructing rank-1 lattices we determined for $I^d_{\mathrm{ac},K}$. Table 3.9 presents lattice sizes M for reconstructing rank-1 lattices for two-dimensional axis crosses, which are of particular interest. Even these two-dimensional frequency index sets needs at least reconstructing rank-1 lattice sizes, that are approximately K^2. More specific, we observe

$$M_{\mathrm{Cor3.4}} = \min\{M \text{ prime}\colon M > 2K^2 + 2\}$$

Axis crosses $I^d_{\mathrm{ac},1024}$ – Reconstructing Rank-1 Lattices $\Lambda(\boldsymbol{z}, M, I^d_{\mathrm{ac},1024})$					
d	$\lvert I^d_{\mathrm{ac},1024}\rvert$	$M_{\mathrm{Cor3.4}}$	$M_{\mathrm{Alg3.3+Alg3.5}}$	$M_{\mathrm{Alg3.7}}$	$M_{\mathrm{Alg3.8}}$
2	4 097	2 097 169	1 050 626	2 099 201	1 050 626
3	6 145	4 194 319	1 051 651	2 100 229	1 051 651
4	8 193	6 291 469	1 052 677	2 101 479	1 052 677
5	10 241	8 388 617	1 477 439	2 104 685	1 477 439
10	20 481	18 874 379	1 897 299	5 467 793	1 897 299
15	30 721	29 360 147	1 995 677	10 999 396	1 995 677
20	40 961	39 845 899	2 108 463	18 558 909	2 108 463

Table 3.10: Cardinalities of reconstructing rank-1 lattices for axis cross frequency index sets $I^d_{\mathrm{ac},1024}$ found by applying Corollary 3.4, Algorithm 3.3 and 3.5, Algorithm 3.7, and Algorithm 3.8.

and

$$M_{\mathrm{Alg3.3+Alg3.5}} = M_{\mathrm{Alg3.8}} = (K+1)^2 + 1.$$

Surprisingly, the resulting reconstructing rank-1 lattice sizes $M_{\mathrm{Alg3.7}}$ of Algorithm 3.7 are even larger than the theoretical lattice sizes $M_{\mathrm{Cor3.4}}$ determined by Corollary 3.4 for dimension $d = 2$.

However, the equality $M_{\mathrm{Cor3.4}} = \min\{M \text{ prime}\colon M > 2(d-1)K^2 + 2\}$ can be proved by counting the elements of the difference sets $\mathcal{D}(I^d_{\mathrm{ac},K})$ for arbitrary K and dimensions d. Table 3.10 presents the reconstructing rank-1 lattice sizes for axis crosses $I^d_{\mathrm{ac},1024}$. We computed such tables for all dimensions d up to 20 and different K that are powers of 2. In all our numerical experiments, we observed big gaps between the rank-1 lattice sizes of $M_{\mathrm{Alg3.3+Alg3.5}} = M_{\mathrm{Alg3.8}}$ for dimensions $d = 4$ and $d = 5$, cf. Table 3.10. Perhaps, this is caused by the structure of the found generating vectors $\boldsymbol{z}$. In particular, the generating vectors $\boldsymbol{z}$ are given by $\boldsymbol{z} = (1, K+1, K+2, K+3, \ldots)$, where the components z_{s_0} are the smallest positive integers that are relatively prime to all previous components z_s, $s = 2, \ldots, s_0 - 1$.

Nevertheless, we observe a slowly increasing sequence of reconstructing rank-1 lattice sizes for fixed K and growing dimension d in particular with respect to the fast growing sequence of the cardinalities of the difference sets $\mathcal{D}(I^d_{\mathrm{ac},K})$.

In contrast to the investigated axis crosses, we have to expect faster growing reconstructing rank-1 lattice sizes for weighted energy-norm based hyperbolic crosses $I^{d,\boldsymbol{\gamma},\alpha,\beta}_{\mathrm{ehc},N}$ for specific smoothness parameters α and β, weights $\boldsymbol{\gamma}$, and parameters N, since the corresponding difference sets may be of much higher cardinality and more complicated structure. In particular, the structure of the difference set $\mathcal{D}(I^{d,\boldsymbol{\gamma},\alpha,\beta}_{\mathrm{ehc},N})$ mainly affects the reconstruction property of a rank-1 lattice, since the corresponding integer dual lattice, see (3.11), must not touch the difference set. □

3.8.4 Arbitrary Sparse Frequency Index Sets

In a various number of applications, one assumes that all frequencies that are large in the order of magnitude of their absolute values have frequency indices that are contained in a d-dimensional cube of a fixed edge length. Certainly, one is interested in the frequency index set I and, in addition, the value of the corresponding frequencies. We will not discuss the identification problem here.

However, once one has identified a potentially unstructured frequency index set $I \subset \mathbb{Z}^d$, one is usually interested in a stable sampling scheme of a suitable cardinality. Certainly, rank-1 lattices offer a suitable possibility in order to sample trigonometric polynomials supported on an arbitrary frequency index set I.

In detail, we assume that the frequency index set I is a set of d-dimensional integer vectors that are contained in a box $[a,b]^d$, $a < b$, of an edge length $b - a < |I| - 1$. Then there exists a reconstructing rank-1 lattice $\Lambda(\boldsymbol{z}, M, I)$ of size M, $|I| \leq M \lesssim |I|^2$, cf. Corollary 3.4, such that the corresponding Fourier matrix $\boldsymbol{A} = \left(\mathrm{e}^{2\pi\mathrm{i}\frac{j}{M}\boldsymbol{k}\cdot\boldsymbol{z}}\right)_{j=0,\ldots,M-1,\boldsymbol{k}\in I}$ has orthogonal columns, i.e., $\boldsymbol{A}$ is perfectly stable.

Naturally, the difference set $\mathcal{D}(I)$ of a completely unstructured frequency index set I has a cardinality near the upper bound $|\mathcal{D}(I)| \leq |I|(|I|-1)+1$. Accordingly, we expect that the lower bound M_{lb} in Corollary 3.4 is of the same order in the cardinality of I. Consequently, our theoretical result guarantees the existence of a rank-1 lattice of the size $\frac{2}{3}(|\mathcal{D}(I)|+7) \leq \frac{2}{3}(|I|^2 - |I| + 8)$ that guarantees the unique reconstruction of all trigonometric polynomials supported on the frequency index set I. Moreover, the strategy mentioned in Table 3.1 determines reconstructing rank-1 lattices of a cardinality M, $|I| \leq M \leq \frac{2}{3}(|I|^2 - |I| + 8)$.

The frequency index sets I, that we use for determining the results of Table 3.11, are sets of integer vectors that are taken randomly from the uniformly distributed set $[-128, 128]^d \cap \mathbb{Z}^d$, $d = 2, 4, 8, 16, 32, 64, 128, 256$ and $d = 512, 1024$ only for small cardinalities of I due to the huge memory requirements of the computation of the difference set $\mathcal{D}(I)$. Except for dimension $d = 2$, where the difference sets are not as unstructured as in higher dimensions, we obtain that the number $M_{\mathrm{Cor3.4}}$ is very close to the number $\frac{|I|(|I|-1)+1}{2}$, which verifies in some sense that the cardinality of the difference set $\mathcal{D}(I)$ is indeed almost as big as $|I|^2$ as expected. The corresponding rank-1 lattice sizes $M_{\mathrm{Alg3.3+Alg3.5}}$, $M_{\mathrm{Alg3.7}}$, and $M_{\mathrm{Alg3.8}}$ are much smaller and in the same order of magnitude. However, we also recognize that all determined lattice sizes M seem to depend quadratically on the cardinality $|I|$ of the frequency index set I since doubling the cardinality of I yields approximately fourfold reconstructing rank-1 lattice sizes. Anyway, the most important observation on the numerical examples in Table 3.11 is that the rank-1 lattice sizes M of the reconstructing rank-1 lattices $\Lambda(\boldsymbol{z}, M, I)$ for frequency index sets I of a specific cardinality do not depend on the dimension d—at least for higher dimensions $d \geq 4$. In fact, we observed that the cardinalities of $\mathcal{D}(I)_{\downarrow 4}$ and $\mathcal{D}(I)_{\downarrow s}$, $s > 4$, hardly differ and, in addition, that the lattice sizes M and a suitable generating vector $\boldsymbol{z}$ is (almost) completely determined after the component–by–component step in the fourth dimension of our approaches.

3.9 Summary

In this chapter we considered rank-1 lattices as spatial discretizations in the d-dimensional torus $\mathbb{T}^d$. The evaluation of multivariate trigonometric polynomials $f = \sum_{\boldsymbol{k}\in I} \hat{f}_{\boldsymbol{k}} \mathrm{e}^{2\pi\mathrm{i}\boldsymbol{k}\cdot\circ} \in \Pi_I$, where the Fourier coefficients $\hat{f}_{\boldsymbol{k}}$, $\boldsymbol{k} \in I$, are given, at all nodes of a rank-1 lattice $\Lambda(\boldsymbol{z}, M)$ simplifies to a rearrangement and accumulations of the multivariate Fourier coefficients $\hat{f}_{\boldsymbol{k}}$, $\boldsymbol{k} \in I$, and a subsequent one-dimensional fast Fourier transform. The complexity of this evaluation is in $\mathcal{O}\left(M \log M + d|I|\right)$, see Section 3.1 for the details.

A corresponding unique reconstruction of multivariate trigonometric polynomials $f \in \Pi_I$ from sampling values along a rank-1 lattice $\Lambda(\boldsymbol{z}, M)$ is only possible if the corresponding Fourier matrix $\boldsymbol{A}$, cf. (2.7), consists of pairwise orthogonal columns, i.e., the matrix $\boldsymbol{A}^*\boldsymbol{A} = M\boldsymbol{I}$ holds and, thus, the condition number of $\boldsymbol{A}$ is one. We called a rank-1 lattice that

Sparse frequency index sets I – Reconstructing Rank-1 Lattices $\Lambda(\boldsymbol{z}, M, I)$					
	d	$M_{\text{Cor3.4}}$	$M_{\text{Alg3.3+Alg3.5}}$	$M_{\text{Alg3.7}}$	$M_{\text{Alg3.8}}$
$\lvert I\rvert = 750$	2	87 211	16 906	24 968	16 906
	4	279 817	24 708	33 759	24 278
	8	279 847	23 930	35 965	22 055
	16	279 863	27 672	39 781	24 028
	32	279 847	24 207	35 622	23 367
	64	279 857	23 965	34 913	21 977
	128	279 847	26 723	30 252	19 975
	256	279 883	27 449	31 933	20 457
	512	279 913	27 674	33 997	26 087
	1 024	279 883	27 081	40 654	26 965
$\lvert I\rvert = 1500$	2	114 259	51 767	54 029	51 767
	4	1 119 857	74 689	109 860	67 121
	8	1 120 001	86 680	100 149	85 882
	16	1 120 019	83 642	99 885	68 893
	32	1 119 949	68 515	105 304	79 440
	64	1 120 001	87 263	94 786	91 600
	128	1 120 019	101 866	88 794	82 731
	256	1 120 073	80 428	124 532	75 873
	512	1 120 051	100 146	122 559	83 723
$\lvert I\rvert = 3000$	2	126 713	62 819	62 819	62 819
	4	4 480 261	273 432	484 353	273 432
	8	4 481 137	311 380	364 226	250 617
	16	4 481 189	247 178	392 284	270 578
	32	4 481 311	306 413	378 129	286 970
	64	4 481 311	319 451	396 427	323 385
	128	4 481 369	312 365	411 125	319 329
	256	4 481 311	313 037	411 137	301 271
$\lvert I\rvert = 6000$	2	130 073	65 455	65 455	65 455
	4	17 912 899	1 026 554	1 366 076	1 026 554
	8	17 927 237	1 117 781	1 513 793	903 149
	16	17 927 807	1 042 108	1 483 023	1 048 182
	32	17 927 449	1 075 536	1 411 194	972 288
	64	17 927 509	1 058 443	1 462 364	1 048 111
	128	17 927 729	980 062	1 324 691	855 800
	256	17 927 587	1 089 369	1 540 621	1 030 930

Table 3.11: Cardinalities of reconstructing rank-1 lattices for arbitrary frequency index sets I that are chosen uniformly distributed from $[-128, 128]^d$.

entails such a Fourier matrix $\boldsymbol{A}$ for a fixed frequency index set I reconstructing rank-1 lattice $\Lambda(\boldsymbol{z}, M, I)$ for the frequency index set I. In addition, we stress on the fact that the reconstruction can be done using a one-dimensional fast Fourier transform and a subsequent rearrangement of the corresponding result. We specified the details on the computations in Algorithm 3.2. The corresponding complexity of the fast reconstruction is also bounded by $\mathcal{O}\left(M \log M + d|I|\right)$.

We determine sufficient conditions on the lattice size M such that there exists a reconstructing rank-1 lattice $\Lambda(\boldsymbol{z}, M, I)$ for the frequency index set I, cf. Corollary 3.4. In particular, this lattice size crucially depends on the structure of the difference set $\mathcal{D}(I)$ of the frequency index set I. Additionally, the found conditions on M allow for the component–by–component construction of a generating vector $\boldsymbol{z}$ of a reconstructing rank-1 lattice $\Lambda(\boldsymbol{z}, M, I)$, which enables us to give a deterministic suitable construction method for reconstructing rank-1 lattices, cf. Algorithm 3.3.

Due to the fact that $\boldsymbol{A}^*\boldsymbol{A} = M\boldsymbol{I}$ necessarily holds for a reconstructing rank-1 lattice $\Lambda(\boldsymbol{z}, M, I)$ for the frequency index set I, we get an extremely stable and fast algorithm for the reconstruction of multivariate trigonometric polynomials. Furthermore, we use the same algorithm, i.e., Algorithm 3.2, in order to compute approximations $\tilde{S}_I f = \sum_{\boldsymbol{k}\in I} \hat{\tilde{f}}_{\boldsymbol{k}} \mathrm{e}^{2\pi \mathrm{i} \boldsymbol{k}\cdot\circ} \in \Pi_I$ of functions $f \in \mathcal{A}_\omega(\mathbb{T}^d)$ and proved concrete error estimates in Theorem 3.11. In detail, the approximation $\tilde{S}_I f \in \Pi_I$ is a suitable approximation of f, if the exact Fourier partial sum $S_I f \in \Pi_I$ approximates f well and the approximated Fourier coefficients $\hat{\tilde{f}}_{\boldsymbol{k}}$, $\boldsymbol{k} \in I$, of f are computed using a lattice rule based on a reconstructing rank-1 lattice for I. In addition to the general approximation results, we discussed the extension of the approximation algorithm to an interpolation algorithm. More precisely, if a reconstructing rank-1 lattice $\Lambda(\boldsymbol{z}, M, I)$ for the frequency index set I is already determined, one extends the frequency index set I to $\tilde{I}$ such that $|\tilde{I}| = M$ holds and the reconstruction property is preserved, i.e., $\Lambda(\boldsymbol{z}, M, \tilde{I}) = \Lambda(\boldsymbol{z}, M, I)$, cf. Algorithm 3.6. The corresponding error estimates for $\tilde{S}_I f$ spread to $\tilde{S}_{\tilde{I}} f$, see Theorem 3.13.

By means of some examples, we illustrate that tractability properties of an approximation problem may be determined using our rank-1 lattice approach. In detail, the dependence of the cardinality of the frequency index set $I_N = \{\boldsymbol{k} \in \mathbb{Z}^d \colon \omega(\boldsymbol{k}) \leq N\}$ on the parameter N and the dimension d may allow for explicit statements on the tractability of approximation problems in spaces $\mathcal{A}_\omega(\mathbb{T}^d)$, cf. Section 3.6.

Moreover, we discuss some improvements of our search algorithms for reconstructing rank-1 lattices. Specifically, we present two basic deterministic component–by–component algorithms that constructs reconstructing rank-1 lattices for a given frequency index set I and has only low memory requirements. The main advantage of Algorithms 3.7 and 3.8 is that we determine whole reconstructing rank-1 lattices, i.e., the generating vectors $\boldsymbol{z}$ and in particular the lattice sizes M, by means of a component–by–component construction.

Finally, we treated the specific frequency index sets that are introduced in Chapter 2. We showed that reconstructing rank-1 lattices are suitable spatial discretizations in order to uniquely reconstruct trigonometric polynomials with frequencies supported on ℓ_p-balls, weighted hyperbolic crosses and weighted energy-norm based hyperbolic crosses. In particular, we applied our theoretical findings from this chapter and Chapter 2 and proved the following statements.

- There exist reconstructing rank-1 lattices $\Lambda(\boldsymbol{z}, M, I_{p,N}^{d,\boldsymbol{\gamma}})$ for ℓ_p-balls, where the number M of sampling values is optimal with respect to N, i.e., $M \lesssim N^d$, cf. Corollary 3.18.
- There exist reconstructing rank-1 lattices $\Lambda(\boldsymbol{z}, M, I_{\mathrm{ehc},N}^{d,\boldsymbol{\gamma},\alpha,\beta})$ for weighted energy-norm

based hyperbolic crosses, where the number M of sampling values is optimal with respect to N, i.e., $M \lesssim N^2$, and the additional assumption that the condition number $\mathrm{cond}_2(\boldsymbol{A})$ of the corresponding Fourier matrix $\boldsymbol{A}$ is one, cf. Corollary 3.26.

- There exist reconstructing rank-1 lattices $\Lambda(\boldsymbol{z}, M, I^{d,\boldsymbol{\gamma}}_{\mathrm{hc},N})$ for weighted hyperbolic crosses, where the number M of sampling values is optimal with respect to the assumption $\mathrm{cond}_2(\boldsymbol{A}) = 1$ and N up to logarithmic factors $\log N$, i.e., $M \lesssim N^2(\log N)^{d-2}$, cf. Corollary 3.23.

Additionally, we constructed reconstructing rank-1 lattices for specific frequency index sets and demonstrated the proved properties.

Chapter 4

Generated Sets

The most important advantage of sampling along rank-1 lattice nodes is the rank-1 structure of the sampling set and the associated simplification of the evaluation and reconstruction of multidimensional trigonometric polynomials, cf. Chapter 3. In detail, we use simple pre- or post-computations and only one one-dimensional (inverse) fast Fourier transform in order to evaluate or reconstruct multivariate trigonometric polynomials.

The stated advantages of rank-1 lattices and the availability of efficient algorithms and corresponding implementations for nonequispaced discrete Fourier transforms lead us to a generalization of this concept. In contrast to the definition of rank-1 lattices, we will allow real valued vectors as generating vectors in this chapter, cf. (3.1). Consequently, we define for a generating vector $\boldsymbol{r} \in \mathbb{R}^d$ and for a size $M \in \mathbb{N}$ the sampling set

$$\Lambda(\boldsymbol{r}, M) := \{\boldsymbol{x}_j := j\boldsymbol{r} \bmod \mathbf{1} \in \mathbb{T}^d \colon j = 0, \ldots, M-1\} \tag{4.1}$$

and call it a *generated set*. A two-dimensional sketch of the construction of a generated set is illustrated in Figure 4.1. Note that we change our definition comparing to rank-1 lattices. Nevertheless, for a fixed M and with $\boldsymbol{r} \in M^{-1}\mathbb{Z}^d$ we also obtain rank-1 lattices. Accordingly, each rank-1 lattice is also a generated set. In contrast to rank-1 lattices, we lose the group structure by allowing $\boldsymbol{r} \in \mathbb{R}^d$.

Specifically, a sequence $\big(j(r_1, \ldots, r_d)^\top \bmod \mathbf{1}\big)_{j \in \mathbb{N}_0}$ is uniformly distributed in the d-dimensional torus if and only if $r_s \in \mathbb{R} \setminus \mathbb{Q}$, $s = 1, \ldots, d$, and $r_1, \ldots, r_d$ are linearly independent over $\mathbb{Q}$, cf. [Wey16]. In [Ost82, Lar88], the authors determine upper bounds on discrepancies, which are quality measures for integration errors, for sampling sets $\Lambda(\boldsymbol{r}, M)$, $r_s \in \mathbb{R} \setminus \mathbb{Q}$, $s = 1, \ldots, d$, and $r_1, \ldots, r_d$ linearly independent over $\mathbb{Q}$.

Certainly, we are interested in reconstruction and approximation problems and, thus, take the results of K. Gröchenig, B. M. Pötscher, and H. Rauhut, cf. [GPR10], into account. Due to their results, with high probability we expect Fourier matrices $\boldsymbol{A}$, cf. (2.7), that have a small condition number, where the frequency index set I is given and fixed and the sampling set $\mathcal{X} \subset \mathbb{T}^d$ consists of sufficiently many independent and identically uniformly distributed sampling nodes $\boldsymbol{x} \in \mathbb{T}^d$. In particular, the number of sampling nodes $|\mathcal{X}|$ is bounded by terms $C|I| \log |I|$, where the term C does not depend on I but moderately on the target condition number of $\boldsymbol{A}$ and slightly on the probability.

Since the sequence $\big(j(r_1, \ldots, r_d)^\top \bmod \mathbf{1}\big)_{j=0,\ldots,M-1}$ may tend to the uniform distribution on the d-dimensional torus as M tends to infinity, we may get Fourier matrices $\boldsymbol{A}$ of full column rank and, in addition, a small condition number of $\boldsymbol{A}$ for large enough M.

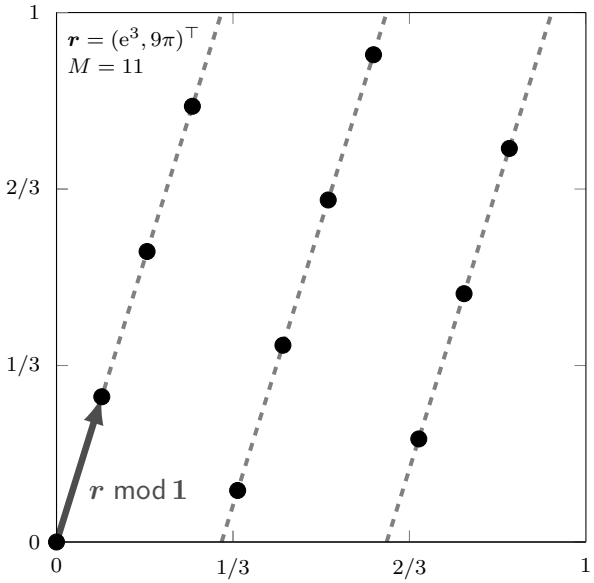

Figure 4.1: Generated set construction sketch.

On the other hand, we cannot treat irrational numbers in numerical applications due to the finite number representations on the used machines. Consequently, we shift our interest to sampling sets that are spanned by one real valued vector and use a suitable rational valued vector that is representable as usual floating point numbers in concrete applications.

However, the rank-1 structure of generated sets allows for a simultaneous evaluation of a trigonometric polynomial $f \in \Pi_I$ at all nodes of a generated set, i.e., the computation of the matrix vector product $\boldsymbol{A}\hat{\boldsymbol{f}}$, where $\boldsymbol{A}$ is the Fourier matrix, using simple pre-computations and a one-dimensional nonequispaced fast Fourier transform (NFFT), cf. Section 4.2. Similar to the rank-1 lattice approach, we have to assume Fourier matrices $\boldsymbol{A}$ of full column rank in order to compute a unique inversion of $\boldsymbol{A}$ using the pseudoinverse $(\boldsymbol{A}^*\boldsymbol{A})^{-1}\boldsymbol{A}^*$. We call a generated set that allows for the inversion of $\boldsymbol{A}^*\boldsymbol{A}$ reconstructing generated set for the frequency index set I, since the corresponding pseudoinverse $(\boldsymbol{A}^*\boldsymbol{A})^{-1}\boldsymbol{A}^*$ allows for the exact reconstruction of all trigonometric polynomials $f \in \Pi_I$ from the sampling values along this generated set, see Section 4.3.

In particular, we develop an algorithm that searches for reconstructing generated sets for a given frequency index set I and a target condition number for the matrix $\boldsymbol{A}$ in Section 4.4. The low computational costs of the search algorithm that uses a continuous optimization method, the guarantee on the condition number of $\boldsymbol{A}$, and the fast computations of the matrix vector products concerning $\boldsymbol{A}$ and an iterative method, i.e., a conjugate gradient method (CG), computing the pseudoinverse of $\boldsymbol{A}$ are the main advantages of generated sets.

Furthermore, we analyzed the approximation properties of the suggested sampling method. We prove upper bounds on the $L_2(\mathbb{T}^d)$ approximation error of our sampling method, which are equivalent to the estimates for rank-1 lattices, cf. Section 4.5. At this point, we would like to stress that we bounded the approximation error in the $L_\infty(\mathbb{T}^d)$ norm for rank-1 lattices indeed. Table 4.1 lists the most important details of the differences of the rank-1 lattice approach and the generated set approach.

In Section 4.6, we compare specific reconstructing generated sets found by our search method to reconstructing rank-1 lattices that we have determined in Chapter 3. The corre-

	Rank-1 Lattice	Generated Set
Evaluation	FFT $\mathcal{O}\left(M \log M + d\lvert I\rvert\right)$ Algorithm 3.1	NFFT $\mathcal{O}\left(M \log M + (d - \log \epsilon)\lvert I\rvert\right)$ Algorithm 4.1
Search technique for reconstructing sampling set	discrete component–by–component Algorithms 3.3 & 3.8	continuous simplex search method Algorithm 4.5
Reconstruction	FFT $\mathcal{O}\left(M \log M + d\lvert I\rvert\right)$ Algorithm 3.2	NFFT & CG $\mathcal{O}\left(r_{\varepsilon,\kappa}(M \log M + (d - \log \epsilon)\lvert I\rvert)\right)$ Algorithm 4.3
Error estimate for approximation	$\lVert f - \tilde{S}_{I_N} f \rvert L_\infty(\mathbb{T}^d)\rVert$ $\leq 2N^{-1}\lVert f\rvert\mathcal{A}_\omega(\mathbb{T}^d)\rVert$ Theorem 3.11	$\lVert f - \breve{S}_{I_N} f \rvert L_2(\mathbb{T}^d)\rVert$ $\leq C_\delta N^{-1}\lVert f\rvert\mathcal{A}_\omega(\mathbb{T}^d)\rVert$ Theorem 4.12

Table 4.1: Characteristics of rank-1 lattice and generated set sampling for comparison.

sponding number of sampling values that are needed in order to get stable Fourier matrices $\boldsymbol{A}$ are of our particular interest. In general, the cardinalities of reconstructing generated sets and reconstructing rank-1 lattices for the specific frequency index sets are similar—at least in its order of magnitude.

4.1 Motivation

At first, we consider a simple theoretical example, that motivates the intensive study of generated sets. The starting point is Remark 3.6 which states that for arbitrary $M' \in \mathbb{N}$ there exist frequency index sets I containing only two elements, i.e., $|I| = 2$, such that there exists no reconstructing rank-1 lattice $\Lambda(\boldsymbol{z}, M, I)$, where $M \leq M'$.

Lemma 4.1. *[Opposite of Remark 3.6] For arbitrary $d \in \mathbb{N}$, and arbitrary index set $I \subset \mathbb{Z}^d$ with $|I| = 2$, there exists a generated set $\Lambda(\boldsymbol{r}, M)$ of size $M = 2$ with perfectly stable Fourier matrix $\boldsymbol{A} = \left(\mathrm{e}^{2\pi \mathrm{i} j \boldsymbol{k}\cdot\boldsymbol{r}}\right)_{j=0,1;\, \boldsymbol{k}\in I}$, i.e., $\boldsymbol{A}^*\boldsymbol{A} = 2\boldsymbol{I}$.*

Proof. Let $\boldsymbol{h} \in I$ and $\boldsymbol{k} \in I$ and $\boldsymbol{h} \neq \boldsymbol{k}$ the two elements of the index set I. We define the matrix $\boldsymbol{C} = \begin{pmatrix} h_1 & \cdots & h_d \\ k_1 & \cdots & k_d \end{pmatrix}$ and distinguish three different cases.

- $\boldsymbol{h} = \boldsymbol{0}, \boldsymbol{k} \neq \boldsymbol{0}$ or $\boldsymbol{h} \neq \boldsymbol{0}, \boldsymbol{k} = \boldsymbol{0}$
  W.l.o.g. we assume $\boldsymbol{h} = \boldsymbol{0}$ and $\boldsymbol{k} \neq \boldsymbol{0}$. Then there exists an integer $s_0 \in \{1, \ldots, d\}$ with $k_{s_0} \neq 0$. We determine the generating vector $\boldsymbol{r}$ with $r_s = \begin{cases} 0 & \text{for } s \neq s_0, \\ \frac{1}{2k_s} & \text{for } s = s_0, \end{cases}$ and obtain $\boldsymbol{C}\boldsymbol{r} = \begin{pmatrix} \boldsymbol{h}\cdot\boldsymbol{r} \\ \boldsymbol{k}\cdot\boldsymbol{r} \end{pmatrix} = \begin{pmatrix} 0 \\ \frac{1}{2} \end{pmatrix}$.
- $\boldsymbol{h} \neq \boldsymbol{0}, \boldsymbol{k} = \lambda\boldsymbol{h}$ with $\lambda \in \mathbb{R} \setminus \{0, 1\}$
  Due to $\boldsymbol{h} \neq \boldsymbol{0}$ we can find an $s_0 \in \{1, \ldots, d\}$ with $h_{s_0} \neq 0$. A suitable generating vector

$\boldsymbol{r}$ is given by $r_s = \begin{cases} 0 & \text{for } s \neq s_0, \\ \frac{1}{2(\lambda-1)h_s} & \text{for } s = s_0, \end{cases}$ and we calculate

$$\boldsymbol{C}\boldsymbol{r} = \begin{pmatrix} \boldsymbol{h}\cdot\boldsymbol{r} \\ \boldsymbol{k}\cdot\boldsymbol{r} \end{pmatrix} = \begin{pmatrix} \frac{1}{2(\lambda-1)} \\ \frac{1}{2(\lambda-1)} + \frac{1}{2} \end{pmatrix}$$

- $\boldsymbol{h} \neq \boldsymbol{0}, \boldsymbol{k} \neq \lambda\boldsymbol{h}$ for all $\lambda \in \mathbb{R}$
  In order to obtain the current case, we have to require $d \geq 2$. Due to $\boldsymbol{h} \neq \boldsymbol{0} \neq \boldsymbol{k}$ and $\boldsymbol{h}$ and $\boldsymbol{k}$ are linear independent, the matrix $\boldsymbol{C}$ has full row rank. Consequently, we obtain the vector $\begin{pmatrix} 0 \\ \frac{1}{2} \end{pmatrix}$ in the image of $\boldsymbol{C}$ and we can find at least one solution of $\boldsymbol{C}\boldsymbol{r} = \begin{pmatrix} 0 \\ \frac{1}{2} \end{pmatrix}$. We determine a suitable $\boldsymbol{r}$ computing the solution of the normal equation of the second kind $\boldsymbol{C}\boldsymbol{C}^*\tilde{\boldsymbol{r}} = \begin{pmatrix} 0 \\ \frac{1}{2} \end{pmatrix}, \boldsymbol{r} = \boldsymbol{C}^*\tilde{\boldsymbol{r}}$.

For each of the three different cases we determined a generating vector $\boldsymbol{r}$ that fulfills $\boldsymbol{C}\boldsymbol{r} = \begin{pmatrix} c \\ c + \frac{1}{2} \end{pmatrix}$, $c \in \mathbb{R}$. We obtain that the Fourier matrix

$$\boldsymbol{A} = \left(\mathrm{e}^{2\pi\mathrm{i}j\boldsymbol{k}\cdot\boldsymbol{r}}\right)_{j=0,1;\,\boldsymbol{k}\in I} = \begin{pmatrix} 1 & 1 \\ \mathrm{e}^{2\pi\mathrm{i}c} & -\mathrm{e}^{2\pi\mathrm{i}c} \end{pmatrix},$$

is unitary up to the constant factor $\frac{1}{\sqrt{2}}$. Accordingly, the discrete Fourier transform with frequency index set I and corresponding sampling scheme $\Lambda(\boldsymbol{r}, 2)$ has condition number 1. ∎

According to the last lemma, for each multivariate trigonometric polynomial with frequencies supported on only two d-dimensional indices there exists a generated set of cardinality 2 such that the Fourier matrix $\boldsymbol{A}$ is perfectly stable. In particular, we can reconstruct the trigonometric polynomial in a stable and unique way applying the adjoint Fourier matrix $\boldsymbol{A}^*$ to the two-dimensional vector of the sampling values. In contrast to sampling along rank-1 lattices, the number of samples needed for the reconstruction is independent of the specific frequency indices of the trigonometric polynomial, cf. Remark 3.6.

In the next sections, we analyze different properties of generated sets in detail.

4.2 Evaluation of Multivariate Trigonometric Polynomials

We assume the index set $I \subset \mathbb{Z}^d$ being of finite cardinality and $f(\boldsymbol{x}) = \sum_{\boldsymbol{k}\in I} \hat{f}_{\boldsymbol{k}} \mathrm{e}^{2\pi\mathrm{i}\boldsymbol{k}\cdot\boldsymbol{x}} \in \Pi_I$. Our task is to evaluate f at all nodes $\boldsymbol{x}_j$, $j = 0, \ldots, M-1$, of the generated set $\Lambda(\boldsymbol{r}, M)$. We exploit the structure of the generated set $\Lambda(\boldsymbol{r}, M)$ and achieve

$$f(\boldsymbol{x}_j) = \sum_{\boldsymbol{k}\in I} \hat{f}_{\boldsymbol{k}} \mathrm{e}^{2\pi\mathrm{i}j\boldsymbol{k}\cdot\boldsymbol{r}} = \sum_{y\in\mathcal{Y}} \left(\sum_{\substack{\boldsymbol{k}\in I \\ \boldsymbol{k}\cdot\boldsymbol{r}\equiv y \pmod 1}} \hat{f}_{\boldsymbol{k}} \right) \mathrm{e}^{2\pi\mathrm{i}jy} = \sum_{y\in\mathcal{Y}} \hat{g}_y \mathrm{e}^{2\pi\mathrm{i}jy}, \tag{4.2}$$

where $\mathcal{Y} := \{\boldsymbol{k}\cdot\boldsymbol{r} \bmod 1 : \ \boldsymbol{k} \in I\}$ and $\hat{g}_y = \sum_{\substack{\boldsymbol{k}\in I \\ \boldsymbol{k}\cdot\boldsymbol{r}\equiv y \pmod 1}} \hat{f}_{\boldsymbol{k}}$.

Algorithm 4.1 Evaluation of a trigonometric polynomial at a generated set

Input:	$M \in \mathbb{N}$	cardinality of generated set $\Lambda(\boldsymbol{r}, M)$
	$\boldsymbol{r} \in \mathbb{R}^d$	generating vector of generated set $\Lambda(\boldsymbol{r}, M)$
	$I \subset \mathbb{Z}^d$	frequency index set of finite cardinality
	$\hat{\boldsymbol{f}} = \left(\hat{f}_{\boldsymbol{k}}\right)_{\boldsymbol{k} \in I}$	Fourier coefficients of $f \in \Pi_I$
for each $\boldsymbol{k} \in I$ ***do***		
$y_{\boldsymbol{k}} = \boldsymbol{k} \cdot \boldsymbol{r} \bmod 1$		
end for		
$\boldsymbol{f} = \text{adjNFFT\_1D}(\hat{\boldsymbol{f}}, \boldsymbol{y}, M)$		
Output:	$\boldsymbol{f} = \boldsymbol{A}\hat{\boldsymbol{f}} = \left(f\left(j\boldsymbol{r} \bmod \boldsymbol{1}\right)\right)_{j=0}^{M-1}$	function values of $f \in \Pi_I$

Concretely, the right hand side of equation (4.2) is an adjoint one-dimensional nonequispaced discrete Fourier transform (NDFT). In order to evaluate the trigonometric polynomial $f \in \Pi_I$ at all nodes of the generated set $\Lambda(\boldsymbol{r}, M)$ we have to pre-compute the corresponding values $y = \boldsymbol{k} \cdot \boldsymbol{r} \bmod 1$ for all $\boldsymbol{k} \in I$. This pre-computation step causes a complexity of $\mathcal{O}(d|I|)$. We compute the following adjoint NDFT using the adjoint one-dimensional *nonequispaced fast Fourier transform* (NFFT) with a complexity of $\mathcal{O}(M \log M + |\log \varepsilon||I|)$, cf. [KKP09], where ε describes the accuracy of the (adjoint) NFFT algorithm. We end up with a total complexity of $\mathcal{O}(M \log M + (|\log \varepsilon| + d)|I|)$. Pre-computing $\boldsymbol{k} \cdot \boldsymbol{r} \bmod 1$ and storing the corresponding mapping saves some complexity in the case that one evaluates several trigonometric polynomials from Π_I at all nodes of $\Lambda(\boldsymbol{r}, M)$. So we obtain a complexity of $\mathcal{O}(M \log M + |\log \varepsilon||I|)$. We outlined the described approach in Algorithm 4.1, where the function adjNFFT_1D is an adjoint one-dimensional NFFT. Note that one has to specify some accuracy parameters in order to use the NFFT software library, cf. [KKP09]. At this juncture, we leave these parameters out for reasons of simplification.

Algorithm 4.1 indicates the fast evaluation of multivariate trigonometric polynomials $f \in \Pi_I$ with frequencies supported on arbitrary index sets I. Please note the conformity with the evaluation of $f \in \Pi_I$ at rank-1 lattice nodes, cf. Section 3.1.

4.3 Reconstruction of Multivariate Trigonometric Polynomials

In this section, we analyze sufficient conditions on generated sets $\Lambda(\boldsymbol{r}, M)$ that allow for the unique reconstruction of a trigonometric polynomial with frequencies supported on a fixed index set I. In the following, each $\Lambda(\boldsymbol{r}, M)$ with this property is called *reconstructing generated set* for the index set I. The notation $\Lambda(\boldsymbol{r}, M, I)$ symbolizes the reconstruction property of $\Lambda(\boldsymbol{r}, M)$ with respect to I. Due to the fact that each (reconstructing) rank-1 lattice is also a (reconstructing) generated set, we can apply the existence results from Corollary 3.4.

In order to investigate the reconstruction property of a given sampling scheme we consider the corresponding Fourier matrix $\boldsymbol{A}$. In our specific case the matrix $\boldsymbol{A}$ is given by the frequency index set I, the generating vector $\boldsymbol{r}$, and the generated set size M, and reads as follows

$$\boldsymbol{A} = \boldsymbol{A}(I, \boldsymbol{r}, M) := \left(\mathrm{e}^{2\pi \mathrm{i} j \boldsymbol{k} \cdot \boldsymbol{r}}\right)_{j=0,\ldots,M-1;\, \boldsymbol{k} \in I}. \tag{4.3}$$

Below, we will use the notation $\boldsymbol{A}$ as far as possible. In cases where we consider various

different Fourier matrices, we will use the explicit notation $\boldsymbol{A}(I, \boldsymbol{r}, M)$.

Certainly, the reconstruction of multivariate trigonometric polynomials supported on the frequency index set I requires a number of samples M not smaller than the number of frequency indices $|I|$. In detail, the matrix $\boldsymbol{A}$ needs a full column rank and thus at least as many rows as columns. The essential condition on the generating vector $\boldsymbol{r}$ guaranteeing that $\Lambda(\boldsymbol{r}, M)$, $M \geq |I|$, is a reconstructing generated set is specified in the following lemma.

Lemma 4.2. *Let the frequency index set I of finite cardinality and the generated set $\Lambda(\boldsymbol{r}, M)$, $M \geq |I|$, be given. Then the Fourier matrix $\boldsymbol{A}(I, \boldsymbol{r}, M)$ in (4.3) is*

- *either of full column rank, i.e., $\boldsymbol{k} \cdot \boldsymbol{r} \not\equiv \boldsymbol{h} \cdot \boldsymbol{r} \pmod 1$ for all $\boldsymbol{k} \neq \boldsymbol{h}$, $\boldsymbol{k}, \boldsymbol{h} \in I$,*
- *or has at least two identical columns.*

Proof. The Fourier matrix $\boldsymbol{A}(I, \boldsymbol{r}, M)$ is a transposed Vandermonde matrix. The first $|I|$ rows of $\boldsymbol{A}(I, \boldsymbol{r}, M)$ form a square Vandermonde matrix $\boldsymbol{A}(I, \boldsymbol{r}, |I|)$. We number the frequency indices contained in I, i.e., $I = \{\boldsymbol{k}_1, \ldots, \boldsymbol{k}_{|I|}\}$. According to [HJ85, Sec. 0.9.11], the corresponding determinant is given by

$$\det(\boldsymbol{A}(I, \boldsymbol{r}, |I|)) = \prod_{1 \leq \ell < l \leq |I|} (\mathrm{e}^{2\pi \mathrm{i} y_l} - \mathrm{e}^{2\pi \mathrm{i} y_\ell}),$$

where $y_l = \boldsymbol{k}_l \cdot \boldsymbol{r}$. The determinant $\det(\boldsymbol{A}(I, \boldsymbol{r}, |I|))$ is nonzero iff $\mathrm{e}^{2\pi \mathrm{i} y_l}(1 - \mathrm{e}^{2\pi \mathrm{i} y_\ell - y_l}) \neq 0$ for all $1 \leq \ell < l \leq |I|$, i.e., all differences $y_\ell - y_l$, $1 \leq \ell < l \leq |I|$ have to be non-integer. Using the definition of y_l and $y_\ell - y_l = -(y_l - y_\ell)$, we obtain the condition $\boldsymbol{k}_l \cdot \boldsymbol{r} \not\equiv \boldsymbol{k}_\ell \cdot \boldsymbol{r} \pmod 1$ for all $\boldsymbol{k}_l \neq \boldsymbol{k}_\ell$, $\boldsymbol{k}_l, \boldsymbol{k}_\ell \in I$, in order to obtain a regular matrix $\boldsymbol{A}(I, \boldsymbol{r}, |I|)$. The regularity of $\boldsymbol{A}(I, \boldsymbol{r}, |I|)$ yields that the rows of $\boldsymbol{A}(I, \boldsymbol{r}, |I|)$ and hence the first $|I|$ rows of $\boldsymbol{A}(I, \boldsymbol{r}, M)$, $M \geq |I|$, are linear independent. Accordingly, the rank of $\boldsymbol{A}(I, \boldsymbol{r}, M)$ is at least $|I|$. Since the matrix $\boldsymbol{A}(I, \boldsymbol{r}, M)$ has $|I|$ columns, the rank of $\boldsymbol{A}(I, \boldsymbol{r}, M)$ is exactly $|I|$, i.e., the matrix $\boldsymbol{A}(I, \boldsymbol{r}, M)$ has full column rank. On the other hand, let us assume that there exist $l \neq \ell$ such that $\boldsymbol{k}_l \cdot \boldsymbol{r} \equiv \boldsymbol{k}_\ell \cdot \boldsymbol{r} \pmod 1$. Then the terms $\mathrm{e}^{2\pi \mathrm{i} y_l}$ and $\mathrm{e}^{2\pi \mathrm{i} y_\ell}$ produce the same entries in the columns numbered with l and ℓ within the transposed Vandermonde matrix $\boldsymbol{A}(I, \boldsymbol{r}, M)$. Consequently, we have at least two identical columns in $\boldsymbol{A}(I, \boldsymbol{r}, M)$. ∎

According to Lemma 4.2 and assuming $M \geq |I|$, the generating vector $\boldsymbol{r} \in \mathbb{R}^d$ determines the reconstruction property of the generated set $\Lambda(\boldsymbol{r}, M)$ with respect to I. In detail, we recognize the necessary condition

$$|\mathcal{Y}(I, \boldsymbol{r})| = |I|,$$

where $\mathcal{Y}(I, \boldsymbol{r}) := \{\boldsymbol{k} \cdot \boldsymbol{r} \bmod 1 \colon \boldsymbol{k} \in I\} \subset \mathbb{T}^d$ is a discrete subset of the one-dimensional torus. For an arbitrary fixed frequency index set I we are interested in the existence of generating vectors $\boldsymbol{r}$ fulfilling $|\mathcal{Y}(I, \boldsymbol{r})| = |I|$. In fact we simply show, that we can consider $\boldsymbol{r} \in (0, 1)^d$ as uniformly distributed random variable and the probability of choosing $\boldsymbol{r}$ such that $|\mathcal{Y}(I, \boldsymbol{r})| = |I|$ is one.

Lemma 4.3. *Let $I \subset \mathbb{Z}^d$ of finite cardinality. Then, the Lebesgue measure of the set*

$$G(I) := \left\{ \boldsymbol{r} \in (0, 1)^d \colon |\mathcal{Y}(I, \boldsymbol{r})| = |I| \right\}$$

is one, i.e., in formula $\lambda_d(G(I)) = 1$.

Proof. We show that the Lebesgue measure of the complement $G(I)^{\complement}$ of $G(I)$ is zero.

$$\begin{aligned} G(I)^{\complement} &= \left\{ \boldsymbol{r} \in (0,1)^d \colon |\mathcal{Y}(I,\boldsymbol{r})| < |I| \right\} \\ &= \left\{ \boldsymbol{r} \in (0,1)^d \colon \exists \boldsymbol{k}_1, \boldsymbol{k}_2 \in I \text{ s.t. } \boldsymbol{k}_1 \cdot \boldsymbol{r} \equiv \boldsymbol{k}_2 \cdot \boldsymbol{r} \pmod 1 \right\} \\ &= \left\{ \boldsymbol{r} \in (0,1)^d \colon \exists \boldsymbol{k} \in \mathcal{D}(I) \text{ s.t. } \boldsymbol{k} \cdot \boldsymbol{r} \equiv 0 \pmod 1 \right\} \\ &= \bigcup_{\boldsymbol{k} \in \mathcal{D}(I)} \bigcup_{a \in \mathbb{Z}} \left\{ \boldsymbol{r} \in (0,1)^d \colon \boldsymbol{k} \cdot \boldsymbol{r} = a \right\}. \end{aligned}$$

Since the frequency index set I is of finite cardinality, the difference set $\mathcal{D}(I)$, cf. (2.11), is embedded in an unweighted ℓ_1-ball of appropriate size L, i.e., $\mathcal{D}(I) \subset I_{1,L}^{d,\mathbf{1}}$, where $I_{1,L}^{d,\mathbf{1}}$ is defined in Equation (2.15). We estimate $|\boldsymbol{k} \cdot \boldsymbol{r}| \leq \|\boldsymbol{k}\|_1 \leq L$ and conclude

$$\begin{aligned} G(I)^{\complement} &= \bigcup_{\boldsymbol{k} \in \mathcal{D}(I)} \bigcup_{a=-L}^{L} \left\{ \boldsymbol{r} \in (0,1)^d \colon \boldsymbol{k} \cdot \boldsymbol{r} = a \right\} \\ &\subset \bigcup_{\boldsymbol{k} \in \mathcal{D}(I)} \bigcup_{a=-L}^{L} \left\{ \boldsymbol{r} \in \mathbb{R}^d \colon \boldsymbol{k} \cdot \boldsymbol{r} = a \right\}. \end{aligned}$$

In the last line, we see that a finite union of vector hyperplanes of dimension $d-1$ covers the set $G(I)^{\complement}$. Each of this vector hyperplanes has d-dimensional Lebesgue measure zero. ∎

Due to the last lemma, we observe that we can randomly choose a generating vector $\boldsymbol{r} \in (0,1)^d$ and we can expect that the corresponding generated set $\Lambda(\boldsymbol{r}, M)$, $M \geq |I|$, is a reconstructing generated set with respect to the frequency index set I. At this point, we would like to remind the reader that we cannot expect to choose $\boldsymbol{r}$ randomly over the real vectors contained in $(0,1)^d$ in numerical applications. Using a number representation of finite precision, we choose $\boldsymbol{r}$ randomly over a discrete subset of finite cardinality contained in $(0,1)^d$ and, thus, each candidate $\boldsymbol{r}$ with $|\mathcal{Y}(I,\boldsymbol{r})| < |I|$ will be chosen with a probability larger than zero, provided that such $\boldsymbol{r}$ is representable on the machine.

Up to now, we investigated the reconstruction properties of generated sets from a theoretical point of view and showed that this mainly depends on the frequency index set and the generating vector. The next lemma points out the concrete method we will use in order to reconstruct trigonometric polynomials $f \in \Pi_I$ from the sampling values $\left(f\left(\frac{j}{M}\boldsymbol{r}\right)\right)_{j=0}^{M-1}$ along a reconstructing generated set $\Lambda(\boldsymbol{r}, M, I)$.

Lemma 4.4. *Let the dimension $d \in \mathbb{N}$, the frequency index set $I \subset \mathbb{Z}^d$ of finite cardinality, and the reconstructing generated set $\Lambda(\boldsymbol{r}, M, I)$ be given, i.e., the corresponding Fourier matrix $\boldsymbol{A}$, cf.* (4.3)*, is of full column rank. We assume that the vector $\boldsymbol{f} = (f(j\boldsymbol{r}))_{j=0}^{M-1} \in \mathbb{C}^M$ belongs to the image of $\boldsymbol{A}$. Then we can uniquely reconstruct the Fourier coefficients $\hat{\boldsymbol{f}} \in \mathbb{C}^{|I|}$ of the trigonometric polynomial $f \in \Pi_I$ satisfying $\boldsymbol{A}\hat{\boldsymbol{f}} = \boldsymbol{f}$.*

Proof. Due to the full column rank of $\boldsymbol{A}$ we obtain a unique solution $\hat{\boldsymbol{f}}$ of the normal equation $\boldsymbol{A}^*\boldsymbol{A}\hat{\boldsymbol{f}} = \boldsymbol{A}^*\boldsymbol{f}$. In addition, $\boldsymbol{A}\hat{\boldsymbol{f}}$ and $\boldsymbol{f} \in \left\{ \boldsymbol{A}\boldsymbol{x} : \boldsymbol{x} \in \mathbb{C}^{|I|} \right\} \subset \mathbb{C}^M$ are orthogonal to the null space of $\boldsymbol{A}^*$. Consequently, $\boldsymbol{A}\hat{\boldsymbol{f}} - \boldsymbol{f}$ is orthogonal to the null space of $\boldsymbol{A}^*$ and $\boldsymbol{A}^*\left(\boldsymbol{A}\hat{\boldsymbol{f}} - \boldsymbol{f}\right) = \boldsymbol{0}$ implies $\boldsymbol{A}\hat{\boldsymbol{f}} - \boldsymbol{f} = \boldsymbol{0}$. ∎

Algorithm 4.2 Adjoint of the evaluation of a trigonometric polynomial at a generated set

Input:	$\boldsymbol{r} \in \mathbb{R}^d$	generating vector of generated set $\Lambda(\boldsymbol{r}, M)$
	$I \subset \mathbb{Z}^d$	frequency index set of finite cardinality
	$\boldsymbol{f} = (f(j\boldsymbol{r} \bmod \mathbf{1}))_{j=0}^{M-1}$	function values of $f \in \Pi_I$ at the generated set nodes

for each $\boldsymbol{k} \in I$ ***do***
  $y_{\boldsymbol{k}} = \boldsymbol{k} \cdot \boldsymbol{r} \bmod 1$
end for
$\hat{\boldsymbol{g}} = \text{NFFT\_1D}(\boldsymbol{f}, \boldsymbol{y}, \text{length}(\boldsymbol{f}))$

Output:	$\hat{\boldsymbol{g}} = \boldsymbol{A}^* \boldsymbol{f}$	result of adjoint Fourier transform

Algorithm 4.3 Reconstruction of a trigonometric polynomial from sampling values along a generated set

Input:	$\boldsymbol{r} \in \mathbb{R}^d$	generating vector of $\Lambda(\boldsymbol{r}, M)$
	$I \subset \mathbb{Z}^d$	frequency index set of finite cardinality
	$\boldsymbol{f} = (f(j\boldsymbol{r} \bmod \mathbf{1}))_{j=0}^{M-1}$	function values of $f \in \Pi_I$ at the generated set nodes

$M = \text{length}(\boldsymbol{f})$
for each $\boldsymbol{k} \in I$ ***do***
  $y_{\boldsymbol{k}} = \boldsymbol{k} \cdot \boldsymbol{r} \bmod 1$
end for
$\boldsymbol{b} = \text{NFFT\_1D}(\boldsymbol{f}, \boldsymbol{y}, M)$
solve
$$\text{NFFT\_1D}\left(\text{adjNFFT\_1D}\left(\hat{\tilde{\boldsymbol{f}}}, \boldsymbol{y}, M\right), \boldsymbol{y}, M\right) = \boldsymbol{b}$$
using an iterative method

Output:	$\hat{\tilde{\boldsymbol{f}}} = \underset{\boldsymbol{x} \in \mathbb{C}^{\lvert I \rvert}}{\text{argmin}} \lVert \boldsymbol{A}\boldsymbol{x} - \boldsymbol{f} \rvert \ell_2(M) \rVert$	approximated Fourier coefficients of f

The proof of the last lemma uses the normal equation to calculate a unique solution of $\boldsymbol{A}\hat{\boldsymbol{f}} = \boldsymbol{f}$, $f \in \Pi_I$. Due to the full column rank of $\boldsymbol{A}$ we observe a full rank square matrix $\boldsymbol{A}^*\boldsymbol{A}$. In order to solve $\boldsymbol{A}\hat{\boldsymbol{f}} = \boldsymbol{f}$ we compute

$$\hat{\boldsymbol{f}} = (\boldsymbol{A}^*\boldsymbol{A})^{-1}\boldsymbol{A}^*\boldsymbol{f}.$$

Of course, we use iterative solvers applying only the matrices $\boldsymbol{A}$ and $\boldsymbol{A}^*$ instead of computing the inverse of $\boldsymbol{A}^*\boldsymbol{A}$. Furthermore, we use Algorithm 4.1 and Algorithm 4.2 computing the matrix times vector products in a fast way. Note that both matrix times vector products can be realized with a complexity of $\mathcal{O}(M \log M + (|\log \varepsilon| + d)|I|)$, where ε describes the accuracy of the one-dimensional NFFT. We condensed the strategy to reconstruct multivariate trigonometric polynomials with frequencies supported on an index set $I \subset \mathbb{Z}^d$ using samples along a generated set in Algorithm 4.3. This Algorithm mentioned the usage of an iterative method in order to solve the normal equation. A small condition number of the matrix $\boldsymbol{A}^*\boldsymbol{A}$ guarantees the fast convergence of most of these iterative methods. Accordingly, the condition number indicates not only the stability of the problem, but also characterizes the computational complexity of the reconstruction algorithm. In particular, we estimate the number of iterations of a conjugate gradient method (CG) applied on $\boldsymbol{A}^*\boldsymbol{A}\boldsymbol{x} = \boldsymbol{b}$ such that

we achieve a relative error of at most ϵ in Algorithm 4.3. We stress the fact that the accuracy parameter ε of the NFFT and the relative error ϵ do not have a direct relationship to each other here.

Lemma 4.5. *Let the dimension $d \in \mathbb{N}$, the frequency index set $I \subset \mathbb{Z}^d$ of finite cardinality, $\Lambda(\boldsymbol{r}, M, I)$ a reconstructing generated set for I, $\boldsymbol{f} \in \mathbb{C}^M$, and $\epsilon < 1$ be given. In addition, let $\boldsymbol{x}_0 = \boldsymbol{0}$ and $\boldsymbol{x}_r$ the result of the rth iteration of the conjugate gradient method, cf. [Bjö96], applied to solve $\boldsymbol{A}^*\boldsymbol{A}\boldsymbol{x} = \boldsymbol{A}^*\boldsymbol{f}$. The corresponding exact solution is denoted by $\boldsymbol{x}_*$. Then the number*

$$r_\epsilon := \left\lceil \frac{\log_2 \epsilon - 1}{\log_2\left(\operatorname{cond}_2(\boldsymbol{A}) - 1\right) - \log_2\left(\operatorname{cond}_2(\boldsymbol{A}) + 1\right)} \right\rceil \tag{4.4}$$

gives an iteration number of the conjugate gradient method guaranteeing a relative error

$$\frac{\|\boldsymbol{x}_* - \boldsymbol{x}_r | \ell_2(|I|)\|}{\|\boldsymbol{x}_* | \ell_2(|I|)\|} \leq \epsilon, \text{ for all } r \geq r_\epsilon.$$

The condition number of the non-square matrix $\boldsymbol{A}$ is given by $\operatorname{cond}_2(\boldsymbol{A}) = \sqrt{\operatorname{cond}_2(\boldsymbol{A}^*\boldsymbol{A})}$.

Proof. We apply the standard estimate for the convergence of the conjugate gradient method, cf. e.g. [Bjö96, p. 289], similar to the proof of [Kun06, Corollary 3.5]. For $\boldsymbol{x}_* = \boldsymbol{0}$ the exact solution is $\boldsymbol{x}_0$ and all results of the iterations of the conjugate gradient method are $\boldsymbol{0}$. With $\boldsymbol{x}_* \neq \boldsymbol{0}$, $r \geq r_\epsilon$, and

$$r \log_2 \left(\frac{\operatorname{cond}_2(\boldsymbol{A}) - 1}{\operatorname{cond}_2(\boldsymbol{A}) + 1} \right) \leq r_\epsilon \log_2 \left(\frac{\operatorname{cond}_2(\boldsymbol{A}) - 1}{\operatorname{cond}_2(\boldsymbol{A}) + 1} \right) \leq \log_2 \frac{\epsilon}{2}$$

we obtain

$$\epsilon \geq 2 \left(\frac{\operatorname{cond}_2(\boldsymbol{A}) - 1}{\operatorname{cond}_2(\boldsymbol{A}) + 1} \right)^{r_\epsilon} \geq 2 \left(\frac{\operatorname{cond}_2(\boldsymbol{A}) - 1}{\operatorname{cond}_2(\boldsymbol{A}) + 1} \right)^{r} \geq \frac{\|\boldsymbol{x}_* - \boldsymbol{x}_r | \ell_2(|I|)\|}{\|\boldsymbol{x}_* - \boldsymbol{x}_0 | \ell_2(|I|)\|} = \frac{\|\boldsymbol{x}_* - \boldsymbol{x}_r | \ell_2(|I|)\|}{\|\boldsymbol{x}_* | \ell_2(|I|)\|}.$$

■

Please note that the number of iterations needed to achieve a relative error smaller or equal ϵ only depends logarithmically on ϵ. Furthermore, we stress the fact that large condition numbers of $\boldsymbol{A}$ yields small absolute values of the denominators inside the ceiling of (4.4). For example $\operatorname{cond}_2(\boldsymbol{A}) = 300$ causes a value of $\log_2 \left(\frac{\operatorname{cond}_2(\boldsymbol{A})+1}{\operatorname{cond}_2(\boldsymbol{A})-1} \right)$ smaller than 10^{-2}. In detail, r_ϵ depends almost linearly on the condition number of $\boldsymbol{A}$ provided that $\operatorname{cond}_2(\boldsymbol{A}) \geq 2$. In fact, the slope of the function $a(t) = \frac{1}{\log_2(t+1) - \log_2(t-1)}$ is contained in the interval $(\frac{\log 2}{2}, \frac{\log 4}{3 \log^2 3}] \subset (0.3465, 0.3829]$ provided that $t \geq 2$ and tends to $\frac{\log 2}{2}$ as t tends to infinity, cf. Figure 4.2 for illustration. Accordingly, in addition to the stability of the given problem the condition number characterizes the convergence properties of the reconstruction algorithm.

4.4 Stability

We are interested in the condition number corresponding to the $\ell_2(|I|)$ norm which is defined as

$$\operatorname{cond}_2(\boldsymbol{A}^*\boldsymbol{A}) = \frac{\lambda_{\max}(\boldsymbol{A}^*\boldsymbol{A})}{\lambda_{\min}(\boldsymbol{A}^*\boldsymbol{A})}.$$

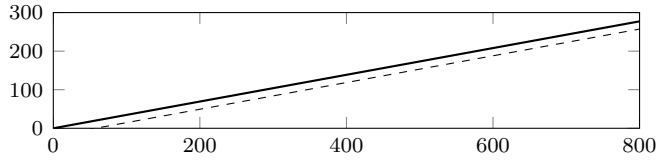

Figure 4.2: Thick line: $a(t) = \left[\log_2(\frac{t+1}{t-1})\right]^{-1}$, dashed line: $b(t) = \frac{\log 2}{2}t - 20$.

Here $\lambda_{\max}(\boldsymbol{A}^*\boldsymbol{A})$ and $\lambda_{\min}(\boldsymbol{A}^*\boldsymbol{A})$ denote the maximal and minimal absolute value of the eigenvalues of $\boldsymbol{A}^*\boldsymbol{A}$, respectively. In order to consider the condition number of $\boldsymbol{A}^*\boldsymbol{A}$ with $\boldsymbol{A}$ as stated in (4.3) we assume $\Lambda(\boldsymbol{r}, M)$ being a reconstructing generated set. Otherwise we obtain that the matrix $\boldsymbol{A}^*\boldsymbol{A}$ is not of full rank, which means that the smallest eigenvalue of $\boldsymbol{A}^*\boldsymbol{A}$ is zero and the condition number is infinite.

We consider the entries of the matrix $\boldsymbol{A}^*\boldsymbol{A}$ and obtain

$$(\boldsymbol{A}^*\boldsymbol{A})_{\boldsymbol{k},\boldsymbol{h}} = \sum_{j=0}^{M-1} \mathrm{e}^{2\pi \mathrm{i} j(\boldsymbol{h}-\boldsymbol{k})\cdot\boldsymbol{r}} =: D_M(\boldsymbol{h}\cdot\boldsymbol{r} - \boldsymbol{k}\cdot\boldsymbol{r}), \quad \boldsymbol{k},\boldsymbol{h} \in I. \tag{4.5}$$

Here, the function D_M is the one-dimensional *Dirichlet kernel*

$$D_M(x) = \begin{cases} M & \text{for } x \in \mathbb{Z}, \\ \mathrm{e}^{\pi \mathrm{i}(M-1)x} \frac{\sin(M\pi x)}{\sin(\pi x)} & \text{for } x \in \mathbb{R} \setminus \mathbb{Z}. \end{cases} \tag{4.6}$$

A more instructive notation gives us

$$(\boldsymbol{A}^*\boldsymbol{A})_{\boldsymbol{k},\boldsymbol{h}} = D_M(y_{\boldsymbol{h}} - y_{\boldsymbol{k}}). \tag{4.7}$$

with $y_{\boldsymbol{k}} = \boldsymbol{k}\cdot\boldsymbol{r} \mod 1$ for all $\boldsymbol{k} \in I$. Due to the necessity of the full rank property of the matrix $\boldsymbol{A}^*\boldsymbol{A}$, we require that the sequence $(y_{\boldsymbol{k}})_{\boldsymbol{k}\in I}$ contains pairwise distinct components. In addition, Equation (4.7) shows that the reconstruction problem is nothing more than a normal equation of the second kind of an under-determined linear system which is a one-dimensional nonequispaced discrete Fourier transform, cf. [KP07], in fact. This interpretation directly leads to the approach indicated in Algorithm 4.3.

Besides the convergence properties of the conjugate gradient method applicable in Algorithm 4.3, the condition number characterizes the stability concerning round-off errors of the given problem.

Of course, for a fixed frequency index set I and a given generated set $\Lambda(\boldsymbol{r}, M)$ one can determine the smallest and the largest eigenvalues of the matrix $\boldsymbol{A}^*\boldsymbol{A}$ and compute the condition number numerically. One can use the condition number depending on the generating vector $\boldsymbol{r}$ and the number of elements M in order to classify the generated set. Basically, we are interested in generated sets with a relatively small M and a condition number as small as possible.

We look at the condition number of $\boldsymbol{A}^*\boldsymbol{A}$ as a rate of quality of a given generated set $\Lambda(\boldsymbol{r}, M)$. Consequently, for fixed M and frequency index set $I \subset \mathbb{Z}^d$ we are interested in a generating vector $\boldsymbol{r} \in \mathbb{R}^d$ ensuring a relatively small condition number of $\boldsymbol{A}^*\boldsymbol{A}$. A direct optimization of the condition number leads to huge computational costs. Hence, we score the generated set based on an upper bound on the condition number $\mathrm{cond}_2(\boldsymbol{A}^*\boldsymbol{A})$ of the corresponding matrix . We consider an upper bound on the condition number which is based on the radii of Gershgorin circles, cf. [Ger31] or [Axe96, Section 4.2].

Lemma 4.6. *[Gershgorin circle theorem applied on $\boldsymbol{A}^*\boldsymbol{A}$] Let the dimension $d \in \mathbb{N}$, the frequency index set $I \subset \mathbb{Z}^d$ of finite cardinality, $\Lambda(\boldsymbol{r}, M)$ a generated set, and the corresponding matrix $\boldsymbol{A}^*\boldsymbol{A}$ of full rank. Then the interval $[M - R(\boldsymbol{A}^*\boldsymbol{A}), M + R(\boldsymbol{A}^*\boldsymbol{A})]$ with*

$$R(\boldsymbol{A}^*\boldsymbol{A}) := \max_{\boldsymbol{h}\in I} \sum_{\substack{\boldsymbol{k}\in I \\ \boldsymbol{k}\neq\boldsymbol{h}}} |D_M((\boldsymbol{k}-\boldsymbol{h})\cdot\boldsymbol{r})| \tag{4.8}$$

contains all eigenvalues of $\boldsymbol{A}^*\boldsymbol{A}$. We name $R(\boldsymbol{A}^*\boldsymbol{A})$ the maximum Gershgorin circle radius *of $\boldsymbol{A}^*\boldsymbol{A}$.*

Proof. We apply the Gershgorin circle theorem and obtain all eigenvalues of the matrix $\boldsymbol{A}^*\boldsymbol{A}$ in the union of all circles

$$\left\{ z \in \mathbb{C} :\ |z - (\boldsymbol{A}^*\boldsymbol{A})_{\boldsymbol{h},\boldsymbol{h}}| \le \sum_{\substack{\boldsymbol{k}\in I \\ \boldsymbol{k}\neq\boldsymbol{h}}} |(\boldsymbol{A}^*\boldsymbol{A})_{\boldsymbol{h},\boldsymbol{k}}| \right\}, \quad \boldsymbol{h} \in I.$$

Since the matrix $\boldsymbol{A}^*\boldsymbol{A}$ is a Hermitian matrix, i.e., self-adjoint, all eigenvalues of $\boldsymbol{A}^*\boldsymbol{A}$ are necessarily real. In addition, all diagonal elements of the matrix $\boldsymbol{A}^*\boldsymbol{A}$ equal M. Consequently, with (4.5) we obtain

$$\bigcup_{\boldsymbol{h}\in I} \left\{ x \in \mathbb{R} :\ |x - M| \le \sum_{\substack{\boldsymbol{k}\in I \\ \boldsymbol{k}\neq\boldsymbol{h}}} |D_M((\boldsymbol{k}-\boldsymbol{h})\cdot\boldsymbol{r})| \right\} = [M - R(\boldsymbol{A}^*\boldsymbol{A}), M + R(\boldsymbol{A}^*\boldsymbol{A})].$$

■

With $R(\boldsymbol{A}^*\boldsymbol{A})$ as stated in (4.8) we get an upper bound on the condition number of $\boldsymbol{A}^*\boldsymbol{A}$ in the following way

$$\begin{aligned} \operatorname{cond}_2(\boldsymbol{A}^*\boldsymbol{A}) = \frac{\lambda_{\max}(\boldsymbol{A}^*\boldsymbol{A})}{\lambda_{\min}(\boldsymbol{A}^*\boldsymbol{A})} &\le \frac{\max\{|x| :\ x \in [M - R(\boldsymbol{A}^*\boldsymbol{A}), M + R(\boldsymbol{A}^*\boldsymbol{A})]\}}{\min\{|x| :\ x \in [M - R(\boldsymbol{A}^*\boldsymbol{A}), M + R(\boldsymbol{A}^*\boldsymbol{A})]\}} \\ &= \begin{cases} \infty & \text{for } R(\boldsymbol{A}^*\boldsymbol{A}) \ge M, \\ \frac{M+R(\boldsymbol{A}^*\boldsymbol{A})}{M-R(\boldsymbol{A}^*\boldsymbol{A})} & \text{for } 0 \le R(\boldsymbol{A}^*\boldsymbol{A}) < M. \end{cases} \end{aligned}$$

Consequently, $R(\boldsymbol{A}^*\boldsymbol{A})$ needs to be smaller than M in order to suitably estimate the condition number of $\boldsymbol{A}^*\boldsymbol{A}$. In order to estimate the maximum Gershgorin circle radius we collect some basic facts about the Dirichlet kernel D_M in the next

Lemma 4.7. *Let $M \in \mathbb{N}$ and $D_M(x)$ the Dirichlet kernel as defined in (4.6) be given. Then the following equalities and inequality hold*

$$\begin{aligned} &|D_M(x)| = |D_M(-x)| = |D_M(x+k)| \qquad \text{for } x \in \mathbb{R} \text{ and } k \in \mathbb{Z}, \text{ and} \\ &|D_M(x)| \le \frac{1}{2x} \qquad \text{for } x \in \left(0, \frac{1}{2}\right]. \end{aligned}$$

Proof. The symmetry and the one-periodicity of the absolute value of D_M can be seen from (4.6). Applying $2x \le \sin \pi x$ for $x \in (0, 1/2]$ yields

$$|D_M(x)| = \left| \frac{\sin M\pi x}{\sin \pi x} \right| \le \frac{1}{\sin \pi x} \le \frac{1}{2x}.$$

■

Theorem 4.8. *Let the dimension $d \in \mathbb{N}$, the frequency index set $I \subset \mathbb{Z}^d$ of finite cardinality, and the generated set $\Lambda(\boldsymbol{r}, M)$ be given. We determine $y_{\boldsymbol{h}} = \boldsymbol{h} \cdot \boldsymbol{r} \bmod 1$ for each $\boldsymbol{h} \in I$ and assume the sequence of $y_{\boldsymbol{h}}$'s being sorted in ascending order, i.e., $0 \le y_{\boldsymbol{h}_1} \le y_{\boldsymbol{h}_2} \le \ldots \le y_{\boldsymbol{h}_{|I|}}$, $\boldsymbol{y} = \left(y_{\boldsymbol{h}_j}\right)_{j=1}^{|I|}$. We define the sequence of gaps $\boldsymbol{g}$ in $\boldsymbol{y}$ as*

$$g_j = \begin{cases} y_{\boldsymbol{h}_1} - y_{\boldsymbol{h}_{|I|}} + 1 & \text{for } j = 1, \\ y_{\boldsymbol{h}_j} - y_{\boldsymbol{h}_{j-1}} & \text{for } j = 2, \ldots, |I|. \end{cases}$$

Then, we can estimate the Gershgorin circle radius by

$$R(\boldsymbol{A}^*\boldsymbol{A}) \le \rho(\boldsymbol{A}^*\boldsymbol{A}) := \sum_{l=1}^{\left\lfloor \frac{|I|}{2} \right\rfloor} \left(\sum_{k=1}^{l} g_{p(k)} \right)^{-1}. \tag{4.9}$$

Here, the function p is a permutation of the sequence $1, \ldots, |I|$ arranging $g_{p(k)} \le g_{p(k+1)}$ for all $1 \le k < |I|$. We name $\rho(\boldsymbol{A}^*\boldsymbol{A})$ upper bound on the maximum Gershgorin circle radius *of $\boldsymbol{A}^*\boldsymbol{A}$.*

Proof. We consider the sequence $\left(g_{p(k)}\right)_{k=1}^{|I|}$. For $g_{p(1)} = 0$ we obtain at least one pair $\boldsymbol{k}, \boldsymbol{h} \in I$, $\boldsymbol{h} \neq \boldsymbol{k}$, with $y_{\boldsymbol{h}} = y_{\boldsymbol{k}}$. Accordingly, the matrix $\boldsymbol{A}^*\boldsymbol{A}$ contains at least two identical columns and thus is not of full rank. So, there exists no or no unique solution of $\boldsymbol{A}^*\boldsymbol{A}\boldsymbol{x} = \boldsymbol{b}$. The smallest eigenvalue of the matrix $\boldsymbol{A}^*\boldsymbol{A}$ is zero. On the other hand, the corresponding upper bound $\rho(\boldsymbol{A}^*\boldsymbol{A})$ of the Gershgorin circle radius of $\boldsymbol{A}^*\boldsymbol{A}$ is infinite. Certainly, the interval $[-\infty, \infty]$ contains all eigenvalues of $\boldsymbol{A}^*\boldsymbol{A}$.

Now, let us assume $g_{p(1)} > 0$. We consider the Gershgorin radius of the matrix $\boldsymbol{A}^*\boldsymbol{A}$ corresponding to the row of $\boldsymbol{A}^*\boldsymbol{A}$ with index $\boldsymbol{h} \in I$, $y_{\boldsymbol{h}} = \boldsymbol{h} \cdot \boldsymbol{r} \bmod 1$. Due to the assumption $g_{p(1)} > 0$, we have $y_{\boldsymbol{h}} - y_{\boldsymbol{k}} \in (-1, 0) \cup (0, 1)$ for all $\boldsymbol{k} \in I$ with $\boldsymbol{h} \neq \boldsymbol{k}$. Consequently we obtain

$$\sum_{\substack{\boldsymbol{k} \in I \\ \boldsymbol{k} \neq \boldsymbol{h}}} |D_M(y_{\boldsymbol{k}} - y_{\boldsymbol{h}})| = \sum_{\substack{\boldsymbol{k} \in I \\ \boldsymbol{k} \neq \boldsymbol{h}}} \left| \frac{\sin(M\pi(y_{\boldsymbol{k}} - y_{\boldsymbol{h}}))}{\sin(\pi(y_{\boldsymbol{k}} - y_{\boldsymbol{h}}))} \right|.$$

We split the index set $I \setminus \{\boldsymbol{h}\}$ in the two disjoint subsets

$$\begin{aligned} J_1 &:= \{\boldsymbol{k} \in I : \ (y_{\boldsymbol{h}} - y_{\boldsymbol{k}}) \bmod 1 \in (0, 1/2]\} \qquad \text{and} \\ J_2 &:= \{\boldsymbol{k} \in I : \ (y_{\boldsymbol{k}} - y_{\boldsymbol{h}}) \bmod 1 \in (0, 1/2)\}. \end{aligned}$$

Using the one-periodicity of D_M and $|D_M(-x)| = |D_M(x)| \le (2x)^{-1}$ for all $x \in (0, 1/2]$ we deduce

$$\begin{aligned} \sum_{\substack{\boldsymbol{k} \in I \\ \boldsymbol{k} \neq \boldsymbol{h}}} \left| \frac{\sin(M\pi(y_{\boldsymbol{k}} - y_{\boldsymbol{h}}))}{\sin(\pi(y_{\boldsymbol{k}} - y_{\boldsymbol{h}}))} \right| &\le \sum_{\boldsymbol{k} \in J_1} \left| \frac{\sin(M\pi(y_{\boldsymbol{k}} - y_{\boldsymbol{h}}))}{\sin(\pi(y_{\boldsymbol{k}} - y_{\boldsymbol{h}}))} \right| + \sum_{\boldsymbol{k} \in J_2} \left| \frac{\sin(M\pi(y_{\boldsymbol{k}} - y_{\boldsymbol{h}}))}{\sin(\pi(y_{\boldsymbol{k}} - y_{\boldsymbol{h}}))} \right| \\ &= \sum_{\boldsymbol{k} \in J_1} \left| \frac{\sin(M\pi(y_{\boldsymbol{k}} - y_{\boldsymbol{h}}))}{\sin(\pi((y_{\boldsymbol{k}} - y_{\boldsymbol{h}}) \bmod 1))} \right| + \sum_{\boldsymbol{k} \in J_2} \left| \frac{\sin(M\pi(y_{\boldsymbol{k}} - y_{\boldsymbol{h}}))}{\sin(\pi((y_{\boldsymbol{k}} - y_{\boldsymbol{h}}) \bmod 1))} \right| \\ &\le \frac{1}{2} \sum_{\boldsymbol{k} \in J_1} \frac{1}{(y_{\boldsymbol{h}} - y_{\boldsymbol{k}}) \bmod 1} + \frac{1}{2} \sum_{\boldsymbol{k} \in J_2} \frac{1}{(y_{\boldsymbol{k}} - y_{\boldsymbol{h}}) \bmod 1}. \end{aligned}$$

Now, we estimate the differences $y_{\boldsymbol{k}} - y_{\boldsymbol{h}} \bmod 1$. In principle we interpret the index set J_1 as the indices of the left neighbors of $y_{\boldsymbol{h}}$. So, the distance of the nearest neighbor on the left hand side to $y_{\boldsymbol{h}}$ is at least $g_{p(1)}$. Clearly, the second nearest neighbor at the left hand side brings a distance of at least $g_{p(1)} + g_{p(2)}$. In general, the jth nearest neighbor to the left of $y_{\boldsymbol{h}}$ has a distance not less than $\sum_{l=1}^{j} g_{p(l)}$ to $y_{\boldsymbol{h}}$. The index set J_2 can be interpreted as the index set of the right neighbors of $y_{\boldsymbol{h}}$ and we determine the lower bounds on the distances in the same way as done for the left neighbors. We obtain

$$\sum_{\substack{\boldsymbol{k}\in I\\ \boldsymbol{k}\neq\boldsymbol{h}}} \left| \frac{\sin(M\pi(y_{\boldsymbol{k}} - y_{\boldsymbol{h}}))}{\sin(\pi(y_{\boldsymbol{k}} - y_{\boldsymbol{h}}))} \right| \leq \frac{1}{2} \sum_{j=1}^{|J_1|} \left(\sum_{l=1}^{j} g_{p(l)} \right)^{-1} + \frac{1}{2} \sum_{j=1}^{|J_2|} \left(\sum_{l=1}^{j} g_{p(l)} \right)^{-1}$$

and balance the two sums applying $\sum_{l=1}^{j} g_{p(l)} \leq \sum_{l=1}^{t} g_{p(l)}$ for $j \leq t$ and $|J_1 \cup J_2| = |I| - 1$

$$\sum_{\substack{\boldsymbol{k}\in I\\ \boldsymbol{k}\neq\boldsymbol{h}}} \left| \frac{\sin(M\pi(y_{\boldsymbol{k}} - y_{\boldsymbol{h}}))}{\sin(\pi(y_{\boldsymbol{k}} - y_{\boldsymbol{h}}))} \right| \leq \sum_{j=1}^{\left\lfloor \frac{|I|}{2} \right\rfloor} \left(\sum_{l=1}^{j} g_{p(l)} \right)^{-1}.$$

The right hand side is independent of $\boldsymbol{h}$ now. Hence, each Gershgorin circle radius is bounded by the right hand side and the assertion holds. ∎

Remark 4.9. We stress the fact that the right hand side of $\rho(\boldsymbol{A}^*\boldsymbol{A})$ does not depend on M. The upper bound on the Gershgorin circle radius $\rho(\boldsymbol{A}^*\boldsymbol{A})$ only depends on the generating vector $\boldsymbol{r}$. Hence, for a fixed frequency index set $I \subset \mathbb{Z}^d$ and a fixed generated set $\Lambda(\boldsymbol{r}, M)$ the value of $\rho(\boldsymbol{A}^*\boldsymbol{A})$ is an upper bound on the Gershgorin circle radii for all matrices contained in the set of matrices $\left\{ \boldsymbol{B}^*\boldsymbol{B} : \ \boldsymbol{B} = \left(\mathrm{e}^{2\pi \mathrm{i} j \boldsymbol{k}\cdot\boldsymbol{r}}\right)_{j=1,\dots,M'-1,\ \boldsymbol{k}\in I}, M' \in \mathbb{N} \right\}$. Consistently, we denote $\rho(I, \boldsymbol{r}) := \rho(\boldsymbol{A}^*\boldsymbol{A})$. ∎

Corollary 4.10. *Let the dimension $d \in \mathbb{N}$, the frequency index set $I \subset \mathbb{Z}^d$ of finite cardinality, $|I| > 1$, the generating vector $\boldsymbol{r} \in \mathbb{R}^d$, and the upper bound on the Gershgorin circle radius $\rho(I, \boldsymbol{r}) := \rho(\boldsymbol{A}^*\boldsymbol{A})$ as stated in Theorem 4.8 be given. In addition, we assume $\rho(I, \boldsymbol{r}) < \infty$, the constant $C \in \mathbb{R}$, $C > 1$, and*

$$M \geq M(I, \boldsymbol{r}, C) := \left\lceil \frac{C+1}{C-1} \rho(I, \boldsymbol{r}) \right\rceil. \tag{4.10}$$

Then, we estimate the condition number of $\boldsymbol{A}(I, \boldsymbol{r}, M)^*\boldsymbol{A}(I, \boldsymbol{r}, M)$ by

$$\mathrm{cond}_2(\boldsymbol{A}^*\boldsymbol{A}) \leq C.$$

Proof. Assuming $M \geq \frac{C+1}{C-1}\rho(I, \boldsymbol{r})$, we obtain

$$C \geq \frac{M + \rho(I, \boldsymbol{r})}{M - \rho(I, \boldsymbol{r})} \geq \frac{M + R(\boldsymbol{A}^*\boldsymbol{A})}{M - R(\boldsymbol{A}^*\boldsymbol{A})} \geq \mathrm{cond}_2(\boldsymbol{A}^*\boldsymbol{A}).$$

∎

Algorithm 4.4 Computing the upper bound $\rho(\boldsymbol{A}^*\boldsymbol{A})$ of the maximum Gershgorin circle radius

Input:	$\boldsymbol{r} \in \mathbb{R}^d$	real valued generating vector
	$I \subset \mathbb{Z}^d$	frequency index set of finite cardinality

for $j = 1, \ldots, |I|$ ***do***
  $y_j = \boldsymbol{k}_j \cdot \boldsymbol{r} \bmod 1$
end for
$\boldsymbol{y} = \mathrm{SORT}(\boldsymbol{y})$
$g_1 = y_1 - y_{|I|} + 1$
for $j = 2, \ldots, |I|$ ***do***
  $g_j = y_j - y_{j-1}$
end for
$\boldsymbol{g} = \mathrm{SORT}(\boldsymbol{g})$
$\rho = 0$, $a = 0$
for $j = 1, \ldots, \left\lfloor \frac{I}{2} \right\rfloor$ ***do***
  $a = a + g_j$
  $\rho = \rho + \frac{1}{a}$
end for

Output:	$\rho = \rho(I, \boldsymbol{r})$	upper bound on the maximum Gershgorin circle radius, cf. (4.9)

Remark 4.11. In Corollary 4.10, we determine $M = M(I, \boldsymbol{r}, C)$ guaranteeing that the condition number $\mathrm{cond}_2(\boldsymbol{A}) = \sqrt{\mathrm{cond}_2(\boldsymbol{A}^*\boldsymbol{A})}$ of the Fourier matrix $\boldsymbol{A} = \left(\mathrm{e}^{2\pi \mathrm{i} j \boldsymbol{k}\cdot\boldsymbol{r}}\right)_{j=0,\ldots,M-1,\boldsymbol{k}\in I}$ is bounded by $\sqrt{C}$ for a given frequency index set I and generating vector $\boldsymbol{r}$. The number $M(I, \boldsymbol{r}, C)$ is essentially based on the upper bound $\rho(I, \boldsymbol{r})$ on the Gershgorin circle radius $R(\boldsymbol{A}^*\boldsymbol{A})$.

In order to determine the upper bound $\rho(I, \boldsymbol{r})$ of the radii of all Gershgorin circles in Theorem 4.8, we estimated the absolute value of the Dirichlet kernel $D_M(\circ)$ by a monotonically non-increasing upper bound $|2 \circ |^{-1}$ in $\left[0, \frac{1}{2}\right]$. Due to the continuity of $|D_M(\circ)|$ and $\frac{1}{2\circ}$ in $\left(0, \frac{1}{2}\right]$ and the condition $|D_M(\frac{t}{M})| = 0 < \frac{M}{|2t|} = |2\frac{t}{M}|^{-1}$ for $t \in \mathbb{Z} \setminus M\mathbb{Z}$, the upper bound and the absolute value of the kernel D_M possibly differ widely. In addition, we sorted the pairwise distances of the sorted sequence $\left(y_{\boldsymbol{h}_j}\right)_{j=1,\ldots,|I|}$ in a worst case scenario. Thus, we also have to expect some differences between the estimated and the exact maximum Gershgorin radius. Altogether, we obtain an estimate $\rho(I, \boldsymbol{r})$ of the maximum Gershgorin radius $R(\boldsymbol{A}^*\boldsymbol{A})$ which eventually is much larger than the exact maximum Gershgorin circle radius. ■

According to Corollary 4.10, we can determine a number $M(I, \boldsymbol{r}, C)$ from (4.10) for each $C > 1$ and each generating vector $\boldsymbol{r} \in \mathbb{R}^d$ with a unique sequence $(\boldsymbol{h} \cdot \boldsymbol{r} \mod 1)_{\boldsymbol{h}\in I}$, i.e., $|\{y : y = \boldsymbol{h} \cdot \boldsymbol{r} \bmod 1, \boldsymbol{h} \in I\}| = |I|$. The resulting reconstructing generated set $\Lambda(\boldsymbol{r}, M(I, \boldsymbol{r}, C), I)$ guarantees that the condition number of the corresponding Fourier matrix $\boldsymbol{A}^*\boldsymbol{A}$ is not larger than C. The essential part of determining the right hand side of (4.10) is the computation of $\rho(I, \boldsymbol{r})$ for a given generating vector $\boldsymbol{r}$. Algorithm 4.4 indicates an efficient method to compute $\rho(I, \boldsymbol{r})$ with a complexity of $\mathcal{O}\left(|I|(\log|I| + d)\right)$.

Taking Remark 4.9 into account, we can interpret the variation of the generated set size M in detail. Increasing M means shifting the interval of fixed length $2\rho(I, \boldsymbol{r})$ containing all eigenvalues to the right at the real numbers, i.e., in the case $M > \rho(I, \boldsymbol{r})$ the upper bound $\frac{M+\rho(I,\boldsymbol{r})}{M-\rho(I,\boldsymbol{r})}$ of the condition number of the corresponding Fourier matrices slightly decreases

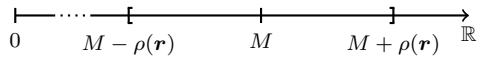

Figure 4.3: Schematic diagram of the interval containing the eigenvalues of the matrix $\boldsymbol{A}^*\boldsymbol{A}$.

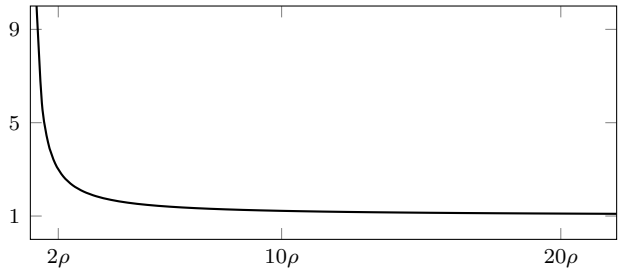

Figure 4.4: The estimator $\frac{M+\rho}{M-\rho}$ of the condition number of the matrix $\boldsymbol{A}^*\boldsymbol{A}$ depending on the relation of M and ρ.

with growing number M of samples, cf. Figures 4.3 and 4.4 for illustration.

Due to the fact that the number $M(I, \boldsymbol{r}, C)$ depends linearly on the value $\rho(I, \boldsymbol{r})$, cf. Corollary 4.10, and we are interested in sampling sets of small cardinalities, we assess the vector $\boldsymbol{r}$ using its ρ-value. In other words, for a given frequency index set I we prefer generating vectors $\boldsymbol{r}$ such that the value $\rho(I, \boldsymbol{r})$ is as small as possible. Thus, we are interested in an approach that determines minimizers of ρ for a given frequency index set I. Local minimizer of ρ can be found using Algorithm 4.5. This algorithm numerically searches for local mimimizers using a simplex search method according to the famous Nelder-Mead method, cf. [NM65]. The simplex search method uses only function evaluations of ρ, which are fast realized by Algorithm 4.4. The functional $\rho(I, \circ)$ has uncountable many poles, e.g., there exist $d-1$-dimensional hyperplanes such that all values $\rho(I, \boldsymbol{r})$, where $\boldsymbol{r}$ is from the hyperplane, are infinite, confer the proof of Lemma 4.3 for details. The huge set of poles and some numerical tests lead us to the conjecture, that nonlinear optimization techniques using also derivatives or approximations of derivatives do not improve the results of Algorithm 4.5 in general.

Algorithm 4.5 Search for suitable reconstructing generated set $\Lambda(\boldsymbol{r}, M, I)$

Input:	$I \subset \mathbb{Z}^d$	frequency index set of finite cardinality
	$C \in \mathbb{R}$	target condition number $C > 1$

d = dimension of elements in I
$\boldsymbol{r}_0$ = random start vector in $(0,1)^d$
$\boldsymbol{r}^\bullet$ = fminsearch$^\dagger(\rho, \boldsymbol{r}_0)$ using Algorithm 4.4
$M(I, \boldsymbol{r}^\bullet, C) = \left\lceil \frac{C+1}{C-1} \rho(I, \boldsymbol{r}^\bullet) \right\rceil$

Output:	$\boldsymbol{r}^\bullet$	generating vector
	$M(I, \boldsymbol{r}^\bullet, C)$	generated set size guaranteeing $\mathrm{cond}_2(\boldsymbol{A}^*\boldsymbol{A}) \leq C$

† function name from MATLAB® [MAT], in detail a simplex search method, according to [NM65], using suitable additional parameters

4.5 Approximation of Multivariate Periodic Functions

In order to approximate a function $f \in \mathcal{A}_\omega(\mathbb{T}^d)$, see (2.9), using sampling values along a generated set $\Lambda(\boldsymbol{r}, M)$ we have to solve the following over-determined system of linear equations

$$\boldsymbol{A}\hat{\check{\boldsymbol{f}}} \approx \boldsymbol{f}, \qquad \boldsymbol{A} = \left(\mathrm{e}^{2\pi \mathrm{i} j \boldsymbol{k}\cdot\boldsymbol{r}}\right)_{j=0,\dots,M-1;\,\boldsymbol{k}\in I}, \; \boldsymbol{f} = (f(j\boldsymbol{r} \bmod \mathbf{1}))_{j=0,\dots,M-1}.$$

Here, the frequency index sets $I \subset \mathbb{Z}^d$ determines the space of trigonometric polynomials where the approximant $\check{S}_I f \in \Pi_I$, $f(\boldsymbol{x}) := \sum_{\boldsymbol{k}\in I} \hat{\check{f}}_{\boldsymbol{k}} \mathrm{e}^{2\pi \mathrm{i}\boldsymbol{k}\cdot\boldsymbol{x}}$, comes from.

We approximate the function $f \in \mathcal{A}_\omega(\mathbb{T}^d)$ computing the Fourier coefficients $\left(\hat{\check{f}}_{\boldsymbol{k}}\right)_{\boldsymbol{k}\in I} \in \mathbb{C}^{|I|}$ of the approximant $\check{S}_I f$ as the solution of the normal equation

$$\boldsymbol{A}^*\boldsymbol{A}\hat{\check{\boldsymbol{f}}} = \boldsymbol{A}^*\boldsymbol{f}$$

which is equivalent to solve the linear least squares problem

$$\|\boldsymbol{A}\hat{\check{\boldsymbol{f}}} - \boldsymbol{f}\|_2 \to \min,$$

cf. [Bjö96]. More precisely, we use Algorithm 4.3 in order to compute the approximated Fourier coefficients $\left(\hat{\check{f}}_{\boldsymbol{k}}\right)_{\boldsymbol{k}\in I}$.

Theorem 4.12. *Let $f \in \mathcal{A}_\omega(\mathbb{T}^d)$ and $I_N = \{\boldsymbol{k} \in \mathbb{Z}^d : \omega(\boldsymbol{k}) \le N\}$ of finite cardinality. Additionally we assume $\Lambda(\boldsymbol{r}, M, I_N)$ is a reconstructing generated set for I_N with corresponding Fourier matrix $\boldsymbol{A}$ and the Gershgorin radius of $\boldsymbol{A}^*\boldsymbol{A}$ bounded by δM with $\delta < 1$. Then we estimate the error of the approximation of f*

$$\check{S}_{I_N} f(\boldsymbol{x}) = \sum_{\boldsymbol{k}\in I_N} \hat{\check{f}}_{\boldsymbol{k}} \mathrm{e}^{2\pi \mathrm{i}\boldsymbol{k}\boldsymbol{x}},$$

with

$$\left(\hat{\check{f}}_{\boldsymbol{k}}\right)_{\boldsymbol{k}\in I_N} := \operatorname*{argmin}_{\hat{\boldsymbol{g}}\in\mathbb{C}^{|I_N|}} \|\boldsymbol{A}\hat{\boldsymbol{g}} - \boldsymbol{f}|l_2(M)\| \text{ and } \boldsymbol{f} = (f(j\boldsymbol{r} \bmod \mathbf{1}))_{j=0}^{M-1},$$

by

$$\|f - \check{S}_{I_N} f|L_2(\mathbb{T}^d)\| \le \left(1 + \frac{1}{\sqrt{1-\delta}}\right) N^{-1} \|f|\mathcal{A}_\omega(\mathbb{T}^d)\|. \tag{4.11}$$

Proof. We estimate the $L_2(\mathbb{T}^d)$ error of the approximation $\check{S}_{I_N} f$ of f using Parseval's identity and the triangle inequality of the ℓ_2-norm

$$\|f - \check{S}_{I_N} f|L_2(\mathbb{T}^d)\| \le \left\|\left(\hat{f}_{\boldsymbol{k}} - \hat{\check{f}}_{\boldsymbol{k}}\right)_{\boldsymbol{k}\in I_N} |\ell_2(I_N)\right\| + \left\|\left(\hat{f}_{\boldsymbol{k}}\right)_{\boldsymbol{k}\in\mathbb{Z}^d\setminus I_N} |\ell_2(\mathbb{Z}^d \setminus I_N)\right\|. \tag{4.12}$$

In order to estimate the left summand at the right hand side of (4.12), we apply

$$\begin{aligned}\boldsymbol{A}^*\boldsymbol{A}\left(\hat{\check{f}}_{\boldsymbol{k}} - \hat{f}_{\boldsymbol{k}}\right)_{\boldsymbol{k}\in I_N} &= \boldsymbol{A}^*\boldsymbol{f} - \boldsymbol{A}^*\left(\boldsymbol{f} - \left(\sum_{\boldsymbol{k}\in\mathbb{Z}^d\setminus I_N} \hat{f}_{\boldsymbol{k}} \mathrm{e}^{2\pi \mathrm{i} j \boldsymbol{k}\cdot\boldsymbol{r}}\right)_{j=0}^{M-1}\right) \\ &= \boldsymbol{A}^*\left(\sum_{\boldsymbol{k}\in\mathbb{Z}^d\setminus I_N} \hat{f}_{\boldsymbol{k}} \mathrm{e}^{2\pi \mathrm{i} j \boldsymbol{k}\cdot\boldsymbol{r}}\right)_{j=0}^{M-1}\end{aligned}$$

and obtain

$$\left\| \left(\hat{f}_{\boldsymbol{k}} - \hat{\tilde{f}}_{\boldsymbol{k}} \right)_{\boldsymbol{k} \in I_N} | \ell_2(I_N) \right\| \leq \| (\boldsymbol{A}^* \boldsymbol{A})^{-1} \boldsymbol{A}^* | \ell_2(M) \to \ell_2(I_N) \| \left\| \boldsymbol{A} \left(\hat{f}_{\boldsymbol{k}} \right)_{\boldsymbol{k} \in I_N} - \boldsymbol{f} | \ell_2(M) \right\|,$$

where $\| (\boldsymbol{A}^* \boldsymbol{A})^{-1} \boldsymbol{A}^* | \ell_2(M) \to \ell_2(I_N) \|$ is the operator norm of $(\boldsymbol{A}^* \boldsymbol{A})^{-1} \boldsymbol{A}^*$ as operator mapping from $\ell_2(M)$ to $\ell_2(I_N)$. According to [Bjö96, Subsection 1.4.3], we estimate the maximal singular value of $(\boldsymbol{A}^* \boldsymbol{A})^{-1} \boldsymbol{A}^*$ using the singular value decomposition of $\boldsymbol{A} = \boldsymbol{U} \boldsymbol{\Sigma} \boldsymbol{V}^*$ with unitary $\boldsymbol{U} \in \mathbb{C}^{M \times M}$, unitary $\boldsymbol{V} \in \mathbb{C}^{|I_N| \times |I_N|}$, and matrix $\boldsymbol{\Sigma} \in \mathbb{R}^{M \times |I_N|}$ with $\Sigma_{j,k} = 0$ for $j \neq k$ and $\Sigma_{j,j} = \sigma_j$ the singular values of $\boldsymbol{A}$, $\sigma_1 \geq \sigma_2 \geq \ldots \geq \sigma_{|I_N|} > 0$. Note that the matrix $\boldsymbol{\Sigma}$ is of full column rank. We achieve

$$\begin{aligned}(\boldsymbol{A}^* \boldsymbol{A})^{-1} \boldsymbol{A}^* &= (\boldsymbol{V} \boldsymbol{\Sigma}^* \boldsymbol{U}^* \boldsymbol{U} \boldsymbol{\Sigma} \boldsymbol{V}^*)^{-1} \boldsymbol{V} \boldsymbol{\Sigma}^* \boldsymbol{U}^* = \boldsymbol{V} \left(\boldsymbol{\Sigma}^* \boldsymbol{\Sigma} \right)^{-1} \boldsymbol{V}^{-1} \boldsymbol{V} \boldsymbol{\Sigma}^* \boldsymbol{U}^* \\ &= \boldsymbol{V} \left(\boldsymbol{\Sigma}^* \boldsymbol{\Sigma} \right)^{-1} \boldsymbol{\Sigma}^* \boldsymbol{U}^* = \boldsymbol{V} \boldsymbol{\Sigma}_{(\boldsymbol{A}^* \boldsymbol{A})^{-1} \boldsymbol{A}^*} \boldsymbol{U}^*.\end{aligned}$$

We identify the singular values of $(\boldsymbol{A}^* \boldsymbol{A})^{-1} \boldsymbol{A}^*$ from the diagonal of $\boldsymbol{\Sigma}_{(\boldsymbol{A}^* \boldsymbol{A})^{-1} \boldsymbol{A}^*}$. The matrix is given by

$$\left(\boldsymbol{\Sigma}_{(\boldsymbol{A}^* \boldsymbol{A})^{-1} \boldsymbol{A}^*} \right)_{j,k} = \begin{cases} 0 & \text{for } k \neq j, \\ \frac{1}{\sigma_j} & \text{for } k = j. \end{cases}$$

This yields

$$\| (\boldsymbol{A}^* \boldsymbol{A})^{-1} \boldsymbol{A}^* | \ell_2(M) \to \ell_2(I_N) \| = \frac{1}{\sigma_{|I_N|}} = \frac{1}{\sqrt{\lambda_{\min}(\boldsymbol{A}^* \boldsymbol{A})}} \leq \frac{1}{\sqrt{M(1-\delta)}}$$

where $\lambda_{\min}(\boldsymbol{A}^* \boldsymbol{A}) > 0$ is the smallest eigenvalue of $\boldsymbol{A}^* \boldsymbol{A}$. Applying

$$\left| \left(\boldsymbol{A} \left(\hat{f}_{\boldsymbol{k}} \right)_{\boldsymbol{k} \in I_N} \right)_j - f(j \boldsymbol{r} \bmod \boldsymbol{1}) \right| = \left| \sum_{\boldsymbol{k} \in \mathbb{Z}^d \setminus I_N} \hat{f}_{\boldsymbol{k}} \mathrm{e}^{2 \pi \mathrm{i} j \boldsymbol{k} \cdot \boldsymbol{r}} \right| \leq \sum_{\boldsymbol{k} \in \mathbb{Z}^d \setminus I_N} |\hat{f}_{\boldsymbol{k}}|$$

and

$$\left\| \left(\hat{f}_{\boldsymbol{k}} - \hat{\tilde{f}}_{\boldsymbol{k}} \right)_{\boldsymbol{k} \in I_N} | \ell_2(I_N) \right\| \leq \frac{1}{\sqrt{M(1-\delta)}} \sqrt{M} \left\| \boldsymbol{A} \left(\hat{f}_{\boldsymbol{k}} \right)_{\boldsymbol{k} \in I_N} - \boldsymbol{f} | \ell_\infty(M) \right\|$$

we conclude

$$\begin{aligned}\| f - \breve{S}_{I_N} f | L_2(\mathbb{T}^d) \| &\leq \frac{1}{\sqrt{1-\delta}} \left\| \left(\hat{f}_{\boldsymbol{k}} \right)_{\boldsymbol{k} \in \mathbb{Z}^d \setminus I_N} | \ell_1(\mathbb{Z}^d \setminus I_N) \right\| + \left\| \left(\hat{f}_{\boldsymbol{k}} \right)_{\boldsymbol{k} \in \mathbb{Z}^d \setminus I_N} | \ell_1(\mathbb{Z}^d \setminus I_N) \right\| \\ &= \left(1 + \frac{1}{\sqrt{1-\delta}} \right) \left\| \left(\hat{f}_{\boldsymbol{k}} \right)_{\boldsymbol{k} \in \mathbb{Z}^d \setminus I_N} | \ell_1(\mathbb{Z}^d \setminus I_N) \right\| \\ &\leq \left(1 + \frac{1}{\sqrt{1-\delta}} \right) \frac{1}{N} \| f | \mathcal{A}_\omega(\mathbb{T}^d) \|.\end{aligned}$$

■

The estimate (4.11) of the approximation error for the generated set sampling is closely related to the approximation result from Theorem 3.11. This theorem specifies error estimates for approximations computed from sampling values along reconstructing rank-1 lattices. The

corresponding findings are in some sense sharper than the results from Theorem 4.12. In detail, we proved in Theorem 3.11 that the $L_\infty(\mathbb{T}^d)$ error of an approximation $\tilde{S}_{I_N} f$ that is computed from sampling values along a reconstructing rank-1 lattice for $I_N := \{\boldsymbol{k} \in \mathbb{Z}^d \colon \omega(\boldsymbol{k}) \leq N\}$ is bounded by $2/N$ times the norm of f in the space $\mathcal{A}_\omega(\mathbb{T}^d)$. As a matter of course, the $L_2(\mathbb{T}^d)$ error of this approximation is also bounded by the same terms since the inequality $\|f|L_2(\mathbb{T}^d)\| \leq \|f|L_\infty(\mathbb{T}^d)\|$ holds for all functions $f \in \mathcal{A}(\mathbb{T}^d)$. The proofs of the Theorems 3.11 and 4.12 use different methods. More specifically, the proof of the $L_\infty(\mathbb{T}^d)$ error bound in Theorem 3.11 exploits the detailed aliasing formula, cf. (3.12), that is known for the rank-1 lattice sampling. We could not find a similar suitable formula for generated sets. Nevertheless, one can find a nice similarity in the results. Since each reconstructing generated set $\Lambda(\boldsymbol{r}, M, I_N)$ with $\boldsymbol{r} \in M^{-1}\mathbb{Z}^d$ is in fact a reconstructing rank-1 lattice, we obtain $\delta = 0$ in Theorem 4.12 and this yields the inequality

$$\|f - \breve{S}_{I_N} f|L_2(\mathbb{T}^d)\| \leq 2N^{-1}\|f|\mathcal{A}_\omega(\mathbb{T}^d)\|.$$

On the other hand, we estimate

$$\|f - \tilde{S}_{I_N} f|L_2(\mathbb{T}^d)\| \leq \|f - \tilde{S}_{I_N} f|L_\infty(\mathbb{T}^d)\| \leq 2N^{-1}\|f|\mathcal{A}_\omega(\mathbb{T}^d)\|,$$

where $\tilde{S}_{I_N} f$ is the approximant of f found by sampling along the reconstructing rank-1 lattice $\Lambda(\boldsymbol{z}, M, I_N)$, $\boldsymbol{z} = M\boldsymbol{r} \in \mathbb{Z}^d$, cf. Theorem 3.11. Actually, the operators $\breve{S}_{I_N}$ and $\tilde{S}_{I_N}$ are identical and both Theorems bound the $L_2(\mathbb{T}^d)$ error from above using exactly the same terms—even the small constants are identical.

Furthermore, we would like to stress that the right hand side of the estimates of both Theorems are only two- and C_δ-folds of the worst case error caused by the approximation of f by the exact Fourier partial sum $S_{I_N} f$, cf. (2.10), which is the best possible approximation of f in Π_{I_N}, cf. Lemma 2.2.

4.6 Specific Frequency Index Sets

In order to compute reconstructing generated sets $\Lambda(\boldsymbol{r}, M, I)$ of small sizes M, we fix the parameter $C = 7$ in (4.10). According to this, we obtain

$$M(I, \boldsymbol{r}, C) = \left\lceil \frac{4}{3}\rho(I, \boldsymbol{r}) \right\rceil \qquad \text{and thus} \qquad \rho(I, \boldsymbol{r}) \leq \frac{3}{4}M.$$

Bounding the condition number of $\boldsymbol{A}^*\boldsymbol{A}$ from above by $C = 7$, the CG algorithm used in Algorithm 4.3 needs at most a number

$$r_\epsilon := \left\lceil \frac{\log_2 \epsilon - 1}{\log_2\left(\operatorname{cond}_2(\boldsymbol{A}) - 1\right) - \log_2\left(\operatorname{cond}_2(\boldsymbol{A}) + 1\right)} \right\rceil \leq 1 - 3\log_{10}(\epsilon)$$

of iterations in order to ensure a relative ℓ_2-error of the reconstructed Fourier coefficients $\hat{\hat{\boldsymbol{f}}}$ not larger than ϵ, i.e.,

$$\frac{\|(\boldsymbol{A}^*\boldsymbol{A})^{-1}\boldsymbol{A}^*\boldsymbol{f} - \hat{\hat{\boldsymbol{f}}}|\ell_2(|I|)\|}{\|(\boldsymbol{A}^*\boldsymbol{A})^{-1}\boldsymbol{A}^*\boldsymbol{f}|\ell_2(|I|)\|} \leq \epsilon.$$

In addition, considering matrices $\boldsymbol{A}^*\boldsymbol{A}$ having a condition number $\operatorname{cond}_2(\boldsymbol{A}^*\boldsymbol{A}) \leq 7$, we estimate the approximation error in Theorem 4.12 by

$$\|f - \breve{S}_{I_N} f|L_2(\mathbb{T}^d)\| \leq \frac{3}{N}\|f|\mathcal{A}_\omega(\mathbb{T}^d)\|.$$

So far, we presented the theoretical results for the setting of this section of examples. In order to show the outstanding properties of the generating vectors found by Algorithm 4.5, we compute condition numbers $\kappa = \operatorname{cond}_2(\boldsymbol{A}^*\boldsymbol{A})$ and its estimates κ_{G} based on the maximum Gershgorin circle radius $R(\boldsymbol{A}^*\boldsymbol{A})$, cf. (4.8). Since we know that the output $M(I, \boldsymbol{r}^\bullet, C)$ of Algorithm 4.5 may be not optimal, cf. Remark 4.11, we are interested in smaller $M < M(I, \boldsymbol{r}^\bullet, C)$ guaranteeing that the condition number of the matrix $\boldsymbol{A}(I, \boldsymbol{r}^\bullet, M)$ is also bounded by C. Accordingly, we apply the following strategy. We compute some local minimizers $\boldsymbol{r}^\bullet$ using Algorithm 4.5, choose that $\boldsymbol{r}^\bullet$, where $M(I, \boldsymbol{r}^\bullet, C)$ is the smallest one, and denote this generating vector by $\boldsymbol{r}^\#$. Once we have fixed $\boldsymbol{r}^\#$, we compute the minimal power of two

$$M_{\mathrm{G}}(I, \boldsymbol{r}^\#, C) := \min_{n \in \mathbb{N}} \left\{ 2^n \colon R(\boldsymbol{A}(I, \boldsymbol{r}^\#, 2^n)^* \boldsymbol{A}(I, \boldsymbol{r}^\#, 2^n)) \leq \tfrac{C-1}{C+1} 2^n \right\}, \tag{4.13}$$

such that the maximum Gershgorin circle radius

$$R\left(\boldsymbol{A}\left(I, \boldsymbol{r}^\#, M_{\mathrm{G}}(I, \boldsymbol{r}^\#, C)\right)^* \boldsymbol{A}\left(I, \boldsymbol{r}^\#, M_{\mathrm{G}}(I, \boldsymbol{r}^\#, C)\right)\right)$$

allows for the estimate $\operatorname{cond}_2(\boldsymbol{A}(I, \boldsymbol{r}^\#, M_{\mathrm{G}}(I, \boldsymbol{r}^\#, C))^* \boldsymbol{A}(I, \boldsymbol{r}^\#, M_{\mathrm{G}}(I, \boldsymbol{r}^\#, C))) \leq C$, i.e., $M_{\mathrm{G}}(I, \boldsymbol{r}^\#, C)$ many multiples of $\boldsymbol{r}^\#$ are enough in order to stably sample trigonometric polynomials with frequencies supported on the frequency index set I. Due to the fact that we determine the number $M(I, \boldsymbol{r}^\#, C)$ based on an upper bound on the Gershgorin circle radius, which itself only allows for an estimate of the condition number of the considered matrix from above, we are also interested in a heuristic rule of thumb that determines a more or less good approximation of an $M < M(I, \boldsymbol{r}^\#, C)$ such that the condition number $\operatorname{cond}_2(\boldsymbol{A}(I, \boldsymbol{r}^\#, M)^* \boldsymbol{A}(I, \boldsymbol{r}^\#, M))$ is bounded near C.

Motivated by our numerical tests, cf. Tables 4.5 and 4.6, we determine the lower bound

$$\sum_{k=1}^{\left\lfloor \frac{|I|}{2} \right\rfloor} \left(\frac{k}{|I|} \right)^{-1} \leq \rho(\boldsymbol{r}, I)$$

on the functional $\rho(\boldsymbol{r}, I)$ and obtain equality, iff the sequence of $(y_{\boldsymbol{h}})_{\boldsymbol{h} \in I}$, see Theorem 4.8 for its definition, is an equispaced lattice on the one-dimensional torus. In that case we can translate $y_{\boldsymbol{h}}$ such that $y_{\boldsymbol{h}_1} = 0$ and apply an equispaced FFT of length $|I|$ to reconstruct all Fourier coefficients supported on I. In other words, a frequency index set I and a generating vector $\boldsymbol{r}$ implying an equispaced sequence $(y_{\boldsymbol{h}})_{\boldsymbol{h} \in I}$ causes an $M(I, \boldsymbol{r}, C)$ that is oversized by a factor of at least $\sum_{k=1}^{\left\lfloor \frac{|I|}{2} \right\rfloor} k^{-1}$. Now, we deduce the heuristically large enough generated set size

$$M^\natural(I, \boldsymbol{r}, C) := \left\lfloor M(I, \boldsymbol{r}, C) \left(\sum_{k=1}^{\left\lfloor \frac{|I|}{2} \right\rfloor} k^{-1} \right)^{-1} \right\rfloor. \tag{4.14}$$

In detail, we can estimate the harmonic number $H_L = \sum_{k=1}^{L} k^{-1}$, $L \in \mathbb{N}$, using the inequalities one finds in [Hav09] given by D. W. DeTemple in [DeT91]

$$\ln\left(L + \frac{1}{2}\right) + \gamma + \frac{1}{24(L+1)^2} \leq H_L \leq \ln\left(L + \frac{1}{2}\right) + \gamma + \frac{1}{24L^2},$$

where $\gamma = 0.5772156649\ldots$ is the Euler–Mascheroni constant here. Consequently, the relation of the numbers $M(I,\boldsymbol{r},C)$ and $M^\natural(I,\boldsymbol{r},C)$ is approximately given by $\ln(|I|)$, i.e., $\frac{M(I,\boldsymbol{r},C)}{M^\natural(I,\boldsymbol{r},C)} \sim \ln(|I|)$.

Our main focus is on the stability of the corresponding Fourier transform and thus the condition numbers of the matrices $\boldsymbol{A}^*\boldsymbol{A}$. We denote the condition numbers $\kappa := \operatorname{cond}_2(\boldsymbol{A}^*\boldsymbol{A})$ and its estimates $\kappa_{\mathrm{G}} := \frac{M+R(\boldsymbol{A}^*\boldsymbol{A})}{M-R(\boldsymbol{A}^*\boldsymbol{A})}$ by the following explicit notations

$$\kappa(I,\boldsymbol{r},M) := \operatorname{cond}_2\left(\boldsymbol{A}(I,\boldsymbol{r},M)^*\boldsymbol{A}(I,\boldsymbol{r},M)\right), \tag{4.15}$$

$$\kappa_{\mathrm{G}}(I,\boldsymbol{r},M) := \frac{M + R(\boldsymbol{A}(I,\boldsymbol{r},M)^*\boldsymbol{A}(I,\boldsymbol{r},M))}{M - R(\boldsymbol{A}(I,\boldsymbol{r},M)^*\boldsymbol{A}(I,\boldsymbol{r},M))} \tag{4.16}$$

and shorten them using

$$\begin{aligned}
&\kappa(I,\boldsymbol{r},M,C) := \kappa(I,\boldsymbol{r},M(I,\boldsymbol{r},C)), && \kappa_{\mathrm{G}}(I,\boldsymbol{r},M,C) := \kappa_{\mathrm{G}}(I,\boldsymbol{r},M(I,\boldsymbol{r},C)),\\
&\kappa(I,\boldsymbol{r},M_{\mathrm{G}},C) := \kappa(I,\boldsymbol{r},M_{\mathrm{G}}(I,\boldsymbol{r},C)), && \kappa_{\mathrm{G}}(I,\boldsymbol{r},M_{\mathrm{G}},C) := \kappa_{\mathrm{G}}(I,\boldsymbol{r},M_{\mathrm{G}}(I,\boldsymbol{r},C)),\\
&\kappa(I,\boldsymbol{r},M^\natural,C) := \kappa(I,\boldsymbol{r},M^\natural(I,\boldsymbol{r},C)), && \kappa_{\mathrm{G}}(I,\boldsymbol{r},M^\natural,C) := \kappa_{\mathrm{G}}(I,\boldsymbol{r},M^\natural(I,\boldsymbol{r},C)).
\end{aligned} \tag{4.17}$$

If we assume $\rho(I,\boldsymbol{r})$ is finite and $M \geq |I|$, we obtain that the matrix $\boldsymbol{A}(I,\boldsymbol{r},M)^*\boldsymbol{A}(I,\boldsymbol{r},M)$ is a regular and positive-definite Hermitian matrix,

$$\boldsymbol{x}^*\boldsymbol{A}^*\boldsymbol{A}\boldsymbol{x} = (\boldsymbol{A}\boldsymbol{x})^*\boldsymbol{A}\boldsymbol{x} = \|\boldsymbol{A}\boldsymbol{x}|\ell_2(M)\| > 0 \quad \forall \boldsymbol{x} \in \mathbb{C}^{|I|} \setminus \{\boldsymbol{0}\},$$

and thus all eigenvalues are positive real values and larger than zero. Nevertheless, the minimum of the interval $[M - R(\boldsymbol{A}(I,\boldsymbol{r},M)^*\boldsymbol{A}(I,\boldsymbol{r},M)), M + R(\boldsymbol{A}(I,\boldsymbol{r},M)^*\boldsymbol{A}(I,\boldsymbol{r},M))]$ is non-positive for $M \leq R(\boldsymbol{A}(I,\boldsymbol{r},M)^*\boldsymbol{A}(I,\boldsymbol{r},M))$ and, consequently, the estimated condition number $\kappa_{\mathrm{G}}(I,\boldsymbol{r},M)$ becomes infinite or negative. In these cases, each positive real number near zero is a candidate for the smallest eigenvalue of the matrix $\boldsymbol{A}(I,\boldsymbol{r},M)^*\boldsymbol{A}(I,\boldsymbol{r},M)$. Accordingly, the condition number of the matrix $\boldsymbol{A}(I,\boldsymbol{r},M)^*\boldsymbol{A}(I,\boldsymbol{r},M)$ can be arbitrarily large, i.e., $\kappa_{\mathrm{G}}(I,\boldsymbol{r},M) = \infty$ and $\kappa_{\mathrm{G}}(I,\boldsymbol{r},M) < 0$ indicates that we cannot estimate the condition number of the matrix $\boldsymbol{A}(I,\boldsymbol{r},M)^*\boldsymbol{A}(I,\boldsymbol{r},M)$ using the Gershgorin circle radius.

4.6.1 Weighted ℓ_p-balls

As a first example, we would like to treat a weight function that yields convex frequency index sets. Since weighted ℓ_∞-balls are well investigated, cf. [ST89], tensor products of equispaced sampling schemes provide perfectly stable spatial discretizations, and the corresponding fast algorithm, the multidimensional fast Fourier transform, is well known, we focus on frequency index sets of a more difficult structure. In particular, we will consider weighted ℓ_1-balls as convex frequency index sets and, in addition, $\ell_{1/2}$-balls as non-convex ℓ_p-balls.

Example 4.13. We consider the same ℓ_1-ball frequency index sets as investigated in Example 3.20 and compare the reconstructing generated sets to the corresponding reconstructing rank-1 lattices. Accordingly, we fix the weights $\boldsymbol{\gamma} = \left(0.9^{s-1}\right)_{s\in\mathbb{N}}$ compute the frequency index sets $I = I_{1,N}^{d,\boldsymbol{\gamma}}$, $N = 2, 6, 10$, for dimensions d from two up to its effective dimension d_{eff}, cf. (3.18), and apply Algorithm 4.5 in order to determine reconstructing generated sets as described in the introduction of this section. The corresponding generated set sizes $M(I,\boldsymbol{r}^\#,7)$, $M_{\mathrm{G}}(I,\boldsymbol{r}^\#,7)$, $M^\natural(I,\boldsymbol{r}^\#,7)$ and the estimates $\kappa_{\mathrm{G}}(I,\boldsymbol{r}^\#,M,7)$, $\kappa_{\mathrm{G}}(I,\boldsymbol{r}^\#,M_{\mathrm{G}},7)$, and $\kappa_{\mathrm{G}}(I,\boldsymbol{r}^\#,M^\natural,7)$ of the condition numbers of the corresponding Fourier matrices $\boldsymbol{A}^*\boldsymbol{A}$, are presented in Tables 4.2, 4.3, and 4.4. Furthermore, we computed the exact condition

Weighted ℓ_1-balls $I_{1,2}^{d,\gamma}$ – Reconstructing Generated Sets $\Lambda(\boldsymbol{r}, M, I_{1,2}^{d,\gamma})$								
d	$\lvert I_{1,2}^{d,\gamma}\rvert$	$M(I,\boldsymbol{r}^\#,7)$	$\kappa_{\mathrm{G}}(I,\boldsymbol{r}^\#,M,7)$	$M_{\mathrm{G}}(I,\boldsymbol{r}^\#,7)$	$\kappa_{\mathrm{G}}(I,\boldsymbol{r}^\#,M_{\mathrm{G}},7)$	$M^\natural(I,\boldsymbol{r}^\#,7)$	$\kappa_{\mathrm{G}}(I,\boldsymbol{r}^\#,M^\natural,7)$	$\kappa(I,\boldsymbol{r}^\#,M^\natural,7)$
2	7	18	2.3357	16	2.5508	9	7.9460	2.0000
3	9	26	1.8889	16	3.9364	12	8.6678	2.5572
4	11	34	1.8333	32	1.9091	14	24.8025	2.5356
5	13	46	2.2856	32	3.1964	18	45.4228	2.6772
6	15	54	2.2128	32	2.9649	20	-172.3200	2.7966
7	17	66	2.4026	64	2.2784	24	-30.5293	2.6388

Table 4.2: Generated set sizes $M(I,\boldsymbol{r}^\#,7)$, $M_{\mathrm{G}}(I,\boldsymbol{r}^\#,7)$, $M^\natural(I,\boldsymbol{r}^\#,7)$, estimated condition numbers κ_{G}, cf. (4.16) and (4.17), and condition numbers $\kappa(I,\boldsymbol{r},M^\natural,7)$, cf. (4.17), for weighted ℓ_1-ball frequency index sets $I = I_{1,2}^{d,\gamma}$, $\boldsymbol{\gamma} = \left(0.9^{s-1}\right)_{s\in\mathbb{N}}$.

numbers $\kappa(I,\boldsymbol{r}^\#,M^\natural,7)$ for the reconstructing generated sets $\Lambda(\boldsymbol{r}^\#,M^\natural(I,\boldsymbol{r}^\#,7),I)$, where $|I| < 25\,000$, since there are several cases where the numbers $\kappa_{\mathrm{G}}(I,\boldsymbol{r}^\#,M^\natural,7)$ do not bound the condition number of the matrices $\boldsymbol{A}^*\boldsymbol{A}$. In fact, all the computed condition numbers $\kappa(I,\boldsymbol{r}^\#,M^\natural,7)$ are less than three.

At first, we compare the results of our theoretical findings in Corollaries 3.4 and 4.10, i.e., we compare our generated set sizes from Tables 4.2, 4.3, and 4.4 to the rank-1 lattices sizes from Tables 3.3, 3.4, and 3.5. We observe that the determined generated set sizes $M(I,\boldsymbol{r}^\#,7)$ are larger than the lattice sizes $M_{\mathrm{Cor3.4}}$ by a factor up to approximately eight. However, we stress the fact that the computation of $M_{\mathrm{Cor3.4}}$ involves the computation of the difference sets, which needs a lot of memory and time. On the contrary, the generated set sizes $M(I,\boldsymbol{r}^\#,7)$ are results of our search Algorithm 4.5 and arise during the search for suitable generating vectors $\boldsymbol{r}$ by the way.

Furthermore, we compare the generated set sizes $M_{\mathrm{G}}(I,\boldsymbol{r}^\#,7)$ and $M^\natural(I,\boldsymbol{r}^\#,7)$ against the rank-1 lattice sizes $M_{\mathrm{Alg3.3+Alg3.5}}$ and $M_{\mathrm{Alg3.8}}$. In detail, we observe generated set sizes that are larger than the lattice sizes by a factor up to approximately ten. Despite larger oversampling factors $M_{\mathrm{G}}(I,\boldsymbol{r}^\#,7)/|I|$ of reconstructing generated sets compared to those of reconstructing rank-1 lattices $M_{\mathrm{Alg3.3+Alg3.5}}/|I|$, the found reconstructing generated sets $\Lambda(\boldsymbol{r}^\#,M_{\mathrm{G}}(I,\boldsymbol{r}^\#,7),I)$ have numbers of sampling nodes that are—at least for larger dimensions d and parameters N—considerably less than those needed by applying an embedding approach as mentioned in Example 3.20, see also Table 3.2.

At this point we should mention, that the computation of $M^\natural(I,\boldsymbol{r}^\#,7)$ involves (almost) no additional computational costs. The computation of $M_{\mathrm{G}}(I,\boldsymbol{r}^\#,7)$ has a complexity that is bounded by $C|I|^2\log M(I,\boldsymbol{r}^\#,7) + 2d|I|$ and can be done without essential memory usage—clearly the memory should contain the values of $y_{\boldsymbol{k}} = \boldsymbol{k}\cdot\boldsymbol{r}$, $\boldsymbol{k}\in I$, in order to compute all Gershgorin radii of the matrices $\boldsymbol{A}(I,\boldsymbol{r},2^m)^*\boldsymbol{A}(I,\boldsymbol{r},2^m)$, $m = \lceil\log_2|I|\rceil,\ldots,\lfloor\log_2 M(I,\boldsymbol{r}^\#,7)\rfloor$. The term C only depends on the computational complexity of the evaluation of the sine function since we compute the absolute values of all entries of the matrices $\boldsymbol{A}(I,\boldsymbol{r},2^m)^*\boldsymbol{A}(I,\boldsymbol{r},2^m)$, cf. (4.7). In particular, the constant C does not depend on the dimension d.

Weighted ℓ_1-balls $I_{1,6}^{d,\boldsymbol{\gamma}}$ – Reconstructing Generated Sets $\Lambda(\boldsymbol{r}, M, I_{1,6}^{d,\boldsymbol{\gamma}})$								
d	$\lvert I_{1,6}^{d,\boldsymbol{\gamma}}\rvert$	$M(I,\boldsymbol{r}^{\#},7)$	$\kappa_{\mathrm{G}}(I,\boldsymbol{r}^{\#},M,7)$	$M_{\mathrm{G}}(I,\boldsymbol{r}^{\#},7)$	$\kappa_{\mathrm{G}}(I,\boldsymbol{r}^{\#},M_{\mathrm{G}},7)$	$M^{\natural}(I,\boldsymbol{r}^{\#},7)$	$\kappa_{\mathrm{G}}(I,\boldsymbol{r}^{\#},M^{\natural},7)$	$\kappa(I,\boldsymbol{r}^{\#},M^{\natural},7)$
2	63	360	2.1066	256	2.7861	89	-6.1365	2.0000
3	227	2 199	1.7209	1 024	4.9325	414	-4.4752	2.2349
4	551	8 609	1.6476	2 048	5.3565	1 389	-5.5349	1.9991
5	997	25 570	1.4249	8 192	3.2054	3 766	-5.8051	2.0938
6	1 567	58 582	1.3953	16 384	3.8851	8 090	-13.6403	2.0012
7	2 169	126 671	1.2854	32 768	3.1516	16 741	-259.7592	2.0231
8	2 697	188 828	1.2161	32 768	5.3597	24 258	18.8615	1.9258
9	3 121	249 116	1.2532	65 536	2.5502	31 414	9.2822	1.8275
10	3 433	283 980	1.2517	65 536	2.9557	35 385	14.2974	1.9386
11	3 653	361 453	1.1881	65 536	3.5917	44 693	12.4097	2.0564
12	3 799	406 239	1.2639	65 536	5.7006	49 989	5.2574	1.7902
13	3 877	510 590	1.2030	65 536	3.9957	62 673	4.0355	1.6235
14	3 911	482 280	1.2343	131 072	2.2897	59 134	7.4497	2.0566
15	3 933	485 456	1.1723	65 536	5.2095	59 483	4.3564	1.7814
16	3 943	400 322	1.1924	65 536	4.8344	49 036	4.9136	1.7534
17	3 945	438 061	1.2092	65 536	4.8976	53 655	4.8469	1.8470
18	3 947	485 004	1.1607	65 536	5.4885	59 401	5.9468	1.7913

Table 4.3: Generated set sizes $M(I,\boldsymbol{r}^{\#},7)$, $M_{\mathrm{G}}(I,\boldsymbol{r}^{\#},7)$, $M^{\natural}(I,\boldsymbol{r}^{\#},7)$, estimated condition numbers κ_{G}, cf. (4.16) and (4.17), and condition numbers $\kappa(I,\boldsymbol{r},M^{\natural},7)$, cf. (4.17), for weighted ℓ_1-ball frequency index sets $I = I_{1,6}^{d,\boldsymbol{\gamma}}$, $\boldsymbol{\gamma} = \left(0.9^{s-1}\right)_{s\in\mathbb{N}}$.

In accordance to Remark 4.11, we observe that the estimates $\kappa_{\mathrm{G}}(I,\boldsymbol{r}^{\#},M,7)$ on the condition numbers of the matrices $\boldsymbol{A}(I,\boldsymbol{r},M)^*\boldsymbol{A}(I,\boldsymbol{r},M)$ are non-monotonic with respect to the number M of sampling values. Our numerical findings confirm the same behavior even for the exact condition numbers $\kappa(I,\boldsymbol{r}^{\#},M,7)$. In particular, one can use the initial findings from Lemma 4.1 in order to construct a nice minimal example. Thus, the condition numbers of the matrices $\boldsymbol{A}(I,\boldsymbol{r},M+1)^*\boldsymbol{A}(I,\boldsymbol{r},M+1)$ may be larger than those of $\boldsymbol{A}(I,\boldsymbol{r},M)^*\boldsymbol{A}(I,\boldsymbol{r},M)$. However, for a fixed generating vector $\boldsymbol{r}$ and a fixed frequency index set I the condition number varies within the fixed interval $\left[1, \frac{M+\rho(\boldsymbol{r},I)}{M-\rho(\boldsymbol{r},I)}\right]$ as long as $M > \rho(\boldsymbol{r},I)$ holds. □

Example 4.14. Similar to Example 3.21 we would like to treat weighted non-convex ℓ_p-balls. Specifically, we fix the parameters $p = 1/2$, $\boldsymbol{\gamma} = \left(0.9^{s-1}\right)_{s\in\mathbb{N}}$, and $N = 35$ and compare the found reconstructing generated set sizes, that are listed in Table 4.5, to the rank-1 lattice sizes presented in Table 3.7. In general, we observe larger cardinalities for reconstructing generated sets than for reconstructing rank-1 lattices. Up to dimension $d = 10$ the generated set sizes $M(I,\boldsymbol{r}^{\#},7)$ are less than four times the rank-1 lattice sizes $M_{\mathrm{Cor3.4}}$. Similarly, we observe that the generated set sizes $M^{\natural}(I,\boldsymbol{r}^{\#},7)$ are not larger than ten times the rank-1 lattice sizes $M_{\mathrm{Alg3.3+Alg3.5}}$ or $M_{\mathrm{Alg3.8}}$. Since we consider frequency index sets of substantial cardinality

Weighted ℓ_1-balls $I_{1,10}^{d,\boldsymbol{\gamma}}$ – Reconstructing Generated Sets $\Lambda(\boldsymbol{r}, M, I_{1,10}^{d,\boldsymbol{\gamma}})$								
d	$\lvert I_{1,10}^{d,\boldsymbol{\gamma}}\rvert$	$M(I,\boldsymbol{r}^{\#},7)$	$\kappa_{\mathrm{G}}(I,\boldsymbol{r}^{\#},M,7)$	$M_{\mathrm{G}}(I,\boldsymbol{r}^{\#},7)$	$\kappa_{\mathrm{G}}(I,\boldsymbol{r}^{\#},M_{\mathrm{G}},7)$	$M^{\natural}(I,\boldsymbol{r}^{\#},7)$	$\kappa_{\mathrm{G}}(I,\boldsymbol{r}^{\#},M^{\natural},7)$	$\kappa(I,\boldsymbol{r}^{\#},M^{\natural},7)$
2	183	1 311	1.9759	1 024	2.5340	257	-3.9695	2.0000
3	983	12 431	1.5478	4 096	4.0563	1 834	-3.2507	2.2125
4	3 741	88 554	1.5012	32 768	2.6445	10 917	-3.8293	2.1301
5	10 569	470 305	1.2737	131 072	3.6799	51 400	-5.7059	2.0243
6	23 431	1 716 851	1.2750	262 144	3.7796	172 619	-9.7223	2.0232
7	43 081	5 179 281	1.2085	1 048 576	2.7806	490 698	8.1427	–
8	67 857	10 773 726	1.1357	2 097 152	2.3746	978 608	24.3931	–
9	94 693	25 047 401	1.1162	2 097 152	4.4027	2 208 285	4.8482	–
10	120 251	40 082 509	1.1579	4 194 304	4.1762	3 460 936	3.9950	–
11	142 261	50 120 683	1.1177	4 194 304	3.2392	4 265 776	3.3211	–
12	159 611	68 346 777	1.1042	4 194 304	5.7392	5 760 580	3.2268	–
13	172 079	92 708 602	1.0968	8 388 608	4.1251	7 764 684	4.3660	–
14	180 383	95 547 471	1.0908	8 388 608	3.6335	7 970 986	3.6633	–
15	185 551	147 089 331	1.0683	8 388 608	6.1100	12 241 985	2.5929	–
16	188 531	138 940 316	1.0974	8 388 608	4.8203	11 548 443	2.4997	–
17	190 085	140 891 818	1.1128	8 388 608	6.8848	11 702 663	3.4279	–
18	190 819	171 448 313	1.0740	16 777 216	3.0043	14 236 169	2.3026	–
19	191 105	139 003 851	1.0899	8 388 608	5.7615	11 540 716	2.1610	–
20	191 207	155 186 701	1.1208	16 777 216	3.2687	12 883 717	3.3075	–
21	191 233	141 303 357	1.0985	16 777 216	3.0772	11 730 979	3.0025	–
22	191 235	130 564 751	1.1008	8 388 608	3.8759	10 839 452	3.1905	–

Table 4.4: Generated set sizes $M(I,\boldsymbol{r}^{\#},7)$, $M_{\mathrm{G}}(I,\boldsymbol{r}^{\#},7)$, $M^{\natural}(I,\boldsymbol{r}^{\#},7)$, estimated condition numbers κ_{G}, cf. (4.16) and (4.17), and condition numbers $\kappa(I,\boldsymbol{r},M^{\natural},7)$, cf. (4.17), for weighted ℓ_1-ball frequency index sets $I = I_{1,10}^{d,\boldsymbol{\gamma}}$, $\boldsymbol{\gamma} = \left(0.9^{s-1}\right)_{s\in\mathbb{N}}$.

$|I|$, dimension d, and structure, the oversampling factors up to 400 for the reconstructing generated sets are acceptable, in particular with respect to the relatively fast search Algorithm 4.5. □

We note that the reconstructing generated set sizes are not too far away from the corresponding reconstructing rank-1 lattice sizes for ℓ_p-ball frequency index sets of reasonable cardinality—even for non-convex ℓ_p-balls, i.e., $0 < p < 1$.

4.6.2 Weighted Hyperbolic Crosses

Due to the fact that each reconstructing rank-1 lattice is also a reconstructing generated set for a specific frequency index set I, the existence results for reconstructing rank-1 lattices, cf. Corollary 3.4, apply directly to reconstructing generated sets. Our search strategy for reconstructing generated sets is based on a continuous optimization method which can only

Weighted $\ell_{1/2}$-balls $I^{d,\boldsymbol{\gamma}}_{1/2,35}$ – Reconstructing Generated Sets $\Lambda(\boldsymbol{r}, M, I^{d,\boldsymbol{\gamma}}_{1/2,35})$								
d	$\lvert I^{d,\boldsymbol{\gamma}}_{1/2,35}\rvert$	$M(I,\boldsymbol{r}^{\#},7)$	$\kappa_{\mathrm{G}}(I,\boldsymbol{r}^{\#},M,7)$	$M_{\mathrm{G}}(I,\boldsymbol{r}^{\#},7)$	$\kappa_{\mathrm{G}}(I,\boldsymbol{r}^{\#},M_{\mathrm{G}},7)$	$M^{\natural}(I,\boldsymbol{r}^{\#},7)$	$\kappa_{\mathrm{G}}(I,\boldsymbol{r}^{\#},M^{\natural},7)$	$\kappa(I,\boldsymbol{r}^{\#},M^{\natural},7)$
2	749	14 307	1.643	8 192	1.872	2 200	-4.989	2.057
3	3 285	169 538	1.321	16 384	4.640	21 242	-69.617	1.893
4	8 835	1 037 473	1.188	131 072	6.582	115 653	4.626	1.552
5	18 019	4 652 262	1.137	524 288	3.643	480 444	3.231	1.573
6	30 263	12 670 321	1.164	1 048 576	3.271	1 241 975	3.230	1.843
7	44 867	30 464 506	1.087	2 097 152	4.144	2 875 223	2.631	1.786
8	60 479	65 209 353	1.085	8 388 608	2.044	5 985 738	2.475	1.744
9	76 109	76 113 188	1.120	8 388 608	2.249	6 842 255	2.183	1.647
10	90 983	155 571 721	1.108	16 777 216	2.001	13 764 368	2.182	1.737
11	104 615	214 018 985	1.064	16 777 216	3.762	18 704 502	2.101	–
12	116 571	310 727 610	1.087	33 554 432	2.067	26 902 068	1.971	–
13	126 761	301 779 850	1.077	33 554 432	1.832	25 939 191	2.128	–
14	135 105	426 149 997	1.076	33 554 432	2.290	36 429 690	2.108	–
15	141 877	471 661 378	1.073	33 554 432	3.487	40 152 382	1.983	–
16	147 195	397 110 673	1.065	33 554 432	2.005	33 700 336	1.987	–
17	151 371	613 800 095	1.075	33 554 432	6.085	51 966 058	1.843	–
18	154 569	605 304 755	1.073	67 108 864	2.238	51 156 271	2.002	–
19	156 955	566 656 688	1.067	33 554 432	3.848	47 828 078	1.641	–
20	158 715	609 848 421	1.071	33 554 432	6.248	51 425 231	2.096	–
21	159 999	540 794 630	1.064	33 554 432	3.160	45 571 334	2.633	–
22	160 917	636 159 526	1.067	67 108 864	1.909	53 581 650	1.700	–
23	161 551	576 314 229	1.079	33 554 432	4.947	48 525 004	1.746	–
24	161 965	515 658 324	1.074	33 554 432	2.816	43 408 491	2.062	–
25	162 221	684 218 540	1.061	67 108 864	1.716	57 590 355	1.709	–
26	162 381	559 140 055	1.070	33 554 432	4.811	47 058 653	1.946	–
27	162 477	628 385 517	1.074	67 108 864	1.835	52 883 897	2.221	–
28	162 549	659 006 471	1.070	33 554 432	4.803	55 458 838	2.131	–
29	162 595	591 983 153	1.070	33 554 432	6.218	49 817 290	1.764	–
30	162 621	657 959 603	1.095	67 108 864	1.707	55 368 675	2.695	–
31	162 631	538 222 519	1.102	33 554 432	4.759	45 292 315	2.136	–
32	162 633	493 595 180	1.070	33 554 432	2.695	41 536 808	1.865	–
33	162 635	499 030 445	1.075	33 554 432	4.577	41 994 150	2.552	–
34	162 637	573 600 550	1.069	33 554 432	4.969	48 269 285	1.722	–
35	162 637	495 029 394	1.058	33 554 432	2.918	41 657 413	1.855	–

Table 4.5: Generated set sizes $M(I,\boldsymbol{r}^{\#},7)$, $M_{\mathrm{G}}(I,\boldsymbol{r}^{\#},7)$, $M^{\natural}(I,\boldsymbol{r}^{\#},7)$,estimated condition numbers κ_{G}, cf. (4.16) and (4.17), and condition numbers $\kappa(I,\boldsymbol{r},M^{\natural},7)$, cf. (4.17), for weighted $\ell_{1/2}$-ball frequency index sets $I = I^{d,\boldsymbol{\gamma}}_{1/2,35}$, $\boldsymbol{\gamma} = \left(0.9^{s-1}\right)_{s\in\mathbb{N}}$.

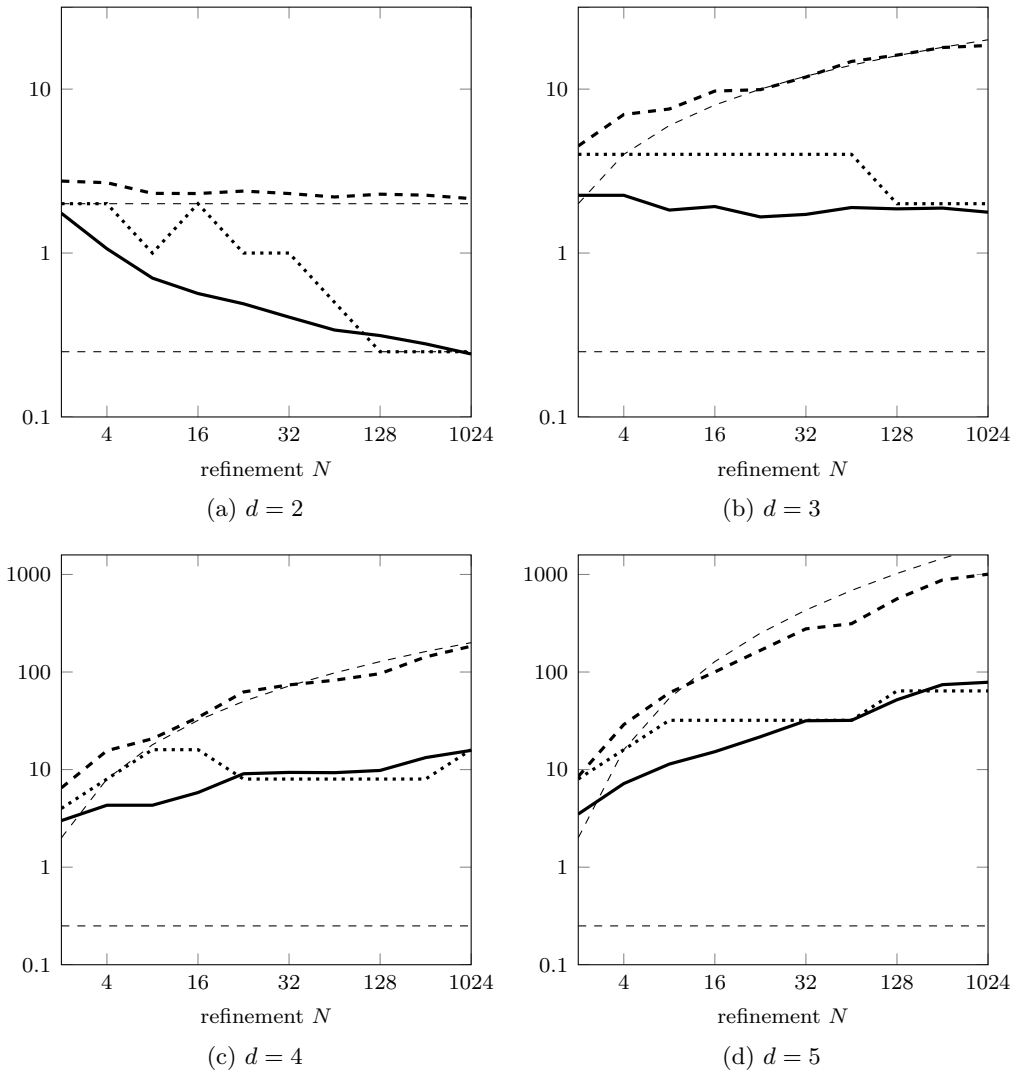

(a) $d = 2$ (b) $d = 3$

(c) $d = 4$ (d) $d = 5$

Figure 4.5: Cardinalities of stable ($C = 7$) reconstructing generated sets for weighted hyperbolic crosses $I := I^{d,\boldsymbol{\gamma}}_{\mathrm{hc},N}$ of different dimensions d for comparison. Upper dashed: $2(\log_2 N)^{d-2}$, lower dashed: $1/4$, thick dashed: $M(I, \boldsymbol{r}^{\#}, 7)/N^2$, thick dotted: $M_{\mathrm{G}}(I, \boldsymbol{r}^{\#}, 7)/N^2$, thick solid: $M^{\natural}(I, \boldsymbol{r}^{\#}, 7)/N^2$, $\boldsymbol{\gamma} = \left(\frac{1}{2}\right)_{s\in\mathbb{N}}$.

find local minimizers of the functional ρ, cf. (4.9). In general, we do not find global minimizers using this method.

We would like to consider one of the most interesting questions in this area: Can we expect the same asymptotic behavior for reconstructing rank-1 lattice sizes and reconstructing generated set sizes using the presented search methods?

In particular, we consider the behavior of the cardinalities of reconstructing generated sets for weighted hyperbolic crosses with respect to the parameter N.

Example 4.15. We computed reconstructing generated sets for weighted hyperbolic crosses $I = I^{d,\boldsymbol{\gamma}}_{\mathrm{hc},N}$ for $d = 2, \ldots, 5$ and $N = 2, 4, \ldots, 1\,024$. Specifically, we obtain reconstructing generated sets of sizes $M(I, \boldsymbol{r}^{\#}, 7)$, $M_{\mathrm{G}}(I, \boldsymbol{r}^{\#}, 7)$, $M^{\natural}(I, \boldsymbol{r}^{\#}, 7)$, as introduced in this section.

Similar to Example 3.24, we plotted the functions $2(\log_2(N))^{d-2}$ and $1/4$ and the values of $M(I, \boldsymbol{r}^\#, 7)/N^2$, $M_{\mathrm{G}}(I, \boldsymbol{r}^\#, 7)/N^2$, $M^\natural(I, \boldsymbol{r}^\#, 7)/N^2$ in Figure 4.5 for dimensions $d = 2, 3, 4, 5$. Accordingly, the thin dashed lines ($2(\log_2(N))^{d-2}$ and $1/4$) are exactly the same as plotted for rank-1 lattices. We compare the plots to those presented in Figure 3.2. The most interesting observations are:

1. The plots of $M(I, \boldsymbol{r}^\#, 7)/N^2$ behave like the function $2(\log_2(N))^{d-2}$ and thus like $M_{\mathrm{Cor3.4}}/N^2$.

2. The plotted values of $M_{\mathrm{G}}(I, \boldsymbol{r}^\#, 7)/N^2$ and $M^\natural(I, \boldsymbol{r}^\#, 7)/N^2$ grow similar to the plots of $M_{\mathrm{Alg3.7}}/N^2$ and $M_{\mathrm{Alg3.8}}/N^2$ in Figure 3.2.

3. In most cases we obtain generated set sizes $M(I, \boldsymbol{r}^\#, 7)$ ($M_{\mathrm{G}}(I, \boldsymbol{r}^\#, 7)$ or $M^\natural(I, \boldsymbol{r}^\#, 7)$) that are larger than the rank-1 lattice sizes $M_{\mathrm{Cor3.4}}$ ($M_{\mathrm{Alg3.8}}$) determined in Example 3.24.

Thus, we recognize similar behaviors for our determined reconstructing generated set sizes and reconstructing rank-1 lattice sizes with respect to the parameter N. As also mentioned in Example 3.24 for reconstructing rank-1 lattices, we observe an asymptotic behavior of the cardinalities of our reconstructing generated sets $\Lambda(\boldsymbol{r}^\#, M, I^{d,\boldsymbol{\gamma}}_{\mathrm{hc},N})$, $M = M_{\mathrm{G}}(I, \boldsymbol{r}^\#, 7)$ or $M = M^\natural(I, \boldsymbol{r}^\#, 7)$, that differs from the lower bound $N^2/4$ and also from the upper bound $N^2(\log N)^{d-2}$.

Although the most reconstructing generated set sizes $M^\natural(I, \boldsymbol{r}^\#, 7)$ are even significantly larger than the rank-1 lattice sizes $M_{\mathrm{Alg3.8}}$, we would like to emphasize the practical advantages of the generated set approach. In particular, applications that causes varying frequency index sets, i.e., time dependent partial differential equations, may benefit from well adapted frequency index sets and corresponding suitable sampling sets. Clearly, we need fast methods in order to determine such sampling sets in order to compute a lot of time steps. Consequently, generated sets might be preferred to rank-1 lattices since the corresponding search algorithm, cf. Algorithm 4.5, determines suitable generated sets in a relatively fast way.

Again, we stress the fact that almost all determined reconstructing generated sets $\Lambda(\boldsymbol{r}^\#, M, I^{d,\boldsymbol{\gamma}}_{\mathrm{hc},N})$, $M = M(I, \boldsymbol{r}^\#, 7)$, $M = M_{\mathrm{G}}(I, \boldsymbol{r}^\#, 7)$, or $M = M^\natural(I, \boldsymbol{r}^\#, 7)$, induce Fourier matrices $\boldsymbol{A} = \left(\mathrm{e}^{2\pi\mathrm{i}\boldsymbol{k}\cdot\boldsymbol{x}}\right)_{\boldsymbol{x}\in\Lambda(\boldsymbol{r}^\#, M, I^{d,\boldsymbol{\gamma}}_{\mathrm{hc},N}), \boldsymbol{k}\in I^{d,\boldsymbol{\gamma}}_{\mathrm{hc},N}}$, such that the condition numbers of the matrices $\boldsymbol{A}^*\boldsymbol{A}$ are bounded by three actually. □

Example 4.16. We consider equally weighted hyperbolic crosses $I^{d,\boldsymbol{\gamma}}_{\mathrm{hc},N}$ of different dimensions d, parameters $N = 4, 2^{2.5}$ and fixed weights $\gamma_s = \left(\frac{108972864000}{2122061\pi^{10}}\right)^{1/10} \approx 0.941686$, $s = 1, \ldots, d$, similar to Example 3.25. In Table 4.6, we present stable reconstructing generated sets for these weighted hyperbolic crosses $I^{d,\boldsymbol{\gamma}}_{\mathrm{hc},N}$. In general, we observe that the cardinalities of the generated sets are up to approximately five times larger than the lattice sizes of the reconstructing rank-1 lattices we presented in Table 3.8. Nevertheless, sampling schemes with comparable reconstruction properties has cardinalities in the same order of magnitude. We notice that all exactly determined condition numbers are less than three actually.

At this point, we would like to stress that the limit of the cardinality of the weighted hyperbolic crosses $I^{d,\boldsymbol{\gamma}}_{\mathrm{hc},N}$ of approximately one million is not caused by our search method, i.e., Algorithm 4.5. Quite the contrary, we check the properties of the determined generated sets by computing the exact Gershgorin circle radii. The corresponding complexity is in $\Theta\left(|I|^2\right)$ and, thus, the bottleneck here. □

Weighted hyperbolic crosses $I^{d,\gamma}_{\mathrm{hc},N}$ – Reconstructing Generated Sets $\Lambda(\boldsymbol{r}, M, I^{d,\gamma}_{\mathrm{hc},N})$									
	d	$\lvert I^{d,\gamma}_{\mathrm{hc},N}\rvert$	$M(I,\boldsymbol{r}^{\#},7)$	$\kappa_{\mathrm{G}}(I,\boldsymbol{r}^{\#},M,7)$	$M_{\mathrm{G}}(I,\boldsymbol{r}^{\#},7)$	$\kappa_{\mathrm{G}}(I,\boldsymbol{r}^{\#},M_{\mathrm{G}},7)$	$M^{\natural}(I,\boldsymbol{r}^{\#},7)$	$\kappa_{\mathrm{G}}(I,\boldsymbol{r}^{\#},M^{\natural},7)$	$\kappa(I,\boldsymbol{r}^{\#},M^{\natural},7)$
$N=4$	2	33	158	2.0655	128	2.5990	46	-9.3958	2.4702
	3	135	1 124	1.9964	512	4.0671	234	-4.7711	2.2959
	4	513	7 203	1.6336	4 096	2.7259	1 176	-4.7668	2.1102
	5	1 703	53 432	1.3602	16 384	2.3190	7 295	-8.3791	2.0167
	6	5 217	343 833	1.2639	65 536	3.2891	40 720	78.7394	1.8761
	7	15 655	1 691 514	1.2045	262 144	2.6203	177 258	17.8978	1.9187
	8	47 617	7 668 584	1.1314	1 048 576	3.7965	719 716	5.6432	1.6474
	9	148 167	48 791 878	1.0846	4 194 304	3.9202	4 138 354	3.6469	–
	10	469 409	210 333 486	1.0957	16 777 216	3.6974	16 250 377	3.7299	–
$N=2^{5/2}$	2	61	379	2.0086	256	3.0994	94	-6.4329	2.4149
	3	255	3 215	1.7037	2 048	2.3693	592	-5.7753	2.1553
	4	1 001	24 387	1.3488	8 192	2.2781	3 590	-6.6803	1.9993
	5	3 843	173 537	1.3132	32 768	3.3784	21 324	-19.0376	1.7747
	6	13 125	1 074 309	1.2395	262 144	1.8144	114 698	-15.1377	1.9459
	7	40 407	4 793 474	1.1925	1 048 576	1.9742	456 920	16.0385	–
	8	117 905	30 724 067	1.1083	2 097 152	4.9095	2 657 399	3.2846	–
	9	341 307	175 872 820	1.0708	16 777 216	2.7536	13 930 955	2.9900	–
	10	1 007 629	849 340 491	1.0789	67 108 864	2.0387	61 963 186	2.1041	–

Table 4.6: Generated set sizes $M(I,\boldsymbol{r}^{\#},7)$, $M_{\mathrm{G}}(I,\boldsymbol{r}^{\#},7)$, $M^{\natural}(I,\boldsymbol{r}^{\#},7)$, estimated condition numbers κ_{G}, cf. (4.16) and (4.17), and condition numbers κ, cf. (4.15) and (4.17), for hyperbolic cross frequency index sets $I = I^{d,\gamma}_{\mathrm{hc},N}$, $\boldsymbol{\gamma} = \left(\frac{2122061\pi^{10}}{108972864000}\right)^{-1/10}\mathbf{1}$.

4.6.3 Arbitrary Sparse Frequency Index Sets

Since we would like to compare the numerical results of this section with those of Section 3.8.4, we computed reconstructing generated sets for exactly the same randomly chosen frequency index sets as considered in Section 3.8.4. We present the corresponding generated set sizes M, M_G and $M^{\natural}$, estimates of the condition numbers κ_G, and condition numbers κ in Table 4.7. Similar to the numerical results for reconstructing rank-1 lattices, the two-dimensional frequency index sets $I \subset [-128,128]^2 \cap \mathbb{Z}^2$ seem to have some additional structure, which may be caused by the high density of the two-dimensional frequency index sets I within the discrete set $[-128,128]^2 \cap \mathbb{Z}^2$. Accordingly, we focus on the frequency index sets of higher dimensions $d = 4,\dots,1024$.

At first we consider fixed dimension d and growing cardinalities $|I|$. Similar to the reconstructing rank-1 lattices, we obtain approximately fourfold generated set sizes for doubled cardinalities of frequency index sets. Consequently, the generated set sizes grow approximately as the squared cardinality of the frequency index set I.

Furthermore, we obtain cardinalities of the reconstructing generated sets that are similar to the rank-1 lattice sizes presented in Table 3.11 in the order of magnitude. In particular, the values within the tuples $(M(I,\boldsymbol{r}^{\#},7), M_{\mathrm{Cor3.4}})$ and $(M^{\natural}(I,\boldsymbol{r}^{\#},7), M_{\mathrm{Alg3.3+Alg3.5}}, M_{\mathrm{Alg3.8}})$

Arbitrary frequency index sets I – Reconstructing Generated Sets $\Lambda(\boldsymbol{r}, M, I)$								
	d	$M(I, \boldsymbol{r}^{\#}, 7)$	$\kappa_{\mathrm{G}}(I, \boldsymbol{r}^{\#}, M, 7)$	$M_{\mathrm{G}}(I, \boldsymbol{r}^{\#}, 7)$	$\kappa_{\mathrm{G}}(I, \boldsymbol{r}^{\#}, M_{\mathrm{G}}, 7)$	$M^{\natural}(I, \boldsymbol{r}^{\#}, 7)$	$\kappa_{\mathrm{G}}(I, \boldsymbol{r}^{\#}, M^{\natural}, 7)$	$\kappa(I, \boldsymbol{r}^{\#}, M^{\natural}, 7)$
$\lvert I\rvert = 750$	2	175 855	1.1864	32 768	2.3435	27 031	1.4358	1.1318
	4	264 274	1.1023	32 768	3.7252	40 623	2.8878	1.8521
	8	207 848	1.1601	32 768	2.3929	31 949	2.3647	1.6115
	16	142 567	1.1579	16 384	3.6510	21 914	2.5299	1.6179
	32	118 850	1.2556	16 384	2.6977	18 269	3.5602	1.7384
	64	105 529	1.1733	16 384	3.4507	16 221	3.3623	1.8754
	128	77 779	1.2484	16 384	3.8866	11 955	6.4992	1.9725
	256	67 399	1.2437	16 384	2.3913	10 360	7.4982	2.0225
	512	67 769	1.2234	8 192	6.0333	10 417	7.6357	2.0920
	1 024	67 735	1.2824	8 192	6.8689	10 412	4.6306	1.8402
$\lvert I\rvert = 1500$	2	424 770	1.1208	65 536	1.9321	59 012	1.2895	1.0806
	4	886 339	1.1403	131 072	1.7242	123 137	1.9850	1.7794
	8	833 773	1.1028	131 072	1.7028	115 834	2.3318	1.8294
	16	605 972	1.1661	65 536	4.9773	84 186	2.7771	1.8020
	32	476 273	1.1135	65 536	2.3508	66 167	2.3054	1.5975
	64	412 495	1.1794	65 536	2.7616	57 307	2.9043	1.7450
	128	329 227	1.1875	32 768	6.0854	45 738	2.5163	1.6943
	256	246 535	1.1782	32 768	3.5957	34 250	3.5141	1.8048
	512	293 640	1.1882	32 768	4.5122	40 794	4.2008	1.8058
$\lvert I\rvert = 3000$	2	604 908	1.1771	65 536	2.2606	76 660	2.1397	1.3249
	4	3 039 764	1.0971	262 144	6.1060	385 230	2.1546	1.9630
	8	3 120 064	1.0790	262 144	5.6093	395 406	2.0191	1.8691
	16	2 678 164	1.1122	262 144	3.4153	339 404	1.7900	1.6055
	32	1 880 963	1.1026	262 144	2.1722	238 375	2.0828	1.6177
	64	1 515 685	1.1517	262 144	2.6016	192 083	2.2648	1.7525
	128	1 229 923	1.1056	131 072	2.1753	155 868	2.3957	1.6649
	256	1 140 653	1.1424	131 072	2.6274	144 555	2.4377	1.7032
$\lvert I\rvert = 6000$	2	709 484	1.2538	65 536	3.9082	82 654	14.1339	1.8350
	4	12 771 978	1.1030	1 048 576	5.1820	1 487 925	2.1443	1.9841
	8	12 550 893	1.1073	1 048 576	4.9586	1 462 169	2.2041	2.0689
	16	10 643 820	1.1082	1 048 576	3.0549	1 239 996	2.0480	1.8882
	32	7 923 112	1.1037	1 048 576	2.0819	923 036	2.2783	1.7199
	64	6 625 638	1.1216	524 288	5.7345	771 881	1.8552	1.6084
	128	5 544 914	1.1285	524 288	2.8288	645 978	2.1266	1.6709
	256	4 771 193	1.1108	524 288	2.6301	555 840	2.3159	1.6784

Table 4.7: Generated set sizes $M(I, \boldsymbol{r}^{\#}, 7)$, $M_{\mathrm{G}}(I, \boldsymbol{r}^{\#}, 7)$, $M^{\natural}(I, \boldsymbol{r}^{\#}, 7)$, estimated condition numbers κ_{G}, cf. (4.16) and (4.17), and condition numbers κ, cf. (4.15) and (4.17), for arbitrary frequency index sets I chosen uniformly distributed from $[-128, 128]^d$.

are very close to each other.

To this end, we focus on fixed cardinalities of the frequency index sets I and growing dimensions. We observe that the cardinalities of the found reconstructing generated sets mildly decrease with growing dimensions. In other words, an increasing number of degrees of freedom of the functional ρ results in a lower minimal value. This behavior seems to be somehow natural. In fact, for large dimensions $d \gg |I|$ and randomly chosen $|I|$ we have a high probability that all elements contained in I are linearly independent. Thus, let us assume that all elements of the frequency index set I are linearly independent. Then, the matrix

$$\boldsymbol{K} = \left(\begin{array}{cccc} \boldsymbol{k}_1, & \boldsymbol{k}_2, & \cdots, & \boldsymbol{k}_{|I|} \end{array} \right) \in \mathbb{Z}^{d \times |I|},$$

that contains each element of I as one column, has full column rank and we obtain that the vector $\frac{1}{|I|}(0, 1, \ldots, |I|-1)^\top$ is in the range of $\boldsymbol{K}^\top$. Hence, we compute a generating vector $\boldsymbol{r} \in \mathbb{R}^d$ as the solution of the system of linear equations

$$\boldsymbol{K}^\top \boldsymbol{r} = \frac{1}{|I|}(0, 1, \ldots, |I|-1)^\top.$$

Consequently, the vector $\boldsymbol{r}$ is an optimal choice of a generating vector, since the corresponding Fourier matrix $\boldsymbol{A} = \left(\mathrm{e}^{2\pi \mathrm{i} j \boldsymbol{k}_l \cdot \boldsymbol{r}}\right)_{j=0,\ldots,|I|-1,\, l=1,\ldots,|I|} = \left(\mathrm{e}^{2\pi \mathrm{i} \frac{jl}{|I|}}\right)_{j,l=0,\ldots,|I|-1}$ simplifies to a Fourier matrix of a one-dimensional discrete Fourier transform and, thus, is a unitary matrix up to some constant. In addition, we obtain an optimal cardinality $|I|$ of the reconstructing generated set $\Lambda(\boldsymbol{r}, |I|, I)$. Furthermore the vector $\boldsymbol{r}$ is a global minimizer of $\rho(I, \circ)$ and the corresponding value is given by $\rho(I, \boldsymbol{r}) = |I| \sum_{j=1}^{\left\lfloor \frac{|I|}{2} \right\rfloor} j^{-1}$.

We stress the fact that we cannot expect a similar behavior for structured frequency index sets I since the condition $d \gg |I|$ and the linear independence of the elements of the frequency index sets I is usually violated.

4.7 Summary

The basic subject of this chapter was the generalization of the rank-1 lattice approach that is presented in Chapter 3. We simply allowed real valued vectors as generating vectors of the sampling scheme with rank-1 structure.

We exploited this rank-1 structure of generated sets $\Lambda(\boldsymbol{r}, M)$ in order to evaluate a trigonometric polynomial at all nodes of a generated set similar to the rank-1 lattice approach. The only difference is the application of a one-dimensional adjoint nonequispaced fast Fourier transform instead of an equispaced fast Fourier transform. The corresponding complexity of the evaluation problem is in $\mathcal{O}\left(M \log M + (|\log \varepsilon| + d)|I|\right)$, where ε describes the accuracy of the one-dimensional nonequispaced fast Fourier transform, see Section 4.2 for all details.

Since a fast evaluation of multivariate trigonometric polynomials along generated sets is guaranteed, we focus on the reconstruction problem, i.e., the unique reconstruction of all frequencies $\hat{f}_{\boldsymbol{k}} \in \mathbb{C}$, $\boldsymbol{k} \in I$, of the trigonometric polynomials $f \in \Pi_I$ from the sampling values $f(\boldsymbol{x})$, $\boldsymbol{x} \in \Lambda(\boldsymbol{r}, M)$. The necessary condition on the corresponding Fourier matrix $\boldsymbol{A}$ is that $\boldsymbol{A}$ needs full column rank, which is fulfilled if and only if the conditions $|\{\boldsymbol{k} \cdot \boldsymbol{r} \bmod 1 \colon \boldsymbol{k} \in I\}| = |I|$ and $M \geq |I|$ are fulfilled, cf. Lemma 4.2. We gave a fast algorithm for the reconstruction problem that applies a conjugate gradient method to one-dimensional nonequispaced fast Fourier transforms and corresponding adjoint nonequispaced fast Fourier transforms, cf. Algorithm 4.3. The computational complexity of one step of the conjugate

gradient method is bounded by $\mathcal{O}\left(M \log M + (|\log \varepsilon| + d)|I|\right)$. Certainly, the number of needed steps of the conjugate gradient method crucially depends on the condition number of the corresponding Fourier matrix $\boldsymbol{A}$, cf. Lemma 4.5. Thus, the condition number of the matrix $\boldsymbol{A}$ describes the stability of the given problem and somehow the computational complexity of the reconstruction problem.

Furthermore, we considered the approximation of functions $f \in \mathcal{A}_\omega(\mathbb{T}^d)$ using trigonometric polynomials $\breve{S}_{I_N} f \in \Pi_{I_N}$ that well approximates the Fourier partial sums $S_{I_N} f$ of f. Here, we compute $\breve{S}_{I_N} f$ from sampling values of f that are taken along a reconstructing generated set for I_N. In particular, we estimate the $L_2(\mathbb{T}^d)$ error of the approximation by the term N^{-1} times the norm of f in $\mathcal{A}_\omega(\mathbb{T}^d)$ times a term that depends inversely proportional on the smallest singular value of $\boldsymbol{A}$ and, thus, can be bounded from above by the condition number of $\boldsymbol{A}$, cf. Theorem 4.12.

In order to estimate the stability, or more precisely the condition number, of the Fourier matrix $\boldsymbol{A}$, where $\Lambda(\boldsymbol{r}, M)$ and I are given, we considered the Gershgorin circle radii of the matrix $\boldsymbol{A}^*\boldsymbol{A}$ and gave an upper bound $\rho(I, \boldsymbol{r})$ on the maximum Gershgorin circle radius. Note that all centers of the Gershgorin circles are identical. The upper bound on the maximum Gershgorin circle radius only depends on the distances of successive elements within the set $\{\boldsymbol{k} \cdot \boldsymbol{r} \bmod 1 \colon \boldsymbol{k} \in I\}$ and is fast computable in $\mathcal{O}\left(|I|(\log |I| + d)\right)$, cf. Theorem 4.8 and Algorithm 4.4. In addition, we can simply compute a generated set size $M(I, \boldsymbol{r}, C)$, which depends linearly on $\rho(I, \boldsymbol{r})$, such that the corresponding matrix $\boldsymbol{A}^*\boldsymbol{A}$, $\boldsymbol{A} = \left(\mathrm{e}^{2\pi \mathrm{i} \boldsymbol{k} \cdot \boldsymbol{x}}\right)_{\boldsymbol{x} \in \Lambda(\boldsymbol{r}, M(I, \boldsymbol{r}, C)), \boldsymbol{k} \in I'}$ has a condition number smaller or equal to $C > 1$, cf. Corollary 4.10. For that reason, we use $\rho(I, \boldsymbol{r})$ in order to rate the reconstruction properties of a generating vector $\boldsymbol{r}$ for a given frequency index set I.

We suggest to numerically minimize the functional $\rho(I, \circ) : \mathbb{T}^d \to \mathbb{R} \cup \{\infty\}$ in order to achieve suitable generated sets, i.e., generated sets that consists of a small number of sampling nodes and guarantees a small condition number of $\boldsymbol{A}$. Due to the fact that the functional $\rho(I, \circ)$ may has poles on $d-1$- dimensional subsets of $\mathbb{T}^d$, we restrict ourselves to evaluations of $\rho(I, \circ)$ in order to find local minimizers of $\rho(I, \circ)$. Accordingly, we use a simplex search method for the optimization of $\rho(I, \circ)$, cf. Algorithm 4.5. In contrast to the rank-1 lattice search algorithm, which is a discrete component–by–component type algorithm, the search algorithm for generated sets is based on a continuous search method. We compute the corresponding evaluations of $\rho(I, \circ)$ in a fast way. The related algorithm needs only few memory, cf. Algorithm 4.4.

We demonstrate the search algorithm for generated sets, cf. Algorithm 4.5, on specific frequency index sets. To this end, we computed stable reconstructing generated sets for weighted ℓ_p-balls, weighted hyperbolic crosses, and randomly chosen frequency index sets and compare the results to the reconstructing rank-1 lattices that we determined in Chapter 3. The numerical tests heuristically motivate that the theoretically found $M(I, \boldsymbol{r}, C)$ may suffer from the rough estimate of the maximum Gershgorin circle radius and even a smaller number of sampling values are enough in order to obtain small condition numbers of the Fourier matrix $\boldsymbol{A}$. In general, the number of sampling nodes of the stable generated sets and the reconstructing rank-1 lattices that we determined using our search algorithms are broadly similar.

Chapter 5

Applications and Numerical Examples

In this chapter, we present some examples with detailed theoretical error analysis and corresponding numerical tests. More precisely, we specified some error estimates in the $L_\infty(\mathbb{T}^d)$ norm in Chapter 3. In the following, we will illustrate their validity by some specific examples. In particular, we have to compute or estimate the $L_\infty(\mathbb{T}^d)$ norm of different functions. Due to the fact, that we do not only want to approximate the $L_\infty(\mathbb{T}^d)$ norm of a function using a finite set of sampling values, we will compute an upper bound on it. More specifically, we estimate

$$\begin{aligned}\|f-t|L_\infty(\mathbb{T}^d)\| \leq \|f-t|\mathcal{A}(\mathbb{T}^d)\| &= \sum_{\boldsymbol{k}\in\mathbb{Z}^d} |\hat{f}_{\boldsymbol{k}} - \hat{t}_{\boldsymbol{k}}| \\ &= \sum_{\boldsymbol{k}\in\mathbb{Z}^d} |\hat{f}_{\boldsymbol{k}}| - \sum_{\boldsymbol{k}\in I} |\hat{f}_{\boldsymbol{k}}| + \sum_{\boldsymbol{k}\in I} |\hat{f}_{\boldsymbol{k}} - \hat{t}_{\boldsymbol{k}}| \\ &= \|f|\mathcal{A}(\mathbb{T}^d)\| + \sum_{\boldsymbol{k}\in I} \left(|\hat{f}_{\boldsymbol{k}} - \hat{t}_{\boldsymbol{k}}| - |\hat{f}_{\boldsymbol{k}}| \right) =: \operatorname{err}(f,t,\mathcal{A}(\mathbb{T}^d)), \end{aligned} \tag{5.1}$$

where $f \in \mathcal{A}(\mathbb{T}^d)$ belongs to the Wiener algebra and $t \in \Pi_I$ is a trigonometric polynomial with frequencies supported on the index set $I \subset \mathbb{Z}^d$, $|I| < \infty$. We name $\operatorname{err}(f,t,\mathcal{A}(\mathbb{T}^d))$ the error of the approximation t of f in the space $\mathcal{A}(\mathbb{T}^d)$, which is in fact an upper bound on the $L_\infty(\mathbb{T}^d)$ norm of $f-t$. At this point, we would like to stress that we checked the relevance of the upper bound $\operatorname{err}(f,t,\mathcal{A}(\mathbb{T}^d))$ of the $L_\infty(\mathbb{T}^d)$ error in (5.1) by evaluating the considered test functions f and corresponding approximations t at suitable rank-1 lattices. Indeed, we found sampling nodes $\boldsymbol{x} \in \mathbb{T}^d$ where the error $f(\boldsymbol{x}) - t(\boldsymbol{x})$ was in the order of magnitude of the upper bound $\operatorname{err}(f,t,\mathcal{A}(\mathbb{T}^d))$ in all our numerical tests.

Furthermore, we proved some error estimates in Chapter 4, where the error is measured in the $L_2(\mathbb{T}^d)$ norm. Similar to (5.1), we estimate

$$\|f-t|L_2(\mathbb{T}^d)\|^2 = \sum_{\boldsymbol{k}\in\mathbb{Z}^d} |\hat{f}_{\boldsymbol{k}} - \hat{t}_{\boldsymbol{k}}|^2 = \sum_{\boldsymbol{k}\in\mathbb{Z}^d} |\hat{f}_{\boldsymbol{k}}|^2 + \sum_{\boldsymbol{k}\in I} \left(|\hat{f}_{\boldsymbol{k}} - \hat{t}_{\boldsymbol{k}}|^2 - |\hat{f}_{\boldsymbol{k}}|^2 \right)$$

using Parseval's identity and the requirement that $t \in \Pi_I$ is a trigonometric polynomial with frequencies supported on the frequency index set I. Since we sum up a large number of differences of squared rounded floating point numbers, we have to expect that the right hand side of the equality may sum up to some negative value. Thus, we will compute the values

of the $L_2(\mathbb{T}^d)$ error by

$$\|f - t|L_2(\mathbb{T}^d)\| = \left| \|f|L_2(\mathbb{T}^d)\|^2 + \sum_{\boldsymbol{k} \in I} \left(|\hat{f}_{\boldsymbol{k}} - \hat{t}_{\boldsymbol{k}}|^2 - |\hat{f}_{\boldsymbol{k}}|^2 \right) \right|^{1/2} =: \operatorname{err}(f, t, L_2(\mathbb{T}^d)).$$

We stress the fact that we do not apply the asymptotically best possible theoretical error estimates in this section. More precisely, we estimate the approximation errors in Theorems 3.11 and 4.12 by the norm of the function $f \in \mathcal{A}_\omega(\mathbb{T}^d)$ in the specific function space $\mathcal{A}_\omega(\mathbb{T}^d)$, the term N^{-1}, and terms $C_\delta \geq 2$ and 2 that depend on the smallest singular value of the involved Fourier matrices $\boldsymbol{A}(I_N, \Lambda(\boldsymbol{r}, M))$ and $\boldsymbol{A}(I_N, \Lambda(\boldsymbol{z}, M))$, respectively. In general, the norm of a fixed function $f \in \mathcal{A}_\omega(\mathbb{T}^d)$ in the space $\mathcal{A}_\omega(\mathbb{T}^d)$ is monotone in ω, i.e., the larger ω the larger the norm of the function f in $\mathcal{A}_\omega(\mathbb{T}^d)$.

For our numerical examples, we do not choose the weight function ω best possible with respect to the smoothness of our test functions f, since we have to expect large norms of f in the corresponding function spaces $\mathcal{A}_\omega(\mathbb{T}^d)$ and, thus, we cannot expect adequate error estimates for numerical manageable problem sizes, i.e., reasonable cardinalities of the frequency index sets I. For that reason, we consider weight functions ω that yield meaningful error estimates already for relatively small values of N. The chosen weight functions ω are somehow a tradeoff between small norms of f on the one hand and a suitable decay of the error estimates with respect to N on the other. In most of our examples, we exploit the smoothness of the test functions, i.e., the decay of the Fourier coefficients of the test functions, with the exception of (almost) one order of smoothness in order to give theoretical error bounds of practical usefulness.

We would like to stress the fact that all of our test functions in this chapter are functions that vary considerably, and do not tend to zero for growing dimension d. Specifically, the range of our functions do not reduce for growing dimensions d. Quite the contrary, the ranges expand for the polynomial test function, cf. Sections 5.1.1 and 5.2.1, and mildly expand for the periodic test function, cf. Section 5.1.2, if the dimension d increases.

We compute approximations of different test functions in Section 5.1 and demonstrate that the weights $\boldsymbol{\gamma}$ used to define weighted frequency index sets, cf. Section 2.3, are of particular interest and may cause more or less sparse and suitable frequency index sets I in different dimensions.

In Section 5.2, we discuss the application of trigonometric spectral methods on Poisson's equation in arbitrary dimensions d. We stress the fact that the presented methods can also be applied to more general partial differential equations as described in [LH03].

Moreover, we illustrate a usual approach to treat the approximation problem for non-periodic functions using FFT methods in Section 5.3. Similar approaches have already been studied in the field of numerical integration in order to apply suitable cubature rules for periodic functions to non-periodic functions, cf. [Hic02, CDLP07, DNP14].

5.1 Approximation of Periodic Functions

In this section, we will demonstrate the outstanding properties of the approximation methods specified in Chapters 3 and 4. We approximate functions from specific function spaces $\mathcal{A}_\omega(\mathbb{T}^d)$ by approximated Fourier partial sums and compare the theoretical findings to the numerical results.

The first example is a tensor product of a ten times continuously differentiable one-dimensional test function that is polynomial on the torus $\mathbb{T}$. Well adapted frequency index

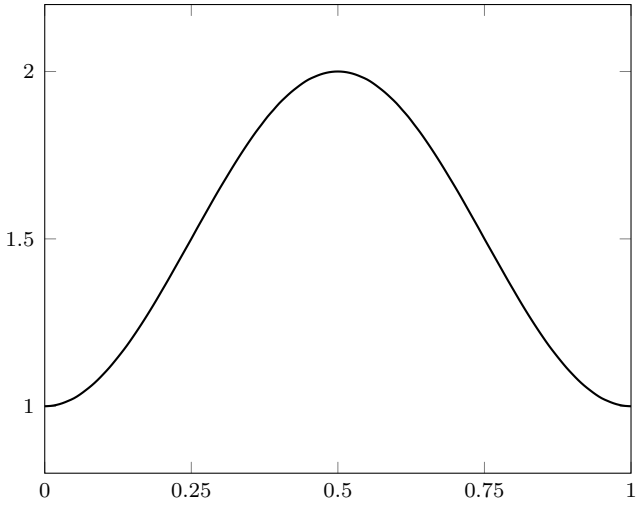

Figure 5.1: One period of the polynomial test function $v(x)$.

sets for the approximation of such a multivariate periodic function are weighted hyperbolic crosses.

We also treat a second test function in this section, which is also a suitable weighted tensor product of a one-dimensional test function. In particular, the one-dimensional function is an infinitely many times continuously differentiable function and, thus, has exponentially decaying Fourier coefficients. The corresponding weighted tensor product of such functions are well approximated using trigonometric polynomials supported on weighted ℓ_p-balls. In our numerical tests, we use d-dimensional ℓ_1-balls up to dimensions d larger than 20.

5.1.1 Polynomial Test Function

As first example we consider the following univariate function

$$v(x) = \begin{cases} \frac{4096}{4146}(2x^{12} - 12x^{11} + 22x^{10} - 33x^8 + 44x^6 - 33x^4 + 10x^2) + 1 & \text{for } x \in [0,1], \\ v(x - \lfloor x \rfloor) & \text{for } x \in \mathbb{R} \setminus [0,1], \end{cases}$$

cf. Figure 5.1 for an illustration, and construct the multivariate function $u_d(\boldsymbol{x}) = \prod_{s=1}^{d} v(x_s)$. We define a suitable weight function $\omega_a^d(\boldsymbol{k}) = \prod_{s=1}^{d} \max(1, a|k_s|^{10})$ with $a = \frac{2122061\pi^{10}}{108972864000} \approx 1.82364$ and calculate the weighted norms of v and u in $\mathcal{A}_{\omega_a^d}(\mathbb{T}^d)$ using the Fourier coefficients of the univariate function v given in Table 5.1

$$\begin{aligned} \|v|\mathcal{A}_{\omega_a^1}(\mathbb{T})\| &= \hat{v}_0 + 2\sum_{k=1}^{\infty} \omega_a^1(k)\hat{v}_k \\ &= \frac{6143}{4095} + 2\sum_{k=1}^{\infty} \frac{2122061(\pi k)^{10}}{108972864000} \frac{159667200}{691(\pi k)^{12}} \\ &= \frac{6143}{4095} + \frac{6142}{4095} = 3 \\ \|u_d|\mathcal{A}_{\omega_a^d}(\mathbb{T}^d)\| &= \prod_{s=1}^{d} \|v|\mathcal{A}_{\omega_a^1}(\mathbb{T})\| = 3^d. \end{aligned}$$

$p(x)$			$\hat{p}_0$					$\hat{p}_k,\ k \neq 0$
$p_2(x)$	$=$	$5(x(x-1))^2$	$\frac{1}{6}$					$-\frac{30}{4(k\pi)^4}$
$p_3(x)$	$=$	$-10(x(x-1))^3$	$\frac{1}{14}$				$-\frac{450}{4(k\pi)^6}$	$+\frac{30}{4(k\pi)^4}$
$p_4(x)$	$=$	$\frac{17}{2}(x(x-1))^4$	$\frac{17}{1260}$			$-\frac{5355}{4(k\pi)^8}$	$+\frac{510}{4(k\pi)^6}$	
$p_5(x)$	$=$	$-4(x(x-1))^5$	$\frac{1}{693}$		$-\frac{56700}{4(k\pi)^{10}}$	$+\frac{6300}{4(k\pi)^8}$	$-\frac{60}{4(k\pi)^6}$	
$p_6(x)$	$=$	$(x(x-1))^6$	$\frac{1}{12012}$	$-\frac{467775}{4(k\pi)^{12}}$	$+\frac{56700}{4(k\pi)^{10}}$	$-\frac{945}{4(k\pi)^8}$		
		$\sum_{j=2}^{6} p_j(x)$	$\frac{691}{2730}$	$-\frac{467775}{4(k\pi)^{12}}$				
$v(x)$	$=$	$1+\frac{4096}{2073}\sum_{j=2}^{6} p_j(x)$	$\frac{6143}{4095}$	$-\frac{159667200}{691(k\pi)^{12}}$				

Table 5.1: Construction of the polynomial test function v and its Fourier coefficients.

Thus, we estimate the $L_2(\mathbb{T}^d)$ and the $L_\infty(\mathbb{T}^d)$ errors by

$$\|u_d - \tilde{S}_{I_K^{d,a}} u_d | L_2(\mathbb{T}^d)\| \leq \|u_d - \tilde{S}_{I_K^{d,a}} u_d | L_\infty(\mathbb{T}^d)\| \leq 2K^{-1} \|u_d | \mathcal{A}_{\omega_a^d}(\mathbb{T}^d)\| \tag{5.2}$$

and

$$\|u_d - \breve{S}_{I_K^{d,a}} u_d | L_2(\mathbb{T}^d)\| \leq C_\delta K^{-1} \|u_d | \mathcal{A}_{\omega_a^d}(\mathbb{T}^d)\|, \tag{5.3}$$

where $\tilde{S}_{I_K^{d,a}} u_d$ and $\breve{S}_{I_K^{d,a}} u_d$ are approximations of u_d based on sampling along a reconstructing rank-1 lattice and a reconstructing generated set for $I_K^{d,a} := \{\boldsymbol{k} \in \mathbb{Z}^d : \omega_a^d(\boldsymbol{k}) \leq K\}$, respectively. The general error estimates can be found in Theorems 3.11 and 4.12. We analyze the weight function ω_a^d and obtain

$$\prod_{s=1}^{d} \max(1, a|k_s|^{10}) \leq K \quad \Leftrightarrow \quad \prod_{s=1}^{d} \max(1, a^{1/10}|k_s|) \leq K^{1/10} =: N.$$

Thus, the corresponding frequency index sets $I_K^{d,a}$ are determined by

$$I_K^{d,a} = \{\boldsymbol{k} \in \mathbb{Z}^d : \omega_a^d(\boldsymbol{k}) \leq K\} = \{\boldsymbol{k} \in \mathbb{Z}^d : \prod_{s=1}^{d} \max(1, a^{1/10} k_s) \leq N\} =: I_{\mathrm{hc},N}^{d,\boldsymbol{\gamma}_a}.$$

Accordingly, $I_K^{d,a} = I_{\mathrm{hc},N}^{d,\boldsymbol{\gamma}_a}$ are just weighted hyperbolic crosses $I_{\mathrm{hc},N}^{d,\boldsymbol{\gamma}_a}$ with weights $\gamma_{a,s} = a^{-1/10} \approx 0.941686$ for $s = 1, \ldots, d$, cf. (2.17).

Hence, the a priori estimates (5.2) and (5.3) of the corresponding accuracy of the approximation of u_d yield

$$\|u_d - \tilde{S}_{I_{\mathrm{hc},N}^{d,\boldsymbol{\gamma}_a}} u_d | L_\infty(\mathbb{T}^d)\| \leq 2 \frac{3^d}{N^{10}} \tag{5.4}$$

and

$$\|u_d - t_d | L_2(\mathbb{T}^d)\| \leq \frac{3^d}{N^{10}} \begin{cases} 2 & \text{for } t_d = \tilde{S}_{I_{\mathrm{hc},N}^{d,\boldsymbol{\gamma}_a}} u_d, \\ C_\delta & \text{for } t_d = \breve{S}_{I_{\mathrm{hc},N}^{d,\boldsymbol{\gamma}_a}} u_d. \end{cases} \tag{5.5}$$

	$N = 4$		$N = 2^{5/2}$		$N = 8$	
d	$3^d/N^{10}$	$\lvert I^{d,\boldsymbol{\gamma}_a}_{\mathrm{hc},N}\rvert$	$3^d/N^{10}$	$\lvert I^{d,\boldsymbol{\gamma}_a}_{\mathrm{hc},N}\rvert$	$3^d/N^{10}$	$\lvert I^{d,\boldsymbol{\gamma}_a}_{\mathrm{hc},N}\rvert$
2	8.583e-06	33	2.682e-07	61	8.382e-09	93
3	2.575e-05	135	8.047e-07	255	2.515e-08	435
4	7.725e-05	513	2.414e-06	1 001	7.544e-08	1 865
5	2.317e-04	1 703	7.242e-06	3 843	2.263e-07	6 823
6	6.952e-04	5 217	2.173e-05	13 125	6.789e-07	22 917
7	2.086e-03	15 655	6.518e-05	40 407	2.037e-06	75 435
8	6.257e-03	47 617	1.955e-04	117 905	6.110e-06	248 785
9	1.877e-02	148 167	5.866e-04	341 307	1.833e-05	823 167
10	5.631e-02	469 409	1.760e-03	1 007 629	5.499e-05	2 729 709

Table 5.2: Cardinalities $\lvert I^{d,\boldsymbol{\gamma}_a}_{\mathrm{hc},N}\rvert$ of frequency index sets of hyperbolic cross type and values of the main term of the theoretical error bounds (5.4) and (5.5), $\boldsymbol{\gamma}_a = \left(\left(\frac{108972864000}{2122061}\right)^{1/10} \frac{1}{\pi}\right)_{s=1}^{d}$.

Table 5.2 specifies the corresponding values of $\frac{3^d}{N^{10}}$ for different $N = 2^2, 2^{5/2}, 2^3$ and presents the cardinalities of the frequency index sets $I_K^{d,a} = I^{d,\boldsymbol{\gamma}_a}_{\mathrm{hc},N}$. Clearly, we obtain a priori error estimates in the spaces $L_\infty(\mathbb{T}^d)$ and $L_2(\mathbb{T}^d)$ by multiplying these values by 2 and C_δ for approximations $\tilde{S}_{I^{d,\boldsymbol{\gamma}_a}_{\mathrm{hc},N}} u_d$ and $\breve{S}_{I^{d,\boldsymbol{\gamma}_a}_{\mathrm{hc},N}} u_d$, respectively.

The last error estimates mainly depends on the norm of u_d in the function space $\mathcal{A}_{\omega_a^d}(\mathbb{T}^d)$ and, thus, on the weight function ω_a^d, that we have chosen in order to compute the norm of the functions u_d. In particular, one can change the value of a and obtain, in some sense, a more suitable weight function. We will choose $b = \frac{2475853\pi^{10}}{54486432000}$ in order to compare the two weights ω_a^d and ω_b^d. At a first glance, the weight function ω_b^d causes a norm of u_d

$$\|u_d|\mathcal{A}_{\omega_b^d}(\mathbb{T}^d)\| = \prod_{s=1}^{d} \|v|\mathcal{A}_{\omega_b^1}(\mathbb{T})\| = 5^d,$$

which is much larger than the norm of u_d in the space $\mathcal{A}_{\omega_a^d}(\mathbb{T}^d)$ and, thus, has counterproductive effects with respect to our approximation estimate

$$\|u_d - \tilde{S}_{I_K^{d,b}} u_d|L_\infty(\mathbb{T}^d)\| \leq 2\frac{5^d}{N^{10}} \tag{5.6}$$

and

$$\|u_d - t_d|L_2(\mathbb{T}^d)\| \leq \frac{5^d}{N^{10}} \begin{cases} 2 & \text{for } t_d = \tilde{S}_{I_K^{d,b}} u_d, \\ C_\delta & \text{for } t_d = \breve{S}_{I_K^{d,b}} u_d, \end{cases} \tag{5.7}$$

where the frequency index set $I_K^{d,b}$ is defined by $I_K^{d,b} := \{\boldsymbol{k} \in \mathbb{Z}^d \colon \omega_b^d(\boldsymbol{k}) = \prod_{s=1}^{d} \max(1, b|k_s|) \leq K\}$ and $\tilde{S}_{I_K^{d,b}} u_d$ and $\breve{S}_{I_K^{d,b}} u_d$ are determined from samples of related reconstructing rank-1 lattices and related reconstructing generated sets, respectively. Only on a second glance, we obtain that the cardinalities of the frequency index sets $I_K^{d,b}$ are much

	$N = 4$		$N = 2^{5/2}$		$N = 8$	
d	$5^d/N^{10}$	$\lvert I_{\mathrm{hc},N}^{d,\boldsymbol{\gamma}_b}\rvert$	$5^d/N^{10}$	$\lvert I_{\mathrm{hc},N}^{d,\boldsymbol{\gamma}_b}\rvert$	$5^d/N^{10}$	$\lvert I_{\mathrm{hc},N}^{d,\boldsymbol{\gamma}_b}\rvert$
2	2.384e-05	25	7.451e-07	49	2.328e-08	65
3	1.192e-04	87	3.725e-06	177	1.164e-07	285
4	5.960e-04	305	1.863e-05	593	5.821e-07	1 105
5	2.980e-03	903	9.313e-05	1 833	2.910e-06	3 613
6	1.490e-02	2 313	4.657e-04	5 409	1.455e-05	10 737
7	7.451e-02	5 463	2.328e-03	15 921	7.276e-05	30 285
8	3.725e-01	12 641	1.164e-02	45 921	3.638e-04	83 169
9	1.863e+00	30 087	5.821e-02	125 577	1.819e-03	227 565
10	9.313e+00	74 745	2.910e-01	321 489	9.095e-03	623 329

Table 5.3: Cardinalities $\lvert I_{\mathrm{hc},N}^{d,\boldsymbol{\gamma}_b}\rvert$ of frequency index sets of hyperbolic cross type and values of the main term of the theoretical error bounds (5.6) and (5.7), $\boldsymbol{\gamma}_b = \left(\left(\frac{54486432000}{2475853}\right)^{1/10}\frac{1}{\pi}\right)_{s=1}^{d}$.

smaller than those of the frequency index sets $I_K^{d,a}$, at least for smaller dimensions. According to the considerations from above, we get $I_K^{d,b} = I_{\mathrm{hc},N}^{d,\boldsymbol{\gamma}_b}$, where the parameters N and $\boldsymbol{\gamma}_b$ are given by $N = K^{1/10}$ and $\boldsymbol{\gamma}_b = \left(\left(\frac{54486432000}{2475853\pi^10}\right)^{1/10}\right)_{s=1}^{d}$ ($\gamma_{b,s} \approx 0.865180$). Table 5.3 presents the values $\frac{5^d}{N^{10}}$ for different d and $N = 2^2, 2^{5/2}, 2^3$ connected with the cardinalities of the frequency index sets $I_K^{d,b} = I_{\mathrm{hc},N}^{d,\boldsymbol{\gamma}_b}$.

Numerical Example 5.1. For dimensions $d = 1, \ldots, 10$, parameters $N = 2^2$ and $N = 2^{5/2}$, we gave reconstructing rank-1 lattices for the frequency index sets $I_{\mathrm{hc},N}^{d,\boldsymbol{\gamma}_a}$ in Table 3.8. Consequently, we apply our strategy in order to approximate the function $u_d = \prod_{s=1}^{d} v(x_s)$ using a Fourier partial sum $\tilde{S}_{I_{\mathrm{hc},N}^{d,\boldsymbol{\gamma}_a}} u_d(\boldsymbol{x}) = \sum_{\boldsymbol{k}\in I_{\mathrm{hc},2^l}^{d,\boldsymbol{\gamma}_a}} \hat{\tilde{u}}_{d,\boldsymbol{k}} \mathrm{e}^{2\pi\mathrm{i}\boldsymbol{k}\cdot\boldsymbol{x}}$ for different dimensions $d = 2, \ldots, 10$ and hyperbolic crosses of different expansions $N = 2^2, 2^{5/2}$.

The theoretical error bounds can be achieved by multiplying the values contained in Table 5.2 by two. In fact, we determine the $L_2(\mathbb{T}^d)$ errors $\mathrm{err}\left(u_d, \tilde{S}_{I_{\mathrm{hc},N}^{d,\boldsymbol{\gamma}_a}} u_d, L_2(\mathbb{T}^d)\right)$, cf. (5.3), and error bounds $\mathrm{err}\left(u_d, \tilde{S}_{I_{\mathrm{hc},N}^{d,\boldsymbol{\gamma}_a}} u_d, \mathcal{A}(\mathbb{T}^d)\right)$, cf. (5.1), on the $L_\infty(\mathbb{T}^d)$ error as given in Table 5.4. In addition to it, we specified the cardinalities of the corresponding frequency index sets $I_{\mathrm{hc},N}^{d,\boldsymbol{\gamma}_a}$ and the reconstructing rank-1 lattices $\Lambda(\boldsymbol{z}, M, I_{\mathrm{hc},N}^{d,\boldsymbol{\gamma}_a})$.

For comparison, we computed the approximations $\tilde{S}_{I_{\mathrm{hc},N}^{d,\boldsymbol{\gamma}_b}} u_d$, for $d = 1, \ldots, 10$ and $N = 2^{5/2}, 2^3$ and the corresponding $L_2(\mathbb{T}^d)$ errors and the upper bounds on the $L_\infty(\mathbb{T}^d)$ errors. We present these results in Table 5.5.

In general, the errors we computed are much lower than the theoretical error estimates promise. Nevertheless, the upper bounds on the $L_\infty(\mathbb{T}^d)$ errors increase with growing dimension as expected. Specifically, for fixed N, the error bounds multiply by factors near three and five for growing dimension d and approximants $\tilde{S}_{I_{\mathrm{hc},N}^{d,\boldsymbol{\gamma}_a}} u_d$ and $\tilde{S}_{I_{\mathrm{hc},N}^{d,\boldsymbol{\gamma}_b}} u_d$, respectively. In addition, we recognize decreasing errors for growing parameters N. In particular, the errors

Polynomial test function u_d – Rank-1 Lattice Approximation – weights $\boldsymbol{\gamma}_a$								
	$N = 2^2$				$N = 2^{5/2}$			
d	$\lvert I^{d,\boldsymbol{\gamma}_a}_{\mathrm{hc},N}\rvert$	M	$\mathrm{err}_{\mathcal{A}}$	err_2	$\lvert I^{d,\boldsymbol{\gamma}_a}_{\mathrm{hc},N}\rvert$	M	$\mathrm{err}_{\mathcal{A}}$	err_2
2	33	38	2.569e-07	3.425e-08	61	73	2.344e-09	6.664e-08
3	135	186	7.940e-07	6.000e-08	255	449	8.429e-09	1.460e-07
4	513	875	2.114e-06	3.991e-07	1 001	2 497	2.785e-08	4.539e-07
5	1 703	4 037	5.455e-06	2.665e-07	3 843	11 144	9.082e-08	9.791e-10
6	5 217	17 060	1.614e-05	3.546e-06	13 125	45 393	2.901e-07	3.568e-06
7	15 655	61 334	4.726e-05	1.023e-05	40 407	218 084	9.606e-07	1.017e-05
8	47 617	238 682	1.393e-04	1.398e-05	117 905	916 888	3.325e-06	5.363e-06
9	148 167	1 001 977	4.132e-04	1.676e-05	341 307	3 979 598	1.154e-05	1.533e-05
10	469 409	3 458 502	1.176e-03	3.035e-05	1 007 629	17 436 325	3.870e-05	2.827e-05

Table 5.4: Cardinalities $\lvert I^{d,\boldsymbol{\gamma}_a}_{\mathrm{hc},N}\rvert$ of frequency index sets of hyperbolic cross type, lattice sizes $M = \lvert\Lambda(\boldsymbol{z}, M, I^{d,\boldsymbol{\gamma}_a}_{\mathrm{hc},N})\rvert$ of corresponding reconstructing rank-1 lattices, $L_2(\mathbb{T}^d)$ errors $\mathrm{err}_2 = \mathrm{err}\left(u_d, \tilde{S}_{I^{d,\boldsymbol{\gamma}_a}_{\mathrm{hc},N}} u_d, L_2(\mathbb{T}^d)\right)$ and upper bounds $\mathrm{err}_{\mathcal{A}} = \mathrm{err}\left(u_d, \tilde{S}_{I^{d,\boldsymbol{\gamma}_a}_{\mathrm{hc},N}} u_d, \mathcal{A}(\mathbb{T}^d)\right)$ on the $L_\infty(\mathbb{T}^d)$ errors of the approximations $\tilde{S}_{I^{d,\boldsymbol{\gamma}_a}_{\mathrm{hc},N}} u_d$ of u_d, $\boldsymbol{\gamma}_a = \left(\left(\frac{108972864000}{2122061}\right)^{1/10} \frac{1}{\pi}\right)_{s=1}^{d}$.

Polynomial test function u_d – Rank-1 Lattice Approximation – weights $\boldsymbol{\gamma}_b$								
	$N = 2^{5/2}$				$N = 2^3$			
d	$\lvert I^{d,\boldsymbol{\gamma}_b}_{\mathrm{hc},N}\rvert$	M	$\mathrm{err}_{\mathcal{A}}$	err_2	$\lvert I^{d,\boldsymbol{\gamma}_b}_{\mathrm{hc},N}\rvert$	M	$\mathrm{err}_{\mathcal{A}}$	err_2
2	49	58	1.697e-08	6.657e-08	65	90	8.543e-10	6.664e-08
3	177	264	9.656e-08	1.459e-07	285	572	3.732e-09	1.460e-07
4	593	1 384	4.373e-07	4.538e-07	1 105	2 200	1.374e-08	4.539e-07
5	1 833	5 417	1.916e-06	1.292e-08	3 613	11 749	7.459e-08	3.576e-10
6	5 409	18 711	8.125e-06	3.568e-06	10 737	43 794	4.222e-07	3.568e-06
7	15 921	72 959	3.142e-05	1.017e-05	30 285	159 381	2.092e-06	1.017e-05
8	45 921	267 176	1.195e-04	1.389e-05	83 169	644 650	9.231e-06	1.389e-05
9	125 577	971 228	4.682e-04	2.207e-05	227 565	2 511 491	3.713e-05	2.145e-05
10	321 489	3 372 316	1.923e-03	3.441e-05	623 329	8 324 021	1.398e-04	3.482e-05

Table 5.5: Cardinalities $\lvert I^{d,\boldsymbol{\gamma}_b}_{\mathrm{hc},N}\rvert$ of frequency index sets of hyperbolic cross type, lattice sizes $\lvert\Lambda(\boldsymbol{z}, M, I^{d,\boldsymbol{\gamma}_b}_{\mathrm{hc},N})\rvert$ of corresponding reconstructing rank-1 lattices, $L_2(\mathbb{T}^d)$ errors $\mathrm{err}_2 = \mathrm{err}\left(u_d, \tilde{S}_{I^{d,\boldsymbol{\gamma}_b}_{\mathrm{hc},N}} u_d, L_2(\mathbb{T}^d)\right)$ and upper bounds $\mathrm{err}_{\mathcal{A}} = \mathrm{err}\left(u_d, \tilde{S}_{I^{d,\boldsymbol{\gamma}_b}_{\mathrm{hc},N}} u_d, \mathcal{A}(\mathbb{T}^d)\right)$ on the $L_\infty(\mathbb{T}^d)$ errors of approximations $\tilde{S}_{I^{d,\boldsymbol{\gamma}_b}_{\mathrm{hc},N}} u_d$ of u_d, $\boldsymbol{\gamma}_b = \left(\left(\frac{54486432000}{2475853}\right)^{1/10} \frac{1}{\pi}\right)_{s=1}^{d}$.

of the approximants $\tilde{S}_{I^{d,\boldsymbol{\gamma}_a}_{\mathrm{hc},N}} u_d$ decrease by factors near $1/\sqrt{2}^{10} = 1/32$. The approximants

Polynomial test function u_d – Rank-1 Lattice Interpolation – weights $\boldsymbol{\gamma}_a$								
	$N = 2^2$				$N = 2^{5/2}$			
d	$\lvert\tilde{I}^{d,\boldsymbol{\gamma}_a}_{\mathrm{hc},N}\rvert$	M	$\mathrm{err}_{\mathcal{A}}$	err_2	$\lvert\tilde{I}^{d,\boldsymbol{\gamma}_a}_{\mathrm{hc},N}\rvert$	M	$\mathrm{err}_{\mathcal{A}}$	err_2
2	38	38	2.500e-07	1.769e-08	73	73	2.173e-09	7.300e-08
3	186	186	7.214e-07	8.429e-08	449	449	6.681e-09	1.577e-07
4	875	875	1.556e-06	4.373e-07	2 497	2 497	1.409e-08	4.805e-07
5	4 037	4 037	3.433e-06	2.707e-07	11 144	11 144	3.423e-08	1.686e-07
6	17 060	17 060	9.064e-06	3.573e-06	45 393	45 393	8.033e-08	3.592e-06
7	61 334	61 334	2.065e-05	1.040e-05	218 084	218 084	1.701e-07	1.036e-05
8	238 682	238 682	3.950e-05	2.613e-06	916 888	916 888	3.498e-07	1.409e-05
9	1 001 977	1 001 977	9.564e-05	7.341e-05	3 979 598	3 979 598	7.371e-07	7.526e-05
10	3 458 502	3 458 502	1.891e-04	8.764e-05	17 436 325	17 436 325	1.509e-06	8.244e-05

Table 5.6: Cardinalities $\lvert\tilde{I}^{d,\boldsymbol{\gamma}_a}_{\mathrm{hc},N}\rvert$ of interpolating frequency index sets of hyperbolic cross type, lattice sizes $\lvert\Lambda(\boldsymbol{z}, M, \tilde{I}^{d,\boldsymbol{\gamma}_a}_{\mathrm{hc},N})\rvert$ of corresponding reconstructing rank-1 lattices, $L_2(\mathbb{T}^d)$ errors $\mathrm{err}_2 = \mathrm{err}\left(u_d, \tilde{S}_{\tilde{I}^{d,\boldsymbol{\gamma}_a}_{\mathrm{hc},N}} u_d, L_2(\mathbb{T}^d)\right)$ and upper bounds $\mathrm{err}_{\mathcal{A}} = \mathrm{err}\left(u_d, \tilde{S}_{\tilde{I}^{d,\boldsymbol{\gamma}_a}_{\mathrm{hc},N}} u_d, \mathcal{A}(\mathbb{T}^d)\right)$ on the $L_\infty(\mathbb{T}^d)$ errors of approximations $\tilde{S}_{\tilde{I}^{d,\boldsymbol{\gamma}_a}_{\mathrm{hc},N}} u_d$ of u_d, $\boldsymbol{\gamma}_a = \left(\left(\frac{108972864000}{2122061}\right)^{1/10} \frac{1}{\pi}\right)_{s=1}^{d}$.

$\tilde{S}_{I^{d,\boldsymbol{\gamma}_b}_{\mathrm{hc},N}} u_d$ do not reach the same error reduction for increasing N, in particular for larger dimensions d. The $L_2(\mathbb{T}^d)$ errors of all the approximants suffers from rounding errors and only indicate a rough trend. We observe increasing $L_2(\mathbb{T}^d)$ errors for growing dimensions d. □

Numerical Example 5.2. Furthermore, we interpolated the function u_d, cf. Section 3.5, using the same reconstructing rank-1 lattices as used for the computations in Tables 5.4 and 5.5. To this end, we applied Algorithm 3.6 in order to determine the frequency index sets $\tilde{I}^{d,\boldsymbol{\gamma}_a}_{\mathrm{hc},N} \supset I^{d,\boldsymbol{\gamma}_a}_{\mathrm{hc},N}$ and $\tilde{I}^{d,\boldsymbol{\gamma}_b}_{\mathrm{hc},N} \supset I^{d,\boldsymbol{\gamma}_b}_{\mathrm{hc},N}$. The corresponding approximation errors are given in Tables 5.6 and 5.7.

Naturally, the interpolation errors are not greater than the approximation errors. In general, we observe decreased interpolation errors compared to the approximation errors. Particularly for frequency index sets $I^{d,\boldsymbol{\gamma}_a}_{\mathrm{hc},N}$ and $I^{d,\boldsymbol{\gamma}_b}_{\mathrm{hc},N}$ that have reconstructing rank-1 lattices that imply a large oversampling factor, the interpolating frequency index sets $\tilde{I}^{d,\boldsymbol{\gamma}_a}_{\mathrm{hc},N}$ and $\tilde{I}^{d,\boldsymbol{\gamma}_b}_{\mathrm{hc},N}$ contains a lot of additional frequency indices. The corresponding frequencies of u_d are not significantly large but the huge amount of additional approximated frequencies significantly improves the upper bounds on the $L_\infty(\mathbb{T}^d)$ errors. Due to the fact that the number of rounding errors also increases with higher cardinalities of the interpolating frequency index sets during the calculation of the $L_2(\mathbb{T}^d)$ error, we observe even higher $L_2(\mathbb{T}^d)$ errors for interpolation against the expectations. □

Numerical Example 5.3. In addition to the rank-1 lattice approximations, we also computed approximations of the functions u_d from samples along reconstructing generated sets for appropriate frequency index sets. The resulting approximation errors are given in Tables 5.8 and 5.9. We observe error estimates for the $L_\infty(\mathbb{T}^d)$ errors that are very close to those

Polynomial test function u_d – Rank-1 Lattice Interpolation – weights $\boldsymbol{\gamma}_b$								
	$N = 2^{5/2}$				$N = 2^3$			
d	$\lvert\tilde{I}^{d,\boldsymbol{\gamma}_b}_{\mathrm{hc},N}\rvert$	M	$\mathrm{err}_{\mathcal{A}}$	err_2	$\lvert\tilde{I}^{d,\boldsymbol{\gamma}_b}_{\mathrm{hc},N}\rvert$	M	$\mathrm{err}_{\mathcal{A}}$	err_2
2	58	58	1.690e-08	7.293e-08	90	90	5.710e-10	7.300e-08
3	264	264	6.073e-08	1.576e-07	572	572	1.648e-09	1.577e-07
4	1 384	1 384	1.807e-07	4.804e-07	2 200	2 200	4.587e-09	4.805e-07
5	5 417	5 417	4.379e-07	1.693e-07	11 749	11 749	1.187e-08	1.686e-07
6	18 711	18 711	1.376e-06	3.592e-06	43 794	43 794	4.316e-08	3.592e-06
7	72 959	72 959	3.128e-06	1.036e-05	159 381	159 381	1.325e-07	6.616e-06
8	267 176	267 176	1.216e-05	1.272e-05	644 650	644 650	3.587e-07	3.785e-06
9	971 228	971 228	3.124e-05	4.670e-05	2 511 491	2 511 491	1.194e-06	7.309e-05
10	3 372 316	3 372 316	7.618e-05	1.081e-04	8 324 021	8 324 021	3.487e-06	8.348e-05

Table 5.7: Cardinalities $\lvert\tilde{I}^{d,\boldsymbol{\gamma}_b}_{\mathrm{hc},N}\rvert$ of interpolating frequency index sets of hyperbolic cross type, reconstructing rank-1 lattice sizes $\lvert\Lambda(\boldsymbol{z}, M, I^{d,\boldsymbol{\gamma}_b}_{\mathrm{hc},N})\rvert$, $L_2(\mathbb{T}^d)$ errors $\mathrm{err}_2 = \mathrm{err}\left(u_d, \tilde{S}_{\tilde{I}^{d,\boldsymbol{\gamma}_b}_{\mathrm{hc},N}} u_d, L_2(\mathbb{T}^d)\right)$ and upper bounds $\mathrm{err}_{\mathcal{A}} = \mathrm{err}\left(u_d, \tilde{S}_{\tilde{I}^{d,\boldsymbol{\gamma}_b}_{\mathrm{hc},N}} u_d, \mathcal{A}(\mathbb{T}^d)\right)$ on the $L_\infty(\mathbb{T}^d)$ errors of approximations $\tilde{S}_{\tilde{I}^{d,\boldsymbol{\gamma}_b}_{\mathrm{hc},N}} u_d$ of u_d, $\boldsymbol{\gamma}_b = \left(\left(\frac{54486432000}{2475853}\right)^{1/10} \frac{1}{\pi}\right)_{s=1}^{d}$.

Polynomial test function u_d – Generated Set Approximation – weights $\boldsymbol{\gamma}_a$								
	$N = 2^2$				$N = 2^{5/2}$			
d	$\lvert I^{d,\boldsymbol{\gamma}_a}_{\mathrm{hc},N}\rvert$	M	$\mathrm{err}_{\mathcal{A}}$	err_2	$\lvert I^{d,\boldsymbol{\gamma}_a}_{\mathrm{hc},N}\rvert$	M	$\mathrm{err}_{\mathcal{A}}$	err_2
2	33	46	2.644e-07	3.295e-08	61	94	2.206e-09	6.664e-08
3	135	234	8.436e-07	5.767e-08	255	592	8.678e-09	1.460e-07
4	513	1 176	2.157e-06	4.062e-07	1 001	3 590	3.249e-08	4.539e-07
5	1 703	7 295	5.962e-06	2.651e-07	3 843	21 324	1.018e-07	5.766e-10
6	5 217	40 720	1.476e-05	3.563e-06	13 125	114 698	3.167e-07	3.568e-06
7	15 655	177 258	4.540e-05	1.021e-05	40 407	456 920	1.056e-06	1.017e-05
8	47 617	719 716	1.370e-04	1.395e-05	117 905	2 657 399	3.562e-06	5.363e-06
9	148 167	4 138 354	4.110e-04	1.671e-05	341 307	13 930 955	1.294e-05	1.533e-05
10	469 409	16 250 377	1.196e-03	3.041e-05	1 007 629	61 963 186	5.243e-05	2.827e-05

Table 5.8: Cardinalities $\lvert I^{d,\boldsymbol{\gamma}_a}_{\mathrm{hc},N}\rvert$ of frequency index sets of hyperbolic cross type, generated set sizes $M = \lvert\Lambda(\boldsymbol{r}, M, I^{d,\boldsymbol{\gamma}_a}_{\mathrm{hc},N})\rvert$ of corresponding reconstructing generated sets, $L_2(\mathbb{T}^d)$ errors $\mathrm{err}_2 = \mathrm{err}\left(u_d, \tilde{S}_{I^{d,\boldsymbol{\gamma}_a}_{\mathrm{hc},N}} u_d, L_2(\mathbb{T}^d)\right)$ and upper bounds $\mathrm{err}_{\mathcal{A}} = \mathrm{err}\left(u_d, \breve{S}_{I^{d,\boldsymbol{\gamma}_a}_{\mathrm{hc},N}} u_d, \mathcal{A}(\mathbb{T}^d)\right)$ on the $L_\infty(\mathbb{T}^d)$ error of approximations $\breve{S}_{I^{d,\boldsymbol{\gamma}_a}_{\mathrm{hc},N}} u_d$ of u_d, $\boldsymbol{\gamma}_a = \left(\left(\frac{108972864000}{2122061}\right)^{1/10} \frac{1}{\pi}\right)_{s=1}^{d}$.

for the rank-1 lattice approximations, cf. Tables 5.4 and 5.5. Note, that the error bounds for the generated set approximation approach are proved for the $L_2(\mathbb{T}^d)$ error only. The $L_2(\mathbb{T}^d)$ errors have almost the same values as the corresponding errors that occurs by computing the rank-1 lattice approximations.

Polynomial test function u_d – Generated Set Approximation – weights $\boldsymbol{\gamma}_b$								
	$N = 2^{5/2}$				$N = 2^3$			
d	$\lvert I_{\mathrm{hc},N}^{d,\boldsymbol{\gamma}_b}\rvert$	M	$\mathrm{err}_{\mathcal{A}}$	err_2	$\lvert I_{\mathrm{hc},N}^{d,\boldsymbol{\gamma}_b}\rvert$	M	$\mathrm{err}_{\mathcal{A}}$	err_2
2	49	72	1.758e-08	6.657e-08	65	105	1.122e-09	6.664e-08
3	177	377	1.088e-07	1.459e-07	285	609	4.707e-09	1.460e-07
4	593	1 868	4.839e-07	4.539e-07	1 105	4 198	1.571e-08	4.539e-07
5	1 833	8 737	2.176e-06	1.356e-08	3 613	15 977	8.826e-08	4.899e-10
6	5 409	38 557	9.021e-06	3.568e-06	10 737	102 710	4.683e-07	3.568e-06
7	15 921	155 847	3.447e-05	1.017e-05	30 285	428 188	2.207e-06	1.017e-05
8	45 921	796 317	1.248e-04	1.389e-05	83 169	1 910 752	9.672e-06	1.389e-05
9	125 577	3 242 942	4.845e-04	2.769e-05	227 565	8 707 707	3.887e-05	2.728e-05
10	321 489	13 073 944	1.979e-03	3.672e-05	623 329	35 617 319	1.459e-04	3.953e-05

Table 5.9: Cardinalities $\lvert I_{\mathrm{hc},N}^{d,\boldsymbol{\gamma}_b}\rvert$ of frequency index sets of hyperbolic cross type, generated set sizes $\lvert\Lambda(\boldsymbol{r}, M, I_{\mathrm{hc},N}^{d,\boldsymbol{\gamma}_b})\rvert$ of corresponding reconstructing generated sets, $L_2(\mathbb{T}^d)$ errors $\mathrm{err}_2 = \mathrm{err}\left(u_d, \breve{S}_{I_{\mathrm{hc},N}^{d,\boldsymbol{\gamma}_b}} u_d, L_2(\mathbb{T}^d)\right)$ and upper bounds $\mathrm{err}_{\mathcal{A}} = \mathrm{err}\left(u_d, \breve{S}_{I_{\mathrm{hc},N}^{d,\boldsymbol{\gamma}_b}} u_d, \mathcal{A}(\mathbb{T}^d)\right)$ on the $L_\infty(\mathbb{T}^d)$ errors of approximations $\breve{S}_{I_{\mathrm{hc},N}^{d,\boldsymbol{\gamma}_b}} u_d$ of u_d, $\boldsymbol{\gamma}_b = \left(\left(\frac{54486432000}{2475853}\right)^{1/10} \frac{1}{\pi}\right)_{s=1}^{d}$.

We stress the fact that we need more samples in order to guarantee the stable computation of approximations that are based on the generated set sampling compared to the rank-1 lattice approximations. However, our specific examples need not more than five times as many samples for the generated set sampling as needed for the rank-1 lattice sampling. □

Numerical Example 5.4. Finally, we compare the $\mathcal{A}(\mathbb{T}^d)$ errors depending on the frequency index sets $I_{\mathrm{hc},N}^{d,\boldsymbol{\gamma}_a}$ and $I_{\mathrm{hc},N}^{d,\boldsymbol{\gamma}_b}$. To this end, we consider fixed dimension d and compare the approximation errors in relation to the cardinality of the frequency index sets. Thus, we compare the errors of the approximations $\tilde{S}_{I_{\mathrm{hc},N}^{d,\boldsymbol{\gamma}_a}} u_d$ (or $\tilde{S}_{\tilde{I}_{\mathrm{hc},N}^{d,\boldsymbol{\gamma}_a}} u_d$, $\breve{S}_{I_{\mathrm{hc},N}^{d,\boldsymbol{\gamma}_a}} u_d$) to those of $\tilde{S}_{I_{\mathrm{hc},\sqrt{2}N}^{d,\boldsymbol{\gamma}_b}} u_d$ (or $\tilde{S}_{\tilde{I}_{\mathrm{hc},\sqrt{2}N}^{d,\boldsymbol{\gamma}_b}} u_d$, $\breve{S}_{I_{\mathrm{hc},\sqrt{2}N}^{d,\boldsymbol{\gamma}_b}} u_d$) for fixed d and $N = 4, 2^{5/2}$. Generally, we observe smaller errors for the approximating trigonometric polynomials supported on the frequency index sets $I_{\mathrm{hc},\sqrt{2}N}^{d,\boldsymbol{\gamma}_b}$ than for those supported on $I_{\mathrm{hc},N}^{d,\boldsymbol{\gamma}_a}$ for lower dimensions d. For larger dimensions, i.e. $d = 10$, we recognize the contrary. The differences of the errors are mainly caused by the weight functions ω_a^d and ω_b^d. We observe that the frequency index sets $I_{\mathrm{hc},N}^{d,\boldsymbol{\gamma}_a}$ and $I_{\mathrm{hc},\sqrt{2}N}^{d,\boldsymbol{\gamma}_b}$ do not differ widely. In particular, the weight function ω_a^d picks up some more important mixed frequency indices, in the corresponding frequency index sets $I_{\mathrm{hc},N}^{d,\boldsymbol{\gamma}_a}$ in higher dimensions, whereas the weight ω_b^d somehow picks up more frequency indices $\boldsymbol{k}$ in $I_{\mathrm{hc},\sqrt{2}N}^{d,\boldsymbol{\gamma}_b}$ that have a lower mixed order, i.e., a lot of components of $\boldsymbol{k}$ are zero in higher dimensions. The frequency index sets determined by the weight function ω_a^d seems to be more suitable in order to approximate our test function u_d for higher dimensions d. This observation indicates that our polynomial test function u_d requires some kind of a minimum thickness of mixed frequencies in order to get suitable approximating trigonometric polynomials. □

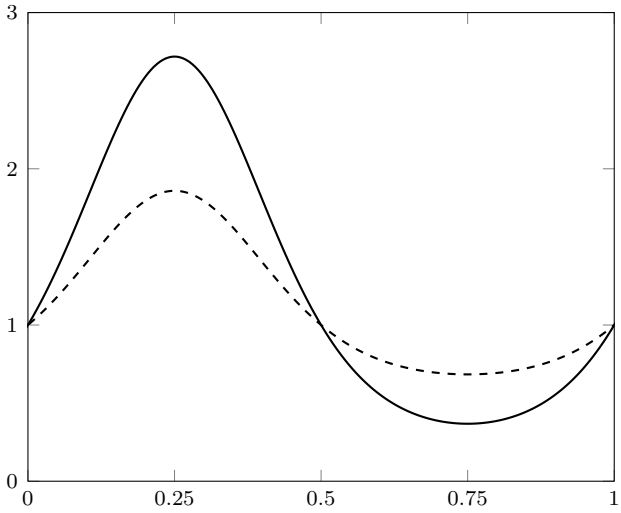

Figure 5.2: The periodic test functions v_η, cf. (5.8), for $\eta = 1$ (solid) and $\eta = 1/2$ (dashed).

5.1.2 Periodic Test Function

Based on the periodic test function used by H. Munthe-Kaas and T. Sørevik, cf. [MS12, Sec. 4, Test function 2], we consider the one-dimensional function

$$v_\eta(x) = 1 + \eta(\mathrm{e}^{\sin(2\pi x)} - 1), \tag{5.8}$$

where $\eta \in (0, 1]$ indicates in some sense the variation of the function v_η, cf. Figure 5.2. We construct the multivariate periodic test functions $f_d^{\boldsymbol{\eta}}$ by tensor products of v_{η_s}, $s = 1, \dots, d$,

$$f_d^{\boldsymbol{\eta}}(\boldsymbol{x}) = \prod_{s=1}^{d} v_{\eta_s}(x_s), \tag{5.9}$$

where $\boldsymbol{\eta} \in (0, 1]^d$ is a real valued vector and its components η_s, $s = 1, \dots, d$, somehow specify the importance of the sth variable.

In addition, we define suitable d-dimensional weight functions

$$\omega_q^d(\boldsymbol{k}) = \prod_{s=1}^{d} \omega_{q+s}(k_s) = \prod_{s=1}^{d} \mathrm{e}^{(10/9)^{q+s}|k_s|} = \mathrm{e}^{(10/9)^{q+1}\sum_{s=1}^{d}(10/9)^{s-1}|k_s|}$$

where the one-dimensional weight function ω_q is given by $\omega_q(k) := \mathrm{e}^{(10/9)^q|k|}$. Due to our approximation results in the Theorems 3.11 and 4.12, we estimate

$$\|f_d^{\boldsymbol{\eta}} - \tilde{S}_{I_K^{q,d}} f_d^{\boldsymbol{\eta}} | L_\infty(\mathbb{T}^d)\| \le 2K^{-1} \|f_d^{\boldsymbol{\eta}} | \mathcal{A}_{\omega_q^d}(\mathbb{T}^d)\| \tag{5.10}$$

$$\|f_d^{\boldsymbol{\eta}} - t_d | L_2(\mathbb{T}^d)\| \le K^{-1} \|f_d^{\boldsymbol{\eta}} | \mathcal{A}_{\omega_q^d}(\mathbb{T}^d)\| \begin{cases} 2 & \text{for } t_d = \tilde{S}_{I_K^{q,d}} f_d^{\boldsymbol{\eta}}, \\ C_\delta & \text{for } t_d = \check{S}_{I_K^{q,d}} f_d^{\boldsymbol{\eta}}, \end{cases} \tag{5.11}$$

where the frequency index set $I_K^{q,d}$ is given by

$$I_K^{q,d} := \{\boldsymbol{k} \in \mathbb{Z}^d \colon \omega_q^d(\boldsymbol{k}) \le K\} = \{\boldsymbol{k} \in \mathbb{Z}^d \colon (10/9)^{q+1} \sum_{s=1}^{d} (10/9)^{s-1}|k_s| \le \log K\}.$$

d	1	3	6	9	12
$\|f_d^{\boldsymbol{\eta}}\|\mathcal{A}_{\omega_0^d}(\mathbb{T}^d)\|$	9.099e+00	2.063e+02	6.583e+03	2.755e+06	1.038e+17
$\|f_d^{\boldsymbol{\eta}}\|\mathcal{A}_{\omega_{-5}^d}(\mathbb{T}^d)\|$	4.863e+00	2.956e+01	9.327e+01	1.704e+02	3.710e+02
$\|f_d^{\boldsymbol{\eta}}\|\mathcal{A}_{\omega_{-10}^d}(\mathbb{T}^d)\|$	3.692e+00	1.404e+01	2.758e+01	3.468e+01	3.907e+01
$\|f_d^{\boldsymbol{\eta}}\|\mathcal{A}_{\omega_{-15}^d}(\mathbb{T}^d)\|$	3.220e+00	9.942e+00	1.659e+01	1.920e+01	2.034e+01
d	15	18	21	22	23
$\|f_d^{\boldsymbol{\eta}}\|\mathcal{A}_{\omega_0^d}(\mathbb{T}^d)\|$	6.892e+65	3.818e+243	6.075e+623	1.079e+808	3.093e+1026
$\|f_d^{\boldsymbol{\eta}}\|\mathcal{A}_{\omega_{-5}^d}(\mathbb{T}^d)\|$	5.198e+04	1.553e+20	1.538e+99	1.583e+157	1.888e+235
$\|f_d^{\boldsymbol{\eta}}\|\mathcal{A}_{\omega_{-10}^d}(\mathbb{T}^d)\|$	4.364e+01	6.117e+01	7.449e+04	1.140e+09	5.731e+16
$\|f_d^{\boldsymbol{\eta}}\|\mathcal{A}_{\omega_{-15}^d}(\mathbb{T}^d)\|$	2.099e+01	2.152e+01	2.235e+01	2.300e+01	2.456e+01

Table 5.10: Approximated norms of the function $f_d^{\boldsymbol{\eta}}$, $\boldsymbol{\eta} = \left(\left(\frac{7}{s+6}\right)^6\right)_{s\in\mathbb{N}}$, in the space $\mathcal{A}_{\omega_q^d}(\mathbb{T}^d)$ for different dimensions d and parameters $q = 0, -5, -10, -15$.

and $\tilde{S}_{I_K^{q,d}} f_d^{\boldsymbol{\eta}}$ and $\breve{S}_{I_K^{q,d}} f_d^{\boldsymbol{\eta}}$ are approximated Fourier partial sums of $f_d^{\boldsymbol{\eta}}$ that have frequency support $I_K^{q,d}$ and are computed from sampling values along reconstructing rank-1 lattices and reconstructing generated sets for $I_K^{q,d}$, respectively.

We define $N := (10/9)^{-q-1} \log K$ and $\boldsymbol{\gamma} := \left(0.9^{s-1}\right)_{s\in\mathbb{N}}$ and obtain that the frequency index set $I_K^{d,q}$ is in fact a weighted ℓ_1-ball of appropriate size, i.e., $I_K^{d,q} = I_{1,N}^{d,\boldsymbol{\gamma}}$.

Accordingly, the error estimates (5.10) and (5.11) yield error estimates

$$\|f_d^{\boldsymbol{\eta}} - \tilde{S}_{I_{1,N}^{d,\boldsymbol{\gamma}}} f_d^{\boldsymbol{\eta}} | L_\infty(\mathbb{T}^d)\| \leq 2\left(\mathrm{e}^{0.9^{-q-1}}\right)^{-N} \|f_d^{\boldsymbol{\eta}} | \mathcal{A}_{\omega_q^d}(\mathbb{T}^d)\| \tag{5.12}$$

and

$$\|f_d^{\boldsymbol{\eta}} - t_d | L_2(\mathbb{T}^d)\| \leq \left(\mathrm{e}^{0.9^{-q-1}}\right)^{-N} \|f_d^{\boldsymbol{\eta}} | \mathcal{A}_{\omega_q^d}(\mathbb{T}^d)\| \begin{cases} 2 & \text{for } t_d = \tilde{S}_{I_{1,N}^{d,\boldsymbol{\gamma}}} f_d^{\boldsymbol{\eta}}, \\ C_\delta & \text{for } t_d = \breve{S}_{I_{1,N}^{d,\boldsymbol{\gamma}}} f_d^{\boldsymbol{\eta}}, \end{cases} \tag{5.13}$$

that decrease exponentially with growing parameter N.

The weight function ω_q^d, which belongs to the norm $\mathcal{A}_{\omega_q^d}(\mathbb{T}^d)$, is in principle a product of exponential functions, where each factor only depends on one dimension. The corresponding bases are strictly larger than one and increase with growing dimension. The growth of the bases mainly depends on the parameter q. Greater values of q cause larger bases and thus higher smoothness of the functions that belongs to $\mathcal{A}_{\omega_q^d}(\mathbb{T}^d)$.

Once we have fixed the parameter q, we get a second perspective to the weight function ω_q^d. Since the bases $\mathrm{e}^{(10/9)^{q+s}}$ of ω_{q+s} grow with growing dimension s, the space $\mathcal{A}_{\omega_q^d}(\mathbb{T}^d)$ consists of functions that becomes more and more smoother with respect to the variable x_s for increasing s.

Example 5.5. In this example, we fix the vector $\boldsymbol{\eta} = \left(\left(\frac{7}{s+6}\right)^6\right)_{s\in\mathbb{N}}$ and consider the functions $f_d^{\boldsymbol{\eta}}$ for $d = 1, \dots, 23$. In particular, we computed norms of $f_d^{\boldsymbol{\eta}}$ in the space $\mathcal{A}_{\omega_q^d}(\mathbb{T}^d)$ for different $q = 0, -5, -10, -15$ given in Table 5.10. Clearly, since the parameter q is an indicator of the smoothness of the functions that belong to $\mathcal{A}_{\omega_q^d}(\mathbb{T}^d)$, i.e., larger q requires more smoothness, the norms of $f_d^{\boldsymbol{\eta}}$ decreases with decreasing parameter q. On the other hand, we observed the number $\mathrm{e}^{0.9^{-q-1}}$ as the base that mainly affects the theoretical error estimates in (5.12). In particular for the chosen parameters q we obtain

$$\mathrm{e}^{0.9^{-q-1}} \approx \begin{cases} 3.0377 & \text{for } q = 0, \\ 1.9273 & \text{for } q = -5, \\ 1.4732 & \text{for } q = -10, \\ 1.2571 & \text{for } q = -15. \end{cases}$$

Consequently, reducing the parameter q decreases the norms of $f_d^{\boldsymbol{\eta}}$ but also decreases the base $\mathrm{e}^{0.9^{-q-1}}$ such that the base to the exponent $-N$ increases. Accordingly, only suitable tradeoffs concerning the parameters q, N, $\boldsymbol{\eta}$, and the dimension d yield suitable a priori error estimates for the approximation $\tilde{S}_{I_{1,N}^{d,\boldsymbol{\gamma}}} f_d^{\boldsymbol{\eta}}$ of $f_d^{\boldsymbol{\eta}}$.

We consider the norm approximations of $f_d^{\boldsymbol{\eta}}$ given in Table 5.10, fix $N = 10$, and obtain the best error estimates

$$\begin{aligned} \|f_d^{\boldsymbol{\eta}} - \tilde{S}_{I_{1,10}^{d,\boldsymbol{\gamma}}} f_d^{\boldsymbol{\eta}} | L_\infty(\mathbb{T}^d)\| &\le 2 \left(\mathrm{e}^{0.9^{-q-1}}\right)^{-10} \|f_d^{\boldsymbol{\eta}} | \mathcal{A}_{\omega_q^d}(\mathbb{T}^d)\| \\ &\le 2 \begin{cases} 0.0984 & \text{for } d \le 6 \quad (q = 0), \\ 0.2411 & \text{for } d \le 9 \quad (q = -5), \\ 0.9065 & \text{for } d \le 15 \quad (q = -10), \\ 2.2686 & \text{for } d \le 21 \quad (q = -15), \end{cases} \end{aligned} \tag{5.14}$$

for the chosen $q = 0, -5, -10, -15$ a priori. We stress the fact that the ranges of the functions $f_d^{\boldsymbol{\eta}}$, $d = 6, \dots, 23$, contain the interval $[0.196, 9.5]$ and are contained in the interval $[0.1867, 10.81]$. Thus, the error bounds on the $L_\infty(\mathbb{T}^d)$ error given in (5.14) are of less quality for higher dimensions d. We would like to point out that the considerations of this example applied to the error estimates in (5.13) bound the $L_2(\mathbb{T}^d)$ error by similar terms. □

In the following, we interpret concrete numerical tests. Particularly, we fixed the sequence $\boldsymbol{\eta} = \left(\left(\frac{7}{s+6}\right)^6\right)_{s\in\mathbb{N}}$ and computed approximations of the function $f_d^{\boldsymbol{\eta}}$ for dimensions d up to 23.

Numerical Example 5.6. We approximated functions $f_d^{\boldsymbol{\eta}}$ by trigonometric polynomials with frequencies supported on weighted ℓ_1-balls $I_{1,N}^{d,\boldsymbol{\gamma}}$, $N = 4, 6, 8, 10$, $\boldsymbol{\gamma} = \left(0.9^{s-1}\right)_{s\in\mathbb{N}}$ from samples along reconstructing rank-1 lattices $\Lambda(\boldsymbol{z}_{\mathrm{Alg3.8}}, M_{\mathrm{Alg3.8}}, I_{1,N}^{d,\boldsymbol{\gamma}})$. The corresponding $L_2(\mathbb{T}^d)$ errors and upper bounds on the $L_\infty(\mathbb{T}^d)$ errors are presented in Tables 5.11 and 5.12. As expected, we observe an exponential decay in the error with respect to growing N for fixed dimension d. For example, we increased N by two and observe error bounds $\mathrm{err}_{\mathcal{A}} := \mathrm{err}\left(f_d^{\boldsymbol{\eta}}, \tilde{S}_{I_{1,N}^{d,\boldsymbol{\gamma}}} f_d^{\boldsymbol{\eta}}, \mathcal{A}(\mathbb{T}^d)\right)$ that decreases by factors larger than 5,4, and 3 in dimensions $d = 6, 9$, and 15, respectively.

Periodic test function $f_d^{\boldsymbol{\eta}}$ – Rank-1 Lattice Approximation								
	$N = 4$				$N = 6$			
d	$\lvert I_{1,4}^{d,\boldsymbol{\gamma}}\rvert$	M	$\mathrm{err}_{\mathcal{A}}$	err_2	$\lvert I_{1,6}^{d,\boldsymbol{\gamma}}\rvert$	M	$\mathrm{err}_{\mathcal{A}}$	err_2
2	27	31	1.638e−01	2.982e−02	63	71	5.027e−03	8.397e−04
3	65	83	4.925e−01	4.431e−02	227	317	2.812e−02	1.883e−03
4	129	181	8.579e−01	5.051e−02	551	918	1.004e−01	3.679e−03
5	193	313	1.215e+00	5.507e−02	997	1 964	1.933e−01	4.658e−03
6	241	422	1.479e+00	5.727e−02	1 567	3 699	2.797e−01	5.316e−03
7	281	545	1.751e+00	6.027e−02	2 169	6 238	3.525e−01	5.656e−03
8	311	545	1.962e+00	6.300e−02	2 697	7 902	4.122e−01	5.999e−03
9	333	591	2.085e+00	6.359e−02	3 121	9 634	4.655e−01	6.293e−03
10	351	614	2.151e+00	6.351e−02	3 433	9 881	5.121e−01	6.566e−03
11	361	614	2.229e+00	6.406e−02	3 653	11 666	5.454e−01	6.717e−03
12	363	614	2.312e+00	6.670e−02	3 799	11 666	5.768e−01	6.920e−03
13	365	614	2.358e+00	6.731e−02	3 877	11 666	6.032e−01	7.089e−03
14	367	614	2.384e+00	6.729e−02	3 911	11 666	6.255e−01	7.186e−03
15	367	614	2.407e+00	6.735e−02	3 933	11 666	6.429e−01	7.257e−03
16	367	614	2.425e+00	6.740e−02	3 943	11 666	6.573e−01	7.316e−03
17	367	614	2.438e+00	6.743e−02	3 945	11 666	6.713e−01	7.405e−03
18	367	614	2.449e+00	6.745e−02	3 947	11 666	6.820e−01	7.492e−03
19	367	614	2.457e+00	6.747e−02	3 947	11 666	6.907e−01	7.544e−03

Table 5.11: Cardinalities $\lvert I_{1,N}^{d,\boldsymbol{\gamma}}\rvert$ of weighted ℓ_1-balls, lattice sizes $\lvert\Lambda(\boldsymbol{z}, M, I_{1,N}^{d,\boldsymbol{\gamma}})\rvert$ of corresponding reconstructing rank-1 lattices, $L_2(\mathbb{T}^d)$ errors $\mathrm{err}_2 := \mathrm{err}\left(f_d^{\boldsymbol{\eta}}, \tilde{S}_{I_{1,N}^{d,\boldsymbol{\gamma}}} f_d^{\boldsymbol{\eta}}, L_2(\mathbb{T}^d)\right)$ and upper bounds $\mathrm{err}_{\mathcal{A}} := \mathrm{err}\left(f_d^{\boldsymbol{\eta}}, \tilde{S}_{I_{1,N}^{d,\boldsymbol{\gamma}}} f_d^{\boldsymbol{\eta}}, \mathcal{A}(\mathbb{T}^d)\right)$ on the $L_\infty(\mathbb{T}^d)$ errors of approximations $\tilde{S}_{I_{1,N}^{d,\boldsymbol{\gamma}}} f_d^{\boldsymbol{\eta}}$ of $f_d^{\boldsymbol{\eta}}$, cf. (5.9), $\boldsymbol{\eta} = \left(\left(\frac{7}{s+6}\right)^6\right)_{s\in\mathbb{N}}$, $\boldsymbol{\gamma} = \left(0.9^{s-1}\right)_{s=1}^d$.

In particular, we focus on the approximations $\tilde{S}_{I_{1,10}^{d,\boldsymbol{\gamma}}} f_d^{\boldsymbol{\eta}}$ and dimensions $d = 6, 9, 15, 21$ in order to compare the error to the theoretical a priori error bounds given in (5.14). We obtain errors $\mathrm{err}\left(f_d^{\boldsymbol{\eta}}, \tilde{S}_{I_{1,N}^{d,\boldsymbol{\gamma}}} f_d^{\boldsymbol{\eta}}, \mathcal{A}(\mathbb{T}^d)\right)$ that are smaller by factors of 24 to 61 than the theoretical bounds from (5.14). Thus, the theoretical error bounds for different dimensions are in some sense equally close to the practical errors. We would like to mention, that we had to adjust the parameters q to the specific dimensions d, the function $f_d^{\boldsymbol{\eta}}$, and $N = 10$ in order to obtain the theoretical error bounds in (5.14). □

Numerical Example 5.7. We also considered the interpolation problem on the functions $f_d^{\boldsymbol{\eta}}$, i.e., we applied Algorithm 3.6 and constructed interpolating frequency index sets $\tilde{I}_{1,N}^{d,\boldsymbol{\gamma}}$, $N = 4, 6, 8, 10$, $\boldsymbol{\gamma} = \left(0.9^{s-1}\right)_{s\in\mathbb{N}}$, for the reconstructing rank-1 lattices $\Lambda(\boldsymbol{z}_{\mathrm{Alg3.8}}, M_{\mathrm{Alg3.8}}, I_{1,N}^{d,\boldsymbol{\gamma}})$. Some of the used reconstructing rank-1 lattices are given in Table 3.4 and 3.5 for $N = 6, 10$.

We do not present detailed tables of the errors of these interpolations since the corre-

Periodic test function $f_d^{\boldsymbol{\eta}}$ – Rank-1 Lattice Approximation

	$N = 8$				$N = 10$			
d	$\lvert I_{1,8}^{d,\boldsymbol{\gamma}}\rvert$	M	$\mathrm{err}_{\mathcal{A}}$	err_2	$\lvert I_{1,10}^{d,\boldsymbol{\gamma}}\rvert$	M	$\mathrm{err}_{\mathcal{A}}$	err_2
2	115	127	8.420e-05	1.350e-05	183	199	8.956e-07	1.468e-07
3	515	695	1.825e-03	1.347e-04	983	1 326	8.929e-05	6.374e-06
4	1 573	2 627	1.035e-02	2.990e-04	3 741	6 387	7.387e-04	1.729e-05
5	3 691	7 778	2.546e-02	4.245e-04	10 569	24 322	2.741e-03	3.377e-05
6	6 955	18 530	4.370e-02	5.219e-04	23 431	64 015	6.013e-03	4.775e-05
7	11 103	36 547	6.359e-02	6.124e-04	43 081	165 954	9.910e-03	6.213e-05
8	15 525	56 704	8.146e-02	6.953e-04	67 857	358 751	1.458e-02	8.102e-05
9	19 671	84 274	9.870e-02	7.814e-04	94 693	561 453	1.974e-02	1.153e-04
10	23 193	105 214	1.146e-01	8.836e-04	120 251	806 670	2.425e-02	1.400e-04
11	25 969	130 235	1.281e-01	9.738e-04	142 261	1 021 007	2.935e-02	1.766e-04
12	27 909	142 745	1.416e-01	1.102e-03	159 611	1 228 093	3.410e-02	2.296e-04
13	29 201	143 789	1.555e-01	1.311e-03	172 079	1 409 797	3.981e-02	3.304e-04
14	29 997	143 789	1.668e-01	1.434e-03	180 383	1 517 004	4.455e-02	3.583e-04
15	30 443	143 789	1.762e-01	1.544e-03	185 551	1 553 233	4.848e-02	3.838e-04
16	30 665	143 789	1.846e-01	1.607e-03	188 531	1 553 253	5.326e-02	4.904e-04
17	30 767	143 789	1.922e-01	1.646e-03	190 085	1 553 253	5.749e-02	5.878e-04
18	30 801	143 789	2.010e-01	1.706e-03	190 819	1 578 919	6.236e-02	6.572e-04
19	30 815	143 789	2.083e-01	1.749e-03	191 105	1 578 919	6.617e-02	6.875e-04
20	30 817	143 789	2.162e-01	1.847e-03	191 207	1 578 919	7.040e-02	7.245e-04
21	30 817	143 789	2.216e-01	1.926e-03	191 233	1 578 919	7.503e-02	7.588e-04
22	30 817	143 789	2.260e-01	1.987e-03	191 235	1 578 919	8.067e-02	8.520e-04
23	30 817	143 789	2.296e-01	2.035e-03	191 235	1 578 919	8.419e-02	9.230e-04

Table 5.12: Cardinalities $\lvert I_{1,N}^{d,\boldsymbol{\gamma}}\rvert$ of weighted ℓ_1-balls, lattice sizes $\lvert\Lambda(\boldsymbol{z}, M, I_{1,N}^{d,\boldsymbol{\gamma}})\rvert$ of corresponding reconstructing rank-1 lattices, $L_2(\mathbb{T}^d)$ errors $\mathrm{err}_2 := \mathrm{err}\left(f_d^{\boldsymbol{\eta}}, \tilde{S}_{I_{1,N}^{d,\boldsymbol{\gamma}}} f_d^{\boldsymbol{\eta}}, L_2(\mathbb{T}^d)\right)$ and upper bounds $\mathrm{err}_{\mathcal{A}} := \mathrm{err}\left(f_d^{\boldsymbol{\eta}}, \tilde{S}_{I_{1,N}^{d,\boldsymbol{\gamma}}} f_d^{\boldsymbol{\eta}}, \mathcal{A}(\mathbb{T}^d)\right)$ on the $L_\infty(\mathbb{T}^d)$ errors of approximations $\tilde{S}_{I_{1,N}^{d,\boldsymbol{\gamma}}} f_d^{\boldsymbol{\eta}}$ of $f_d^{\boldsymbol{\eta}}$, cf. (5.9), $\boldsymbol{\eta} = \left(\left(\frac{7}{s+6}\right)^6\right)_{s\in\mathbb{N}}$, $\boldsymbol{\gamma} = \left(0.9^{s-1}\right)_{s=1}^d$.

sponding approximation errors $\mathrm{err}\left(f_d^{\boldsymbol{\eta}}, \tilde{S}_{I_{1,N}^{d,\boldsymbol{\gamma}}} f_d^{\boldsymbol{\eta}}, \mathcal{A}(\mathbb{T}^d)\right)$ and $\mathrm{err}\left(f_d^{\boldsymbol{\eta}}, \tilde{S}_{I_{1,N}^{d,\boldsymbol{\gamma}}} f_d^{\boldsymbol{\eta}}, L_2(\mathbb{T}^d)\right)$ are only mildly smaller than those for the approximations given in Tables 5.11 and 5.12. We plotted the upper bounds on the approximation errors $\mathrm{err}\left(f_d^{\boldsymbol{\eta}}, \tilde{S}_{I_{1,N}^{d,\boldsymbol{\gamma}}} f_d^{\boldsymbol{\eta}}, \mathcal{A}(\mathbb{T}^d)\right)$ against the upper bounds on the interpolation errors $\mathrm{err}\left(f_d^{\boldsymbol{\eta}}, \tilde{S}_{\tilde{I}_{1,N}^{d,\boldsymbol{\gamma}}} f_d^{\boldsymbol{\eta}}, \mathcal{A}(\mathbb{T}^d)\right)$ for $N = 4, 6, 8, 10$ in Figure 5.3.

In detail, we observe that the interpolation errors are larger than one third of the approximation errors in Tables 5.11 and 5.12. Moreover, we see that the interpolation errors come closer to the approximation errors with growing dimensions d, in general. The

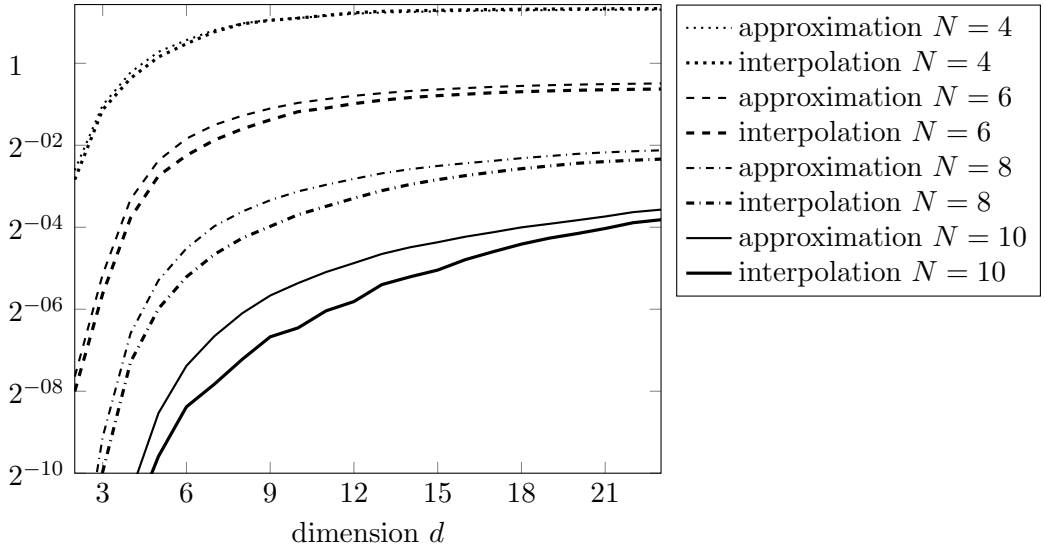

Figure 5.3: Approximation errors $\mathrm{err}\left(f_d^{\boldsymbol{\eta}}, \tilde{S}_{I_{1,N}^{d,\boldsymbol{\gamma}}} f_d^{\boldsymbol{\eta}}, \mathcal{A}(\mathbb{T}^d)\right)$ and $\mathrm{err}\left(f_d^{\boldsymbol{\eta}}, \tilde{S}_{\tilde{I}_{1,N}^{d,\boldsymbol{\gamma}}} f_d^{\boldsymbol{\eta}}, \mathcal{A}(\mathbb{T}^d)\right)$ of approximations and interpolations of the function $f_d^{\boldsymbol{\eta}}$ given in (5.9), $\boldsymbol{\eta} = \left(\left(\frac{7}{s+6}\right)^6\right)$, $N = 4, 6, 8, 10$.

relation of the approximation errors $\mathrm{err}\left(f_d^{\boldsymbol{\eta}}, \tilde{S}_{I_{1,N}^{d,\boldsymbol{\gamma}}} f_d^{\boldsymbol{\eta}}, \mathcal{A}(\mathbb{T}^d)\right)$ and the interpolation errors $\mathrm{err}\left(f_d^{\boldsymbol{\eta}}, \tilde{S}_{\tilde{I}_{1,N}^{d,\boldsymbol{\gamma}}} f_d^{\boldsymbol{\eta}}, \mathcal{A}(\mathbb{T}^d)\right)$ tends to a fixed factor for fixed N and growing dimension d.

This is somehow caused by the finite effective dimension d_{eff} of the frequency index sets $I_{1,N}^{d,\boldsymbol{\gamma}}$, cf. (3.18), for fixed N. In principle, the frequency index sets $I_{1,N}^{d,\boldsymbol{\gamma}}$ do not change by enlarging the dimension $d > d_{\mathrm{eff}}$, i.e. $I_{1,N}^{d,\boldsymbol{\gamma}} = I_{1,N}^{d_{\mathrm{eff}},\boldsymbol{\gamma}} \times \left\{(0)_{s=d_{\mathrm{eff}}+1}^{d}\right\}$. Consequently, the reconstructing rank-1 lattices fulfills $\Lambda(\boldsymbol{z}_{\mathrm{Alg3.8}}, M_{\mathrm{Alg3.8}}, I_{1,N}^{d,\boldsymbol{\gamma}}) = \Lambda(\boldsymbol{z}_{\mathrm{Alg3.8}}, M_{\mathrm{Alg3.8}}, I_{1,N}^{d_{\mathrm{eff}},\boldsymbol{\gamma}}) \times \left\{(0)_{s=d_{\mathrm{eff}}+1}^{d}\right\}$. The effective dimension of the interpolating frequency index set $\tilde{I}_{1,N}^{d,\boldsymbol{\gamma}}$ may differ for different dimensions d that are greater than the effective dimension d_{eff} of the non-interpolating frequency index set $I_{1,N}^{d,\boldsymbol{\gamma}}$. However, for fixed N there exists a number $N' \in \mathbb{R}$ such that $\tilde{I}_{1,N}^{d,\boldsymbol{\gamma}} \subset I_{1,N'}^{d,\boldsymbol{\gamma}}$ for all d and the effective dimension $s_{\mathrm{eff}} := \left\lfloor \frac{\log N'}{\log(10/9)} \right\rfloor + 1$ of $I_{1,N'}^{s,\boldsymbol{\gamma}}$, s large enough, bounds the effective dimension of the interpolating frequency index set $\tilde{I}_{1,N}^{d,\boldsymbol{\gamma}}$ from above. Note, that N' mainly depends on the reconstructing rank-1 lattice for $I_{1,N}^{d_{\mathrm{eff}},\boldsymbol{\gamma}}$ since $\tilde{I}_{1,N}^{d,\boldsymbol{\gamma}}$ depends on this rank-1 lattice.

However, we observe that the frequency index sets $I_{1,N}^{d,\boldsymbol{\gamma}}$ and $\tilde{I}_{1,N}^{d,\boldsymbol{\gamma}}$, $d > s_{\mathrm{eff}}$, contain no element that is nonzero in a component of the sth dimension where $s > s_{\mathrm{eff}}$. Sampling along the reconstructing rank-1 lattices $\Lambda(\boldsymbol{z}_{\mathrm{Alg3.8}}, M_{\mathrm{Alg3.8}}, I_{1,N}^{d,\boldsymbol{\gamma}})$ causes that higher dimensions are sampled only at 0, i.e., we take sampling values $f_d^{\boldsymbol{\eta}}(\boldsymbol{x}_j) = \prod_{s=1}^{d} v_{\eta_s}(x_{j,s}) = \prod_{s=1}^{s_{\mathrm{eff}}} v_{\eta_s}(x_{j,s})$ and thus both, the approximation error and the interpolation error, suffers from a lower effective dimension of the approximation problems. The approximation $\tilde{S}_{I_{1,N}^{d,\boldsymbol{\gamma}}} f_d^{\boldsymbol{\eta}}$ and the interpolation $\tilde{S}_{\tilde{I}_{1,N}^{d,\boldsymbol{\gamma}}} f_d^{\boldsymbol{\eta}}$ do not recognize anything of the higher dimensions and, thus, the approximation

errors for both problems should increase by similar values for growing dimension d from $d = s_{\text{eff}}$ on.

Nevertheless, we obtain relatively small approximation errors since the sequence $\boldsymbol{\eta}$ decreases fast and the variation of the corresponding functions v_{η_s}, $s > s_{\text{eff}}$, is strongly limited. □

5.2 Poisson's Equation in d Dimensions

In this section, we treat Poisson's equation as a representative of elliptic partial differential equations in higher dimensions d. We would like to refer to the paper of H.-J. Bungartz and M. Griebel, cf. [BG99], who suggest to solve Poisson's equation in higher dimensions using a sparse grid approach, and to the book of W. Hackbusch, cf. [Hac12], who uses tensor product approximations—a quite different approach—in order to solve elliptic partial differential equations. Certainly, H. Munthe-Kaas and T. Sørevik presented a rank-1 lattice approach for the numerical treatment of Poisson's equation in [MS12]. We pick up their considerations and solve Poisson's equation on $\mathbb{T}^d$ for different dimensions d. We use periodic boundary conditions, i.e., we consider

$$\Delta u(\boldsymbol{x}) = f(\boldsymbol{x}),\ \boldsymbol{x} \in \mathbb{T}^d, \qquad \text{with } u(\boldsymbol{x}) = u(\boldsymbol{x} + \boldsymbol{l}) \text{ for all } \boldsymbol{x} \in \mathbb{R}^d \text{ and all } \boldsymbol{l} \in \mathbb{Z}^d, \tag{5.15}$$

where the operator Δ is given by $\Delta = \sum_{s=1}^{d} \frac{\partial^2}{\partial x_s^2}$. H. Munthe-Kaas and T. Sørevik used rank-1 lattices found by minimizing different integration errors to solve Poisson's equation in their paper, cf. [MS12]. Now, Algorithms 3.3 and 4.5 offers better adapted methods in order to find suitable sampling sets to solve Poisson's equation in (5.15).

In particular, the strategy to solve partial differential equations that is described in [MS12] is a collocation method, cf. [SB05, Section 7.5] or [STW11, Section 1.2], on rank-1 lattices. D. Li and F. J. Hickernell earlier suggest such an approach in a more general setting, cf. [LH03]. Both papers deal with an interpolation of the right hand side f in (5.15).

In principle, the suggested approach is a numerical solution of a spectral method of Galerkin type, cf. [STW11, Section 1.3] or [SB05, Section 7.5], i.e., one fixes a suitable space of trigonometric polynomials Π_I and calculates an approximate solution of Poisson's equation in the space Π_I.

In detail, we assume $f \in \mathcal{A}(\mathbb{T}^d)$ and calculate

$$\begin{aligned} \hat{f}_{\boldsymbol{k}} :&= \int_{\mathbb{T}^d} f(\boldsymbol{x}) \mathrm{e}^{-2\pi \mathrm{i} \boldsymbol{k}\cdot\boldsymbol{x}} \mathrm{d}x \qquad (5.16)\\ &= \int_{\mathbb{T}^d} \Delta u(\boldsymbol{x}) \mathrm{e}^{-2\pi \mathrm{i} \boldsymbol{k}\cdot\boldsymbol{x}} \mathrm{d}x \\ &= -(2\pi\|\boldsymbol{k}\|_2)^2 \int_{\mathbb{T}^d} \frac{\Delta u(\boldsymbol{x})}{-(2\pi\|\boldsymbol{k}\|_2)^2} \mathrm{e}^{-2\pi \mathrm{i} \boldsymbol{k}\cdot\boldsymbol{x}} \mathrm{d}x = -(2\pi\|\boldsymbol{k}\|_2)^2 \hat{u}_{\boldsymbol{k}} \qquad (5.17) \end{aligned}$$

for all $\boldsymbol{k} \in \mathbb{Z}^d \setminus \{\boldsymbol{0}\}$. In general, we cannot compute all Fourier coefficients $\hat{f}_{\boldsymbol{k}}$, $\boldsymbol{k} \in \mathbb{Z}^d \setminus \{\boldsymbol{0}\}$. Consequently, we are not able to compute the exact solution u of Poisson's equation. In addition, we want to use sampling values of f in order to approximate the Fourier coefficients of f. Thus, we expect some additional errors by the numerical evaluation of the integral in (5.16).

The detailed strategy to compute the solution of Poisson's equation is as follows. We sample f at a sampling set $\mathcal{X}$ and approximate f by a trigonometric polynomial $\tilde{f} \in \Pi_I$,

$\tilde{f}(\boldsymbol{x}) = \sum_{\boldsymbol{k}\in I} \hat{\tilde{f}}_{\boldsymbol{k}} \mathrm{e}^{2\pi \mathrm{i}\boldsymbol{k}\cdot\boldsymbol{x}}$, where the frequency index set I should contain all indices of significant frequencies of f and the approximated Fourier coefficients $\hat{\tilde{f}}_{\boldsymbol{k}}$, $\boldsymbol{k} \in I$, are computed using

$$\boldsymbol{A}^*\boldsymbol{A}\hat{\tilde{\boldsymbol{f}}} = \boldsymbol{A}^*\boldsymbol{f}, \qquad \boldsymbol{A} = \left(\mathrm{e}^{2\pi \mathrm{i}\boldsymbol{k}\cdot\boldsymbol{x}}\right)_{\boldsymbol{x}\in\mathcal{X},\,\boldsymbol{k}\in I}, \; \hat{\tilde{\boldsymbol{f}}} = \left(\hat{\tilde{f}}_{\boldsymbol{k}}\right)_{\boldsymbol{k}\in I}, \; \boldsymbol{f} = (f(\boldsymbol{x}))_{\boldsymbol{x}\in\mathcal{X}}. \tag{5.18}$$

We solve Poisson's equation for this trigonometric polynomial $\tilde{f}$ and achieve a trigonometric polynomial $\tilde{u} \in \Pi_I$ fulfilling $\Delta\tilde{u} = \tilde{f}$. A suitable chosen frequency index set I and a corresponding sampling set $\mathcal{X}$ yield theoretical error bounds guaranteeing that $\tilde{u}$ well approximates u, cf. Theorem 5.8.

We shortly explain how to solve Poisson's equation for trigonometric polynomials $\tilde{u}, \tilde{f} \in \Pi_I$. Poisson's equation reads as follows

$$\begin{aligned}
\Delta\tilde{u}(\boldsymbol{x}) &= \sum_{s=1}^{d} \frac{\partial^2}{\partial x_s^2}\tilde{u}(\boldsymbol{x}) = \sum_{s=1}^{d}\sum_{\boldsymbol{k}\in I} \hat{\tilde{u}}_{\boldsymbol{k}} \frac{\partial^2}{\partial x_s^2}\mathrm{e}^{2\pi \mathrm{i}\boldsymbol{k}\cdot\boldsymbol{x}} \\
&= \sum_{s=1}^{d}\sum_{\boldsymbol{k}\in I} \left(\hat{\tilde{u}}_{\boldsymbol{k}} \prod_{\substack{j=1 \\ j\neq s}}^{d} \mathrm{e}^{2\pi \mathrm{i}k_j x_j} \right) \frac{\partial^2}{\partial x_s^2}\mathrm{e}^{2\pi \mathrm{i}k_s x_s} = \sum_{s=1}^{d}\sum_{\boldsymbol{k}\in I} -2\pi k_s^2 \hat{\tilde{u}}_{\boldsymbol{k}} \mathrm{e}^{2\pi \mathrm{i}\boldsymbol{k}\cdot\boldsymbol{x}} \\
&= \sum_{\boldsymbol{k}\in I} -(2\pi\|\boldsymbol{k}\|_2)^2 \hat{\tilde{u}}_{\boldsymbol{k}} \mathrm{e}^{2\pi \mathrm{i}\boldsymbol{k}\cdot\boldsymbol{x}} = \sum_{\boldsymbol{k}\in I} \hat{\tilde{f}}_{\boldsymbol{k}} \mathrm{e}^{2\pi \mathrm{i}\boldsymbol{k}\cdot\boldsymbol{x}} = \tilde{f}(\boldsymbol{x}).
\end{aligned}$$

Accordingly, we calculate the Fourier coefficients of $\tilde{u}$ from the corresponding Fourier coefficients of $\tilde{f}$

$$\hat{\tilde{u}}_{\boldsymbol{k}} = -\frac{\hat{\tilde{f}}_{\boldsymbol{k}}}{(2\pi\|\boldsymbol{k}\|_2)^2} \tag{5.19}$$

for all $\boldsymbol{k} \in I \setminus \{\boldsymbol{0}\}$. In case of $\boldsymbol{0} \in I$ we need an initial value $u(\boldsymbol{x}_0)$ of u to compute the zeroth Fourier coefficient $\hat{\tilde{u}}_{\boldsymbol{0}}$ of $\tilde{u}$. Knowing this initial value $u(\boldsymbol{x}_0)$ we simply set $\tilde{u}(\boldsymbol{x}_0) := u(\boldsymbol{x}_0)$, determine

$$\tilde{u}(\boldsymbol{x}_0) = \sum_{\boldsymbol{k}\in I} \hat{\tilde{u}}_{\boldsymbol{k}} \mathrm{e}^{2\pi \mathrm{i}\boldsymbol{k}\cdot\boldsymbol{x}_0} := u(\boldsymbol{x}_0)$$

and obtain

$$\hat{\tilde{u}}_{\boldsymbol{0}} = u(\boldsymbol{x}_0) - \sum_{\boldsymbol{k}\in I\setminus\{\boldsymbol{0}\}} \hat{\tilde{u}}_{\boldsymbol{k}} \mathrm{e}^{2\pi \mathrm{i}\boldsymbol{k}\cdot\boldsymbol{x}_0}. \tag{5.20}$$

The last lines outline a strategy to solve Poisson's equation (5.15) approximately. We summarized all the steps in Algorithm 5.1. Once one has determined a suitable frequency index set I, the most important step of Algorithm 5.1 is the computation of the solution of $\boldsymbol{A}^*\boldsymbol{A}\hat{\tilde{\boldsymbol{f}}} = \boldsymbol{A}^*\boldsymbol{f}$, i.e., the approximation $\tilde{f} \in \Pi_I$ of f. In our numerical examples, we will compare our rank-1 lattice approach to different standard methods, i.e., full grid approximations and standard sparse grid approximations using monomials as basis functions. We would like to mention that there are several papers that suggest to solve Poisson's equation using even adaptive sparse grid methods and finite elements, cf. e.g. [Bun92, BG99].

For the moment we focus again on the rank-1 lattice approach and calculate theoretical error bounds for the solution of Algorithm 5.1.

Algorithm 5.1 Solving Poisson's equation

Input:	$I \subset \mathbb{Z}^d$	frequency index set
	$\mathcal{X} \subset \mathbb{T}^d$	sampling set
	$\boldsymbol{f} = (f(\boldsymbol{x}))_{\boldsymbol{x}\in\mathcal{X}}$	sampling values of f
	$u(\boldsymbol{x}_0)$	initial value of u, needed only if $\mathbf{0} \in I$

solve $\boldsymbol{A}^*\boldsymbol{A}\hat{\tilde{\boldsymbol{f}}} = \boldsymbol{A}^*\boldsymbol{f}$
forall $\boldsymbol{k} \in I \setminus \{\mathbf{0}\}$ ***do***
  $\hat{\tilde{u}}_{\boldsymbol{k}} := -\hat{\tilde{f}}_{\boldsymbol{k}}/(2\pi\|\boldsymbol{k}\|_2)^2$
end for
if $\mathbf{0} \in I$ ***then***
  $\hat{\tilde{u}}_{\mathbf{0}} := u(\boldsymbol{x}_0) - \sum_{\boldsymbol{k}\in I\setminus\{\mathbf{0}\}} \hat{\tilde{u}}_{\boldsymbol{k}} \mathrm{e}^{2\pi\mathrm{i}\boldsymbol{k}\cdot\boldsymbol{x}_0}$
end if

Output:	$\hat{\tilde{\boldsymbol{u}}} = \left(\hat{\tilde{u}}_{\boldsymbol{k}}\right)_{\boldsymbol{k}\in I}$	Fourier coefficients of $\tilde{u}$

Theorem 5.8. *Let $\omega : \mathbb{Z}^d \to [1,\infty]$ be a weight function, $N \in \mathbb{R}$ fixed, and $f \in \mathcal{A}_\omega(\mathbb{T}^d)$. As usual, we define $I_N := \{\boldsymbol{k} \in \mathbb{Z}^d : \omega(\boldsymbol{k}) \le N\}$ and we assume that $1 \le |I_N| < \infty$. In addition, let $\mathcal{X} = \Lambda(\boldsymbol{z}, M, I_N)$ be a reconstructing rank-1 lattice for I_N, cf. Section 3.2, and the vector of function values $\boldsymbol{f} = (f(\boldsymbol{x}))_{\boldsymbol{x}\in\Lambda(\boldsymbol{z},M,I_N)}$ and an initial value $u(\boldsymbol{x}_0)$ of u be given. We compute an approximate solution $\tilde{u}$ of $\Delta u = f$ using Algorithm 5.1.*

Then, we estimate the L_∞ error of the approximation $\tilde{u}$ of u in terms of the norm of f in $\mathcal{A}_\omega(\mathbb{T}^d)$ by

$$\|u - \tilde{u}|L_\infty(\mathbb{T}^d)\| \le \frac{1}{\pi^2 N}\|f|\mathcal{A}_\omega(\mathbb{T}^d)\|.$$

Proof. We estimate the $L_\infty(\mathbb{T}^d)$ error using the norm in the Wiener Algebra $\mathcal{A}(\mathbb{T}^d)$ and the knowledge of the function value of u at node $\boldsymbol{x}_0$, i.e. we set $u(\boldsymbol{x}_0) = \tilde{u}(\boldsymbol{x}_0)$,

$$\begin{aligned}
\|u - \tilde{u}|L_\infty(\mathbb{T}^d)\| &\le \sum_{\boldsymbol{k}\in\mathbb{Z}^d} |\hat{u}_{\boldsymbol{k}} - \hat{\tilde{u}}_{\boldsymbol{k}}| \\
&= |\hat{u}_{\mathbf{0}} - \hat{\tilde{u}}_{\mathbf{0}}| + \sum_{\boldsymbol{k}\in I_N\setminus\{\mathbf{0}\}} |\hat{u}_{\boldsymbol{k}} - \hat{\tilde{u}}_{\boldsymbol{k}}| + \sum_{\boldsymbol{k}\in\mathbb{Z}^d\setminus(I_N\cup\{\mathbf{0}\})} |\hat{u}_{\boldsymbol{k}}| \\
&\le \left|\sum_{\boldsymbol{k}\in\mathbb{Z}^d\setminus\mathbf{0}} (\hat{u}_{\boldsymbol{k}} - \hat{\tilde{u}}_{\boldsymbol{k}})\mathrm{e}^{2\pi\mathrm{i}\boldsymbol{k}\cdot\boldsymbol{x}_0}\right| + \sum_{\boldsymbol{k}\in I_N\setminus\{\mathbf{0}\}} |\hat{u}_{\boldsymbol{k}} - \hat{\tilde{u}}_{\boldsymbol{k}}| + \sum_{\boldsymbol{k}\in\mathbb{Z}^d\setminus(I_N\cup\{\mathbf{0}\})} |\hat{u}_{\boldsymbol{k}}| \\
&\le \sum_{\boldsymbol{k}\in\mathbb{Z}^d\setminus\{\mathbf{0}\}} |\hat{u}_{\boldsymbol{k}} - \hat{\tilde{u}}_{\boldsymbol{k}}| + \sum_{\boldsymbol{k}\in I_N\setminus\{\mathbf{0}\}} |\hat{u}_{\boldsymbol{k}} - \hat{\tilde{u}}_{\boldsymbol{k}}| + \sum_{\boldsymbol{k}\in\mathbb{Z}^d\setminus(I_N\cup\{\mathbf{0}\})} |\hat{u}_{\boldsymbol{k}}| \\
&= 2\sum_{\boldsymbol{k}\in I_N\setminus\{\mathbf{0}\}} |\hat{u}_{\boldsymbol{k}} - \hat{\tilde{u}}_{\boldsymbol{k}}| + 2\sum_{\boldsymbol{k}\in\mathbb{Z}^d\setminus(I_N\cup\{\mathbf{0}\})} |\hat{u}_{\boldsymbol{k}}|.
\end{aligned}$$

We put in the relation of f and u and the relation of $\tilde{f}$ and $\tilde{u}$ for $\boldsymbol{k} \in I_N \setminus \{\mathbf{0}\}$, cf. 5.19,

$$\|u - \tilde{u}|L_\infty(\mathbb{T}^d)\| \le 2\sum_{\boldsymbol{k}\in I_N\setminus\{\mathbf{0}\}} (2\pi\|\boldsymbol{k}\|_2)^{-2}|\hat{\tilde{f}}_{\boldsymbol{k}} - \hat{f}_{\boldsymbol{k}}| + 2\sum_{\boldsymbol{k}\in\mathbb{Z}^d\setminus(I_N\cup\{\mathbf{0}\})} (2\pi\|\boldsymbol{k}\|_2)^{-2}|\hat{f}_{\boldsymbol{k}}|,$$

use the aliasing formula for reconstructing rank-1 lattices, cf. (3.12),

$$\begin{aligned}\|u-\tilde{u}|L_\infty(\mathbb{T}^d)\| &\leq 2 \sum_{\boldsymbol{k}\in I_N\setminus\{\boldsymbol{0}\}} (2\pi\|\boldsymbol{k}\|_2)^{-2} \sum_{\boldsymbol{h}\in\Lambda^\perp(\boldsymbol{z},M)\setminus\{\boldsymbol{0}\}} |\hat{f}_{\boldsymbol{k}+\boldsymbol{h}}| \\ &\quad + 2 \sum_{\boldsymbol{k}\in\mathbb{Z}^d\setminus(I_N\cup\{\boldsymbol{0}\})} (2\pi\|\boldsymbol{k}\|_2)^{-2}|\hat{f}_{\boldsymbol{k}}|,\end{aligned}$$

estimate $\|\boldsymbol{k}\|_2^{-2} \leq 1$, $\boldsymbol{k}\in\mathbb{Z}^d\setminus\{\boldsymbol{0}\}$, and extend the range of summation indices of the double sum

$$\begin{aligned}\|u-\tilde{u}|L_\infty(\mathbb{T}^d)\| &\leq \frac{1}{2\pi^2} \sum_{\boldsymbol{k}\in\mathbb{Z}^d\setminus(I\cup\{\boldsymbol{0}\})} |\hat{f}_{\boldsymbol{k}}| + 2 \sum_{\boldsymbol{k}\in\mathbb{Z}^d\setminus(I_N\cup\{\boldsymbol{0}\})} (2\pi\|\boldsymbol{k}\|_2)^{-2}|\hat{f}_{\boldsymbol{k}}| \\ &\leq \frac{1}{\pi^2} \sum_{\boldsymbol{k}\in\mathbb{Z}^d\setminus(I_N\cup\{\boldsymbol{0}\})} |\hat{f}_{\boldsymbol{k}}|,\end{aligned}$$

insert terms $\frac{\omega(\boldsymbol{k})}{\inf_{\boldsymbol{l}\in\mathbb{Z}^d\setminus(I_N\cup\{\boldsymbol{0}\})}\omega(\boldsymbol{l})} \geq 1$, $\boldsymbol{k}\in\mathbb{Z}^d\setminus(I_N\cup\{\boldsymbol{0}\})$,

$$\|u-\tilde{u}|L_\infty(\mathbb{T}^d)\| \leq \frac{1}{\pi^2}\frac{1}{\inf_{\boldsymbol{l}\in\mathbb{Z}^d\setminus(I_N\cup\{\boldsymbol{0}\})}\omega(\boldsymbol{l})} \sum_{\boldsymbol{k}\in\mathbb{Z}^d\setminus(I_N\cup\{\boldsymbol{0}\})} \omega(\boldsymbol{k})|\hat{f}_{\boldsymbol{k}}|,$$

and finally obtain the assertion of the theorem

$$\|u-\tilde{u}|L_\infty(\mathbb{T}^d)\| \leq \frac{1}{\pi^2 N}\|f|\mathcal{A}_\omega(\mathbb{T}^d)\|.$$

■

We stress the fact that the approximation $\tilde{f}\in\Pi_I$ of f in Theorem 5.8 is not an interpolation of f, in general. Consequently, our approach is not a collocation method, i.e., there may exist $\boldsymbol{x}_j\in\Lambda(\boldsymbol{z},M,I)$, where we observe

$$\Delta\tilde{u}(\boldsymbol{x}_j) = \tilde{f}(\boldsymbol{x}_j) \neq f(\boldsymbol{x}_j).$$

Nevertheless, we can use Algorithm 3.6 in order to extend the frequency index set I to an interpolating frequency index set $\tilde{I}$ on the rank-1 lattice $\Lambda(\boldsymbol{z},M,I)$, compute the interpolation $\tilde{S}_{\tilde{I}}f$ of f at $\Lambda(\boldsymbol{z},M,I)$ and the corresponding $\tilde{u}_{\tilde{I}}$ as indicated by Algorithm 5.1, and observe

$$\Delta\tilde{u}_{\tilde{I}}(\boldsymbol{x}_j) = \tilde{S}_{\tilde{I}}f(\boldsymbol{x}_j) = f(\boldsymbol{x}_j)$$

for all $\boldsymbol{x}_j\in\Lambda(\boldsymbol{z},M,I)$. However, we demonstrate the approximation properties of the described approach using the polynomial test function and the rank-1 lattice approximation, i.e., we do not focus on the collocation method.

5.2.1 Polynomial Test Function

We consider the univariate periodic function

$$v(x) = \begin{cases} \frac{4096}{4146}(2x^{12}-12x^{11}+22x^{10}-33x^8+44x^6-33x^4+10x^2)+1 & \text{for } x\in[0,1], \\ v(x-\lfloor x\rfloor) & \text{for } x\in\mathbb{R}\setminus[0,1], \end{cases}$$

see Figure 5.1 for illustration, and construct the multivariate function

$$u_d(\boldsymbol{x}) = \prod_{s=1}^{d} v(x_s) \tag{5.21}$$

as a tensor product. The corresponding Poisson's equation reads as follows

$$\Delta u_d(\boldsymbol{x}) = \sum_{j=1}^{d} \frac{\partial}{\partial^2 x_j} \prod_{s=1}^{d} v(x_s) = \sum_{j=1}^{d} v''(x_j) \prod_{s=1, s\neq j}^{d} v(x_s) = f_d(\boldsymbol{x}).$$

Accordingly, we can estimate the $L_\infty(\mathbb{T}^d)$ error of the approximation $\tilde{u}_{d,K}$, cf. Theorem 5.8,

$$\|u_d - \tilde{u}_{d,K} | L_\infty(\mathbb{T}^d)\| \leq \frac{1}{\pi^2 K} \|f_d | \mathcal{A}_\omega(\mathbb{T}^d)\|, \tag{5.22}$$

where we assume that the function $\tilde{u}_{d,K}$ is the solution of Poisson's equation for the right hand side $\tilde{f} = \tilde{S}_{I_K} f$ and $\tilde{S}_{I_K} f$ is computed from samples of f taken along a reconstructing rank-1 lattice $\Lambda(\boldsymbol{z}, M, I_K)$ for the frequency index set I_K. As usual, we define the frequency index set $I_K := \{\boldsymbol{k} \in \mathbb{Z}^d \colon \omega(\boldsymbol{k}) \leq K\}$.

In particular, we consider suitable weight functions

$$\omega_\mu^d(\boldsymbol{k}) = \prod_{s=1}^{d} \omega_\mu(k_s), \qquad \omega_\mu(k) := \max(1, \mu|k|^8), \tag{5.23}$$

and fix the parameter $\mu = \frac{54\,589\pi^8}{319\,901\,400} \approx 1.619153$. We define $N := K^{1/8}$ and $\boldsymbol{\gamma}_\mu = \left(\mu^{-1/8}\right)_{s\in\mathbb{N}}$, $\gamma_{\mu,s} \approx 0.94154\ldots$, and identify the frequency index sets $I_K^{d,\mu} := \{\boldsymbol{k} \in \mathbb{Z}^d \colon \omega_\mu^d(\boldsymbol{k}) \leq K\}$ as weighted hyperbolic crosses $I_{\mathrm{hc},N}^{d,\boldsymbol{\gamma}_\mu}$.

In order to estimate the $L_\infty(\mathbb{T}^d)$ error $\|u_d - \tilde{u}_{d,K} | L_\infty(\mathbb{T}^d)\|$ we have to calculate at least upper bounds on the norms $\|f_d | \mathcal{A}_{\omega_\mu^d}(\mathbb{T}^d)\|$. In detail, we apply the triangle inequality, exploit the tensor structure of u_d, and achieve

$$\|f_d | \mathcal{A}_{\omega_\mu^d}(\mathbb{T}^d)\| = \left\| \sum_{j=1}^{d} v''(x_j) \prod_{s=1, s\neq j}^{d} v(x_s) | \mathcal{A}_{\omega_\mu^d}(\mathbb{T}^d) \right\| \leq d \|v'' | \mathcal{A}_{\omega_\mu}(\mathbb{T})\| \|v | \mathcal{A}_{\omega_a}(\mathbb{T})\|^{d-1} =: C_{f_d,\mu}.$$

Thus, we calculate the norms of the one-dimensional function v and its second derivative v'',

$$\|v | \mathcal{A}_{\omega_\mu}(\mathbb{T})\| = |\hat{v}_0| + 2\sum_{k=1}^{\infty} \omega_\mu(k) |\hat{v}_k| = \frac{6143}{4095} + 2\sum_{k=1}^{\infty} \frac{54\,589(\pi k)^8}{319\,901\,400} \frac{159667200}{691(\pi k)^{12}} = \frac{221}{93},$$

$$\|v'' | \mathcal{A}_{\omega_\mu}(\mathbb{T})\| = 2\sum_{k=1}^{\infty} \omega_\mu(k)(2\pi k)^2 |\hat{v}_k| = 8\sum_{k=1}^{\infty} \frac{54\,589(\pi k)^{10}}{319\,901\,400} \frac{159\,667\,200}{691(\pi k)^{12}} = \frac{444\,928}{8\,463},$$

and achieve the upper bounds $C_{f_d,\mu}$ on the norms of the functions f_d as given in Table 5.13.

We plug in these norms and obtain from the error estimate in (5.22)

$$\|u_d - \tilde{u}_{d,N}^\mu | L_\infty(\mathbb{T}^d)\| \leq \frac{444\,928}{8\,463} \frac{d}{\pi^2} \left(\frac{221}{93}\right)^{d-1} N^{-8}, \tag{5.24}$$

d	2	3	4	5	6	7	8	9
$C_{f_d,\mu}$	2.50e+02	8.91e+02	2.82e+03	8.38e+03	2.39e+04	6.63e+04	1.80e+05	4.81e+05

Table 5.13: Upper bounds $C_{f_d,\mu}$ on the norms of f_d in the spaces $\mathcal{A}_{\omega_\mu^d}(\mathbb{T}^d)$, for different dimensions d.

Polynomial test function u_d – Rank-1 Lattice Approximation – Poisson's equation									
	N	$\lvert I_{\mathrm{hc},N}^{d,\boldsymbol{\gamma}}\rvert$	M	$\mathrm{err}_{\mathcal{A}}^{\mu}$		N	$\lvert I_{\mathrm{hc},N}^{d,\boldsymbol{\gamma}}\rvert$	M	$\mathrm{err}_{\mathcal{A}}^{\mu}$
$d=2$	4	33	38	4.288e-07	$d=6$	4	5 217	17 060	2.066e-05
	$2^{5/2}$	61	73	4.180e-09		$2^{5/2}$	13 125	45 393	3.535e-07
	8	93	129	1.381e-10		8	22 917	101 545	1.607e-08
$d=3$	4	135	186	1.133e-06	$d=9$	4	148 167	1 001 977	5.742e-04
	$2^{5/2}$	255	449	1.015e-08		$2^{5/2}$	341 307	3 979 598	1.546e-05
	8	435	818	3.071e-10		8	823 167	9 363 203	6.358e-07

Table 5.14: Cardinalities $\lvert I_{\mathrm{hc},N}^{d,\boldsymbol{\gamma}_\mu}\rvert$ of weighted hyperbolic crosses, lattice sizes M of corresponding reconstructing rank-1 lattices $\Lambda(\boldsymbol{z}, M, I_{\mathrm{hc},N}^{d,\boldsymbol{\gamma}_\mu})$, and upper bounds $\mathrm{err}_{\mathcal{A}}^{\mu} := \mathrm{err}\left(u_d, \tilde{u}_{d,N}^{\mu}, \mathcal{A}(\mathbb{T}^d)\right)$ on the $L_\infty(\mathbb{T}^d)$ errors of approximations $\tilde{u}_{d,N}^{\mu}$ of u_d given in (5.21), $\boldsymbol{\gamma}_\mu = \left(\left(\frac{319\,901\,400}{54\,589}\right)^{1/8} \frac{1}{\pi}\right)_{s\in\mathbb{N}}$.

where $\tilde{u}_{d,N}^{\mu}$ is the approximation of u_d that is computed based on the approximation $\tilde{f}_d = \tilde{S}_{I_{\mathrm{hc},N}^{d,\boldsymbol{\gamma}_\mu}} f_d$ of f_d.

We refer to Section 5.1.1, where we have specified the weight function ω_a^d and dealt with the corresponding weighted hyperbolic crosses $I_{\mathrm{hc},N}^{d,\boldsymbol{\gamma}_a}$ with weights $\gamma_{a,s} = \left(\frac{108972864000}{2122061}\right)^{1/10} \frac{1}{\pi} \approx 0.941686$, $s = 1, \ldots, d$. In particular, we obtain the close embedding $I_{\mathrm{hc},N}^{d,\boldsymbol{\gamma}_\mu} \subset I_{\mathrm{hc},N}^{d,\boldsymbol{\gamma}_a}$. In fact, the frequency index sets coincide for the parameters $N = 4, 2^{5/2}, 8$ and dimensions $d = 2, \ldots, 9$.

However, due to the embedding $I_{\mathrm{hc},N}^{d,\boldsymbol{\gamma}_\mu} \subset I_{\mathrm{hc},N}^{d,\boldsymbol{\gamma}_a}$, reconstructing rank-1 lattices $\Lambda(\boldsymbol{z}, M, I_{\mathrm{hc},N}^{d,\boldsymbol{\gamma}_a})$ are also reconstructing rank-1 lattices $\Lambda(\boldsymbol{z}, M, I_{\mathrm{hc},N}^{d,\boldsymbol{\gamma}_\mu})$ for the frequency index sets $I_{\mathrm{hc},N}^{d,\boldsymbol{\gamma}_\mu}$. In the following examples, we apply this observation and compute approximations of f_d from samples along the reconstructing rank-1 lattices that are presented in Table 3.8.

Numerical Example 5.9. At first we would like to compare the practical approximation errors, that we observe from the rank-1 lattice approach, see Table 5.14, to the theoretical error estimate in (5.24). We consider fixed dimension d and increase N by factors of $\sqrt{2}$. We expect that the errors $\|u_d - \tilde{u}_{d,N}^{\mu} | L_\infty(\mathbb{T}^d)\|$ decrease by a factor of at most $1/16 = \sqrt{2}^{-8}$.

The numerical tests in Table 5.14 indicate this behavior even for small parameters N and all dimensions $d = 2, 3, 6, 9$. In fact, the error reduces by factors that are smaller than $1/16$ for fixed dimension $d = 2, \ldots, 9$ and growing $N = 4, 2^{5/2}, 8$.

On the other hand the theoretical estimate (5.24) predicts growing errors for growing dimension d and fixed parameter N. The relation of the theoretical error bound in dimension d to the theoretical error bound in dimension $d-1$ is $\frac{d}{d-1}\frac{221}{93}$. We compare dimension d to dimension $s < d$ and observe the relation of the theoretical error bounds of $\frac{d}{s}\left(\frac{221}{93}\right)^{d-s}$. In

Polynomial test function u_d – Full Grid Approximation – Poisson's equation							
	N	$\lvert I^{d,\mathbf{1}}_{\infty,N}\rvert$	$\mathrm{err}^{\mathrm{FG}}_{\mathcal{A}}$		N	$\lvert I^{d,\mathbf{1}s}_{\infty,N}\rvert$	$\mathrm{err}^{\mathrm{FG}}_{\mathcal{A}}$
$d=2$	3	49	5.081e-07	$d=6$	2	15 625	6.121e-04
	5	121	4.043e-09		4	531 441	1.336e-06
	7	225	1.425e-10		6	4 826 809	2.597e-08
$d=3$	3	343	1.371e-06	$d=9$	1	19 683	9.248e-01
	5	1 331	1.102e-08		2	1 953 125	6.776e-03
	7	3 375	3.884e-10		3	40 353 607	2.161e-04

Table 5.15: Cardinalities $|I^{d,\mathbf{1}}_{\infty,N}|$ of unweighted ℓ_∞-balls and upper bounds $\mathrm{err}^{\mathrm{FG}}_{\mathcal{A}} := \mathrm{err}\left(u_d, \tilde{u}^{\mathrm{FG}}_{d,N}, \mathcal{A}(\mathbb{T}^d)\right)$ on the $L_\infty(\mathbb{T}^d)$ errors of approximations $\tilde{u}^{\mathrm{FG}}_{d,N}$ of u_d given in (5.21).

particular, we calculate the relation of the error bounds in dimension 9 to dimension 6 and in dimension 6 to dimension 3 and get approximately 20 and 27, respectively.

We calculate the same relations for our concrete numerical tests and observe quotients of the 9-dimensional errors divided by the 6-dimensional errors between 27 and 44 for fixed $N = 4, 2^{5/2}, 8$. Considering the same values of N, the 6-dimensional errors divided by the 3-dimensional errors are contained in the interval $[18, 53]$.

Obviously, the theoretical relations do not bound the relations in practice here. However, the practical relations are somehow in the right order of magnitude and do not disagree the theoretical findings, since the practical errors are much smaller than the theoretical bounds in fact. We expect the behavior indicated by the theoretical bound in the asymptotics. □

Since the frequency index sets $I^{d,\boldsymbol{\gamma}_\mu}_{\mathrm{hc},N}$ and, in particular, the corresponding reconstructing rank-1 lattices are of relatively high cardinality, we would like to compare the approximation results against so-called full grid approximations, i.e., trigonometric polynomials $\tilde{u}^{\mathrm{FG}}_{d,N}$ that are computed from approximations $\tilde{S}_{I^{d,\mathbf{1}}_{\infty,N}} f_d$ of f_d. In particular, we computed the trigonometric polynomials $\tilde{S}_{I^{d,\mathbf{1}}_{\infty,N}} f_d$ from sampling values of f_d from tensor product grids

$$\mathcal{X}^d_N = \bigtimes_{s=1}^{d} \left\{0, \frac{1}{2N+1}, \ldots, \frac{2N}{2N+1}\right\}$$

as described in Lemma 2.4. We stress the fact that the corresponding Fourier matrix $\boldsymbol{A} = \left(\mathrm{e}^{2\pi \mathrm{i} \boldsymbol{k}\cdot\boldsymbol{x}}\right)_{\boldsymbol{x}\in\mathcal{X}^d_N, \boldsymbol{k}\in I^{d,\mathbf{1}}_{\infty,N}}$ is unitary up to a scaling factor, i.e., perfectly stable. At this point, we would like to mention that there exist fast algorithms that computes the corresponding d-dimensional discrete Fourier transform in almost linear time with respect to the cardinality of $I^{d,\mathbf{1}}_{\infty,N} = (2N+1)^d$. The concrete complexity is bounded by $C|I^{d,\mathbf{1}}_{\infty,N}| \log |I^{d,\mathbf{1}}_{\infty,N}|$, where the constant C does not depend on d and N. Since the embedding $I^{d,\boldsymbol{\gamma}_\mu}_{\mathrm{hc},N} \subset I^{d,\mathbf{1}}_{\infty,N}$ holds, we also expect an error decay of at least N^{-8} for fixed dimension d.

Numerical Example 5.10. We compare the errors $\mathrm{err}^{\mu}_{\mathcal{A}} := \mathrm{err}\left(u_d, \tilde{u}^{\mu}_{d,N}, \mathcal{A}(\mathbb{T}^d)\right)$ given in Table 5.14 to $\mathrm{err}^{\mathrm{FG}}_{\mathcal{A}} := \mathrm{err}\left(u_d, \tilde{u}^{\mathrm{FG}}_{d,K}, \mathcal{A}(\mathbb{T}^d)\right)$ presented in Table 5.15 with respect to the used number of sampling values M and $|\mathcal{X}^d_K| = |I^{d,\mathbf{1}}_{\infty,K}|$.

Specifically, we use the following approach: For fixed dimension d, we pick out tuples (N, K) where the corresponding errors $\mathrm{err}_{\mathcal{A}}^{\mathrm{FG}}$ and $\mathrm{err}_{\mathcal{A}}^{\mu}$ are in the same order of magnitude. Since, we would like to compare the number of sampling values that are needed in order to achieve the errors $\mathrm{err}_{\mathcal{A}}^{\mathrm{FG}}$ and $\mathrm{err}_{\mathcal{A}}^{\mu}$, we compare the number $|\mathcal{X}_K^d| = |I_{\infty,K}^{d,\mathbf{1}}|$ to the number $M = |\Lambda(\boldsymbol{z}, M, I_{\mathrm{hc},N}^{d,\boldsymbol{\gamma}_\mu})|$, where M is the cardinality of the reconstructing rank-1 lattice for the frequency index set $I_{\mathrm{hc},N}^{d,\boldsymbol{\gamma}_\mu}$. In detail, we consider the quotient $|\mathcal{X}_K^d|/M$.

Due to the results from Corollary 3.23 and the estimates in (3.19), we expect a fixed upper bound on $\frac{|\mathcal{X}_K^d|}{M}$ for dimension $d = 2$. From dimension $d = 3$ on, we expect and also observe growing relations $\frac{|\mathcal{X}_N^d|}{M}$ for increasing errors $\mathrm{err}_{\mathcal{A}}^{\mathrm{FG}} \sim \mathrm{err}_{\mathcal{A}}^{\mu}$.

Naturally, for larger dimensions (in the given tables $d = 6$ and $d = 9$), we notice fast growing quotients $\frac{|\mathcal{X}_K^d|}{M}$ up to more than 47 for increasing errors. We stress the fact that the quotients $\frac{|\mathcal{X}_K^d|}{M}$ grow with further decreasing errors $\mathrm{err}_{\mathcal{A}}^{\mathrm{FG}}$ and $\mathrm{err}_{\mathcal{A}}^{\mu}$, which can be obtained by increasing N and K.

Specifically in dimension $d = 9$, we were not able to compute full grid approximations $\tilde{u}_{d,K}^{\mathrm{FG}}$ of lower errors than 10^{-4}, due to memory limitations on the used machine and the huge cardinalities of $I_{\infty,K}^{9,\mathbf{1}}$, $K \geq 4$, e.g., $|I_{\infty,4}^{9,\mathbf{1}}| = 9^9 = 387\,420\,489$. On the other hand, we computed approximations $\tilde{u}_{9,N}^{\mu}$ based on hyperbolic cross approximations of f_9 up to errors lower than 10^{-6}. We emphasize that we can achieve even lower approximation errors, by determining suitable reconstructing rank-1 lattices for the frequency index sets $I_{\mathrm{hc},K}^{9,\boldsymbol{\gamma}_\mu}$, $K > 8$. □

As a last example, we compare the rank-1 lattice approach to a sparse grid approach. Since we would like to use fast algorithms in order to reconstruct the function f_d, we use a standard dyadic sparse grid interpolation method and the corresponding hyperbolic cross fast Fourier transform, cf. [Hal92]. For that reason, we define the sampling set

$$\mathcal{X} = S_N^d := \bigcup_{\substack{\boldsymbol{j} \in \mathbb{N}_0^d \\ \|\boldsymbol{j}\|_1 = \log_2 N}} \bigtimes_{l=1}^{d} 2^{-j_l}(\mathbb{N}_0 \cap [0, 2^{j_l})),$$

where $N = 2^n$, $n \in \mathbb{N}_0$, is a power of two, and call S_N^d a dyadic sparse grid. It is well known, that the so-called dyadic hyperbolic cross

$$I = H_N^d := \bigcup_{\substack{\boldsymbol{j} \in \mathbb{N}_0^d \\ \|\boldsymbol{j}\|_1 = \log_2 N}} \left(\mathbb{Z}^d \cap \bigtimes_{l=1}^{d} (-2^{-j_l-1}, 2^{j_l-1}] \right),$$

$N = 2^n$, $n \in \mathbb{N}_0$, is a suitable frequency index set, such that one can fast compute trigonometric polynomials with frequencies supported on H_N^d that interpolates the sampling values at the dyadic sparse grid S_N^d using the hyperbolic cross fast Fourier transform (HCFFT), cf. [BD89, Hal92]. In particular, we mention that the cardinalities of dyadic hyperbolic crosses H_N^d and corresponding sparse grids S_N^d coincide.

Due to the results of W. Sickel and T. Ullrich [SU07] we expect error bounds for approximations computed from sampling values taken at sparse grid nodes that are bounded by terms which depends on N at least in the same asymptotic order as the right hand side of (5.24).

Polynomial test function u_d – Sparse Grid Approximation – Poisson's equation							
	N	$\lvert H_N^d\rvert$	$\mathrm{err}_{\mathcal{A}}^{\mathrm{SG}}$		N	$\lvert H_N^d\rvert$	$\mathrm{err}_{\mathcal{A}}^{\mathrm{SG}}$
$d=2$	16	48	1.261e-04	$d=6$	2 048	1 003 136	1.591e-02
	32	112	5.535e-08		4 096	2 664 192	2.346e-05
	64	256	2.601e-11		8 192	6 960 384	2.150e-08
$d=3$	64	688	9.404e-05	$d=9$	1 024	2 719 028	2.570e+01
	128	1 696	5.224e-08		2 048	8 316 200	1.352e+01
	256	4 096	2.789e-11		4 096	24 814 832	5.868e+00

Table 5.16: Cardinalities $|H_N^d| = |S_N^d|$ of dyadic hyperbolic crosses H_N^d and corresponding sparse grids S_N^d and upper bounds $\mathrm{err}_{\mathcal{A}}^{\mathrm{SG}} := \mathrm{err}\left(u_d, \tilde{u}_{d,N}^{\mathrm{SG}}, \mathcal{A}(\mathbb{T}^d)\right)$ on the $L_\infty(\mathbb{T}^d)$ errors of approximations $\tilde{u}_{d,N}^{\mathrm{SG}}$ of u_d given in (5.21).

Numerical Example 5.11. We use the strategy indicated in Algorithm 5.1 and compute approximations $\tilde{u}_{d,N}^{\mathrm{SG}}$ from the interpolations $f_d^{\mathrm{SG}} \in \Pi_{H_N^d}$, where $f_d^{\mathrm{SG}}(\boldsymbol{x}) = f_d(\boldsymbol{x})$ for all $\boldsymbol{x} \in S_N^d$. We stress the fact that we compute the solution $\hat{\boldsymbol{f}}_d^{\mathrm{SG}} = \left(\hat{f}_{d,\boldsymbol{k}}^{\mathrm{SG}}\right)_{\boldsymbol{k}\in H_N^d}$ of $\boldsymbol{A}^*\boldsymbol{A}\hat{\boldsymbol{f}}_d^{\mathrm{SG}} = \boldsymbol{A}^*\boldsymbol{f}_d$, $\boldsymbol{A} = \left(\mathrm{e}^{2\pi\mathrm{i}\boldsymbol{k}\cdot\boldsymbol{x}}\right)_{\boldsymbol{x}\in S_N^d,\,\boldsymbol{k}\in H_N^d}$, $\boldsymbol{f}_d = (f_d(\boldsymbol{x}))_{\boldsymbol{x}\in S_N^d}$, using the inverse hyperbolic cross fast Fourier transform. This is a direct method that calculates the matrix vector product $\boldsymbol{A}^{-1}\boldsymbol{f}_d$ in a fast way, see [Hal92] for details.

At first, we classify the frequency index sets H_N^d. We proved the embedding $H_N^d \subset I_{\mathrm{hc},N}^{d,\mathbf{1/2}}$ in [KKP12], i.e., the dyadic hyperbolic crosses are contained in symmetric hyperbolic crosses with weights $\boldsymbol{\gamma} = \mathbf{1/2} = \left(\frac{1}{2}\right)_{s\in\mathbb{N}}$. Nevertheless, one observes differences $I_{\mathrm{hc},N}^{d,\mathbf{1/2}} \setminus H_N^d$ that are of high cardinality for larger dimensions d and parameters N.

However, we present some numerical results of the sparse grid approach in Table 5.16.

On the one hand, we shortly compare the sparse grid approach to the full grid approach, cf. Table 5.15. For dimensions $d = 2$ and $d = 3$ we need approximately as many sampling nodes as needed for sampling along full grids in order to obtain the same errors. Even in higher dimensions, i.e., $d = 6$ and $d = 9$, we obtain larger errors from the sparse grid sampling than those we achieved using the full grid approach and approximately the same number of sampling nodes.

On the other hand, we compare the standard sparse grid approach to the rank-1 lattice approach. Certainly, we obtain smaller upper bounds on the $L_\infty(\mathbb{T}^d)$ errors using the rank-1 lattice sampling compared to the sparse grid approach measured against the number of used sampling values. As mentioned in Numerical Example 5.4, we observe this behavior due to the fact that the frequency index sets H_N^d are not as suitable as the frequency index sets $I_{\mathrm{hc},N}^{d,\boldsymbol{\gamma}_\mu}$ in order to approximate the function f_d. □

As a consequence of the last examples, we conclude that well adapted suitable frequency index sets I are most important for approximation approaches in higher dimensions. The next numerical examples also illustrates that not only the rough structure but also subtle details of the construction of a frequency index set may cause widely differing approximation errors.

Numerical Example 5.12. We computed different approximations of the solution of Poisson's equation (5.15) for the function u_6, cf. (5.21), in dimension $d = 6$. In detail, we used

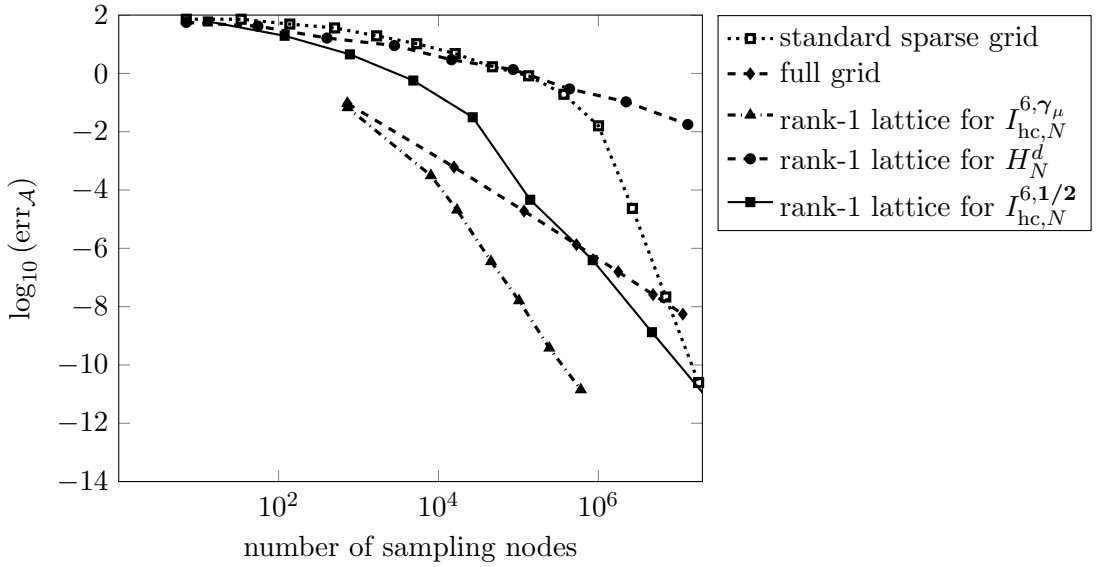

Figure 5.4: Approximation errors $\mathrm{err}_{\mathcal{A}} := \mathrm{err}\left(u_6, p_6, \mathcal{A}(\mathbb{T}^d)\right)$, $p_6 = \tilde{u}_{6,N}^{\mathrm{SG}}$, $p_6 = \tilde{u}_{6,N}^{\mathrm{FG}}$, and $p_6 = \tilde{u}_{6,N}$ for different frequency index sets $I_{\mathrm{hc},N}^{6,\boldsymbol{\gamma}_\mu}$, H_N^d, $I_{\mathrm{hc},N}^{6,\mathbf{1/2}}$ of approximations of u_6 given in (5.21) plotted against the number of used sampling values.

a full grid and a standard sparse grid approach and, in addition, reconstructing rank-1 lattices for the frequency index sets $I_{\mathrm{hc},N}^{6,\boldsymbol{\gamma}_\mu}$, H_N^d, $I_{\mathrm{hc},N}^{6,\mathbf{1/2}}$ in order to compute the corresponding solutions.

In Figure 5.4 we plotted the number of used sampling values against the occurring upper bounds on the $L_\infty(\mathbb{T}^d)$ errors. We list the most important observations:

- As expected, the errors of the standard sparse grid approach decrease faster than the errors of the rank-1 lattice approach for the corresponding dyadic hyperbolic cross H_N^6 and large N.
- The structure of the dyadic hyperbolic cross H_N^6 is suitable in order to approximately solve Poisson's equation for u_6.
- The weighted hyperbolic cross $I_{\mathrm{hc},N}^{6,\mathbf{1/2}}$ is more suitable than the dyadic hyperbolic cross H_N^6 in order to approximate solutions of Poisson's equation for u_6. Even the necessary oversampling caused by the rank-1 lattice approach applied to $I_{\mathrm{hc},N}^{6,\mathbf{1/2}}$ leads to better approximations of u_6 with respect to relatively small numbers of sampling values.
- The asymptotic rate of convergence of the sparse grid approach beats the rates of convergence of all the rank-1 lattice approaches.
- The rank-1 lattice approach applied to the weighted hyperbolic cross $I_{\mathrm{hc},N}^{6,\boldsymbol{\gamma}_\mu}$ cause the minimal errors of all considered approaches for reasonable numbers of sampling values.
- The full grid approach also beats the sparse grid approach for small numbers of sampling values.
- The full grid approach has the worst rate of convergence of all tested approaches.

Finally, we notice that the function u_6 has a lot of relatively large frequencies with mixed indices. For that reason the full grid approach beats the sparse grid approach for small numbers of used sampling values and the least sparse hyperbolic cross $I_{\mathrm{hc},N}^{6,\gamma_\mu}$ seems to be the most adequate frequency index set in order to compute approximate solutions of Poisson's equation for u_d. □

Again, we stress the fact that the computational costs of the approximation of a function f from sampling values along a reconstructing rank-1 lattice for I is bounded from above by $C \max(M \log M, d|I|)$, where the term C does not depend on the frequency index set I, the lattice size M, and the dimension d. We do not compare computational times here since we used a MATLAB® [MAT] implementation of the HCFFT in order to compute the corresponding examples. We refer to [KKP12, Section 4.3], where the authors discuss the differences of the computational times of the rank-1 lattice fast Fourier transform (LFFT) and the HCFFT for reasonable problem sizes. The most impressive observation is that the LFFT outperforms the HCFFT by at least one order of magnitude in the computational times for higher dimensional problems, although the reconstructing rank-1 lattices are of substantially larger cardinality than the corresponding sparse grids.

5.3 Approximation of Non-periodic Functions

There exist a variety of well-adapted fast Fourier transforms, e.g., fast Fourier transforms, nonequispaced fast Fourier transforms, hyperbolic cross fast Fourier transforms, that may be used in order to approximate periodic functions even in higher dimensions. A usual approach is to periodize non-periodic functions in order to apply the algorithms that are already available for the approximation of periodic functions.

However, the qualities of the approximation of the non-periodic function mainly depends on the transform that yields the periodic function. We illustrate one usual transform in Figure 5.5 for dimension $d = 1$. In detail, a non-periodic univariate function $v\colon [0,1] \to \mathbb{R}$ can be periodized using the following approach, that is often used in image processing, see e.g. [DY07]. At first one mirrors the function v at the right hand side of its domain and achieves a function that has the same function values at $x = 0$ and $x = 2$. Then, one scales the new domain $[0,2]$ to $[0,1]$ and periodize this function. This yields a continuous periodic function

$$v_{\mathrm{per}}(x) := \begin{cases} v(2x) & \text{for } 0 \le x < \frac{1}{2}, \\ v(2-2x) & \text{for } \frac{1}{2} \le x < 1, \\ v_{\mathrm{per}}(x - \lfloor x \rfloor) & \text{else,} \end{cases}$$

on the torus $\mathbb{T}$. To summarize, the periodic function v_{per} is given by $v_{\mathrm{per}}(x) = v(\varphi(x - \lfloor x \rfloor))$, $\varphi(x) := 1 - |2x - 1|$.

In the multivariate case, one defines the periodic function f_{per} in the same way—one has to apply the transform on all components of the variable $\boldsymbol{x}$. Accordingly, the periodization of a continuous function $f\colon [0,1]^d \to \mathbb{R}$ is given by the function $f_{\mathrm{per}}(\boldsymbol{x}) = f(\boldsymbol{\varphi}(\boldsymbol{x}))$, where the periodization is realized by $\boldsymbol{\varphi}(\boldsymbol{x}) = (\varphi(x_1 - \lfloor x_1 \rfloor), \ldots, \varphi(x_d - \lfloor x_d \rfloor))^\top$.

Now, one approximates the function f_{per} using a suitable fast Fourier transform. The corresponding approximant also approximates the non-periodic function f since the identity $f(\boldsymbol{x}) = f_{\mathrm{per}}(\frac{\boldsymbol{x}}{2})$, $\boldsymbol{x} \in [0,1]^d$, holds.

We switch to the univariate case and discuss the approximation properties of the periodization approach. The quality of the approximation of the periodic function v_{per} mainly

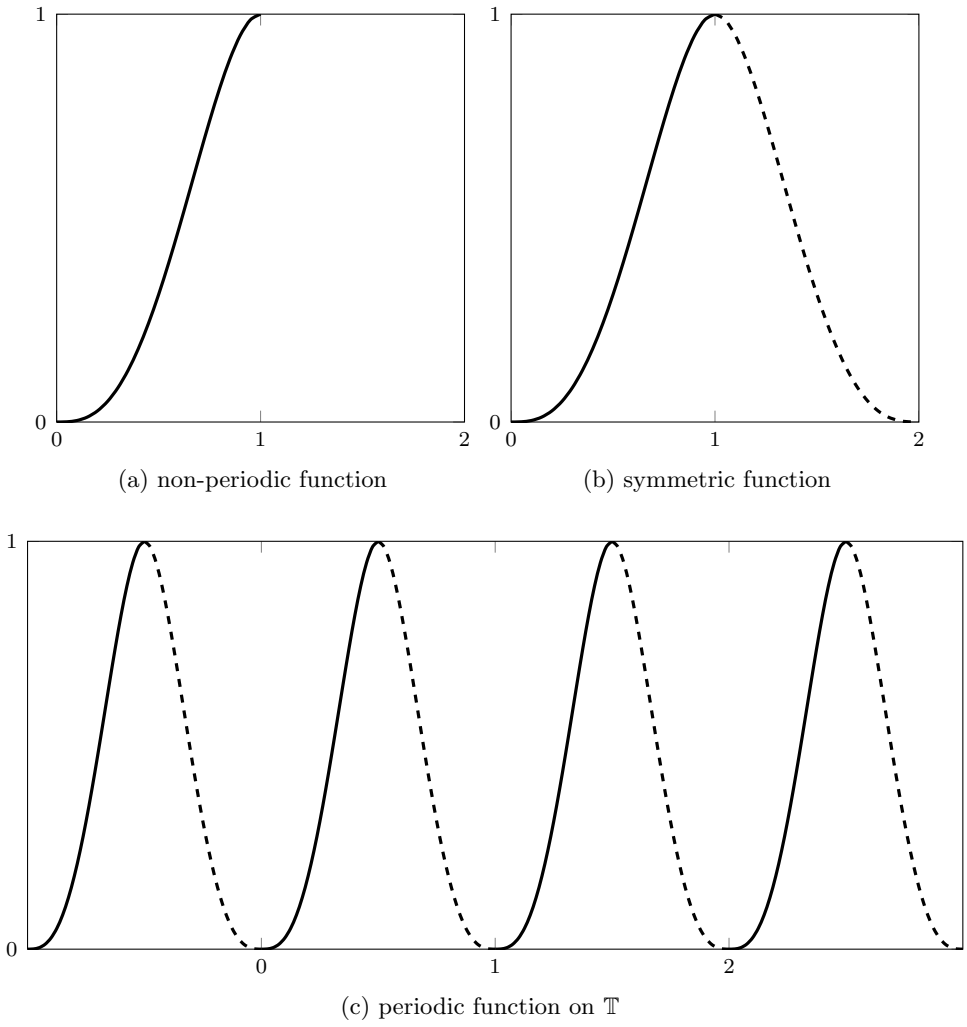

(a) non-periodic function

(b) symmetric function

(c) periodic function on $\mathbb{T}$

Figure 5.5: Sketch of the periodization of non-periodic functions.

depends on the smoothness of v_{per} or, in other words, the decay of its Fourier coefficients. Obviously, the smoothness of the periodized function v_{per} is somehow bounded by the smoothness of the non-periodic function v. In addition, we append the mirrored v to v and periodize this result. Particularly, the smoothness at the tie points, i.e., at $v_{\text{per}}(0)$ and $v_{\text{per}}(\frac{1}{2})$, may corrupt the smoothness of the periodic function v_{per} such that the errors of the periodic approximation approaches may decrease slower than one would expect for functions v of higher smoothness.

Some pre-smoothing steps may overcome these problems. We shortly explain this approach for univariate functions. Hence, we consider a continuous differentiable function $v\colon [0,1] \to \mathbb{R}$ with values $v'(0) \neq 0$ and $v'(1) \neq 0$ of the first derivatives. We assume that we know (or can approximate) the values $v'(0) \neq 0$ and $v'(1) \neq 0$. Then, we construct

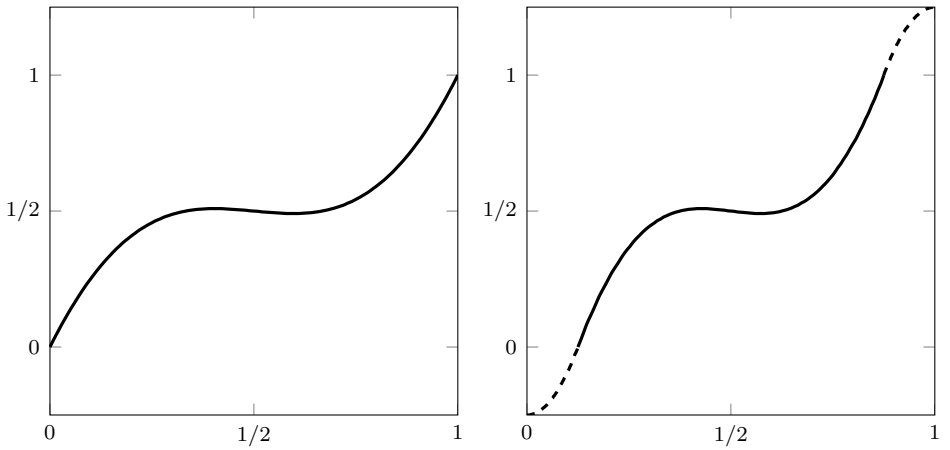

(a) non-periodic function

(b) non-periodic function with slopes zero at the boundary

Figure 5.6: Boundary smoothing with respect to the periodization.

a function

$$\tilde{v}(x) = \begin{cases} v_{\mathrm{l}}(x) & \text{for } 0 \leq x < \varepsilon/2, \\ v\left(\frac{x-\varepsilon/2}{1-\varepsilon}\right) & \text{for } \varepsilon/2 \leq x \leq 1-\varepsilon/2, \\ v_{\mathrm{r}}(x) & \text{for } 1-\varepsilon/2 \leq 1, \end{cases}$$

where the functions v_{l} and v_{r} fulfills

$$\begin{aligned} &v_{\mathrm{l}}'(0) = 0, && v_{\mathrm{l}}(\varepsilon/2) = v(0), && v_{\mathrm{l}}'(\varepsilon/2) = \frac{1}{1-\varepsilon} v'(0), \\ &v_{\mathrm{r}}'(1) = 0, && v_{\mathrm{r}}(1-\varepsilon/2) = v(1), && v_{\mathrm{l}}'(1-\varepsilon/2) = \frac{1}{1-\varepsilon} v'(1). \end{aligned}$$

Figure 5.6 illustrates the mentioned approach. Subsequently, one periodize the function $\tilde{v}$ and achieve a function $\tilde{v}_{\mathrm{per}}$ that is continuously differentiable also at the tie points 0 and $\frac{1}{2}$. We stress the fact that the described approach is of much greater difficulty for higher dimensions d, since the tie points are even tie planes of dimension $d-1$.

Anyway, one can also consider more complicated functions $\boldsymbol{\varphi}$ in order to construct smoothness of higher order at the tie points. In particular for applications in numerical integration, F. J. Hickernell considers those transforms in a more general setting in [Hic02]. Therein, he uses the periodization strategy from above in order to analyze one concrete $\boldsymbol{\varphi}$ and calls it Baker's transformation. In addition, he suggests to consider directly the integration properties of the sampling sets

$$\Lambda_{\boldsymbol{\varphi}}(\boldsymbol{z}, M) := \{\boldsymbol{x} = \boldsymbol{\varphi}(\boldsymbol{x}_j) \colon \boldsymbol{x}_j \in \Lambda(\boldsymbol{z}, M)\} \tag{5.25}$$

in the spaces of non-periodic functions.

Furthermore, J. Dick, D. Nuyens, and F. Pillichshammer, cf. [DNP14], use the sampling schemes $\Lambda_{\boldsymbol{\varphi}}(\boldsymbol{z}, M)$ in order to consider the integration properties of quasi-Monte Carlo rules in functions spaces that are spanned by cosine terms $\left(\prod_{s=1}^{d} \cos(\pi k_s x_s)\right)_{\boldsymbol{k} \in \mathbb{N}_0^d}$, $\boldsymbol{x} \in [0,1]^d$. Due to [CDLP07] the function $\varphi(x) = 1 - |2x-1|$ is called a tent transformation and,

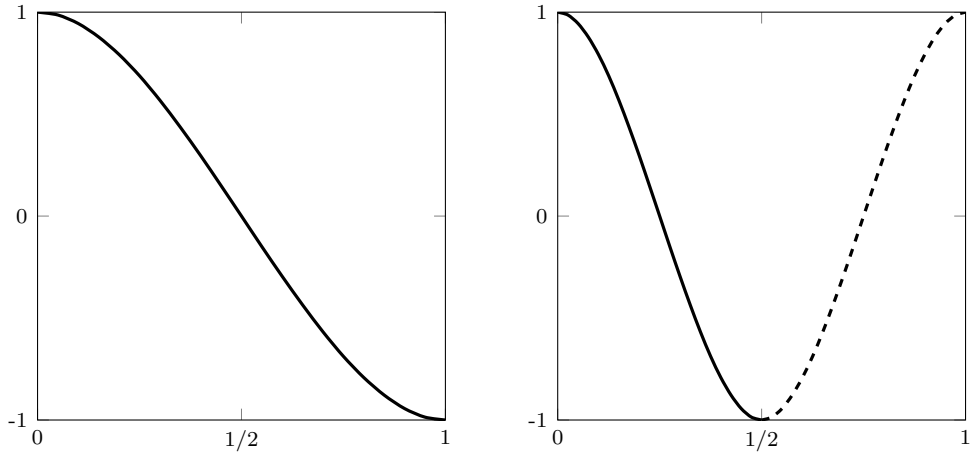

(a) non-periodic polynomial test function v (b) periodized polynomial test function v_{per}

Figure 5.7: Non-periodic polynomial test function v and its periodization v_{per}.

accordingly, the equally weighted quadrature rule based on $\Lambda_{\boldsymbol{\varphi}}(\boldsymbol{z}, M)$ a tent transformed lattice rule. We stress the fact that the periodization of functions that belong to the cosine series space spanned by $\left(\prod_{s=1}^{d} \cos(\pi k_s x_s)\right)_{\boldsymbol{k} \in \mathbb{N}_0^d}$ yield periodic functions spanned by periodic cosine terms, in fact. Thus, the periodization using the tent transformation may not corrupt the smoothness at the tie points in this setting.

However, the cardinality of $\Lambda_{\boldsymbol{\varphi}}(\boldsymbol{z}, M)$ determines the number of sampling values that are taken from the non-periodic multivariate function f in order to sample the periodic function f_{per}. Due to the symmetry of the specific function $\varphi(x) = 1 - |2x - 1|$, i.e., $\varphi(x) = \varphi(1 - x)$ for $x \in [0, \frac{1}{2}]$, and the group structure of rank-1 lattices, we obtain $\varphi(\frac{jz_s}{M} \bmod 1) = \varphi(\frac{(M-j)z_s}{M} \bmod 1)$ for all $s = 1, \ldots, d$ and, thus, $\boldsymbol{\varphi}(\frac{j\boldsymbol{z}}{M} \bmod \mathbf{1}) = \boldsymbol{\varphi}(\frac{(M-j)\boldsymbol{z}}{M} \bmod \mathbf{1})$. Accordingly, the sampling set $\Lambda_{\boldsymbol{\varphi}}(\boldsymbol{z}, M)$ contains at most $\left\lfloor \frac{M+2}{2} \right\rfloor$ sampling nodes.

We approximate sufficiently smooth non-periodic functions f by means of approximated Fourier partial sums of the periodizations f_{per} of f.

5.3.1 Non-periodic Polynomial Test Function

We consider the univariate non-periodic polynomial test function

$$v(x) = 4x^3 - 6x^2 + 1,$$

see Figure 5.7a. Due to the fact, that the function v do not contain a periodic part and the equation $\int_0^1 v(x)\mathrm{d}x = 0$ holds, i.e., the function v is given by the cosine series

$$v(x) = \int_0^1 v(x)\mathrm{d}x + \sum_{k=1}^{\infty} \frac{96}{(2k-1)^4\pi^4} \cos((2k-1)\pi x) = \sum_{k \in \mathbb{Z}} \frac{48}{(2k+1)^4\pi^4} \mathrm{e}^{\pi \mathrm{i}(2k+1)x},$$

only the odd frequencies of the periodic function

$$v_{\mathrm{per}}(x) = \sum_{k \in \mathbb{Z}} \frac{48}{(2k+1)^4\pi^4} \mathrm{e}^{2\pi \mathrm{i}(2k+1)x}$$

are non-zero.

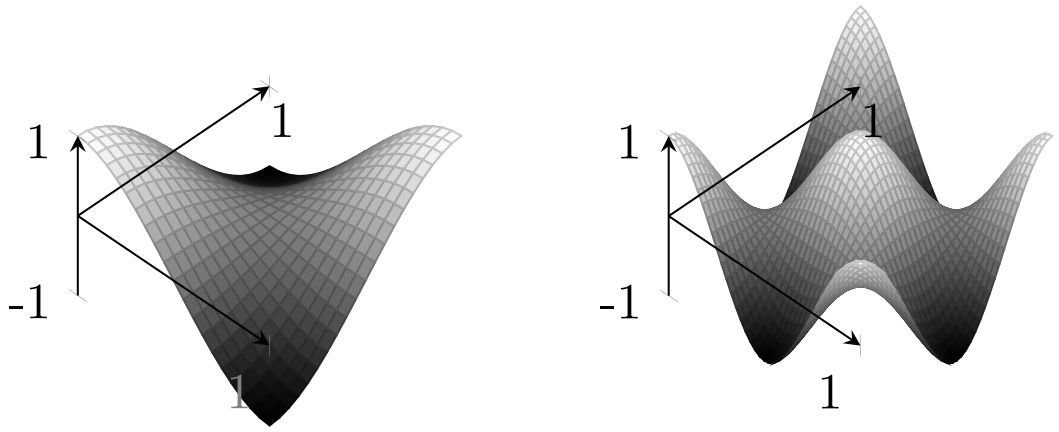

(a) non-periodic test function $d = 2$ (b) periodized test function $d = 2$

Figure 5.8: Two-dimensional test function f^2 and corresponding periodization f^2_{per}.

We define the multivariate non-periodic test function

$$f^d(\boldsymbol{x}) = \prod_{s=1}^{d} v(x_j)$$

as a tensor product of v and similar the periodized test function

$$f^d_{\text{per}}(\boldsymbol{x}) = \prod_{s=1}^{d} v_{\text{per}}(x_j).$$

The Fourier coefficients of v_{per} are given by

$$\hat{v}_{\text{per},k} = \begin{cases} \frac{48}{(k\pi)^4} & \text{for } k \in \mathbb{Z} \setminus 2\mathbb{Z}, \\ 0 & \text{else.} \end{cases}$$

We define a suitable hyperbolic cross weight function $\omega^d(\boldsymbol{k}) := \prod_{s=1}^{d} \max(1, \frac{4}{3}|k_s|)^2$ and conclude from

$$\|v_{\text{per}}|\mathcal{A}_{\omega^1}(\mathbb{T})\| = \sum_{\boldsymbol{k}\in\mathbb{Z}} \omega^1(k)\hat{v}_{\text{per},k} = \frac{64}{3\pi^2} \approx 2.16152$$

the norm of the multivariate periodized test function f^d_{per}

$$\|f^d_{\text{per}}|\mathcal{A}_{\omega^d}(\mathbb{T}^d)\| = \|v_{\text{per}}|\mathcal{A}_{\omega^1}(\mathbb{T})\|^d = \left(\frac{64}{3\pi^2}\right)^d.$$

Consequently, we estimate the $L_\infty(\mathbb{T}^d)$ approximation error by

$$\|f^d_{\text{per}} - \tilde{S}_{I^d_K} f^d_{\text{per}}|L_\infty(\mathbb{T}^d)\| \leq \frac{2}{K}\|f^d_{\text{per}}|\mathcal{A}_{\omega^d}(\mathbb{T}^d)\| = \frac{2}{K}\left(\frac{64}{3\pi^2}\right)^d = \frac{2}{N^2}\left(\frac{64}{3\pi^2}\right)^d, \tag{5.26}$$

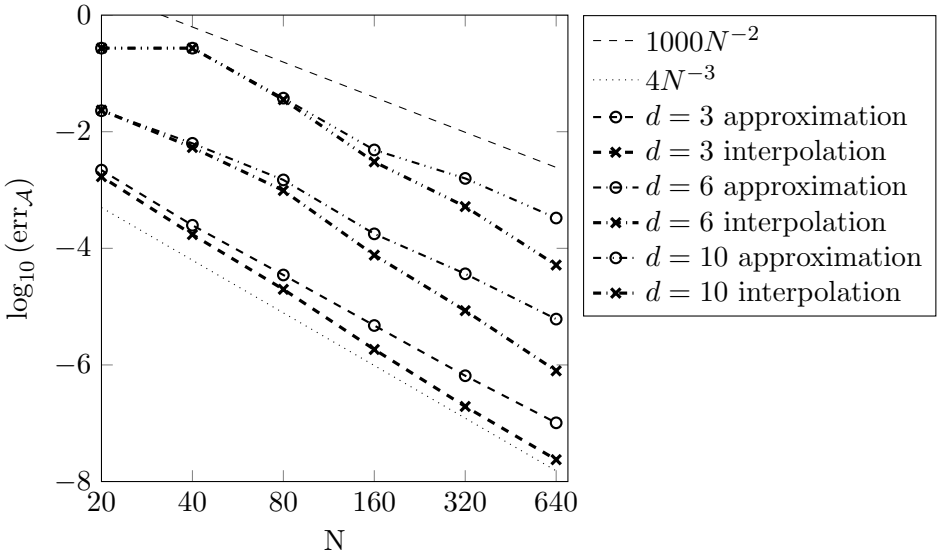

Figure 5.9: Approximation errors $\mathrm{err}_{\mathcal{A}} := \mathrm{err}\left(f_{\mathrm{per}}^d, p, \mathcal{A}(\mathbb{T}^d)\right)$, $p = \tilde{S}_{I_{\mathrm{hc-o},N}^{d,\frac{3}{4}}} f_{\mathrm{per}}^d$ or $p = \tilde{S}_{\tilde{I}_{\mathrm{hc-o},N}^{d,\frac{3}{4}}} f_{\mathrm{per}}^d$, plotted against the parameter N.

where $I_K^d := \{\boldsymbol{k} \in \mathbb{Z}^d \colon \omega^d(\boldsymbol{k}) \leq K\} = \{\boldsymbol{k} \in \mathbb{Z}^d \colon \prod_{s=1}^d \max(1, \frac{4}{3}|k_s|) \leq N\} = I_{\mathrm{hc},N}^{d,\frac{3}{4}}$, $N = \sqrt{K}$, is a frequency index set of hyperbolic cross type, cf. Section 2.3.2. In addition, we will apply the knowledge of the frequency index gaps, i.e., we would like to reconstruct only those frequencies, which are not zero a priori. For that reason, we define the hyperbolic cross of only odd frequency indices by

$$I_{\mathrm{hc-o},N}^{d,\frac{3}{4}} := \left\{ \boldsymbol{k} \in I_{\mathrm{hc},N}^{d,\frac{3}{4}} \colon \prod_{s=1}^{d} (k_s \bmod 2) = 1 \right\},$$

i.e., each frequency index $\boldsymbol{k} \in I_{\mathrm{hc-o},N}^{d,\frac{3}{4}}$ is a vector of only odd nonzero integers. We emphasize, that the theoretical error bounds for $\tilde{S}_{I_{\mathrm{hc},N}^{d,\frac{3}{4}}} f_{\mathrm{per}}^d$ also hold for $\tilde{S}_{I_{\mathrm{hc-o},N}^{d,\frac{3}{4}}} f_{\mathrm{per}}^d$ and are given in (5.26).

Numerical Example 5.13. Concretely, we computed the approximations $\tilde{S}_{I_{\mathrm{hc-o},N}^{d,\frac{3}{4}}} f_{\mathrm{per}}^d$ and the interpolations $\tilde{S}_{\tilde{I}_{\mathrm{hc-o},N}^{d,\frac{3}{4}}} f_{\mathrm{per}}^d$ for different dimensions $d = 3, 6, 10$ and parameters $N = 20, 40, 80, 160, 320, 640$, cf. Figure 5.9. The error estimate in (5.26) predict an error decay of at least N^{-2} for fixed dimension d. We would like to point out that the theoretical error estimates can be improved up to an order of $-3 + \epsilon$ in N for each $\epsilon > 0$ in the asymptotics.

Indeed, the plotted upper bounds of the errors $\mathrm{err}\left(f_{\mathrm{per}}^d, \tilde{S}_{I_{\mathrm{hc-o},N}^{d,\frac{3}{4}}} f_{\mathrm{per}}^d, \mathcal{A}(\mathbb{T}^d)\right)$ of the approximation $\tilde{S}_{I_{\mathrm{hc-o},N}^{d,\frac{3}{4}}} f_{\mathrm{per}}^d$ of f_{per}^d decrease similar to N^{-2} for growing N even for dimension $d = 10$. In addition, we recognize an even faster error decay of the errors $\mathrm{err}\left(f_{\mathrm{per}}^d, \tilde{S}_{\tilde{I}_{\mathrm{hc-o},N}^{d,\frac{3}{4}}} f_{\mathrm{per}}^d, \mathcal{A}(\mathbb{T}^d)\right)$ for the interpolations $\tilde{S}_{\tilde{I}_{\mathrm{hc-o},N}^{d,\frac{3}{4}}} f_{\mathrm{per}}^d$. The interpolation errors

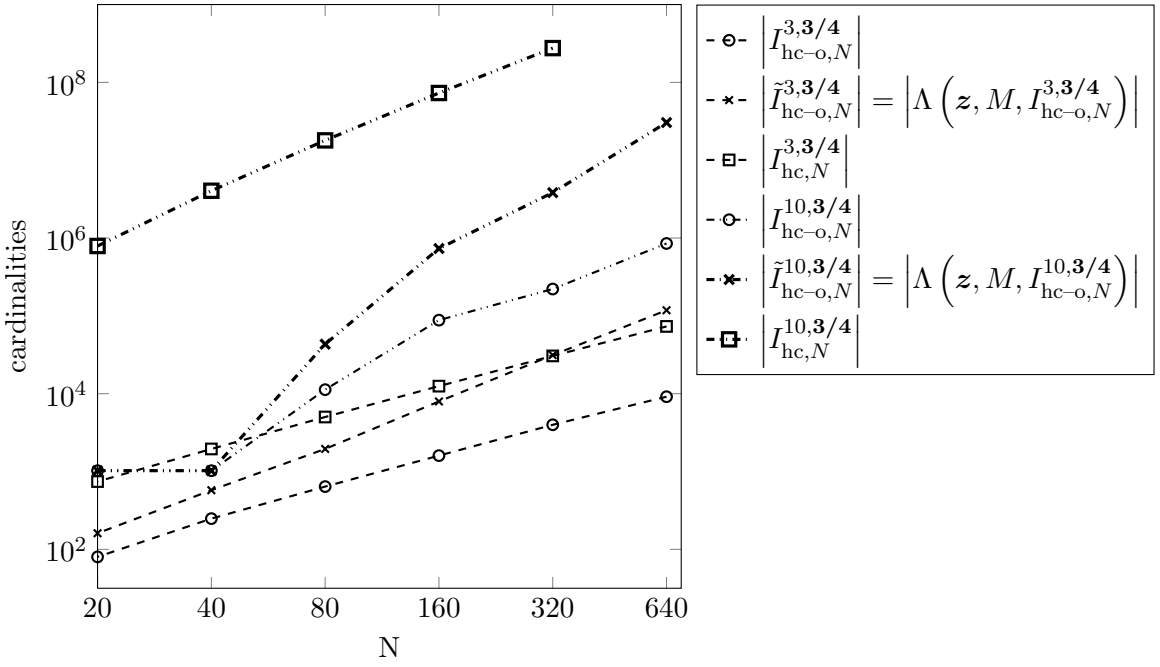

Figure 5.10: Cardinalities of frequency index sets $I^{d,\mathbf{3/4}}_{\text{hc–o},N}$, $\tilde{I}^{d,\mathbf{3/4}}_{\text{hc–o},N}$, and $I^{d,\mathbf{3/4}}_{\text{hc},N}$ plotted against the parameter N, dimensions $d = 3, 10$.

decrease faster than the approximation errors since the interpolating frequency index sets $\tilde{I}^{d,\frac{\mathbf{3}}{\mathbf{4}}}_{\text{hc–o},N}$ contain a huge amount of indices of less significant frequencies of the functions f^d_{per}.

Again, we would like to stress the fact that the frequency index sets $I^{d,\frac{\mathbf{3}}{\mathbf{4}}}_{\text{hc–o},N}$ contain only a few frequency indices of its corresponding supersets $I^{d,\frac{\mathbf{3}}{\mathbf{4}}}_{\text{hc},N}$. Furthermore, the well-adapted interpolating frequency index sets $\tilde{I}^{d,\frac{\mathbf{3}}{\mathbf{4}}}_{\text{hc–o},N}$ consists of much fewer frequencies than $|I^{d,\frac{\mathbf{3}}{\mathbf{4}}}_{\text{hc},N}|$, cf. Figure 5.10.

We consider the absolute values of the errors of the computed approximations and interpolations. The range of the functions f^d and its periodizations f^d_{per} is the whole interval $[-1, 1]$. We achieve error bounds on the $L_\infty(\mathbb{T}^d)$ error that are much smaller than the expected ones and, thus, impressively small with respect to the range of the functions f^d and f^d_{per} even for dimension $d = 10$ and reasonable problem sizes in practice, cf. Figures 5.9 and 5.10.

At the end, we would like to stress the fact that the cardinalities of all the sampling sets $\Lambda_{\boldsymbol{\varphi}}(\boldsymbol{z}, M, I^{d,\frac{\mathbf{3}}{\mathbf{4}}}_{\text{hc–o},N}) := \{\boldsymbol{x} = \boldsymbol{\varphi}(\boldsymbol{x}_j) \colon \boldsymbol{x}_j \in \Lambda(\boldsymbol{z}, M, I^{d,\frac{\mathbf{3}}{\mathbf{4}}}_{\text{hc–o},N})\}$, cf. (5.25), that we used for the approximation of the non-periodic functions f^d are given by the theoretical upper bound $\left\lfloor \frac{M+2}{2} \right\rfloor$ that we determined on page 140. □

5.4 Summary

The last sections treated several approximation problems that may similarly occur in practical applications. We applied the sampling methods that we presented in Chapter 3 in order to compute

- approximations and interpolations of multivariate periodic functions,

- solutions of Poisson's equation in d dimensions as an example of partial differential equations,
- approximations of sufficiently smooth multivariate non-periodic functions.

Additionally, we also dealt with approximations of multivariate periodic functions computed from sampling values along generated sets. We illustrated that our sampling methods yields suitable solutions of these problems if the given frequency index set I is well-adapted to the function that one would like to approximate. Specifically, we treated frequency index sets of different structures, i.e., equally weighted hyperbolic crosses and weighted ℓ_1-balls, and in particular equally weighted hyperbolic crosses with gaps, cf. Section 5.3.1.

We recognize advantages of the rank-1 lattice interpolation approach, cf. Section 3.5, in Section 5.1. In particular, it may be worthwhile to construct a suitable interpolating frequency index set $\tilde{I}_N$ using Algorithm 3.6 for a reconstructing rank-1 lattice $\Lambda(\boldsymbol{z}, M, I_N)$ for the frequency index set I_N. In general, the theoretical error estimates do not improve but the practical approximation errors may decrease due to the amount of additional approximated Fourier coefficients $\hat{\tilde{f}}_{\boldsymbol{k}}$, $\boldsymbol{k} \in \tilde{I}_N \setminus I_N$, especially if the oversampling factor $M/|I_N| \geq 1$ is large. We would like to point out that the computation of the interpolation, i.e., the d-dimensional fast Fourier transform using the already determined interpolating frequency index set $\tilde{I}_N$, cf. Algorithm 3.2, has a complexity of $\mathcal{O}\left(M(d + \log M)\right)$ since $|\tilde{I}_N| = M$, whereas the complexity of the approximation problem is in $\mathcal{O}\left(M \log M + d|I_N|\right)$. Thus, the computational times of both approaches hardly differ for moderate dimension d.

Furthermore, we gave a theoretical error estimate on the approximation error of a Galerkin method that uses the presented rank-1 lattice approach in order to determine approximate solutions of Poisson's equation with periodic boundary conditions in higher dimensions, cf. Theorem 5.8. We illustrated the practicability of this method by means of an example and compared the results to full grid and sparse grid approaches in Section 5.2.1.

In general, the most important observation of our numerical tests is that well chosen frequency index sets may severely reduce the number of degrees of freedom of an approximation of a specific multivariate function. Furthermore, the presented reconstruction approaches for trigonometric polynomials, i.e., reconstructing rank-1 lattices and reconstructing generated sets, offer a universally applicable ansatz with respect to the frequency index set I in order to approximate smooth functions in higher dimensions d.

The development of adaptive methods that reliably determine well-fitting d-dimensional frequency index sets I for functions f that can be arbitrarily sampled is of great interest—and affects another wide field of approximation theory. We only mention the recent developments in sparse fast Fourier transforms, i.e., the computation of frequency indices and frequencies of sparse trigonometric polynomials from a few sampling values, cf. e.g. [HIKP12b, HIKP12a, IKP14], which one might apply on rank-1 lattice sampling. Finally, in this context, we would like to suggest the development of a dimension–by–dimension adaptive approach that uses the presented sampling sets in order to solve both problems—determining a suitable frequency index set I and computing the approximated values of the corresponding frequencies $\hat{f}_{\boldsymbol{k}}$, $\boldsymbol{k} \in I$.

Bibliography

[AB04] A. O. L. Atkin and D. J. Bernstein. Prime sieves using binary quadratic forms. *Math. Comp.*, 73:1023 – 1030 (electronic), 2004. (Cited on page 45.)

[Axe96] O. Axelsson. *Iterative Solution Methods*. Cambridge University Press, Cambridge, 1996. (Cited on page 90.)

[BD89] G. Baszenski and F.-J. Delvos. A discrete Fourier transform scheme for Boolean sums of trigonometric operators. In C. K. Chui, W. Schempp, and K. Zeller, editors, *Multivariate Approximation Theory IV*, ISNM 90, pages 15 – 24. Birkhäuser, Basel, 1989. (Cited on pages 8 and 134.)

[Bey95] G. Beylkin. On the fast Fourier transform of functions with singularities. *Appl. Comput. Harmon. Anal.*, 2:363 – 381, 1995. (Cited on page 9.)

[BG99] H.-J. Bungartz and M. Griebel. A note on the complexity of solving Poisson's equation for spaces of bounded mixed derivatives. *J. Complexity*, 15:167 – 199, 1999. (Cited on pages 31, 73, 127, and 128.)

[BG04] H.-J. Bungartz and M. Griebel. Sparse grids. *Acta Numer.*, 13:147 – 269, 2004. (Cited on pages 8, 27, 30, 31, and 73.)

[Bjö96] Å. Björck. *Numerical Methods for Least Squares Problems*. SIAM, Philadelphia, PA, USA, 1996. (Cited on pages 39, 89, 96, and 97.)

[Bun92] H.-J. Bungartz. An adaptive poisson solver using hierarchical bases and sparse grids. In P. de Groen and R. Beauwens, editors, *Iterative Methods in Linear Algebra*, pages 293 – 310, Amsterdam, 1992. Elsevier. (Cited on page 128.)

[CDLP07] L. L. Cristea, J. Dick, G. Leobacher, and F. Pillichshammer. The tent transformation can improve the convergence rate of quasi-Monte Carlo algorithms using digital nets. *Numer. Math.*, 105:413 – 455, 2007. (Cited on pages 112 and 139.)

[CKN10] R. Cools, F. Y. Kuo, and D. Nuyens. Constructing lattice rules based on weighted degree of exactness and worst case error. *Computing*, 87:63 – 89, 2010. (Cited on pages 9, 28, 40, 41, 46, 55, and 56.)

[CN04] R. Cools and D. Nuyens. Fast algorithms for component-by-component construction of rank-1 lattice rules in shift-invariant reproducing kernel Hilbert spaces. *Math. Comp.*, 75:903 – 920, 2004. (Cited on pages 36 and 56.)

[CN06] R. Cools and D. Nuyens. Fast component-by-component construction, a reprise for different kernels. In H. Niederreiter and D. Talay, editors, *Monte Carlo and Quasi-Monte Carlo Methods 2004*, pages 373 – 387. Springer Berlin Heidelberg, 2006. (Cited on page 56.)

[CN07] R. Cools and D. Nuyens. An overview of fast component-by-component constructions of lattice rules and lattice sequences. *PAMM*, 7:1022609 – 1022610, 2007. (Cited on page 56.)

[CN08] R. Cools and D. Nuyens. A belgian view on lattice rules. In A. Keller, S. Heinrich, and H. Niederreiter, editors, *Monte Carlo and Quasi-Monte Carlo Methods 2006*, pages 3 – 21. Springer Berlin Heidelberg, 2008. (Cited on page 56.)

[CR97] R. Cools and A. V. Reztsov. Different quality indexes for lattice rules. *J. Complexity*, 13:235 – 258, 1997. (Cited on page 46.)

[CT65] J. W. Cooley and J. W. Tukey. An algorithm for machine calculation of complex Fourier series. *Math. Comput.*, 19:297 – 301, 1965. (Cited on pages 7 and 38.)

[DeT91] D. W. DeTemple. The non-integer property of sums of reciprocals of consecutive integers. *Math. Gaz.*, 75:193 – 194, 1991. (Cited on page 99.)

[DKS13] J. Dick, F. Y. Kuo, and I. H. Sloan. High-dimensional integration: The quasi-Monte Carlo way. *Acta Numer.*, 22:133 – 288, 2013. (Cited on page 36.)

[DNP14] J. Dick, D. Nuyens, and F. Pillichshammer. Lattice rules for nonperiodic smooth integrands. *Numerische Mathematik*, 126:259 – 291, 2014. (Cited on pages 112 and 139.)

[DPT94] R. A. DeVore, P. P. Petrushev, and V. N. Temlyakov. Multivariate trigonometric polynomial approximations with frequencies from the hyperbolic cross. *Math. Notes*, 56:900 – 918, 1994. (Cited on pages 8 and 27.)

[DR93] A. Dutt and V. Rokhlin. Fast Fourier transforms for nonequispaced data. *SIAM J. Sci. Stat. Comput.*, 14:1368 – 1393, 1993. (Cited on page 9.)

[DS89] F.-J. Delvos and W. Schempp. *Boolean methods in interpolation and approximation.* Longman Scientific & Technical, Harlow, 1989. (Cited on pages 8 and 27.)

[Dus10] P. Dusart. Estimates of some functions over primes without R.H. `http://arxiv.org/abs/1002.0442v1`, 2010. (Cited on page 43.)

[DY07] L. Demanet and L. Ying. Curvelets and wave atoms for mirror-extended images. In D. Van De Ville, V. K. Goyal, and M. Papadakis, editors, *Proc. SPIE 6701, Wavelets XII,* 67010J, 2007. (Cited on page 137.)

[Erm75] S. M. Ermakov. *Die Monte-Carlo-Methode und verwandte Fragen.* Hochschulbücher für Mathematik. VEB Deutscher Verlag der Wissenschaften, Berlin, 1975. (Cited on pages 21, 33, and 47.)

[Ger31] S. A. Gershgorin. Über die Abgrenzung der Eigenwerte einer Matrix. *Bull. Acad. Sci. URSS*, 1931:749 – 754, 1931. (Cited on page 90.)

[GH14] M. Griebel and J. Hamaekers. Fast discrete Fourier transform on generalized sparse grids. In J. Garcke and D. Pflüger, editors, *Sparse Grids and Applications - Munich 2012*, volume 97 of *Lect. Notes Comput. Sci. Eng.*, pages 75 – 107. Springer International Publishing, 2014. (Cited on pages 8, 31, 51, and 73.)

[GPR10] K. Gröchenig, B. M. Pötscher, and H. Rauhut. Learning trigonometric polynomials from random samples and exponential inequalities for eigenvalues of random matrices. *arXiv:math/0701781v2*, 2010. (Cited on pages 8 and 81.)

[Gra07] V. Gradinaru. Fourier transform on sparse grids: Code design and the time dependent Schrödinger equation. *Computing*, 80:1 – 22, 2007. (Cited on page 8.)

[Hac12] W. Hackbusch. *Tensor spaces and numerical tensor calculus.* Springer, Berlin, 2012. (Cited on page 127.)

[Hal92] K. Hallatschek. Fouriertransformation auf dünnen Gittern mit hierarchischen Basen. *Numer. Math.*, 63:83 – 97, 1992. (Cited on pages 8, 29, 134, and 135.)

[Hav09] J. Havil. *Gamma : Exploring Euler's constant*. Princeton Science Library. Princeton University Press, Princeton, NJ, 10th edition, 2009. (Cited on page 99.)

[Hic02] F. J. Hickernell. Obtaining $O(n^{-2+\epsilon})$ convergence for lattice quadrature rules. In K.-T. Fang, H. Niederreiter, and F. J. Hickernell, editors, *Monte Carlo and Quasi-Monte Carlo Methods 2000*, pages 274 – 289. Springer Berlin Heidelberg, 2002. (Cited on pages 112 and 139.)

[HIKP12a] H. Hassanieh, P. Indyk, D. Katabi, and E. Price. Nearly optimal sparse Fourier transform. In *Proceedings of the Forty-fourth Annual ACM Symposium on Theory of Computing*, pages 563 – 578. ACM, 2012. (Cited on page 144.)

[HIKP12b] H. Hassanieh, P. Indyk, D. Katabi, and E. Price. Simple and practical algorithm for sparse Fourier transform. In *Proceedings of the Twenty-third Annual ACM-SIAM Symposium on Discrete Algorithms*, pages 1183 – 1194. SIAM, 2012. (Cited on page 144.)

[HJ85] R. A. Horn and C. R. Johnson. *Matrix Analysis*. Cambridge University Press, Cambridge, 1985. (Cited on page 86.)

[HW00] F. J. Hickernell and H. Woźniakowski. Integration and approximation in arbitrary dimensions. *Adv. Comput. Math.*, 12:25 – 58, 2000. (Cited on page 22.)

[HW01] F. J. Hickernell and H. Woźniakowski. Tractability of multivariate integration for periodic functions. *J. Complexity*, 17:660 – 682, 2001. (Cited on page 22.)

[IKP14] P. Indyk, M. Kapralov, and E. Price. (Nearly) sample-optimal sparse Fourier transform. In *Proceedings of the Forty-fourth Annual ACM Symposium on Theory of Computing*, pages 563 – 578. ACM, 2014. (Cited on page 144.)

[Käm] L. Kämmerer. LFFT, MATLAB® toolbox for the lattice and generated set based FFT. `http://www.tu-chemnitz.de/~lkae/lfft`. (Cited on page 9.)

[Käm13a] L. Kämmerer. Reconstructing hyperbolic cross trigonometric polynomials by sampling along rank-1 lattices. *SIAM J. Numer. Anal.*, 51:2773 – 2796, 2013. (Cited on pages 9, 29, 69, and 70.)

[Käm13b] L. Kämmerer. Reconstructing multivariate trigonometric polynomials by sampling along generated sets. In J. Dick, F. Y. Kuo, G. W. Peters, and I. H. Sloan, editors, *Monte Carlo and Quasi-Monte Carlo Methods 2012*, pages 439 – 454. Springer Berlin Heidelberg, 2013. (Cited on page 9.)

[Käm14] L. Kämmerer. Reconstructing multivariate trigonometric polynomials from samples along rank-1 lattices. In G. E. Fasshauer and L. L. Schumaker, editors, *Approximation Theory XIV: San Antonio 2013*, pages 255 – 271. Springer International Publishing, 2014. (Cited on page 9.)

[KK11] L. Kämmerer and S. Kunis. On the stability of the hyperbolic cross discrete Fourier transform. *Numer. Math.*, 117:581 – 600, 2011. (Cited on page 8.)

[KKP09] J. Keiner, S. Kunis, and D. Potts. Using NFFT3 - a software library for various nonequispaced fast Fourier transforms. *ACM Trans. Math. Software*, 36:Article 19, 1 – 30, 2009. (Cited on page 85.)

[KKP12] L. Kämmerer, S. Kunis, and D. Potts. Interpolation lattices for hyperbolic cross trigonometric polynomials. *J. Complexity*, 28:76 – 92, 2012. (Cited on pages 9, 29, 135, and 137.)

[Kna00] S. Knapek. Approximation und Kompression mit Tensorprodukt-Multiskalenräumen. Dissertation, Universität Bonn, 2000. (Cited on pages 31 and 73.)

[Kno54] K. Knopp. *Theory and Applications of Infinite Series*. Blackie and Son, Ltd., Glasgow, UK, 1954. (Cited on page 29.)

[Knu76] D. E. Knuth. Big omicron and big omega and big theta. *ACM SIGACT News*, 8(2):18 – 24, 1976. (Cited on page 152.)

[KP07] S. Kunis and D. Potts. Stability results for scattered data interpolation by trigonometric polynomials. *SIAM J. Sci. Comput.*, 29:1403 – 1419, 2007. (Cited on page 90.)

[KPV13] L. Kämmerer, D. Potts, and T. Volkmer. Approximation of multivariate functions by trigonometric polynomials based on rank-1 lattice sampling. *Preprint 145, DFG Priority Program 1324*, 2013. (Cited on pages 9, 31, 51, 52, 54, and 72.)

[KPV14] L. Kämmerer, D. Potts, and T. Volkmer. Approximation of multivariate periodic functions by trigonometric polynomials based on sampling along rank-1 lattice with generating vector of Korobov form. *J. Complexity*, 2014. (Cited on pages 9, 51, and 52.)

[KR08] S. Kunis and H. Rauhut. Random sampling of sparse trigonometric polynomials II, Orthogonal matching pursuit versus basis pursuit. *Found. Comput. Math.*, 8:737 – 763, 2008. (Cited on page 34.)

[KSU14] T. Kühn, W. Sickel, and T. Ullrich. Approximation numbers of Sobolev embeddings—sharp constants and tractability. *J. Complexity*, 30:95 – 116, 2014. (Cited on page 27.)

[KSW06] F. Y. Kuo, I. H. Sloan, and H. Woźniakowski. Lattice rules for multivariate approximation in the worst case setting. In H. Niederreiter and D. Talay, editors, *Monte Carlo and Quasi-Monte Carlo Methods 2004*, pages 289 – 330. Springer Berlin Heidelberg, Berlin, 2006. (Cited on pages 8, 9, and 36.)

[KSW08] F. Y. Kuo, I. H. Sloan, and H. Woźniakowski. Lattice rule algorithms for multivariate approximation in the average case setting. *J. Complexity*, 24:283 – 323, 2008. (Cited on pages 8, 9, and 36.)

[Kun06] S. Kunis. Nonequispaced FFT - Generalisation and Inversion. Dissertation, Institut für Mathematik, Universität zu Lübeck, `http://www.analysis.uni-osnabrueck.de/kunis/`, 2006. (Cited on page 89.)

[KWW09] F. Y. Kuo, G. W. Wasilkowski, and H. Woźniakowski. Lattice algorithms for multivariate L_∞ approximation in the worst-case setting. *Constr. Approx.*, 30:475 – 493, 2009. (Cited on pages 8, 9, and 36.)

[Lar88] G. Larcher. On the distribution of s-dimensional Kronecker-sequences. *Acta Arith.*, 51:335 – 347, 1988. (Cited on page 81.)

[LH03] D. Li and F. J. Hickernell. Trigonometric spectral collocation methods on lattices. In S. Y. Cheng, C.-W. Shu, and T. Tang, editors, *Recent Advances in Scientific Computing and Partial Differential Equations*, volume 330 of *Contemp. Math.*, pages 121 – 132. AMS, 2003. (Cited on pages 8, 36, 38, 50, 112, and 127.)

[Loo11] A. Loo. On the primes in the interval [3n,4n]. *Int. J. Contemp. Math. Sciences*, 6:1871–1882, 2011. (Cited on page 42.)

[LSX09] H. Li, J. Sun, and Y. Xu. Cubature formula and interpolation on the cubic domain. *Numer. Math. Theor. Meth. Appl.*, 2:119 – 152, 2009. (Cited on page 8.)

[MAT] MATLAB®. *Version 8.3 (R2014a)*. The MathWorks, Inc., Natick, Massachusetts, United States. (Cited on pages 95 and 137.)

[MS12] H. Munthe-Kaas and T. Sørevik. Multidimensional pseudo-spectral methods on lattice grids. *Appl. Numer. Math.*, 62:155 – 165, 2012. (Cited on pages 8, 36, 53, 121, and 127.)

[Mys01] I. P. Mysovskikh. Cubature formulae that are exact for trigonometric polynomials. Reports on Numerical Analysis and Applied Mathematics TW 324, Department of Computer Science, K.U.Leuven, 2001. Edited by R. Cools and H. J. Schmid. (Cited on page 26.)

[Nie78] H. Niederreiter. Quasi-Monte Carlo methods and pseudo-random numbers. *B. Am. Math. Soc.*, 84:957 – 1041, 1978. (Cited on pages 8 and 35.)

[NM65] J. A. Nelder and R. Mead. A simplex method for function minimization. *Comput. J.*, 7:308 – 313, 1965. (Cited on page 95.)

[NSW04] E. Novak, I. H. Sloan, and H. Woźniakowski. Tractability of approximation for weighted Korobov spaces on classical and quantum computers. *Found. Comput. Math.*, 4:121 – 156, 2004. (Cited on page 22.)

[NW01] E. Novak and H. Woźniakowski. Intractability results for integration and discrepancy. *J. Complexity*, 17:388 – 441, 2001. (Cited on page 22.)

[NW08] E. Novak and H. Woźniakowski. *Tractability of Multivariate Problems Volume I: Linear Information.* Eur. Math. Society, EMS Tracts in Mathematics Vol 6, 2008. (Cited on pages 22 and 54.)

[NW10] E. Novak and H. Woźniakowski. *Tractability of Multivariate Problems Volume II: Standard Information for Functionals.* Eur. Math. Society, EMS Tracts in Mathematics Vol 12, 2010. (Cited on page 22.)

[NW12] E. Novak and H. Woźniakowski. *Tractability of Multivariate Problems Volume III: Standard Information for Operators.* Eur. Math. Society, EMS Tracts in Mathematics Vol 18, 2012. (Cited on page 22.)

[Ost82] A. Ostrowski. On the error term in multidimensional diophantine approximation. *Acta Arith.*, 41:163 – 183, 1982. (Cited on page 81.)

[PST03] D. Potts, G. Steidl, and M. Tasche. Numerical stability of fast trigonometric transforms - a worst case study. *J. Concrete Appl. Math.*, 1:1 – 36, 2003. (Cited on pages 7 and 37.)

[SB05] J. Stoer and R. Bulirsch. *Numerische Mathematik 2.* Springer-Verlag, Berlin, 4. edition, 2005. (Cited on page 127.)

[Sch96] J. C. Schatzman. Accuracy of the discrete Fourier transform and the fast Fourier transform. *SIAM J. Sci. Comput.*, 17:1150 – 1166, 1996. (Cited on pages 7 and 37.)

[SJ94] I. H. Sloan and S. Joe. *Lattice methods for multiple integration.* Oxford Science Publications. The Clarendon Press Oxford University Press, New York, 1994. (Cited on page 36.)

[SK87] I. H. Sloan and P. J. Kachoyan. Lattice methods for multiple integration: Theory, error analysis and examples. *SIAM J. Numer. Anal.*, 24:116 – 128, 1987. (Cited on page 39.)

[Spr00] F. Sprengel. A class of function spaces and interpolation on sparse grids. *Numer. Funct. Anal. Optim.*, 21:273 – 293, 2000. (Cited on page 27.)

[SR02] I. H. Sloan and A. V. Reztsov. Component-by-component construction of good lattice rules. *Math. Comp.*, 71:263 – 273, 2002. (Cited on pages 35 and 36.)

[SS99a] W. Sickel and F. Sprengel. Interpolation on sparse grids and tensor products of Nikol'skij-Besov spaces. *J. Comput. Anal. Appl.*, 1:263 – 288, 1999. (Cited on page 27.)

[SS99b] W. Sickel and F. Sprengel. Some error estimates for periodic interpolation of functions from Besov spaces. In W. Haussman, K. Jetter, and M. Reimer, editors, *Advances in multivariate approximation*, pages 269 – 287. Wiley-VCH, 1999. (Cited on page 27.)

[ST87] H.-J. Schmeisser and H. Triebel. *Topics in Fourier analysis and function spaces*, volume 42 of *Mathematik und ihre Anwendungen in Physik und Technik*. Akademische Verlagsgesellschaft Geest & Portig K.-G., Leipzig, 1987. (Cited on page 16.)

[ST89] G. Steidl and M. Tasche. Index transforms for multidimensional DFT's and convolutions. *Numer. Math.*, 56:513 – 528, 1989. (Cited on pages 61 and 100.)

[Ste98] G. Steidl. A note on fast Fourier transforms for nonequispaced grids. *Adv. Comput. Math.*, 9:337 – 353, 1998. (Cited on page 9.)

[STW11] J. Shen, T. Tang, and L.-L. Wang. *Spectral Methods*, volume 41 of *Springer Ser. Comput. Math.* Springer-Verlag Berlin Heidelberg, Berlin, 2011. (Cited on page 127.)

[SU07] W. Sickel and T. Ullrich. The Smolyak algorithm, sampling on sparse grids and function spaces of dominating mixed smoothness. *East J. Approx.*, 13:387 – 425, 2007. (Cited on pages 27 and 134.)

[SW01] I. H. Sloan and H. Woźniakowski. Tractability of multivariate integration for weighted Korobov classes. *J. Complexity*, 17:697 – 721, 2001. (Cited on page 22.)

[Tem86] V. N. Temlyakov. Reconstruction of periodic functions of several variables from the values at the nodes of number-theoretic nets. *Anal. Math.*, 12:287 – 305, 1986. In Russian. (Cited on pages 8, 27, 36, and 52.)

[Tem93] V. N. Temlyakov. *Approximation of periodic functions*. Computational Mathematics and Analysis Series. Nova Science Publishers Inc., Commack, NY, 1993. (Cited on page 8.)

[Ull08] T. Ullrich. Smolyak's algorithm, sampling on sparse grids and Sobolev spaces of dominating mixed smoothness. *East J. Approx.*, 14:1 – 38, 2008. (Cited on page 27.)

[Wei12] F. Weisz. Summability of multi-dimensional trigonometric Fourier series. *Surv. Approx. Theory*, 7:1 – 179, 2012. (Cited on page 13.)

[Wey16] H. Weyl. Über die Gleichverteilung von Zahlen mod. Eins. *Mathematische Annalen*, 77:313 – 352, 1916. (Cited on page 81.)

[Xu11] Z. Xu. Deterministic sampling of sparse trigonometric polynomials. *J. Complexity*, 27:133 – 140, 2011. (Cited on page 34.)

[Yse10] H. Yserentant. *Regularity and Approximability of Electronic Wave Functions*. Lecture Notes in Mathematics. Springer-Verlag, Berlin, 2010. (Cited on page 27.)

[Zar72] S. K. Zaremba. La méthode des "bons treillis" pour le calcul des intégrales multiples. In *Applications of number theory to numerical analysis (Proc. Sympos., Univ. Montreal, Montreal, Que., 1971)*, pages 39 – 119. Academic Press, New York, 1972. (Cited on page 46.)

[Zen91] C. Zenger. Sparse grids. In *Parallel algorithms for partial differential equations (Kiel, 1990)*, volume 31 of *Notes Numer. Fluid Mech.*, pages 241 – 251. Vieweg, Braunschweig, Germany, 1991. (Cited on page 27.)

[ZLH06] X. Zeng, K.-T. Leung, and F. J. Hickernell. Error analysis of splines for periodic problems using lattice designs. In H. Niederreiter and D. Talay, editors, *Monte Carlo and Quasi-Monte Carlo Methods 2004*, pages 501 – 514. Springer Berlin Heidelberg, 2006. (Cited on pages 8 and 36.)

Notations

$\mathcal{A}(\mathbb{T}^d)$	Wiener algebra, cf. (2.6).
$\mathcal{A}_\omega(\mathbb{T}^d)$	Weighted function space, subspace of Wiener algebra, cf. (2.9).
$\boldsymbol{A}$	Fourier matrix, cf (2.7).
$\mathbb{C}$	Complex numbers.
$\mathrm{cond}_2(\boldsymbol{A})$	Condition number of the matrix $\boldsymbol{A}$, $\mathrm{cond}_2(\boldsymbol{A}) = \sqrt{\lambda_{\max}(\boldsymbol{A}^*\boldsymbol{A})/\lambda_{\min}(\boldsymbol{A}^*\boldsymbol{A})}$.
$\mathcal{D}(I)$	Difference set of the frequency index set $I \subset \mathbb{Z}^d$, cf. (2.11).
d	Spatial dimension.
ess sup	Essential supremum.
e	Euler's number, $\mathrm{e} = 2.71828182845904\ldots$.
$\boldsymbol{e}_s$	Unit vector in the sth dimension.
$\boldsymbol{I}$	Identity matrix.
i	Imaginary unit.
I	Frequency index set, $I \subset \mathbb{Z}^d$.
$I^{d,\boldsymbol{\gamma},\alpha,\beta}_{\mathrm{ehc},N}$	Weighted energy-norm based hyperbolic cross for $0 < -\alpha < \beta$, cf. (2.21).
$I^{d,\boldsymbol{\gamma}}_{\mathrm{hc},N}$	Weighted hyperbolic cross, cf. (2.17).
$I^{d,\boldsymbol{\gamma}}_{p,N}$	Weighted ℓ_p-ball, cf. (2.15).
$\lambda_{\max}(\boldsymbol{A}^*\boldsymbol{A})$	Maximal eigenvalue of the square matrix $\boldsymbol{A}^*\boldsymbol{A}$.
$\lambda_{\min}(\boldsymbol{A}^*\boldsymbol{A})$	Minimal eigenvalue of the square matrix $\boldsymbol{A}^*\boldsymbol{A}$.
$\Lambda(\boldsymbol{r}, M)$	Generated set of size M with generating vector $\boldsymbol{r} \in \mathbb{R}^d$, cf. (4.1).
$\Lambda(\boldsymbol{r}, M, I)$	Reconstructing generated set for the frequency index set I, see page 85.
$\Lambda(\boldsymbol{z}, M)$	Rank-1 lattice of size M with generating vector $\boldsymbol{z} \in \mathbb{N}^d$, cf. (3.1).
$\Lambda(\boldsymbol{z}, M, I)$	Reconstructing rank-1 lattice for the frequency index set I, see page 39.
$L_p(\mathbb{T}^d)$	Function space of p-integrable functions, cf. (2.2) and (2.3).

$l_p(a)$	Sequence space of p-summable sequences with the usual norm, sequence space of sequences of length a, if $a \in \mathbb{N}$, or over the set a, if $a \subset \mathbb{Z}^d$.
mod	Component–by–component modulo of a vector $\boldsymbol{a} \in \mathbb{R}^d$, $\boldsymbol{a} \bmod \mathbf{1} = (a_s - \lfloor a_s \rfloor)_{s=1}^d$, $\boldsymbol{a} \bmod M = (a_s - \lfloor a_s/M \rfloor M)_{s=1}^d$ for $M \in \mathbb{N}$.
$\mathbb{N}$	Positive integers without zero.
$\mathbb{N}_0$	Positive integers, zero included.
$\Omega\left(g(\boldsymbol{x})\right)$	$f \in \Omega\left(g(\boldsymbol{x})\right) \Leftrightarrow g \in \mathcal{O}\left(f(\boldsymbol{x})\right)$.
$\mathcal{O}\left(g(\boldsymbol{x})\right)$	Denotes the set of functions $f\colon \mathbb{R}^d \mapsto [0,\infty)$ such that there exist positive constants $C_f < \infty$ and $\boldsymbol{n} \in \mathbb{N}^d$ with $f(\boldsymbol{x}) \leq C_f g(\boldsymbol{x})$ for all $\boldsymbol{x} \in \mathbb{R}^d$ with $x_s \geq n_s$, $s = 1,\ldots,d$, C_f depends on f but not on $\boldsymbol{x}$, cf. [Knu76]. Depending on the context, one has to distinguish variables and parameters of the function g.
Π_I	Space of trigonometric polynomials, cf. (2.8).
$\mathbb{Q}$	Rational numbers.
$\mathbb{R}$	Real numbers.
$\boldsymbol{r}$	Vector of real numbers.
$\Theta\left(g(\boldsymbol{x})\right)$	$\Theta\left(g(\boldsymbol{x})\right) = \mathcal{O}\left(g(\boldsymbol{x})\right) \cap \Omega\left(g(\boldsymbol{x})\right)$.
$\mathbb{T}$	One-dimensional torus, $\mathbb{T} \simeq [0,1)$.
$\mathcal{X}$	Sampling scheme on the d-dimensional torus, $\mathcal{X} \subset \mathbb{T}^d$.
$\mathbb{Z}$	Integers.
$\boldsymbol{z}$	Vector of integers.
$\|\circ\|_p$	Usual p norm of a vector.
$\|x\|X\|$	Norm of an element $x \in X$ in the normed space X.

We have listed the most frequently used notations. However, the table is not comprehensive. Several necessary additional notations appear locally throughout the whole work.